

https://dspace.org/

Shock wave interactions with porous plates

Seeraj, Sumil

2009-05-08T08:07:49Z
http://hdl.handle.net/10539/6933

Downloaded from a DSpace repository. https://dspace.org/

Shock Wave Interactions with Porous Plates

Sumil Seeraj

A research report submitted to the Faculty of Engineering, University of the Witwatersrand, Johannesburg, in fulfillment of the requirements for the degree of Master of Science in Engineering.

Johannesburg, December 2007

Declaration

I declare that this research report is my own, unaided work, except where otherwise acknowledged. It is being submitted for the degree of Master of Science in Engineering at the University of the Witwatersrand, Johannesburg, South Africa. It has not been submitted before for any degree or examination in any other University.

_____

Sumil Seeraj

Signed this _____day of _____ 2008

To my family, for their support during my studies.

Acknowledgements

I would like to express my sincere appreciation to Professor B.W. Skews for his guidance and advice throughout the project.

Thank you to Mr. A. Andreis for his technical assistance and advice in the laboratory.

I would like to thank Mr. G.S.M. Li for his assistance with the optical equipment and during testing.

Thank you to the laboratory staff for their advice and assistance in the design and manufacture of the various components required for experimentation.

Finally, I would like to thank the University of the Witwatersrand, Rolls Royce, and the National Research Foundation for sponsoring my postgraduate studies.

Abstract

The idea of creating a material or barrier that attenuates shock and blast waves has long been investigated. Considerable work has been performed on the interactions of shock and blast waves with various materials. The application of permeable solids, porous materials and textiles for the attenuation and reflection of destructive shock waves have been studied extensively. The studies presented herein examine the interaction of shock waves and porous plates in order to ameliorate the hazardous effects of these waves particularly in ducts or channels leading to protected areas or objects. A number of tests were performed in an automated shock tube to determine the effects that a series of directional porous plates had on the initial peak pressure and impulse amelioration experienced by the end wall. Mild steel test specimens, ranging in porosity values from 6.6 % to 41.1 %, were mounted two at a time in the test section of the shock tube. Each plate had directional properties and since four plates were used in the study, a total of forty eight plate configurations were tested. Six pressure transducers were located along the side of the test section and two pressure transducers were located in the end wall of the shock tube in order to measure initial peak pressure and impulse amelioration values experienced by the end wall and to identify the wave interactions involved in the amelioration process. Schlieren photographs were also taken in order to investigate these wave interactions. Tests were run at three different Mach numbers viz. 1.23, 1.35 and 1.42. The separation distances between the plate specimens were varied between 30 mm and 60 mm; however the distance between the downstream plate and the end wall was kept constant at 140mm for all tests. It was found that significant initial peak pressure and impulse amelioration was achievable. The Back & Back plate arrangement produced the greatest initial peak pressure and impulse amelioration with averages values of 73.7 % and 20.45 % respectively. Both the initial peak pressure and impulse amelioration values were found to be dependant on the plate combination porosity. As the porosity of the combination increased, the amelioration values decreased. Complementary plate combinations produced differing results as different wave interactions occur when plate positions were interchanged. The porosity of the combined plates were found to have an overriding influence on the end wall initial peak pressure and impulse amelioration values when compared to the effect that plate arrangement (i.e. geometrical influences) had. For all tests performed in this study, the time period used for the integration of the end wall pressure traces was 9 250 μs. As an acceptable closing time for a blast valve in a shelter's ventilation system is approximately 4 000 μs, the impulse amelioration values for certain plate combinations were recalculated. It was found that using this time period greater impulse amelioration values were produced as the rate of pressure rise, dp/dt, was initially lower at the beginning of the end wall pressure trace. Therefore, the lowest impulse amelioration value (7.9 %) achieved in this study, would produce significant impulse amelioration (20.3 %) if it were to be used in a shelter's ventilation system. Impulse amelioration values were found to increase as the separation distance between

plates were increased. The average impulse amelioration value was found to increase approximately 1 % for a 15mm increase in the distance between plates. The amplitude of the entire end wall pressure trace was found to increase as the incident Mach number was increased. This resulted in greater initial peak pressure and impulse experienced by the end wall. The significant attenuation of the incident shock wave obtained during this study is attributed to the system of multiple reflected and transmitted waves that are produced by the presence of the plate specimens in series. This increases the frequency of shock wave and barrier interactions, when compared to just using a single barrier, creating regions of highly unsteady flow, especially in the air space between the plate specimens. Furthermore, the presence of the series of plates also allows for wave resonance to occur which may further attenuate the strength of the incident shock wave. It is suggested that future studies include numerical techniques in order to further investigate the complex wave processes that occur upon interaction with the plate specimens and confirm the major loss mechanisms of the system.

Contents

Declaration ..... **i**

Acknowledgements ..... **iii**

Abstract ..... **iv**

Contents ..... **vi**

Appendices ..... **x**

List of Figures ..... **xi**

List of Tables ..... **xvi**

List of Symbols ..... **xvii**

1 Introduction **1**

1.1 Importance of the Study **1**

1.2 The Devastating Effects of Exposure to Blast Waves **2**

1.3 Characteristics of Blast Waves **4**

1.4 Blast Waves **6**

1.4.1 The Difference between a Blast and Shock Wave 6

1.4.2 The Generation of a Spherical Blast Wave 8

1.4.3 Measuring the Destructive Capability of a Blast Wave 9

1.5 Applicable Gas Dynamics **11**

1.5.1 Definition of Mach number 11

1.5.2 Normal Shock Waves 12

1.5.3 Moving Normal Shock Waves 12

1.5.4 Reflected Normal Shock Waves 14
1.5.5 Definition of Initial Peak Pressure Amelioration and Impulse Amelioration 15
2 Objectives 16
3 Literature Review 17
3.1 Investigations of the Trapping of Shock Waves 17
3.2 Shock Wave Interactions with Perforated Plates 21
4 Experimental Facilities 33
4.1 Calibration Duct and Related Instruments 33
4.2 The Shock Tube 36
4.2.1 Introduction 36
4.2.2 The Michael Seitz Shock Tube Facility 38
4.2.2.1 The Driver Section 39
4.2.2.2 The Expansion Chamber 40
4.2.2.3 The Test Section 41
4.3 The Data Acquisition System 44
4.4 Instrumentation and Calibration 45
4.4.1 Static Pressure and Temperature Measurement 45
4.4.2 Driver Section Pressure Measurement 45
4.4.3 High Speed Pressure Measurement 45
4.4.4 Calibration of the High Speed Pressure Transducers 45
4.4.5 Shock Tube Mach number Calibration 46
4.5 The Schlieren Optical System 46
4.6 Test Specimens 48
4.6.1 Introduction 48

4.6.2 Test Specimen Properties 50
4.6.3 Mounting of the Test Specimens 51
4.6.4 Plate Combinations and Their Representation 53
4.7 Modification of the Aluminium Test Section Door 54
4.8 Location of Pressure Transducers 55
5 Experimental Procedure and Precautions 57
5.1 Orifice Plate Calibration Procedure 57
5.2 Orifice Plate Calibration Precautions 57
5.3 Operation of the Calibration Duct 58
5.4 Calibration Duct Operating Precautions 59
5.5 Operation of the Shock Tube 59
5.6 Shock Tube Operating Precautions 60
6 Observations 62
6.1 Orifice Plate Calibration Observations 62
6.2 Observations of Pressure Differentials that Occurred Across Test Specimens 64
6.3 Shock Tube Testing Observations 65
6.3.1 Description of Test Data Files 65
7 Shock Tube Data Processing Description 67
8 Processed Shock Tube Data 69
8.1 Normal Test Data 69
8.2 Plate Configuration Test Data 70
8.3 Plate Separation Distance Test Data 73

8.4 Mach number Test Data 74

9 Results and Discussion 75

9.1 Orifice Plate Calibration 75

9.2 Directionality of Test Specimens 76

9.3 Normal Shock Tube Tests 80

9.4 Analysis of the Effects of Plate Arrangement 83

9.4.1 The Effects of Plate Arrangement on the Initial Peak Pressure Amelioration Experienced by the End Wall 84

9.4.2 The Effects of Plate Arrangement on the Impulse Amelioration Experienced by the End Wall 87

9.5 Analysis of the Effects of Plate Combination 91

9.5.1 The Effects of Combined Plate Porosity on the Initial Peak Pressure and Impulse Ameliorations Experienced by the End Wall 94

9.5.2 Analysis of the Trapped Wave Data 97

9.5.3 Analysis of the Reflected Wave Data 99

9.6 Analysis of Pressure Traces 100

9.8.2 End Wall Pressure Trace Analysis of Pl1&Pl2, Pl3&Pl2 and Pl4&Pl2 100

9.8.2 End Wall Pressure Trace Analysis of Pl2&Pl1, Pl2&Pl3 and Pl2&Pl4 102

9.8.2 End Wall Pressure Trace Analysis of the Remaining Plate Combinations 103

9.7 Analysis of Pressure Plots 105

9.8 Analysis of the Effects of Plate Separation Distance 107

9.8.2 The Effects of Plate Separation Distance on the Initial Peak Pressure Amelioration Experienced by the End Wall 109

9.8.2 The Effects of Plate Separation Distance on the Impulse Amelioration Experienced by the End Wall 111

9.9 Analysis of the Effects of Incident Mach number....114

9.10 Wave Diagrams....118

9.11 Schlieren Photographs....122

10 Conclusion....127

11 Recommendations for Future Studies....130

12 References....131

Appendices

Appendix A: Transducer Calibration Constants

Appendix B: Shock Tube Mach number and Diaphragm Calibration

Appendix C: Examples of Pressure Plots for all Plate Combinations Tested

Appendix D: Schlieren Photographs

List of Figures

Figure 1: The Time History of an Ideal Shock Wave As Experienced by an Observer.....6

Figure 2: Time History of an Ideal Blast Wave [Source Baker (1973)].....7

Figure 3: Schematic Diagrams of Spherical and Cylindrical Explosions [Source: Glass (1974)] 9

Figure 4: A Normal Shock Wave Moving With a Constant Velocity 13

Figure 5: Transformation of a Normal Shock Wave.....13

Figure 6: Reflection of a Shock Wave off the End Wall of a Finite Shock Tube.....14

Figure 7: Transformation of a Reflected Shock Wave.....15

Figure 8: Shock Wave Interaction with a Wedge Profile [Skews and Broido (1992)] 18

Figure 9: The Arrangement of Wedges Considered by Skews and Broido (1992).....18

Figure 10: Arrangements That Were Tested by Skews et al. (1995) 19

Figure 11: Results from the Schlieren Photographs Taken of the Physical Tests and the Numerical Analysis Using the Euler Code [Skews et al (1998)] 20

Figure 12: Optimum Blast Arrangement Suggested by Skews et al (1998) 21

Figure 13: Grids Used by Dosanjh (1956) 22

Figure 14: Perforated Plate Specimens Used by Britan et al (2004).....24

Figure 15: The Relationship of Attenuation and x/D_h [Britan et al (2004)] 26

Figure 16: End wall Pressure Traces for Porous Barriers of $\varepsilon = 0.65$ (a) and $\varepsilon = 0.14$ (b), M=1.48 and Δ=589 mm [Britan et al (2006)].....29

Figure 17: Amplitudes of the First Pressure Jump Registered on the End Wall Versus Δ/D_h - Multi-Hole Plate, l=2mm, D_h =4mm, ε=0.4, M=1.48 [Britan et al (2006)] 29

Figure 18: The Amplitude of the First Pressure Jump (B') Versus Porosity, ε - Δ = 100 mm [Britan et al (2006)] **30**

Figure 19: Schematic Description of a Shelter Equipped with Attenuator [Britan et al (2006)] **30**

Figure 20: Photographs of the Calibration Duct **33**

Figure 21: Schematic Representation of the Calibration Duct **34**

Figure 22: Picture of the Brass Orifice Plate **35**

Figure 23: Schematic Representation of a Simple Shock Tube Assembly **36**

Figure 24: Pressure Profile along Shock Tube Before Diaphragm Is Ruptured **37**

Figure 25: Pressure Profile along Shock Tube after Diaphragm Is Ruptured **37**

Figure 26: Schematic Diagram of the 'Seitz' Shock Tube **38**

Figure 27: Cross Section of the Compression Chamber [Whitehouse (2003)] **39**

Figure 28: Photographs of the Driver Section of the Shock Tube **40**

Figure 29: Photograph of the Expansion Chamber and the Test Section **41**

Figure 30: Photograph of the Test Section: A) With Test Specimens and B) Without Test Specimens **42**

Figure 31: Location of Pressure Transducers on the End Wall of the Shock Tube **43**

Figure 32: Photograph of the Control Console **44**

Figure 33: The Schlieren Optical System Used in the Study **47**

Figure 34: Cross Section of the Tapered Hole Geometry **49**

Figure 35: Photograph of the Metal Test Specimens **50**

Figure 36: Exploded View of the Test Specimen Mounting System **51**

Figure 37: Photographs of the Assembled Test Specimen Mounting System **53**

Figure 38: Photographs of the Modified Aluminium Test Section Door.....55

Figure 39: Location of the Test Section Pressure Transducers.....56

Figure 40: Unfiltered Pressure Traces for Pl1Fr&Pl3Fr - M_{set} = 1.42, P_o = 0.83 bar.....68

Figure 41: Filtered Pressure Traces for Pl1Fr&Pl3Fr - M_{set} = 1.42, P_o = 0.83 bar.....68

Figure 42: Orifice Plate Calibration Curve 75

Figure 43: Pressure Differential Results for Plate 1.....76

Figure 44: Pressure Differential Results for Plate 2.....77

Figure 45: Pressure Differential Results for Test Specimens - Air Flow Rate = 0.036 m^3/s 78

Figure 46: Pressure Differential Results for Test Specimens Arranged According to Increasing Plate Porosity - Air Flow Rate = 0.036 m^3/s 79

Figure 47: Overlay of Normal Pressure Traces with Section B of Mounting System Present and Absent In Test Section 81

Figure 48: Photograph of a Normal Shock Wave Passing Through the Test Section with Mounting Section B Present.....82

Figure 49: Overlay of End Wall Plate Arrangement Pressure Traces for Pl1&Pl2 - M_{set} =1.42 84

Figure 50: Initial Peak Pressure Amelioration Values Obtained for the Various Plate Arrangements 85

Figure 51: Initial Peak Pressure Amelioration Values Obtained for the Various Plate Combinations 86

Figure 52: Average Initial Peak Pressure Amelioration Values Obtained For Each Plate Arrangement.....86

Figure 53: Impulse Amelioration Values Obtained for the Various Plate Arrangements.....88

Figure 54: Impulse Amelioration Values Obtained for the Various Plate Combinations 89

Figure 55: Average Impulse Amelioration Obtained For Each Plate Arrangement 89

Figure 56: Initial Peak Pressure Amelioration Values Obtained for the Various Plate Combinations - Back & Back Plate Arrangement 91

Figure 57: Impulse Amelioration Values Obtained for the Various Plate Combinations - Back & Back Plate Arrangement.....92

Figure 58: The Relationship between Initial Peak Pressure Amelioration and Increasing Plate Combination Porosity 95

Figure 59: The Relationship between End Wall Impulse Amelioration and Increasing Plate Combination Porosity 96

Figure 60: Trapped Wave Impulse Values Obtained for the Various Plate Combinations - Back & Back Plate Arrangement.....97

Figure 61: Reflected Wave Impulse Values Obtained for the Various Plate Combinations - Back & Back Plate Arrangement.....99

Figure 62: End Wall Pressure Trace for Pl1&Pl2 - M_{set} = 1.42, Po = 0.83 and d = 30 mm 101

Figure 63: End Wall Pressure Trace for Pl2&Pl3 - M_{set} = 1.42, Po = 0.83 and d = 30 mm 102

Figure 64: End Wall Pressure Trace for Pl1&Pl3 - M_{set} = 1.42, Po = 0.83 and d = 30 mm 104

Figure 65: Pressure Plot for Pl1&Pl2 - M_{set} = 1.42, Po = 0.83 and d = 30 mm.....105

Figure 66: Pressure Plot for Pl4&Pl2 - M_{set} = 1.42, Po = 0.83 and d = 30 mm.....106

Figure 67: Overlay of End Wall Plate Separation Distance Pressure Traces for Pl4&Pl2 - M_{set} =1.42, Back & Back Plate Arrangement 108

Figure 68: Initial Peak Pressure Amelioration Results Obtained for the Various Plate Separation Distances.....109

Figure 69: Initial Peak Pressure Amelioration Results Obtained for the Various Plate Combinations 110

Figure 70: Average Initial Peak Pressure Amelioration Vs Plate Separation Distance 111

Figure 71: Initial Peak Pressure Amelioration Results Obtained for the Various Plate Separation Distances 112

Figure 72: Impulse Amelioration Results Obtained for the Various Plate Combinations 113

Figure 73: Average Impulse Amelioration Vs Plate Separation Distance 113

Figure 74: Overlay of End Wall Pressure Traces for Pl4&Pl3 Obtained for Three Different Incident Mach numbers 115

Figure 75: End Wall Initial Peak Pressure Vs Incident Mach number 116

Figure 76: End Wall Impulse Vs Incident Mach number 116

Figure 77: End Wall Impulse Amelioration Vs Incident Mach number 117

Figure 78: Wave Diagram Illustrating the Wave Processes that Occur 118

Figure 79: Pressure Plot for Pl3&Pl2 - M_{set} = 1.42, d=30mm, Back & Back Plate Arrangement 120

Figure 80: Approximate Incomplete Wave Diagram for Pl3&Pl2 - M_{set} = 1.42, d=30mm, Back & Back Plate Arrangement 120

Figure 81: Schlieren Photographs of Pl2&Pl4 at Time Delays of A) t = 1500 μs, B) t = 1550 μs, C) t = 1650 μs, D) t = 1700 μs, E) t = 1750 μs and F) t = 1800 μs 123

Figure 82: Schlieren Photograph of Pl2&Pl4 at a Time Delay of t = 1500 μs 124

Figure 83: Schlieren Photograph of Pl2&Pl4 at a Time Delay of t = 1550 μs 125

Figure 84: Schlieren Photograph of Pl2&Pl4 at a Time Delay of t = 1650 μs 125

Figure 85: Schlieren Photograph of Pl2&Pl4 at a Time Delay of t = 1700 μs 126

List of Tables

Table 1: Characteristics of the Porous Barriers used by Britan et al (2006) 28

Table 2: Properties of the Composite Test Specimens Used by Seeraj (2004, unpublished) 31

Table 3: Summary of the Test Specimen Geometries and Properties 50

Table 4: Plate Combination and Arrangement Matrix 54

Table 5: Orifice Plate Calibration Data Set 1 62

Table 6: Orifice Plate Calibration Data Set 2 63

Table 7: Pressure Differentials That Occurred Across Metal Test Specimens for Selected Flow Rates 64

Table 8: Extract from a Matlab Data File (*.mat) 66

Table 9: Processed Normal Test Data 70

Table 10: Normal Wave End Wall Initial Peak Pressure and Impulse Values 70

Table 11: Processed Plate Configuration Test Data 71

Table 12: Processed Plate Separation Distance Test Data 73

Table 13: Processed Mach number Test Data 74

Table 14: Summarized Pressure Differential Results for Test Specimens - Air Flow Rate = 0.036 m^3/s 78

Table 15: Comparison of Impulse Amelioration Values Obtained for Different Time Periods of Integration viz. 9 250 μs and 4 000μs. 94

Table 16: Mapping of Plate Combinations with Similar Pressure Plots 106

List of Symbols

A	Area
c	Local Speed of sound
d	Distance between test specimens
D_h	Hydraulic Diameter
ε	Porosity
F	Force
γ	Ratio of specific heats of the gas used
I	Impulse
I^*	Impulse per Unit Area
M	Mach number
P	Pressure
P_o	Atmospheric pressure
Π	Perimeter
R	Universal gas constant
ρ	Air Density
T	Temperature
t	Time
V	Velocity of Fluid

1 Introduction

A shock wave is a very sharp, thin and strong wave front produced by explosions and other phenomena that involve discontinuous finite changes in the pressure, density and temperature of the medium in which it occurs. The kinetic theory of gases predicts that the thickness of a real shock is of the order of magnitude of two or three molecular free paths, approximately 4×10^{-7} cm thick. Shock waves occur in a variety of different forms and the most common forms are those found in nature. Meteor impacts, volcanic explosions, earthquakes and a crack of thunder are examples of shock wave producing phenomena. Shock waves may also be generated by man e.g. nuclear explosions, supersonic flight of an aircraft and even the firing of a gun or the lighting of a firework may produce a shock wave. These phenomena may lead to the loss of property as well as life. Scientists and engineers have been interested in the generation and transmission of blast waves since the latter part of the nineteenth century. Blast waves are a type of shock wave produced from the detonation of munitions, the firing of large caliber guns, and any type of explosion. After World War II the number of reported experimental and analytical studies of air blast phenomena markedly increased. Furthermore, the advent of the nuclear age and supersonic flight has lead to the renewed interest in shock wave research.

1.1 Importance of the Study

Blast waves have a devastating effect on life forms as well as the surrounding environment within close proximity of their origin. When an explosion occurs a blast wave is generated which propagates outwards. This blast wave reflects off any solid surfaces and can cause a larger portion of the damage during an explosion due to higher pressure. This may result in loss of life, environmental damage and damage to property if the source of the explosion is within close vicinity and the explosion is sufficiently strong.

Lavonas (2006) states that in general, most blast injuries are accidental. These incidents include firework mishaps, unintended industrial fuel and chemical explosions, unforeseen explosions in mines, buildings, large vehicles and aircraft which may occur in everyday life. The Concorde incident that occurred in July 2000 is an example of an unforeseen accident that resulted from the impact of an exploded tire fragment upon a wing fuel tank. This caused “water-hammer” shock waves in the fuel that led to a tank rupture and subsequently a catastrophic fire which destroyed the aircraft.

Strategic and intentional explosions are frequently used in war. Lavonas (2003) states that during such times, injuries arising from explosions far out number those from gunshot wounds and in many parts of

the world the reality persists of deadly non-detonated military devices e.g. land mines and hand grenades which are responsible for a significant number of civilian casualties even after hostilities cease. Furthermore, the rise in worldwide terrorism in recent years has shown that explosive devices are not only used by the military anymore. They have also become the choice destructive agent of many terrorists, primarily because the materials used to construct them are so easily accessible. The terrorist attacks on the United States of America in which three aircraft were flown into three buildings on the 11th of September 2001 and the recent London subway bombings in 2005 are examples of the magnitude of injuries and death that can result from a blast mechanism.

The idea of creating a material or barrier that attenuates the devastating effects of blast waves has long been investigated. Over the last thirty years, considerable work has been performed on the interactions of shock and blast waves with various materials. Internationally, research is still underway in order to determine effective methods to dissipate explosive energy and to contain explosive overpressure using blast-mitigating materials. The application of permeable solids, porous materials and solid geometric reflectors for the attenuation and reflection of destructive shock waves and high energy fluid flows has been studied extensively and continue to be studied. Experiments have shown that the attenuation of shock waves is possible however some tests reveal an adverse effect.

This research projects aims to investigate the interaction of shock waves with two porous plates placed in series in order to ameliorate the hazardous effects of these waves.

1.2 The Devastating Effects of Exposure to Blast Waves

Various injuries are incurred if one was exposed to an explosion in air. Mayo & Kluger (2006) states that blast injuries are traditionally divided into 4 categories: primary, secondary, tertiary, and miscellaneous injuries. A patient may suffer injuries caused by more than one of these mechanisms. Primary injuries are caused by the impact of a shock or blast wave on the body. Since air is a compressible medium, primary blast injuries mainly affect the gas containing organs of the body viz. the ear, lungs and gastrointestinal tract. This results in serious internal injuries with no external signs of trauma. Secondary injuries are caused by the direct impact of debris or shrapnel scattered by the explosion and tertiary blast injury is a feature of high-energy explosions. This type of injury occurs when individuals become projectiles, as a result of the impact with the blast wave, and strike other objects. Tertiary injuries include the displacement and amputation of body parts. Miscellaneous blast-related injuries encompass all other injuries caused by explosions. For example if an explosion resulted in a fire or the collapsing of a

building, which kills or injures people, then these injuries are miscellaneous injuries. These miscellaneous injuries may be further classified as being primary, secondary or tertiary injuries.

Glass (1974) states that it is important to note that the natural causes of blast waves result in the loss of life and damage to environment as a result mainly from secondary injuries; however blast waves generated by man from chemical and nuclear explosions are mainly responsible for primary injuries which occur over large areas.

Lavonas (2006) states that in general, only high energy explosions produce severe primary blast injury. Explosives are categorized as low-energy or high-energy. High-energy explosives e.g. ammonium nitrate and trinitrotoluene (TNT), undergo detonation. Detonation is the instantaneous transformation of the original explosive material into gases under extremely high pressure, compressing the surrounding medium, and produces a blast wave. Low order explosives e.g. gunpowder and rocket propellants, burn rapidly and undergo deflagration rather than detonation. They release energy relatively slowly compared to high-order explosives and this results in a subsonic explosion lacking the blast wave that characterizes high order explosives. These explosions are nonetheless extremely destructive and cause secondary, tertiary and miscellaneous injuries.

The occurrence of primary injuries is not a new phenomenon and has been reported as far back as the First World War. Zuckerman (1940) mentions that in the period of 1914 to 1918, men were sometimes picked up dead in the field of an explosion with blood-stained fluid trickling nose or mouth and without signs of serious external injury. Primary injuries include pulmonary barotrauma, tympanic membrane rupture, middle ear damage, eye rupture, and abdominal hemorrhage as well as tearing. The ear is the organ most susceptible to primary blast injury and tympanic membrane rupture is the first indication of blast injury.

Although all gas containing organs in the body are vulnerable to primary injuries, it is injury to the lungs that attracts most attention. Cooper (1996) states that pulmonary barotrauma or blast lung is a serious injury which is compounded by difficult diagnosis in the early stage and is the most common fatal primary injury. Blast lung is the bruising of the lungs in which blood contaminates the alveoli within the lung, reducing the quantity of oxygen carried by the blood. This makes breathing difficult as the airways within the lung fill up with blood. A sign of blast lung is Haemoptysis, the coughing up of blood. Blast lung may include systemic air embolism and the disease may then progress to an acute respiratory disorder, ARD, as a result of direct lung injury or of shock from other body injuries which can be life threatening.

1.3 Characteristics of Blast Waves

The extent and the pattern of injuries inflicted upon a victim exposed to an explosion depend on: the proximity of the victim to the explosion, whether the explosion occurs in a confined space, the medium in which the explosion occurs and the use of body armor.

When an explosion occurs a blast wave is generated and the parameter used to describe the blast intensity is overpressure. This refers to the pressure that is above atmospheric pressure, which results from the instantaneous rise of pressure across the blast wave. The proximity of the person to an explosion is an important factor in primary blast injury. The intensity of an explosion pressure wave declines with the cubed root of the distance from the explosion. A person 3 m from an explosion experiences approximately nine times more overpressure than a person 6 m away.

Another characteristic of blast waves is the injury patterns they produce are dependant on the position of the victim's body in relation to the wave and any reflective/deflecting objects in the environment. Colovos (2001) states that blast waves are reflected by solid surfaces and when a blast wave strikes a wall, it is reflected and the wave's energy is magnified. An explosion that occurs in an enclosed space (including a building, mine, bunker or a relatively lightly constructed enclosed space such as a bus) tends to have similar effects. Injuries are magnified by the effect of reflective surfaces and in such cases a person may suffer increased primary blast injuries as a result of the magnification of the wave's energy due to successive reflections. Hattingh (2000) states that medical professionals focus on the damage caused to the lungs by blast and shock waves for it is considered to be the most critical organ. The threshold overpressure for lung injury to occur is estimated to be between 120 and 185 kPa when exposed to a single short duration blast wave. In cases of multiple exposures, this threshold pressure may be lower, but have not been quantified. Studies conducted by Clemedson and Jonsson (1976) have shown that when blast waves occur inside an enclosure, the threshold pressure for damage is approximately five times lower than for free field waves having the same incident pressure. This is due to the additive effects of reflections or reverberations of the waves from walls and other surfaces which creates complex waves of longer duration and allows greater transfer of energy to the body. Explosions in confined spaces are associated with a higher incidence of primary blast injuries, with more severe injuries and with a higher mortality rate in comparison with explosions in open air. Leibovici et al (1996) investigated four suicidal bombing attacks in Israel which occurred between February 25 1996 and March 4 1996, resulting in a total of 297 casualties. Two bombing incidents occurred in the open air and the other two explosions occurred inside public buses in Jerusalem. In all four cases, the bombs used and the victim density were similar. Results show that penetrating trauma, traumatic limb amputations and the incidence of burns

were similar in both victim groups. However, the confined space casualties had a larger body surface area affected with burns. The confined space explosions resulted in 77.5 % of the victims suffering from blast injuries whereas only 32.4 % of the victims in the open air explosions were affected. The studies concluded that explosions occurring in confined spaces are associated with more dire consequences of mortality and injury severity when compared to explosions in open air.

The medium in which the explosion occurs is an important factor in determining the extent of injury one might be exposed to. Hirsh & Bazini (1969) states that water is a medium of high density and low elasticity therefore underwater blast waves travel further and faster than a wave from a similar explosion occurring in air. The positive pressure phase produced by an underwater explosion is of a higher intensity but of shorter duration than in air. Furthermore, the intensity of this wave in water decreases linearly from the source of the explosion. The positive pressure wave leads to disruption of the water surface and this phenomenon is called "spalling ". Colovos (2001) states that blast waves occurring in water have greater lethality and in such cases injuries incurred are more severe and may also affect the heart, bowels and abdominal organs.

Huller & Bazini (1970) completed the study of 32 sailors who were exposed to an underwater missile explosion which resulted in immersion blast injuries. Similar injuries due to exposure to air blast were noted in all the sailors; however 24 patients had severe abdominal injuries, which include hemorrhaging and tears in the bowel. Four sailors died following operation. The 28 sailors that survived described what they felt immediately after the explosion in their convalescent period. The most common description was that of abdominal pain.

The use of body armour may provide a false sense of security. Body armour does protect a person from shrapnel, but significant underlying blunt trauma may result from exposure to a blast wave or when a projectile is stopped by the protective armour. The advantages of body armour far outweigh this risk though. Studies at the University of the Witwatersrand have been completed to determine the exact mechanism the effect of protective clothing have on lung damage and the overpressure experienced. Hattingh (2000) investigated the interaction of shockwaves with porous textiles and states: ‘It has been found that ballistic vests, foams, copper layers and Kevlar layers amplify the incident shock wave thus increasing the risk of injury.’ Hattingh (2000) further states that when a blast wave strikes the body of someone wearing armour, the wave is reflected against the inside of the protective clothing, producing injuries far greater than if no armour was worn at all. In the case of a projectile impacting with the armour, compression waves behind the armour are caused which propagate into the human tissue. Furthermore, the deformation of the armour can produce additional compression waves which have an

enforcing effect. Therefore, a person wearing body armour cannot be presumed to have been protected from explosion-related injuries. Bugarin (2003) conducted experiments to expand the knowledge of shock amplification by different types of textiles and the geometry of impact. Results of the research state that heavier impermeable textiles such as Kevlar, the material used in the manufacture of bullet proof vests, amplify incident shock wave pressure as much as 400 %.

1.4 Blast Waves

1.4.1 The Difference between a Blast and Shock Wave

As mentioned previously, a blast wave is a type of shock wave produced from an explosive source. This section describes the differences between an ideal blast wave and an ideal shock wave.

In this study, a shock tube was used in order to generate shock waves used in experimentation. The actual passage of a shock wave results in the instantaneous rise of fluid properties viz. pressure, temperature and density. The pressure history as experienced by an observer when subjected to an ideal normal shock wave of magnitude Ps^+ would be as shown in the figure below.

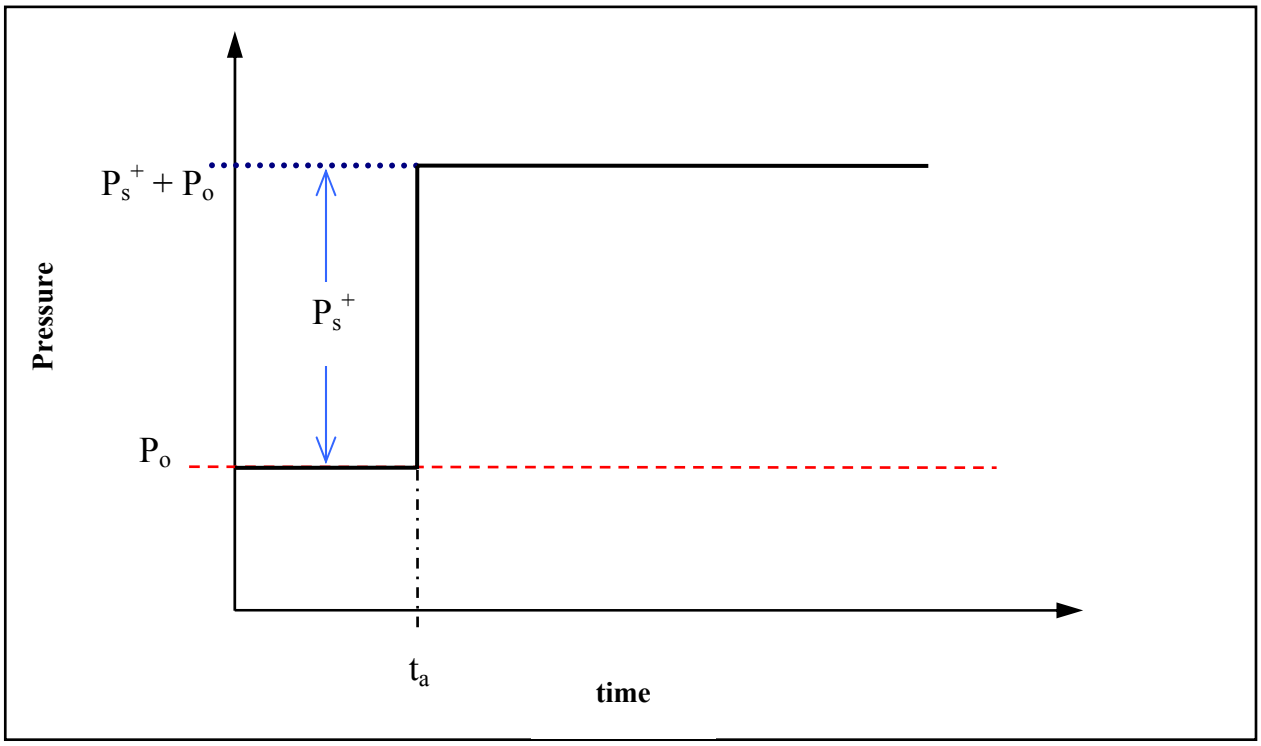


Figure 1: The Time History of an Ideal Shock Wave As Experienced by an Observer

A blast wave results in a similar instantaneous rise in pressure, P_s^+, known as the peak overpressure, but the out rush of gases from the center of the explosion then causes an expansion to below the original atmospheric pressure. Therefore the period of overpressure is followed by a period of negative pressure before returning back to ambient pressure. An ideal or classical blast wave is formed in air by an explosion source and the pressure profile for such a wave as experienced by an observer is shown in the figure below.

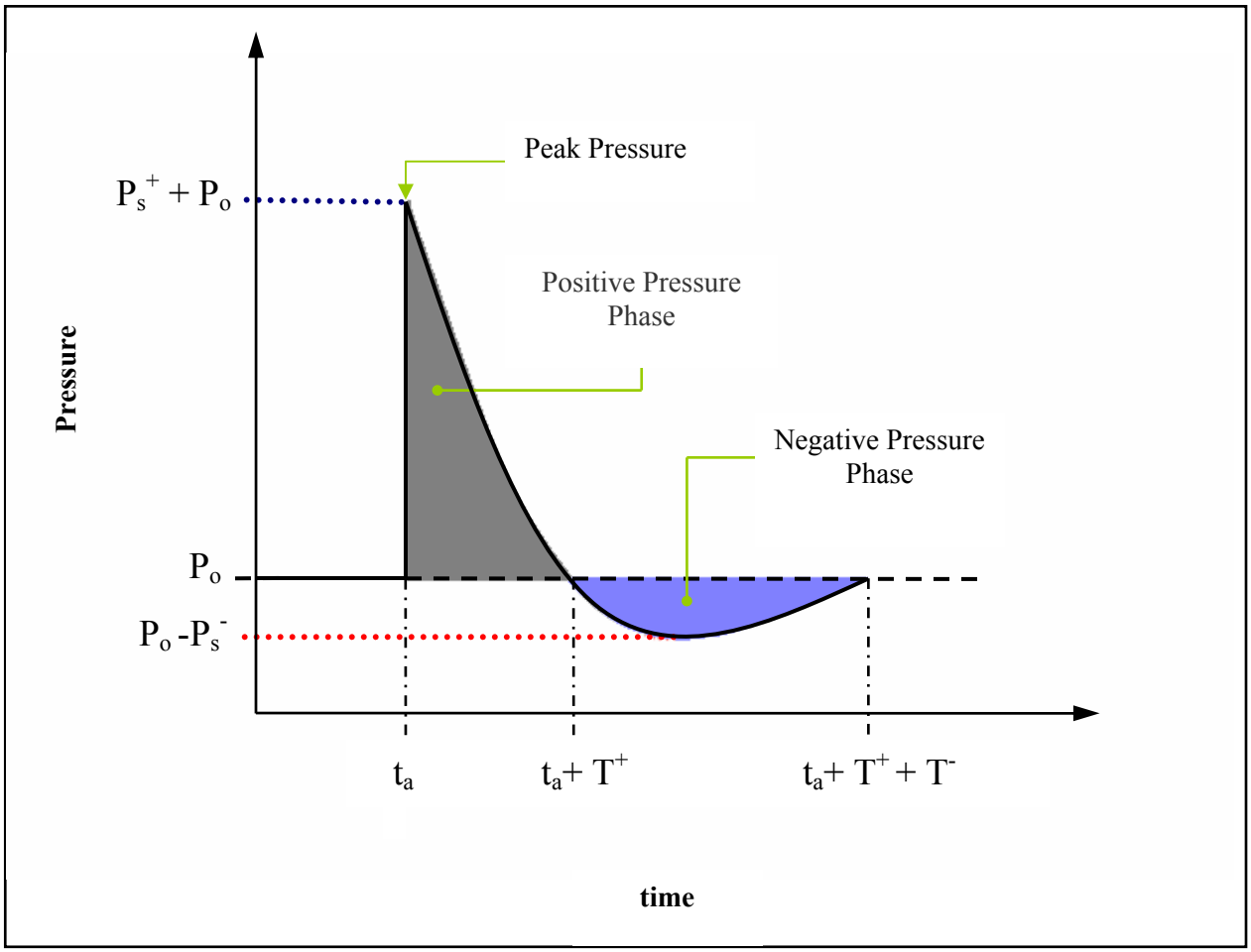


Figure 2: Time History of an Ideal Blast Wave [Source Baker (1973)]

For some time after the explosion the pressure registered is the ambient pressure, P_o. At time t_a, the arrival time, a discontinuity in pressure occurs. The pressure rises abruptly to a value of $P_s^+ + P_o$. The pressure then decays to ambient pressure in the time period, T^+, and then drops to a pressure below atmospheric of magnitude P_s^-. The pressure eventually returns to atmospheric pressure after the time period $T^+ + T^-$. P_s^+ is called the peak side-on overpressure, or merely overpressure. The portion of the time history above the ambient pressure is referred to as the positive phase and that below the ambient pressure is referred to as

the negative phase. The positive phase of the blast wave is dependant on the intensity of the explosion and is generally measured on a time scale of milliseconds.

It is important to note that throughout this study shock waves were used in testing. This is not the same as a blast wave since there is no theoretical pressure drop after the initial shock and that the reflected shock wave has to move into a region of sustained higher pressure upon reflection. Therefore, the use of shock waves for testing instead of blast waves, results in a conservative approach being adopted throughout the study. Furthermore, blast waves typically have a positive phase duration of several milliseconds up to seconds, depending on the energy release and distance from the source. For the size of a typical barrier such as those examined in this work, and also by Britan et al (2006), the pressure drop is small over the transit time of the wave through the barrier and thus the shock wave approximation is acceptable.

1.4.2 The Generation of a Spherical Blast Wave

A blast wave is generated when energy is suddenly released or deposited in a medium (gas, liquid or solid), thereby causing an explosion. In the case of a spherical explosion, Glass (1974) describes the processes that occur as follows:

- Energy is added into the medium instantaneously, resulting in the heating of the medium which creates a high pressure expanding gaseous sphere that drives a blast wave into the surrounding material.
- The blast wave travels supersonically outwards from its source into the medium and abruptly raises the physical properties of the medium.
- A flow is induced behind the blast wave as it travels outwards.
- The intensity of the blast wave decays to a weak disturbance or a sound wave as it engulfs ever greater volumes of the medium and is sufficiently far from the source of the explosion. The distance required by the blast wave to diminish in intensity becomes progressively smaller in a gas, liquid and solid.

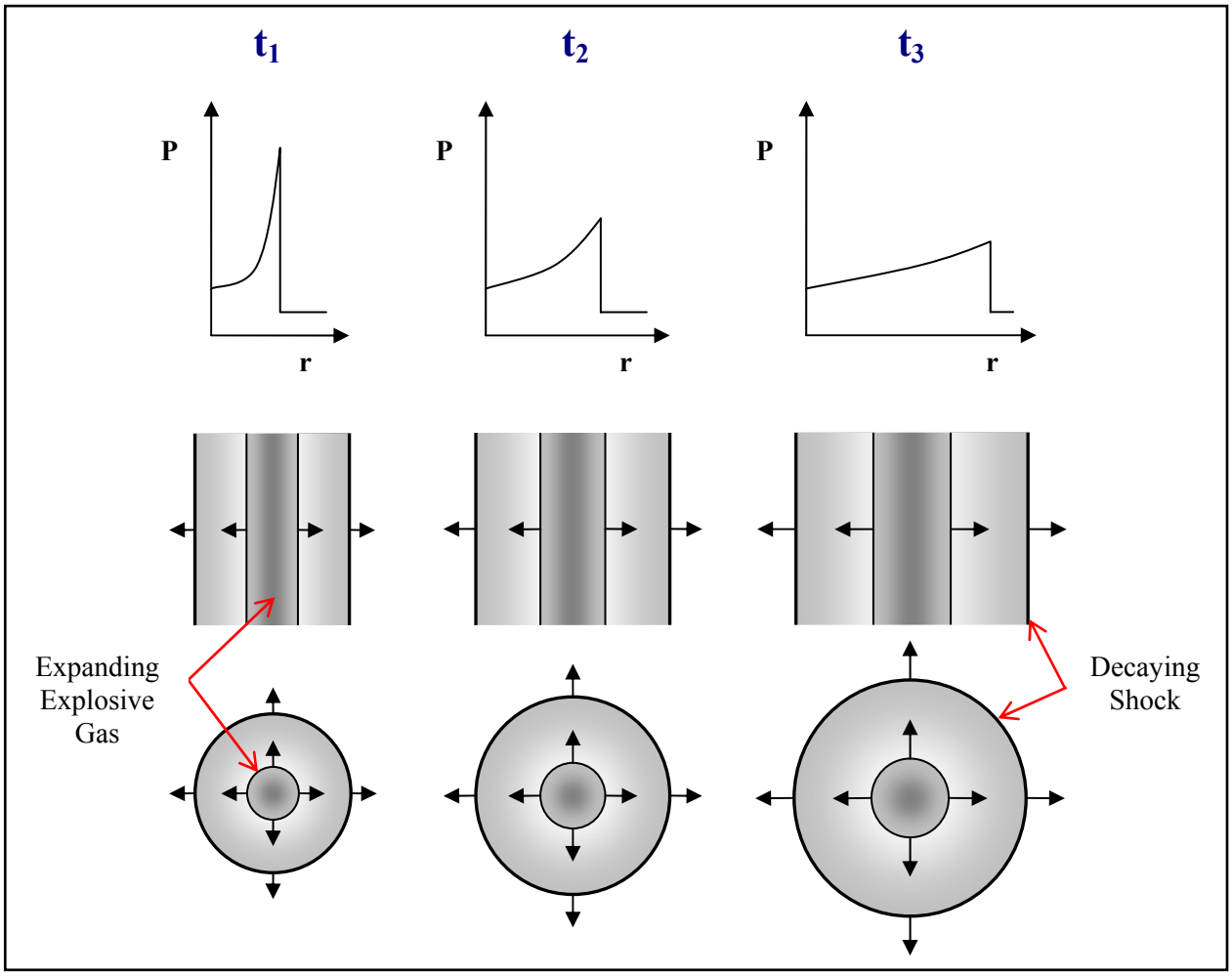


Figure 3: Schematic Diagrams of Spherical and Cylindrical Explosions [Source: Glass (1974)]

At time t_1, the exploding gas creates and drives a steep fronted blast wave with pressure, P, which decays with distance, r, away from the source of the explosion. The explosive gas achieves an oscillatory finite size at time t_2. After time t_3, the volume of air that is engulfed and heated by the shock wave grows with distance. It is in this manner that the shock wave expends its energy and its strength decays. At distances far from the source of the explosion, the shock waves decay to sound waves. [Glass (1974)]

1.4.3 Measuring the Destructive Capability of a Blast Wave

Kinney (1962) states that in order to fully describe a blast wave of the type shown in the Figure 2, three independent characteristics require to be specified viz. the blast intensity, the duration and the impulse of the wave. Besides describing the aspects of a blast wave, these characteristics may be used to quantify the extent of damage that a wave is capable of inflicting.

The initial blast intensity is generally described by specifying the peak overpressure of the blast wave. An observer or object that is subjected to this overpressure experiences an instantaneous lateral force of magnitude equal to the product of the projected area in the plane of the blast wave and the overpressure. The intensity of the blast wave may also be specified by other intensity related items such as Mach number, arrival time or particle velocity which may be used to indirectly calculate the maximum pressure experienced across the blast face.

The duration of the blast wave determines how long forces are applied which in turn determines the ability to cause damage. Since the positive phase of the blast wave produces most damage, the positive pressure duration is generally taken as a measure of the time duration of the entire wave system.

Lastly, the impulse of a blast wave is an important characteristic that is generally used to determine the damage causing ability of a blast wave as it depends on both the peak overpressure as well as the duration of the blast wave. Impulse is defined as the product of force, F, and time and for a blast wave. The impulse per unit projected area is indicated graphically as the area under the pressure time curve of the positive phase of the wave.

$$I = \int_0^{t_a + T^+} F dt \qquad \mathbf{1}$$

$$\text{Since } F = P \times A$$

$$I_{\text{(per unit area)}} = \int_0^{t_a + {}^+T} P dt \qquad \mathbf{2}$$

or

$$I^* = \int_0^{t_a + {}^+T} P dt \qquad \mathbf{3}$$

One may note that in addition to the time and peak overpressure of the blast wave, the rate of decay of the overpressure also affects the magnitude of the impulse of a blast wave.

It is important to note that throughout this study pressure trace data was used to calculate the impulse per unit area experienced by the end wall of the shock tube. Therefore, for the purpose of brevity the term impulse is adopted from here onwards to be equivalent to impulse per unit area.

1.5 Applicable Gas Dynamics

This section outlines basic gas dynamic theory, extracted from John (1969), which was used in the analysis of experimental data obtained during the study.

1.5.1 Definition of Mach number

For a compressible gas, the speed of sound in the gas is c.

$$c^2 = \gamma RT \qquad \textbf{4}$$

$$c = \sqrt{\gamma RT} \qquad \textbf{5}$$

Where:

γ = Ratio of specific heats of the gas used

R = Universal Gas Constant

T = Temperature

The Mach number, M, is used to express the speed of waves generated in a gas relative to the speed of sound ahead of the wave. It is a dimensionless parameter and is defined as the ratio of the fluid velocity, V, to the local sonic velocity.

$$M = \frac{V}{c} \qquad \textbf{6}$$

$$M = \frac{V}{\sqrt{\gamma RT}} \qquad \textbf{7}$$

Where:

c = Local speed of sound

V = Velocity of fluid

M = Mach Number

1.5.2 Normal Shock Waves

When a body travels through a compressible medium such as air at a speed less than the local speed of sound, (M < 1), disturbances propagate outwards from the body at the local speed of sound. These disturbances signal the fluid ahead of the body of its approach and the fluid adjusts to the presence of the body in a smooth manner. If the body travels at a speed greater than the local speed of sound, (M > 1), the fluid ahead of the body is unaware of its approach and there is then a discontinuous adjustment of the fluid properties between the disturbed and undisturbed flow. This discontinuity takes the form of a shock wave. A normal shock wave is a plane shock perpendicular to the flow direction.

Finite variations in pressure, density and temperature occur over a shock thickness comparable to the mean free path of the gas molecules. Standard equations are used to relate these properties across a stationary normal shock wave, as shown below.

$$M_2 = \sqrt{\left[\frac{\left(\frac{2}{\gamma-1} + M_1^{\,2}\right)}{\left(\frac{2\gamma}{\gamma-1}M_1^{\,2} - 1\right)}\right]} \qquad \textbf{8}$$

$$\frac{P_2}{P_1} = \frac{(1+\gamma M_1^{\,2})}{(1+\gamma M_2^{\,2})} \qquad \textbf{9}$$

$$\frac{T_2}{T_1} = \frac{(1+\frac{\gamma-1}{2}M_1^{\,2})}{(1+\frac{\gamma-1}{2}M_2^{\,2})} \qquad \textbf{10}$$

1.5.3 Moving Normal Shock Waves

The shock waves which are generated in shock tubes are moving shock waves and the formulae that have been derived for stationary normal shock waves may also be used to determine the properties across the moving shock. This is done by imposing a reference velocity so that the moving shock appears to be stationary as witnessed by an observer. The static properties of pressure, density and temperature are independent of the reference frame from which they are measured; however attention must be paid to those properties that depend on the velocity of the gas.

To demonstrate the principle, consider a normal shock wave moving at a constant velocity as shown in the figure below.

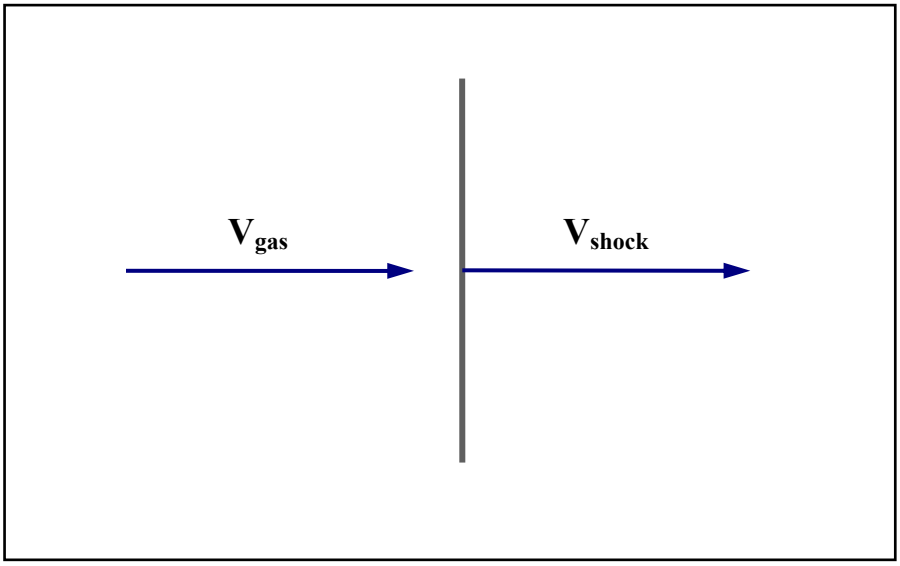


Figure 4: A Normal Shock Wave Moving With a Constant Velocity

In order to bring this shock to rest, the shock velocity is added towards the left. Thus the situation in the figure above has been transformed into a stationary shock problem as shown in the figure below.

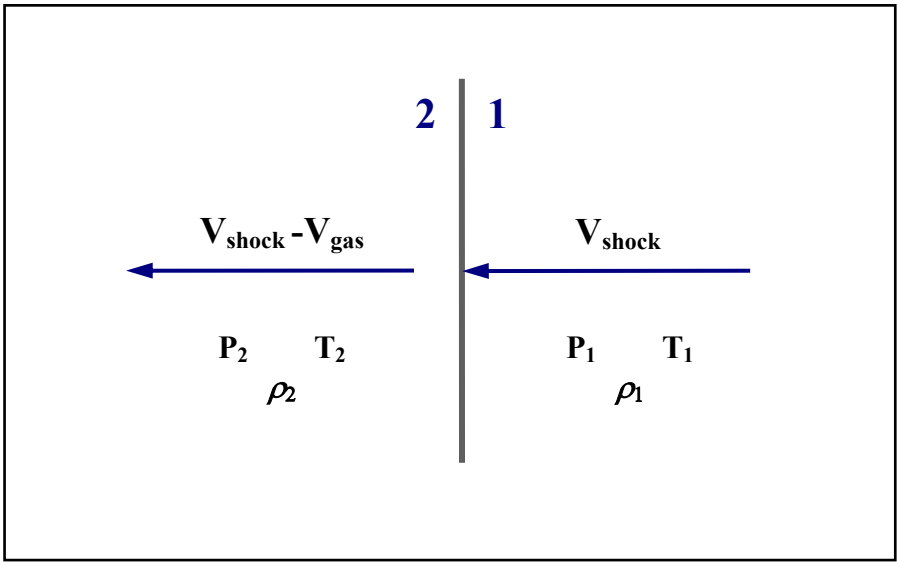


Figure 5: Transformation of a Normal Shock Wave

1.5.4 Reflected Normal Shock Waves

In this study, it was necessary to calculate the velocity of the shock wave reflected off the end wall of the shock tube. As the incident shock wave travels towards the end of a closed shock tube, the gas next to the fixed end of the tube must be at rest and the gas behind the incident shock moves to the right with a velocity less than the velocity of the shock wave, V_{gas}. When the shock wave is reflected of the end wall, the air adjacent to the wall is once again stationary and the reflected shock wave, with a velocity of $V_{ref.shock}$ travels into gas moving to the right with a velocity of V_{gas}. Upon reflection, the temperature, pressure and density of the gas ahead of the reflected shock wave have changed and are no longer at initial conditions.

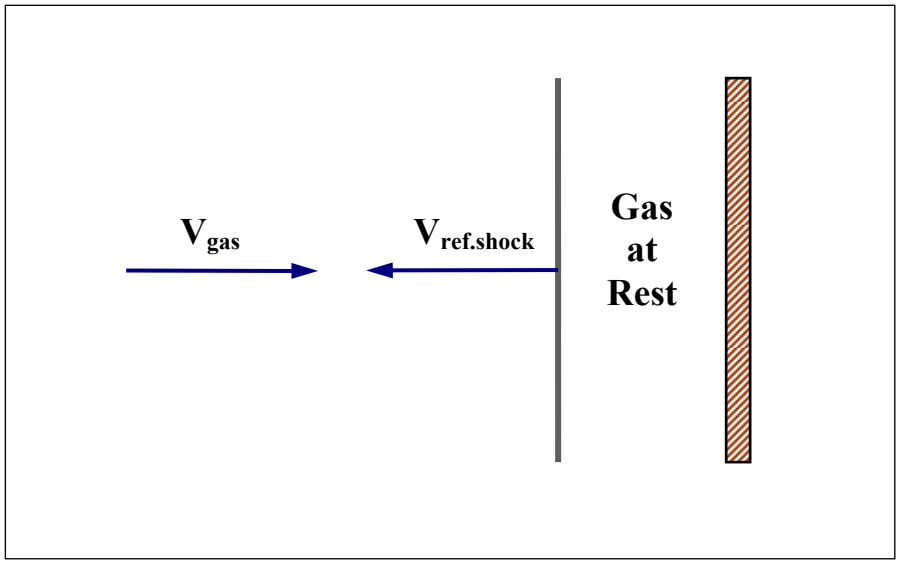


Figure 6: Reflection of a Shock Wave off the End Wall of a Finite Shock Tube

In order to solve for the reflected shock wave velocity, the physical situation is shown in Figure 7 that follows, where the reflected wave is brought to rest by imposing a reference velocity. The velocity, pressure, density and temperature of the gas behind the initial incident shock wave must first be determined. Thereafter, the calculated upstream properties of the incident shock wave together with the normal shock equations may be used in an iterative procedure to solve for the reflected shock wave's velocity and properties.

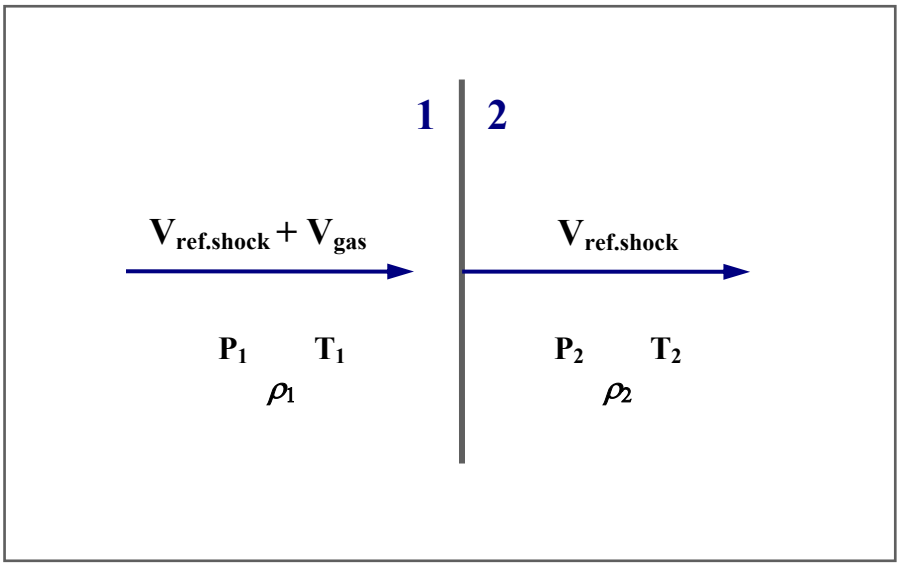


Figure 7: Transformation of a Reflected Shock Wave

1.5.5 Definition of Initial Peak Pressure Amelioration and Impulse Amelioration

The initial peak pressure amelioration experienced by the end wall of the shock tube is defined as the percentage decrease in initial pressure due to the presence of the test specimens as compared to the initial pressure experienced with no test specimens present in test section and is calculated as follows:

$$P_{Amelioration}(\%) = \frac{P_{Bare} - P_{Specimens}}{P_{Bare}} \times 100 \qquad \textbf{11}$$

Where $P_{Specimens}$ and P_{Bare} are the initial peak pressures experienced by the end wall of the shock tube with and without the presence of test specimens respectively.

The impulse amelioration experienced by the end wall of the shock tube is defined as the percentage decrease in impulse due to the presence of the test specimens as compared to the impulse experienced with no test specimens present and is calculated as follows:

$$I^*_{Amelioration}(\%) = \frac{I^*_{Bare} - I^*_{Specimens}}{I^*_{Bare}} \times 100 \qquad \textbf{12}$$

Where $I^*_{Specimens}$ and I^*_{Bare} are the values of impulse experienced on the end wall of the shock tube with and without the presence of test specimens respectively.

2 Objectives

1. Confirm that a shock wave passing through two porous barriers placed in series will ameliorate the initial peak pressure and impulse experienced downstream of the barrier arrangement.

2. Determine the effect that different test conditions have on the initial peak pressure amelioration and impulse amelioration. The effects due to the variation of following test conditions shall be analyzed:

    a. Test specimen arrangement (Plate Arrangement)
    b. Test specimen placement (Plate Combination)
    c. Separation distance between test specimens
    d. Mach number variation

3. Identify the wave processes that occur during the interaction of the shock wave with the porous barriers.

3 Literature Review

The applications of porous media and quenching liquids for the attenuation of the intensity and impulse of potentially destructive shock waves have been studied extensively since the 1940's. This is a fundamental topic in shock dynamics research as it is used in various engineering and industrial applications such as hazardous explosions in mine shafts, industrial pipe works, exhaust systems of internal combustion engines, air conditioning ducts and in design of bomb shelters. The detailed physical processes and flow mechanisms produced as a result of shock waves interacting with blast mitigating materials are extremely complex and are not yet complete. Continuing research aims to develop an understanding as well as develop more precise analytical and numerical models of these complex interaction processes. Furthermore there are continuing efforts to find more effective blast ameliorating materials and systems.

Examples of porous media that have been used in research include: energy absorbing or dissipating foams, liquids in elastic shells, textiles, cellular materials, synthetic plugs, screens, honeycombs structures, perforated plates, wire gauze, orifice plates and granular filters. More specifically, the research involving the interaction of shock waves with perforated plates and shock wave trapping are most pertinent to this study and are discussed in detailed in the following subsections.

3.1 Investigations of the Trapping of Shock Waves

Skews and Broido (1992) investigated the idea of shock wave trapping to ameliorate the hazardous effects of blast waves entering buildings or other structures through air conditioning ducts or similar apertures. An arrangement of triangular barriers which had greater resistance to flow and shock passage in one direction than the other was considered in the study and it was argued that if such arrangements were placed back to back, it would be possible to attenuate the incident shock wave. An incident shock wave could enter the space between the two arrangements without great resistance, producing a weak reflected wave, but would encounter greater resistance in emerging in either direction and undergo a series of reflections in the space between the barriers, effectively trapping the greater part of the incident wave.

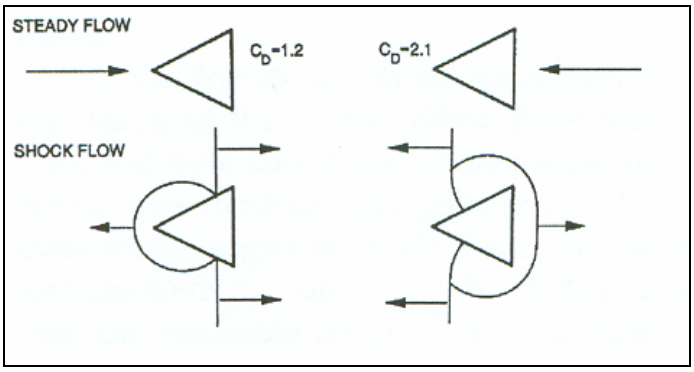


Figure 8: Shock Wave Interaction with a Wedge Profile [Skews and Broido (1992)]

A triangular body or wedge was selected as the barrier geometry since the reflected shock strength is less for such a body with its apex facing the oncoming flow than when the base faces the flow. By arranging these wedge profiles, as shown Figure 9 below, the resulting geometry has a greater resistance to shock passage in one direction than the other.

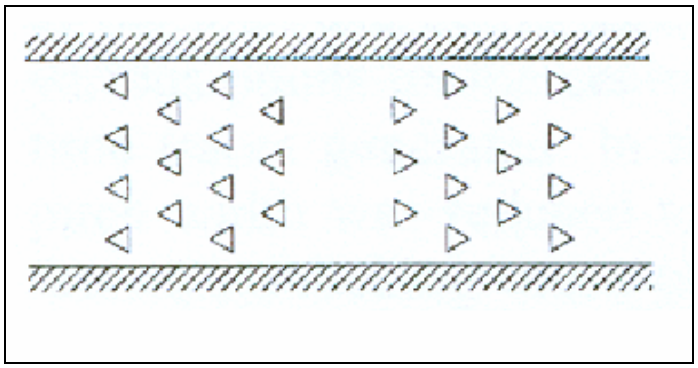


Figure 9: The Arrangement of Wedges Considered by Skews and Broido (1992)

Shock tube tests were performed using this wedge arrangement which had a 50 % blockage and used equilateral triangles as elements of each barrier. Results revealed that for an incident shock Mach number of 1.27, the pressure rise across both the reflected and transmitted waves was 50 % less than that across the incident wave. The incident shock wave entered the space between the two arrangements from the left producing a weak reflected wave. However it encountered greater resistance in emerging in either direction. The shock wave was then reflected in the space between the barriers with little of the wave being transmitted upon each encounter with the barriers on either side. Schlieren photographs revealed that the vortices shed behind each row of elements resulted in strong shock attenuation.

Skews et al. (1998) continued the investigation into the effectiveness of trapping shock waves in a duct in order to enhance attenuation, by means of placing an opposing wedge arrangement in the duct. In this

study, a variety of wedge geometries were analyzed using both numerical and experimental methods in order to determine the effect of geometrical influences on the effectiveness of trapping the incident shock wave.

Previous studies by Bird (1958) showed that for a shock wave moving into a converging channel, the wave energy transmittance decreases with an increasing incidence angle of the shock front. Therefore the strength of the reflected wave for a triangular element arrangement as shown in Figure 8 would be expected to be reduced as the leading edge angle of the triangular elements is reduced. A low change in wave strength would be expected for waves propagating from the opposite direction. Therefore, the effect of wedge angle was outlined as an important geometrical factor to be investigated. Other geometric factors that were also investigated included the degree of duct blockage i.e. the base size of elements, array spacing which influences the vortices shed and the effects of staggering the elements.

A two-dimensional finite element Euler equation solver was used to perform simulations on five wedge arrangements with differing geometric properties to obtain an understanding of the influences these factors had on the trapping of the incident shock wave. Simulations were performed for two different shock wave Mach numbers (M = 1.5 and M = 3) and pressure traces were recorded in order to compare the reflected and transmitted shocks with the incident shock. Shock tube tests were then performed on a physical wedge set with a 10˚ incident angle during which schlieren photographs and pressure traces were taken. This data was then used to verify the results of the numerical simulations. The five wedge arrangements used in the numerical analysis are listed in the figure below together with the arrangement used in the physical shock tube tests.

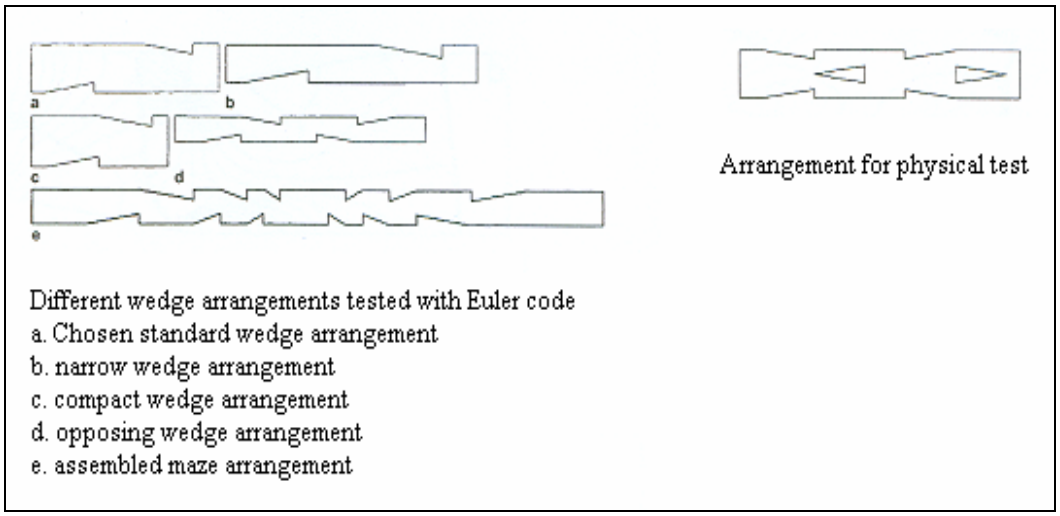


Figure 10: Arrangements That Were Tested by Skews et al. (1995)

The experimental data and schlieren photographs obtained from the shock tube tests were found to correlate fairly well with the results from the numerical simulations. Results of the study indicated that increased transmission of shock strength occurs for the higher Mach number provided that formation of secondary reflected shocks across the entire width of the channel did not occur. The actual shape of the transmitted and the reflected shock waves for both Mach numbers were found to be similar, with the Mach 3 shock being more defined. The effect of increasing the angles of incidence revealed that shock wave transmission decreased and that the reflection of the shock increased for constant Incident Mach Numbers, as expected from the research of Bird (1958). Increases in the duct blockage were found to reduce the amount of transmitted outgoing and ingoing shock significantly. A narrower channel was created when the base width dimensions of the wedges were increased and this restricts the amount of the shock wave transmitted into the maze but also caused a stronger reflected shock to be developed. It was noted that decreasing the permeability of the array of wedges too greatly would lead to significant pressure and flow losses, which is not acceptable if these barriers were to be used in ventilation ducts in certain applications such as mining. This constraint must be taken into consideration depending on the application for use.

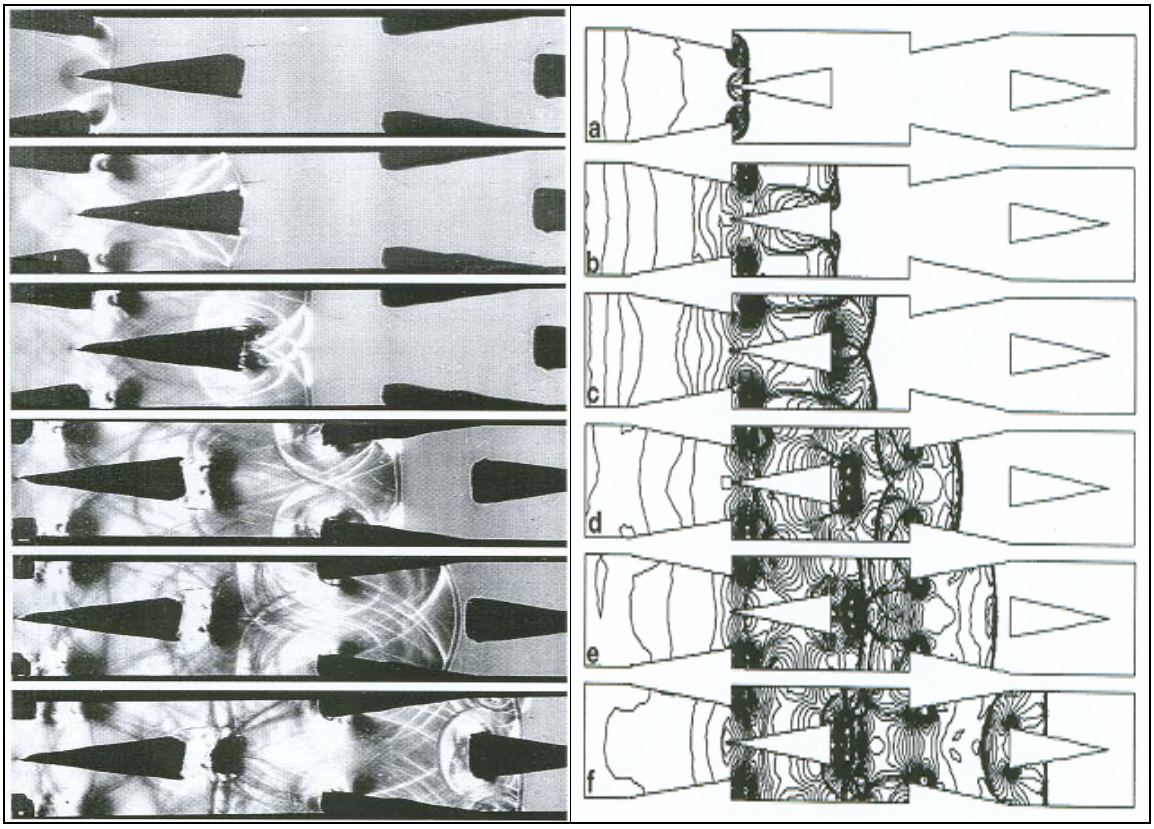


Figure 11: Results from the Schlieren Photographs Taken of the Physical Tests and the Numerical Analysis Using the Euler Code [Skews et al (1998)]

As mentioned previously, the results of the pressure contour plots from the numerical analysis showed a good correlation with that obtained from the schlieren photographs taken of the physical test. These results have been listed in the Figure 11 in order to demonstrate the complex nature of the interactions between the shock waves and the wedge arrangement. Note that the series of schlieren photographs were taken for a Mach =1.37 incident shock wave. The uneven wedge profile is due to the slight excess glue used to fasten elements to the window.

From the analysis of the results obtained, an optimum wedge arrangement design was suggested. The design allows for the incident shock wave to progress into the arrangement with increasing resistance. This was done by the gradual increase in incidence angle of the wedges. The reflected wave strength increases with the increase of the incidence angle, however this wave encounters higher resistance due to the presence of the base (which is increasing in width as one progresses through the arrangement) of the preceding wedge. This creates a weak reflected wave and most of the strength of the incident wave is contained within the structure. Furthermore, the spacing between the opposing wedges is sufficiently large in order to allow the transmitted wave to expand and strengthen into a planar wave front before it strikes the opposing wedges. As seen in the figure below, one space was left every two rows of wedges.

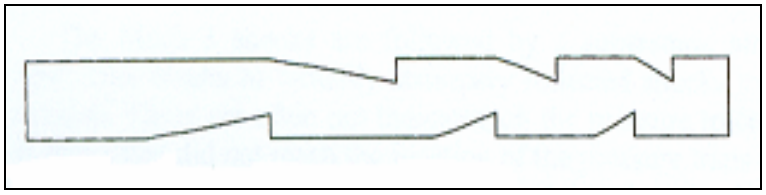


Figure 12: Optimum Blast Arrangement Suggested by Skews et al (1998)

Using the optimum arrangement, a blast barrier may be designed to meet the required reduction of shock strength for the application at hand, by adding more rows of wedges to the maze.

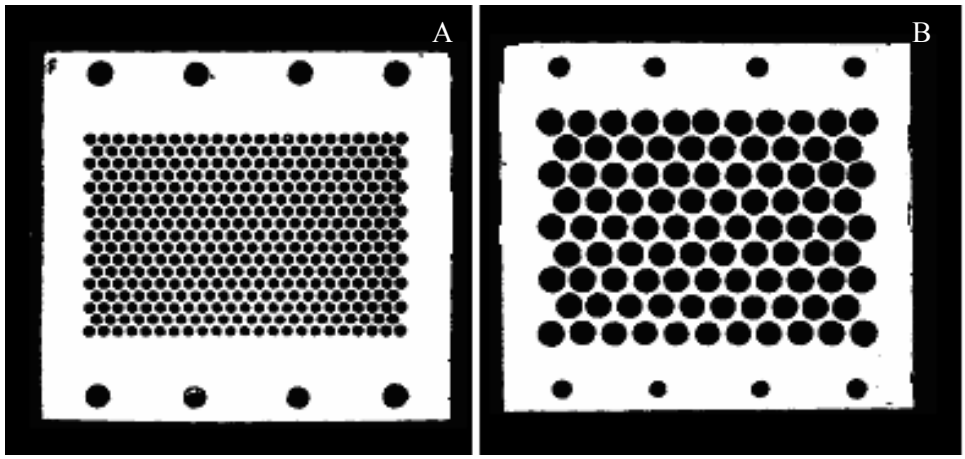
3.2 Shock Wave Interactions with Perforated Plates

The study of the interaction of shock waves with grid-like obstacles started in the 1950s and appears in many engineering applications today. It has been established that ducts and channels act as structured wave guides and when such channels/ducts lead to protected areas or objects, pressure attenuation of a shock or blast wave is desirable. Sufficient pressure amelioration may be attained by the introduction of various types of barriers (perforated plates and/or screens) inside the channel or duct. The presence of the

obstacle modifies the flow field by introducing new shock waves, regions of vortices and considerable turbulence in which the energy of the incident shock wave is dissipated.

Dosanjh (1956) was one of the early researchers to investigate the wave pattern resulting from head on collision of an incident shock wave with a grid-like obstacle and was the first to observe and explain the choking phenomenon of such obstacles. Dosanjh's study contributed significantly towards the understanding of shock-turbulence interactions for the application in aerodynamic noise attenuation. Even though his study did not focus on shock wave attenuation, it is worth while reviewing as it describes the processes that occur as the incident shock wave passes through a grid like obstacle.

Tests were conducted in a steel shock tube with a 15 cm x 10 cm cross section and a length of 8.84 m for a large range of Mach numbers. Two 6.35 mm thick grids with a solidity ratio of 25 % were used in the experiments, where the solidity is defined as the ratio of the total projected solid area of the grid and the total area of the grid exposed to the gas flow. One grid had 6.35 mm holes drilled into it and the other had 13 mm holes drilled into it, as shown in the figure below.



Diameter of Hole = 0.25 inch
Solidity Ratio = 0.25

Diameter of Hole = 0.512 inch
Solidity Ratio = 0.25

Figure 13: Grids Used by Dosanjh (1956)

By means of shadowgraph photography and hot wire techniques the wave patterns developed both upstream and downstream of the obstacle were analyzed. Measurements of the flow field from the shadowgraph pictures and hot wire anemometer were recorded along with the speeds of the incident,

transmitted and reflected shock waves. These results were then used in the calculation of the pressure drop experienced across the grids for different configurations, solidities and Mach numbers.

It was observed that when the incident shock wave interacted with the grid, a reflected wave as well as a transmitted wave was produced. Upon exiting the grid, the transmitted wave was originally distorted into smaller shocklets of similar pattern to the grid, and the drift mass flow behind the front was extremely turbulent. Due to the pressure difference behind the emerging shocklets and the dead air region a diffraction and rarefaction shock pattern was produced. In the process of fanning out, these rarefaction waves weaken the diffracted shocklets and therefore weaken the transmitted wave to a certain extent. Within twelve mesh lengths, the mass flow became essentially uniform and the distorted shocklets merge to form the transmitted wave which was normal as well as plane. In this study, a mesh length was defined as being equivalent to the diameter of the holes in the grid i.e. 6.35mm or 13mm. The transmitted shock wave was then reflected of the end wall of the shock tube and traveled upstream into turbulent contact flow where the interaction of the transmitted reflected wave with the turbulent flow resulted in some dissipation of the shock strength.

Choking of the grid, i.e. when sonic speed is reached somewhere in the grid, occurred when relatively strong incident shock waves were used. A strong incident shock wave created a strong reflected wave with a high pressure related to it. This high pressure region upstream of the grid acted as a reservoir and allowed flow to expand through the grid to a lower pressure region behind the transmitted shock wave. When the required critical pressure was reached the flow of gas, as a result of the pressure differential, reached sonic speed as it passed through the grid and the grid choked. A semi-empirical analysis was conducted in which the grid holes (circular orifices) were modeled as nozzles and this allowed the fairly accurate calculation of the incident Mach number required to choke the grid being tested. Furthermore the pressure drop coefficient calculated in such instances also exhibited the choking of the grid.

Britan et al (2004) conducted the study of shock wave interactions with perforated plates, used as blast attenuators, placed in a channel in order to analyze the flow and wave pattern that resulted downstream of the barrier. The study states that when a shock wave collides head on with a porous obstacle, two processes occur simultaneously. Firstly, a process of shock wave reflection occurs, where part of the shock wave is reflected from the obstacle and travels upstream. The other part of the incident shock wave is transmitted through the obstacle generating a non-steady flow behind it and this process is known as shock wave diffraction. The resulting wave pattern depends on the strength of the incident shock wave and the relative blockage caused by the barrier. Duct blockage or porosity, ε, is defined as the ratio of the cross section of the duct that is open to the flow, A_{op}, and the total area of the duct, A_{tot}.

The research conducted in this paper examined the unsteady flow developed downstream of perforated barriers upon head on collision with incident shock waves both numerically and experimentally. 2-D numerical simulations were conducted on a slit like barrier model only and the flow was modeled as being inviscid and non-conductive by using the Euler equations, as well as being a real flow by using the Navier-Stokes equations. This was done in order to determine if it was acceptable to model the flow as being inviscid and non-conductive as was done in previous studies. In the experimental part of the study, experiments were conducted in a shock tube in order to validate the numerical analysis that included viscous and heat losses. Since previous studies indicated that shock attenuation depends on the barrier's porosity as well as the geometry of the open spaces in the barrier, a number of experiments were further conducted on specimens with different geometries as shown in Figure 14 that follows. This was done in order to determine the effects the geometry had on the developed flow. The shock tube used in the physical experiments had a 32mm x 32 mm cross section and tests were conducted for two different incident Mach numbers viz. M = 1.43 and M = 1.58. Three pressure transducers were located along the length of the shock tube in order to record the pressure history at the different distances downstream of the barrier. Results from the numerical models (Euler and Navier-Stokes) that were developed for the slit-like barrier were compared to the actual pressure traces recorded in the physical experiments. These slit-like barrier models were then extended and applied in the comparison of barriers with different geometries. Particular attention was paid to the distance effect, the time effect and the effect that the geometrical configuration had on the transient pressure field generated downstream of the barrier.

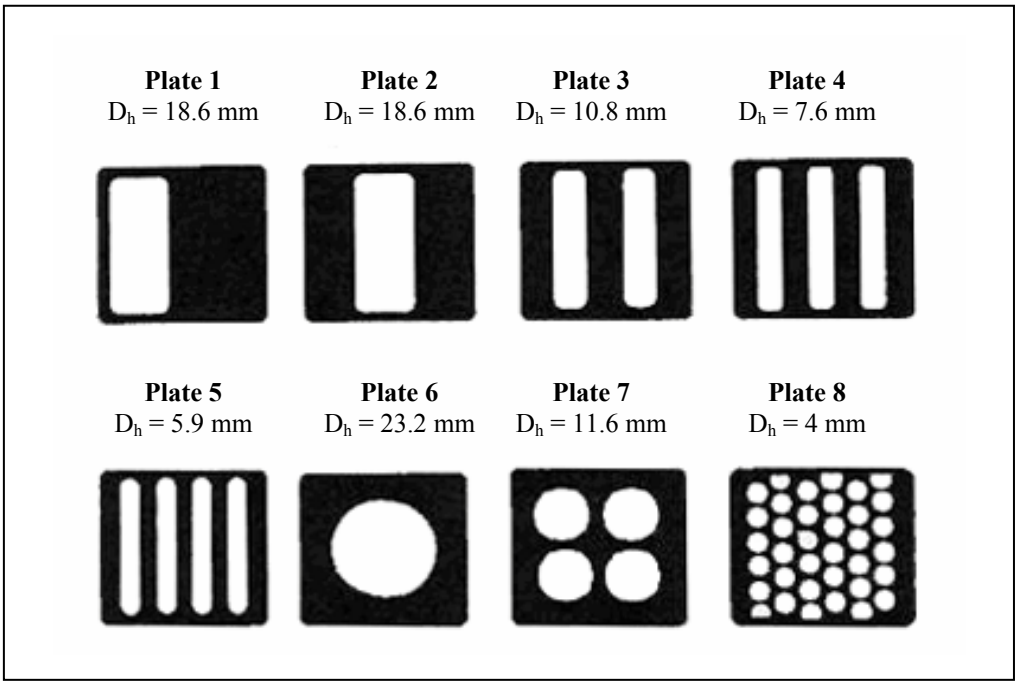


Figure 14: Perforated Plate Specimens Used by Britan et al (2004)

The perforated plates used in the study were of the same porosity ($\varepsilon = 0.4$), but of different geometries. In order to quantify the geometrical effects of the test specimens, a dimensionless parameter know as the hydraulic diameter, D_h, was used. The hydraulic diameter is defined as four times the area of the open space divided by the perimeter of the open space i.e.

$$D_h = 4S/\Pi \qquad \textbf{13}$$

Where S is the area of the open space and Π is the perimeter of the open space.

Analysis of the numerical results reveal that the flow developed closely behind the slit like barrier is initially highly unsteady and in such cases the viscous and heat transfer processes in this mixing region plays a dominant role and contributes significantly to the energy dissipation of the flow. Therefore neglecting these energy loss terms i.e. treating the gas as a perfect fluid by using the Euler equations, results in the incorrect modeling of the flow as non-physical flow behavior occurs. The pressure traces for the numerical simulation based on the Navier-Stokes equation and experimental results for the slit-like case were found to correlate throughout most of the investigated flow duration. This result confirmed the importance of including the heat transfer and viscous terms in the simulation equations.

In the experiments involving the various plates of the same porosity but differing geometrical properties, a fairly good agreement with numerical results were found even though the simulations were conducted for an incident Mach number of M = 1.435. The flow developed behind the transmitted shock wave depends mostly on the distance from the barrier which is defined by the non dimensional parameter x/ D_h, where x is the distance downstream of the barrier. It was found that the flow downstream of the barrier could be divided into two different zones. The flow immediately behind the barrier was highly unsteady and non-uniform (inhomogeneous and non-isotropic) with the maximum production of turbulent kinetic energy. In this region, supersonic jets are the dominant feature and peak attenuation decreases with increasing distance. Further downstream of this region the flow approached a steady and uniform state. The transmitted shock wave reaches a constant pressure jump across its front, which is approximately 65 % of the over-pressure behind the incident shock wave, at a distance of approximately $10 - 15\ D_h$ from the barrier. Most of the attenuation of the transmitted wave occurred in the zone where the flow is highly turbulent due to interactions of the jets and wakes produced by the barrier. For large distances downstream of the barrier, the specific shape of the barrier was found not to influence the pressure as long as the porosity was kept at a constant value. Results gathered from the experiments conducted on the eight barriers indicate that the attenuation of the incident shock wave could be expressed as a function of x/D_h

as shown in Figure 15 that follows. The parameter 'k' is defined as the shock wave attenuation coefficient.

$$k = \Delta p / \Delta p_i \qquad \textbf{14}$$

Where Δp_i is the pressure jump across the incident shock wave before reaching the barrier and Δp is the overpressure recorded after passing through the barrier. The closed points represent the experiments conducted at M = 1.46 and the points on the graph indicate the experiments conducted at M = 1.58.

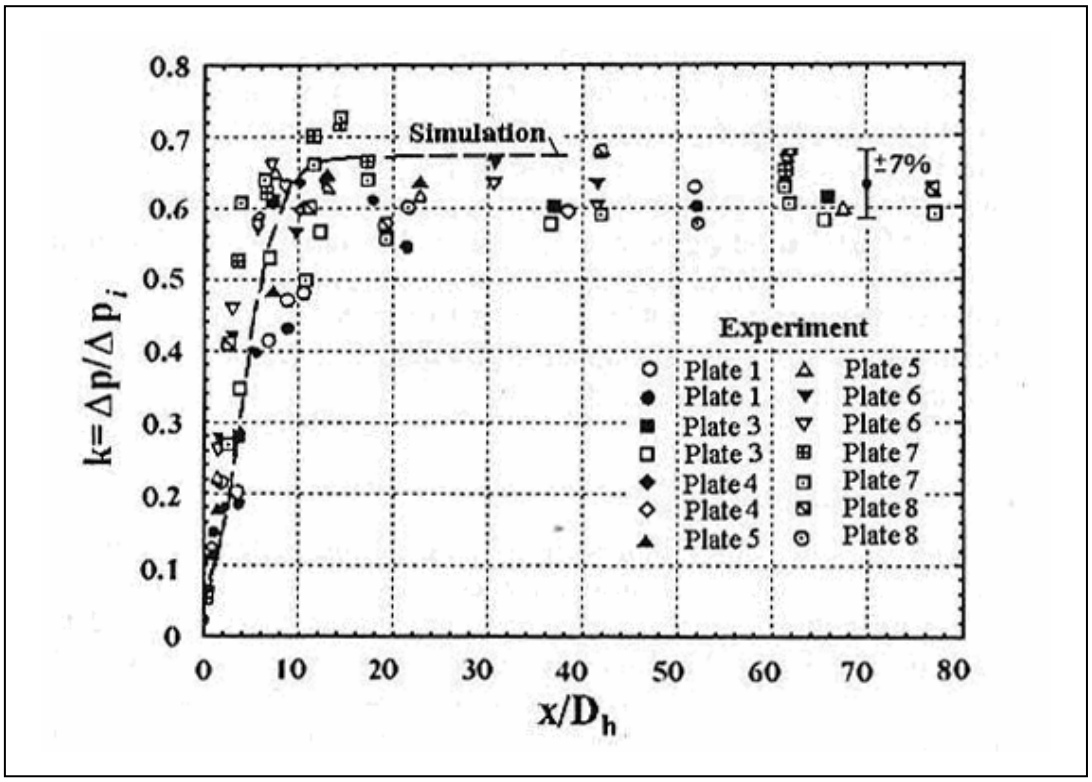


Figure 15: The Relationship of Attenuation and x/D_h [Britan et al (2004)]

It has been stated previously, that when an incident shock wave collides head-on with a porous barrier, two processes occur. A shock wave is reflected from the barrier, which travels upstream, and a transmitted shock wave propagates towards the end wall of the shock tube. When this transmitted wave reaches the end wall, it is reflected back towards the barrier, which is the beginning of a series of reflections that occur in the air gap between barrier and the end wall. Britan et al (2006) continued the analysis of a barrier installed inside a shock tube. Unlike Britan et al (2004), which analyzed the flow developed downstream of the barrier, this study investigated the full cycle of shock reflections that

resulted from the interaction of the incident shock wave with the barrier and the pressure effects experienced on the end wall of the shock tube. A 1-D inviscid flow model was developed to simulate the flow that resulted from the collision and the results from both the numerical simulations and experimentation were then used to develop an optimal design procedure for a shock wave attenuator that may ensure the safety of a shelter's ventilation system.

Previous studies note that the length of the air gap between the barrier and the end wall of the shock tube, Δ, the incident Mach number and the geometrical characteristics of the porous barrier as important parameters that may affect shock wave attenuation. In order to simplify the analysis and since Britan et al (2004) investigated the effects of barriers of the same porosity but different hydraulic diameters, D_h, this study only investigated the effects that barrier porosity, ε, had on the observed peak pressure behind the transmitted shock wave and shock wave attenuation. The main objective of the study focused on the rate of pressure increase dp/dt, acting on the end-wall of the shock tube and the barriers' porosity, since most structures are able to withstand a gradual pressure rise better than an instantaneous rise in pressure. The parameters of barrier porosity, incident Mach number and the length of the air gap were systematically varied in the study to determine the effect that each had on the pressure attenuation experience on the end wall of the shock tube.

Experiments were performed in a shock tube at four different incident shock wave Mach numbers ranging between M = 1.35 and M = 1.7. The details regarding the shock tube have been summarized previously in the review of the study conducted by Britan et al (2004). A series of grids and porous plates were used as shock wave attenuators and are described in Table 1 that follows. Pressure transducers located along the length of the shock tube and in the end wall recorded the pressure history of the wave system for each test. Numerical simulations of the flow resulting from the head-on collision of the incident shock wave with the porous barriers were performed using a 1-D inviscid model. The validity of this model was confirmed by comparing the simulations with the experimental results and numerical results based on a 2-D flow model. Results from the flow model employed were found to correlate fairly well with the results obtained through experimentation.

Table 1: Characteristics of the Porous Barriers used by Britan et al (2006)

No.	Type	Barrier thickness (mm)	Slit length (mm)	Slit width (mm)	Hole diameter (mm)	Wire diameter (mm)	Porosity ε
1	Slit-like plates						
	1 slit	2	32.5	13.00			0.40
	2 slits	2	32.5	6.50			0.40
	3 slits	2	32.5	4.32			0.40
	4 slits	2	32.5	3.25			0.40
	1 shifted slit[a]	2	32.5	13.00			0.40
2	Round hole plates						
	1 hole	2			23.20		0.40
	4 holes	2			11.60		0.40
3	Multi-orifice plate[b]						
		2			4.00		0.40
		2			6.40		0.35
		2			4.80		0.63
		2			5.00		0.25
		2			10.00		0.46
		2			5.80		0.38
		2			3.00		0.38
		2			0.90		0.14
		2			8.00		0.36
		2			3.10		0.34
4	Nets composed of wires						
		0.22				0.11	0.32
		0.08				0.04	0.31
		0.64				0.32	0.36
		0.60				0.30	0.41
		0.70				0.35	0.35
		0.64				0.32	0.42
		0.30				0.15	0.59
		0.08				0.04	0.30
		0.30				0.15	0.39
		0.13				0.06	0.40
		0.24				0.12	0.38
		0.09				0.05	0.43
		1.40				0.70	0.52
		0.33				0.17	0.45
		2.70				1.35	0.65

[a] Slit is shifted from the flow symmetry plane
[b] Holes are uniformly distributed over the plate's surface

The experimental and numerical results revealed that the attenuation of the incident shock wave was largely governed by the strength of the incident shock wave, barrier porosity and the distance between the barrier and the end wall. The pressure signature on the end wall is highly dependant on the porosity of the barrier as shown in Figure 16 that follows.

Notice that the first overpressure recorded at the end wall is almost 3.5 times greater than the pressure observed for the case with the smaller porosity

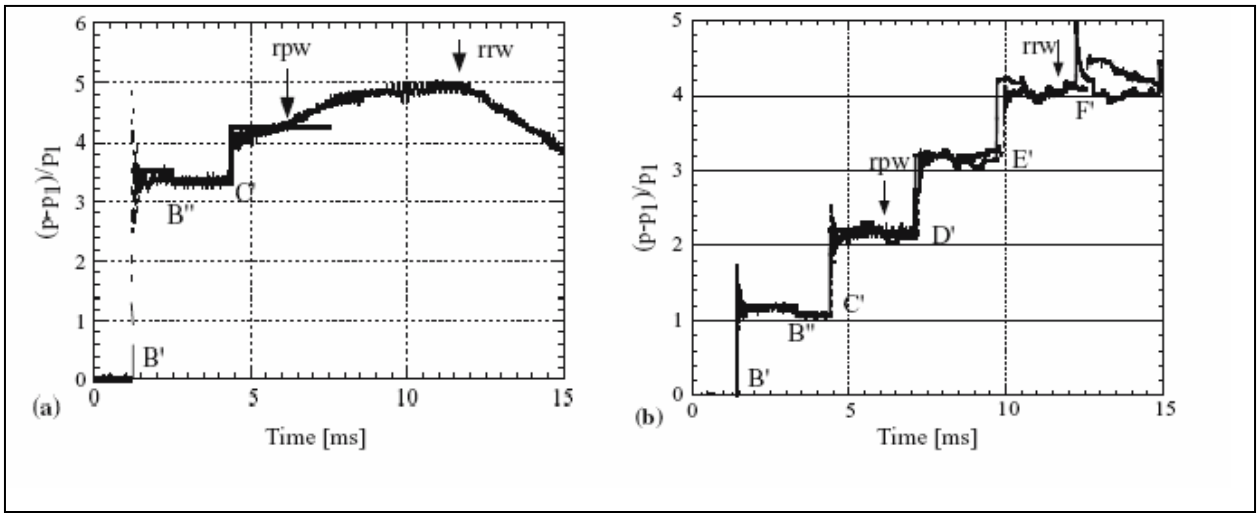


Figure 16: End wall Pressure Traces for Porous Barriers of ε = 0.65 (a) and ε = 0.14 (b), M=1.48 and Δ=589 mm [Britan et al (2006)]

Test data reveals that the amplitude of this first pressure jump experienced by the end wall increases as the porosity of the barrier increases. Furthermore, the attenuation of the transmitted shock wave did not show any dependence on the specific geometry of the barriers tested, but rather on their porosities. It was also found that the amplitude of the pressure jump decreased as the incident Mach number decreased and that this pressure amplitude reduces linearly with increasing distance between the end-wall and the barrier as shown in the diagrams that follow. Note that P_1 refers to the ambient pressure and that P_5 refers to the value obtained when the incidents shock wave reflects from the tube end wall.

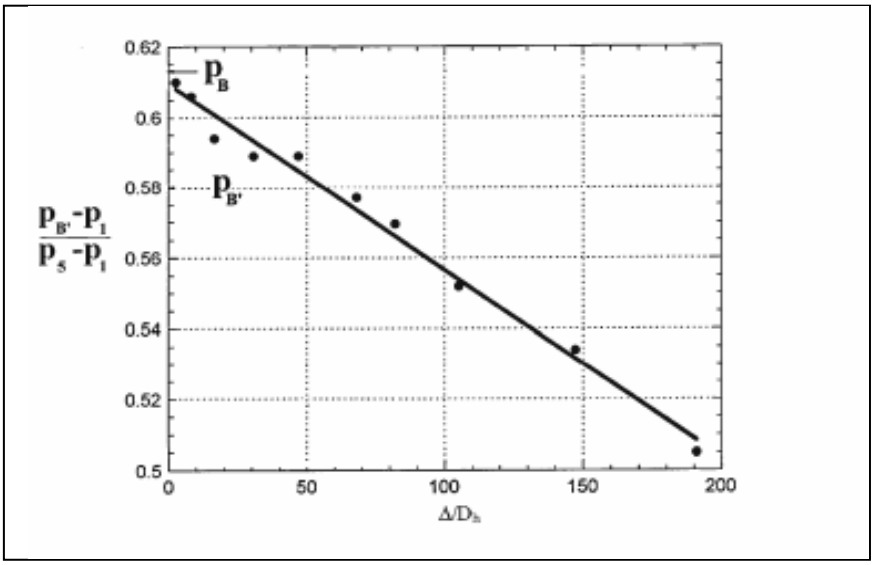


Figure 17: Amplitudes of the First Pressure Jump Registered on the End Wall Versus Δ/D_h - Multi-Hole Plate, l=2mm, D_h=4mm, ε=0.4, M=1.48 [Britan et al (2006)]

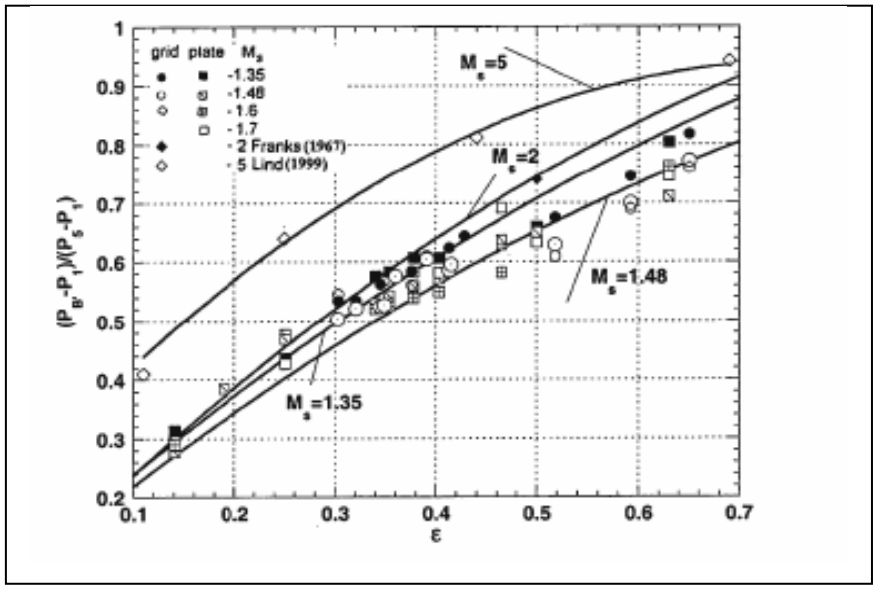


Figure 18: The Amplitude of the First Pressure Jump (B') Versus Porosity, ε - Δ = 100 mm [Britan et al (2006)]

Results of the study were used to develop an optimal attenuator design for a shelter ventilation system. Such attenuators, using porous plates, may be installed in the air ventilation systems of public or military shelters in order to protect the ventilation system from damage as well as the residents of the shelter from primary injuries. These systems are usually equipped with special blast valves which are normally kept in an open position and they close when the over-pressure (or the under-pressure) reaches a predetermined value, generally about 3 bar, with an accepted closing time of the valve of approximately 4 ms. A diagram of such a shelter is shown below.

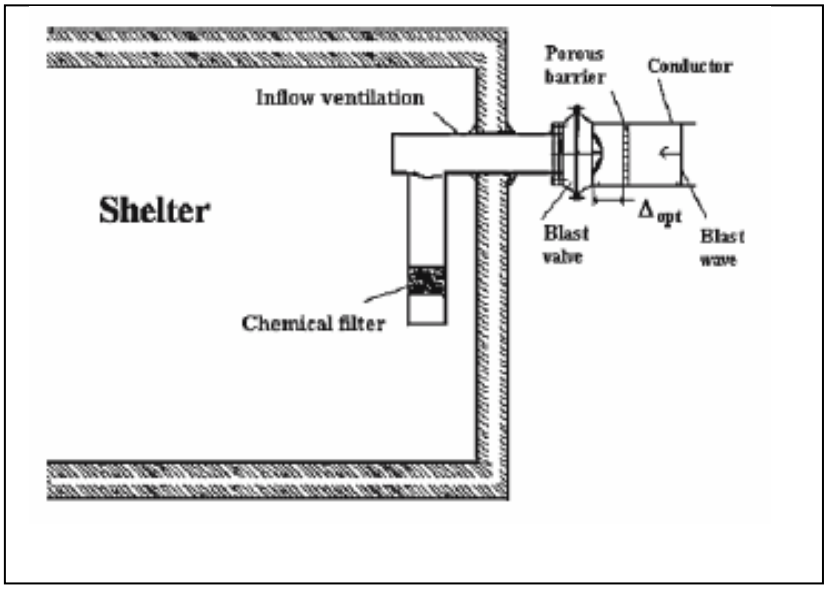


Figure 19: Schematic Description of a Shelter Equipped with Attenuator [Britan et al (2006)]

The presence of the porous barrier in the shock tube does not reduce the final pressure acting on the end wall of the shock tube, but does increase the time period over which this pressure loading acts as shown in Figure 16. Therefore instead of experiencing an instantaneous pressure rise of value P_5, as in the case with no barrier present, the end wall experiences a series of stepped increases in pressure (B' to F') over a longer period of time until the value of P_5 is reached. This makes the presence of a porous barrier in a ventilation duct a suitable shock wave attenuator, as the magnitude of the initial pressure pulse experienced on the end-wall of the ventilation system is reduced due to the timescale of the pressure loading being increased. This may result in the blast valve closing before the pressure of P_5 is reached. In general the presence of an attenuator is to ensure that a strong pressure pulse does not penetrate into the shelter before the blast valve shuts itself. An ideal shock attenuator would ensure that the minimal pressure amplitude of the first pressure jump is only experienced by the end wall of the ventilation system within the time period taken for the blast valve to close. The use of such blast ameliorating systems may also find use in bunkers, mines, industrial pipe-works and galleries.

Seeraj (2004, unpublished) in his final year project, examined the interaction of shock waves and porous barriers in order to ameliorate the hazardous effects of these waves. Test specimens with directional properties (varying resistances when tested front and back) were manufactured from mild steel and carbon fiber composite materials. The four steel test specimens had a tapered hole arrangement drilled into them. The diameter of the holes and their spacings were varied for each specimen. The four composite test specimens were manufactured to have intersecting wedge geometries. The base length and wedge spacings were varied for each test specimen. The properties of the composite specimens are listed in the table that follows. Since the metal test specimens have been used in this study, and to avoid repetition, their properties have been listed in Section 4.6.2 of this report.

Table 2: Properties of the Composite Test Specimens Used by Seeraj (2004, unpublished)

Composite No.	Base Length	Spacing	Mass	Plate Area	Square Side	Square Area	Rows	Columns	No Of Squares	Cut Out Area	Porosity
	[mm]	[mm]	[g]	[mm^2]	[mm]	[mm^2]				[mm^2]	[%]
1	5	10	37.5	13500	5	25	15	7	105	2625	19.4
2	5	7.5	45.6	13500	2.5	6.25	20	9	180	1125	8.3
3	7.5	10	55.7	13500	2.5	6.25	15	7	105	656	4.9
4	7.5	12.5	55.1	13500	5	25	12	5	60	1500	11.1

Free movement of test specimens was required during testing, as it was originally envisaged that these porous barriers would be used in the protective clothing worn by military personnel. This was achieved by mounting the specimens, a known distance from the end wall of the automated shock tube, using screws (which acted as guide rails) allowing free movement. Two pressure transducers were placed in the end wall of the shock tube in order to measure the maximum pressure experienced for each test specimen. Tests were performed for a Mach number of 1.35 and for varying distances from the end wall viz. 2.5 mm, 4.5 mm and 6.5 mm and each test specimen was tested for both its front and back facing the incident shock wave. Contact shadowgraph images were taken to track the motion of the specimen and investigate the wave processes involved.

It was found that upon colliding head-on with the barrier, a wave system similar to that described by Britan et al (2004) occurred. A shock wave is reflected upstream from the barrier and a transmitted wave propagates towards the end wall of the shock tube as the specimen moves towards the end wall of the shock tube due to the impact with the incident wave. When the transmitted shock wave reaches the end wall it is reflected back towards the moving barrier. This begins a series of multiple reflections between the moving barrier and the end wall. Upon colliding with the end wall, the test specimen comes to rest. The results of pressure amplification versus distance from the end wall varied from specimen to specimen and did not exhibit any specific trend. However what is important to note is that negative pressure amplification i.e. attenuation, was achieved. The maximum pressure amplification caused by a steel specimen was approximately 12 %, whereas the maximum caused by a composite specimen was approximately 61 %. Pressure amplification was found to occur as a result of the piston effect, caused by the movement of the test specimen towards the end wall, described by Hattingh (2000) who examined the pressure amplification of a shock wave after it has passed through a textile. In both cases the largest reduction in peak pressure was 10 %, however three out of the four steel plates produced negative values of pressure amplification as compared to one composite specimen. Therefore the metal test specimens revealed more promising results than the composite specimens.

Furthermore, the study revealed that the results obtained were closely related to the mass of the specimens. The use of the metal test specimens in protective clothing for military personnel was not viable as insufficient pressure amelioration is achieved when compared to the mass added to the protective clothing. Therefore, it was decided that such barriers would be suitable for the use in ducts or channels leading to protected areas or objects, as the mass of these barriers would not be a limiting factor.

4 Experimental Facilities

This section outlines the experimental equipment used in the study and their operation.

4.1 Calibration Duct and Related Instruments

An existing calibration duct in the University of the Witwatersrand's Mechanical Engineering Laboratory was modified and used to verify the directional properties of the test specimens. This was done by noting that the pressure drop across each test specimen differed when the side (front/back) of the specimen facing the oncoming air flow was changed.



Figure 20: Photographs of the Calibration Duct

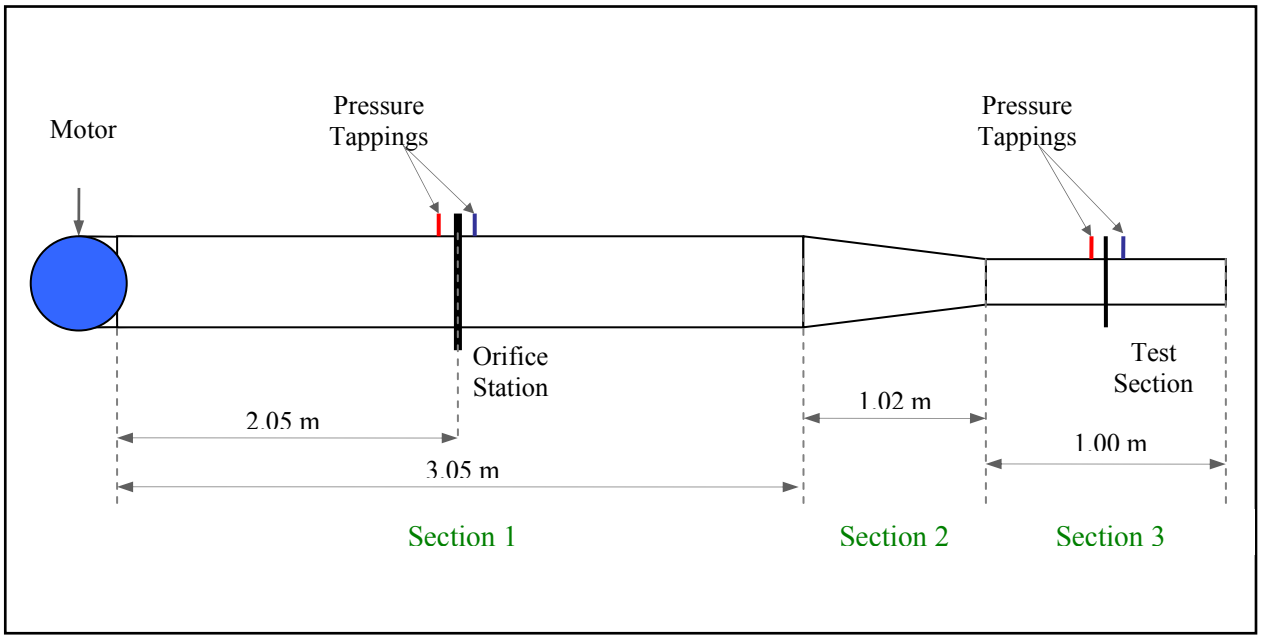


Figure 21: Schematic Representation of the Calibration Duct

The calibration duct consists of a variable speed shunt motor supplying air flow through a 5.07 m long metal duct. The variable speed motor is manufactured by Airflow Developments Ltd. and is rated at 3000 RPM with a maximum output power of 2 HP. Please refer to Picture A in Figure 20.

The duct is divided into three sections corresponding to the change in cross sectional profile. The first section of the duct was pre-existing and has a circular cross section with a diameter of 200 mm and a total length of 3.05m when measured from the motor. A port situated 0.6 m from the motor allowed for the recording of temperature readings of the airflow through the duct. An orifice mounting station is situated in this section of the duct, 2.05 m downstream of the motor, which has a latch sealing system that allows for the easy replacement of orifice plates. Pressure tapings are present on either side of the orifice station in order to determine the air flow rate through the duct. Please refer to Picture B in Figure 20.

The second and third sections of the duct were fabricated in order to accommodate the mounting of test specimens. The second section of the duct converges from the circular cross section to a 180 mm x76 mm rectangular cross section over a length of 2.02 m.

The third section then extends 1 m in length to the end of the duct, venting to atmospheric pressure. The test specimen is mounted midway of this section with pressure tapings, located on either side of the mounting station, allowing for the measurement of the pressure drop that occurs. Please refer to Picture C in Figure 20. The specimen is held in place by means of six bolts which are secured through the flanges to

ensure that an air tight seal is created. Detailed engineering drawings of the calibration duct have been provided in the DVD accompanying this report.

A brass orifice plate conforming to the British Standards Institution (BS EN ISO 5167-1: 1997 with Amendments until Feb 1999) specifications was manufactured and installed in the duct to ensure that a constant air flow rate was used in the testing of the specimens. Pleased refer to the DVD accompanying this report for the detailed engineering drawing of the orifice plate.

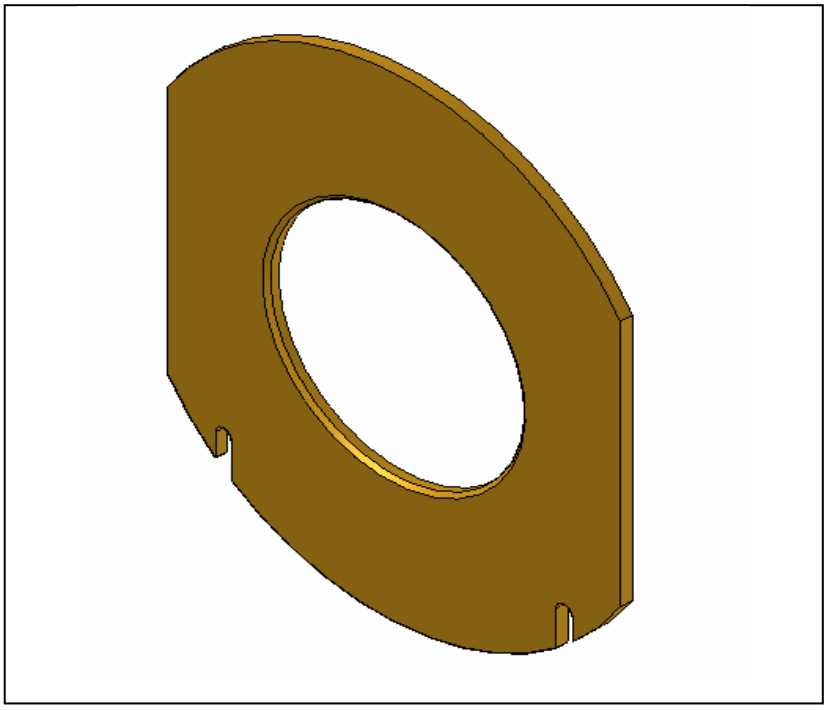


Figure 22: Picture of the Brass Orifice Plate

An AirPro FCO 520 electronic micro- manometer, with a resolution of 1 Pa, was used to measure the differential pressures that occurred at the orifice and testing stations. An Airflow LCA6000 Rotating Vane Anemometer, with a velocity resolution of 0.01 m/s, was used to verify the air flow rate exiting the duct.

4.2 The Shock Tube

4.2.1 Introduction

A shock tube is a device used to generate normal shock waves. It consists essentially of two main sections. These are the compression chamber and expansion chamber. The two sections are separated by a gas tight diaphragm mounted normal to the axis of the tube. A pressure difference is applied across this diaphragm. When this diaphragm is ruptured the high pressure gas in the compression chamber can now move into the expansion chamber. The pressure tends to equalize by means of a shock wave traveling into the expansion chamber and a rarefaction wave traveling into the compression chamber. If the tube is of constant cross-section the shock wave will not be attenuated and the pressure as well as the particle velocity will be constant over a close region behind the shock. This property of the shock tube provides controlled shock wave and gas flow creation.

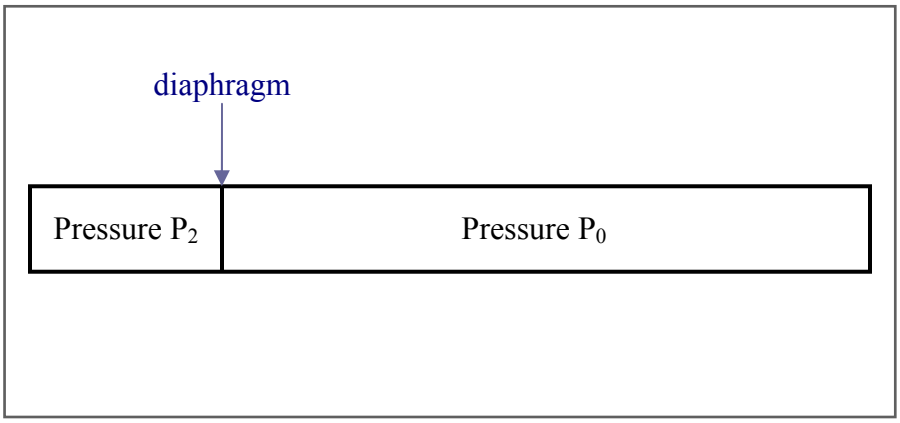


Figure 23: Schematic Representation of a Simple Shock Tube Assembly

Consider the shock tube above. The compression chamber contains a gas at pressure P_2, which is greater than the pressure, P_0, of the gas in the expansion chamber. When the diaphragm separating these two chambers is ruptured a shock wave is propagated into the expansion chamber and a rarefaction wave travels into the compression chamber. The region between the shock front and the tail of the rarefaction wave has constant velocity and pressure. The pressure distribution along the shock tube before and after the diaphragm is ruptured is shown in the figures that follow. [Wright (1961)]

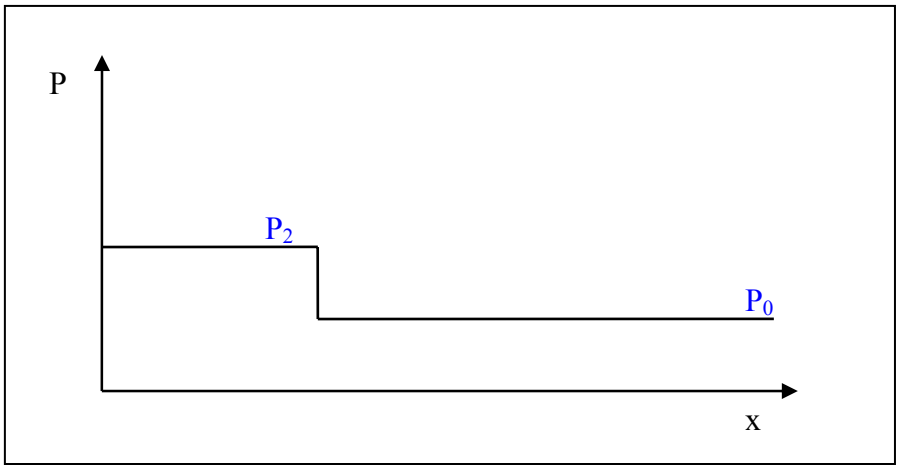


Figure 24: Pressure Profile along Shock Tube Before Diaphragm Is Ruptured

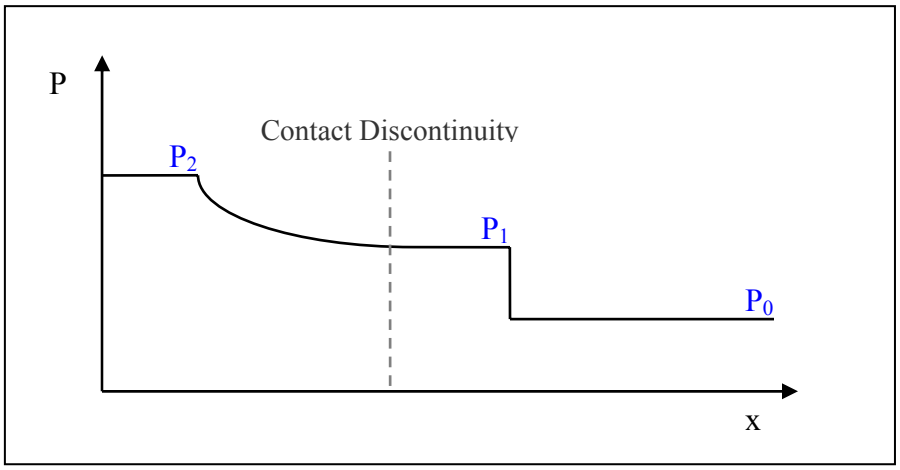


Figure 25: Pressure Profile along Shock Tube after Diaphragm Is Ruptured

A contact surface follows behind the shock wave into the driven section. The dotted line denotes the gas that was originally in the compression chamber before the diaphragm was ruptured and represents the contact surface. This surface is a temperature discontinuity separating the gas compressed by the shock from that cooled by the expansion. The gases on either side of the contact surface travel with the same velocity and have the same pressure, yet there is a density and temperature difference, which distinguishes these two regions. [Wright (1961)]

The initial shock strength and gas velocities are dependent on the pressure ratio across the diaphragm, the initial gas temperature and properties of the gas used.

4.2.2 The Michael Seitz Shock Tube Facility

The fully automated Michael Seitz shock tube in the Mechanical Engineering Laboratory was used in order to conduct tests for the study.

The shock tube consists of three chambers, viz. the compression, intermediate and expansion chambers, with the test section situated at the end of the expansion chamber as shown in Figure 26.

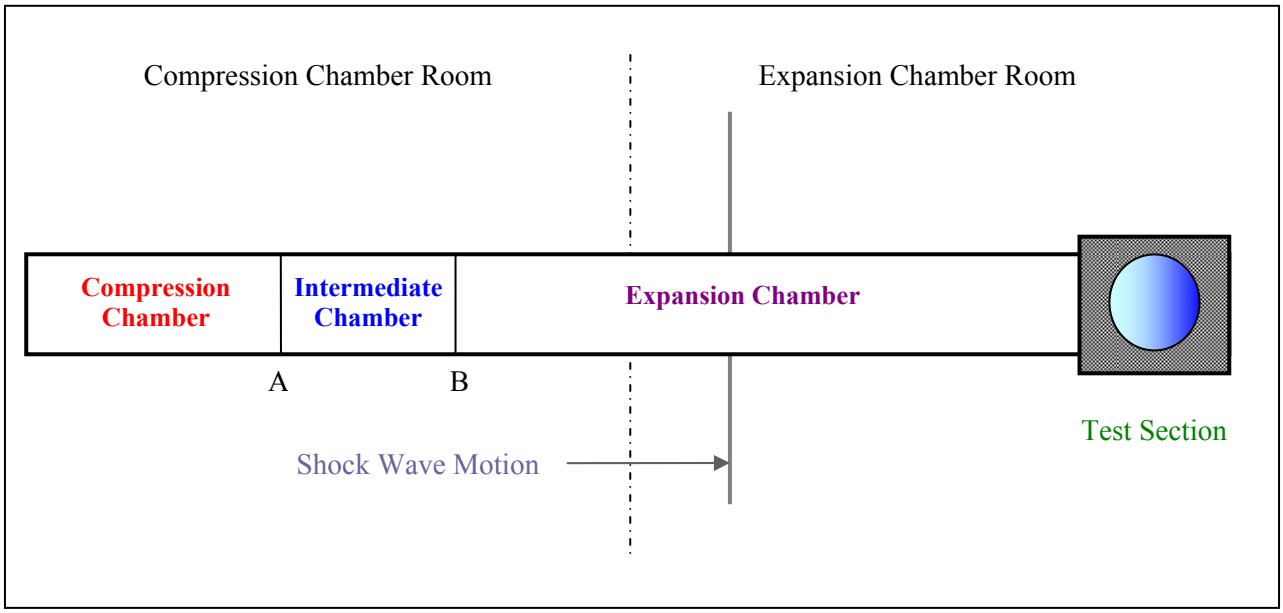


Figure 26: Schematic Diagram of the 'Seitz' Shock Tube

In Figure 26:

A – Position of First Diaphragm (Compression Chamber Diaphragm)

B – Position of Second Diaphragm (Expansion Chamber Diaphragm)

The shock tube extends into two rooms which are referred to as the Compression Chamber and Expansion Chamber rooms. The Compression Chamber room houses the compression and intermediate chambers of the tube as well as part of the expansion chamber. The rest of the expansion chamber, the test section, the control console and optical systems for flow visualization are located in the Expansion Chamber room. The shock tube is calibrated to attain Mach numbers in the range between 1.2 and 1.5 using the atmospheric pressure as the expansion chamber pressure. [Bugarin (2003)]

4.2.2.1 The Driver Section

The driver section of the shock tube consists of a compression and intermediate chamber, with a combined length of approximately 2.28 m. It has a safe operating pressure of 20 bar and is rigidly fixed to a stand which is bolted to the reinforced concrete floor. A double diaphragm arrangement is used in the driver section, which has a two-stage contraction geometry. These two reductions in area occur at the diaphragm station. The first contraction occurs in the compression chamber prior to the first diaphragm where the circular cross section of the compression chamber which has a diameter of 300 mm transforms to a square cross section of dimensions 180 mm x 180 mm. The second reduction in area occurs in the intermediate chamber and transforms the square cross section into a rectangular one, with dimensions of 180 mm x 76 mm, equivalent to the cross section of the expansion chamber. [Whitehouse (2003)]

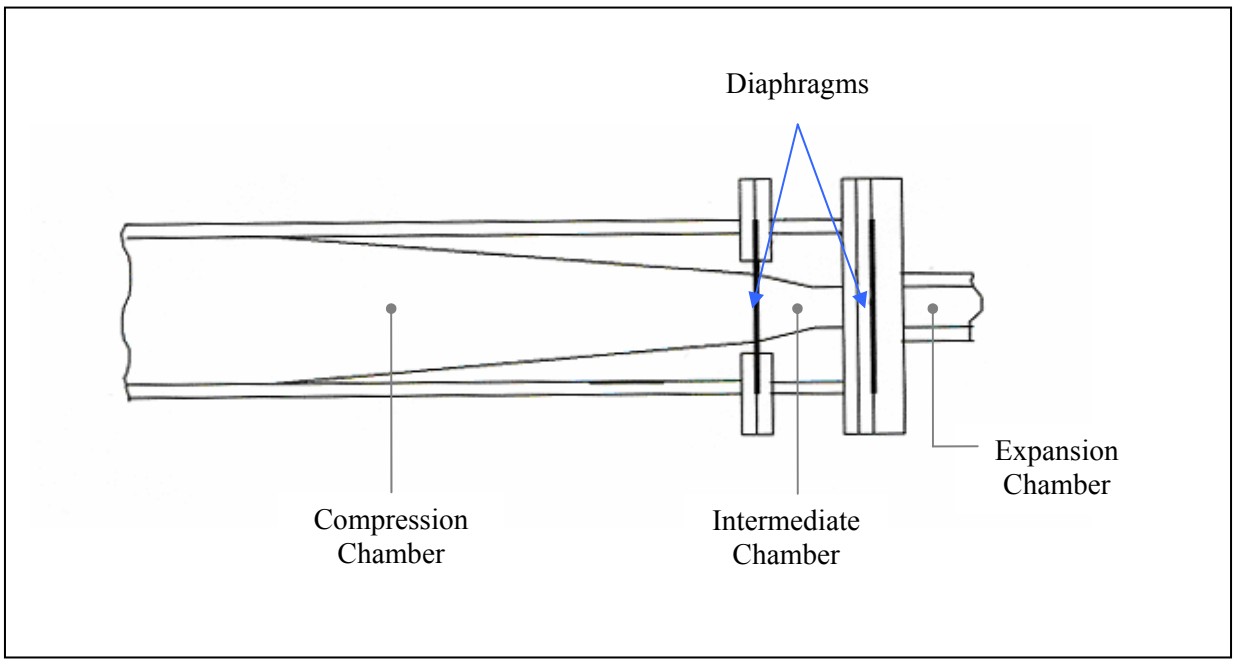


Figure 27: Cross Section of the Compression Chamber [Whitehouse (2003)]

The double diaphragm arrangement allows increased incident shock wave Mach numbers to be attained for a fixed pressure ratio and reduces the distance over which the shock becomes plane. Most importantly, the arrangement allows the diaphragms to burst at a predetermined pressure without the use of a mechanical 'pricker' device. In order to burst the diaphragms, both the intermediate and compression chambers are pressurized simultaneously; however the final pressure of the intermediate chamber is lower than that of the compression chamber. Once the pressurization of both the chambers is complete, the intermediate chamber is vented to the atmosphere which results in the first diaphragm, diaphragm A in Figure 26, bursting due to the overpressure in the compression chamber. The second diaphragm,

diaphragm B in Figure 26, then bursts spontaneously due to the pressure behind the compression wave of the first burst diaphragm. The thickness of the diaphragm plastics used depends on the required Mach number entered by the user. [Seitz (2001)]

A single hydraulic cylinder situated at the rear of the shock tube is used to close and separate all three of the chambers simultaneously. This actuator allows the diaphragms to be clamped between the flanges of the chambers and seals the chambers when the hydraulic ram is extended. When the hydraulic ram is retracted and the compression chamber is open, both the first and second diaphragm stations are opened automatically. The hydraulic actuator and pressurization of the chambers are fully automated and is controlled by the computer in the control console.

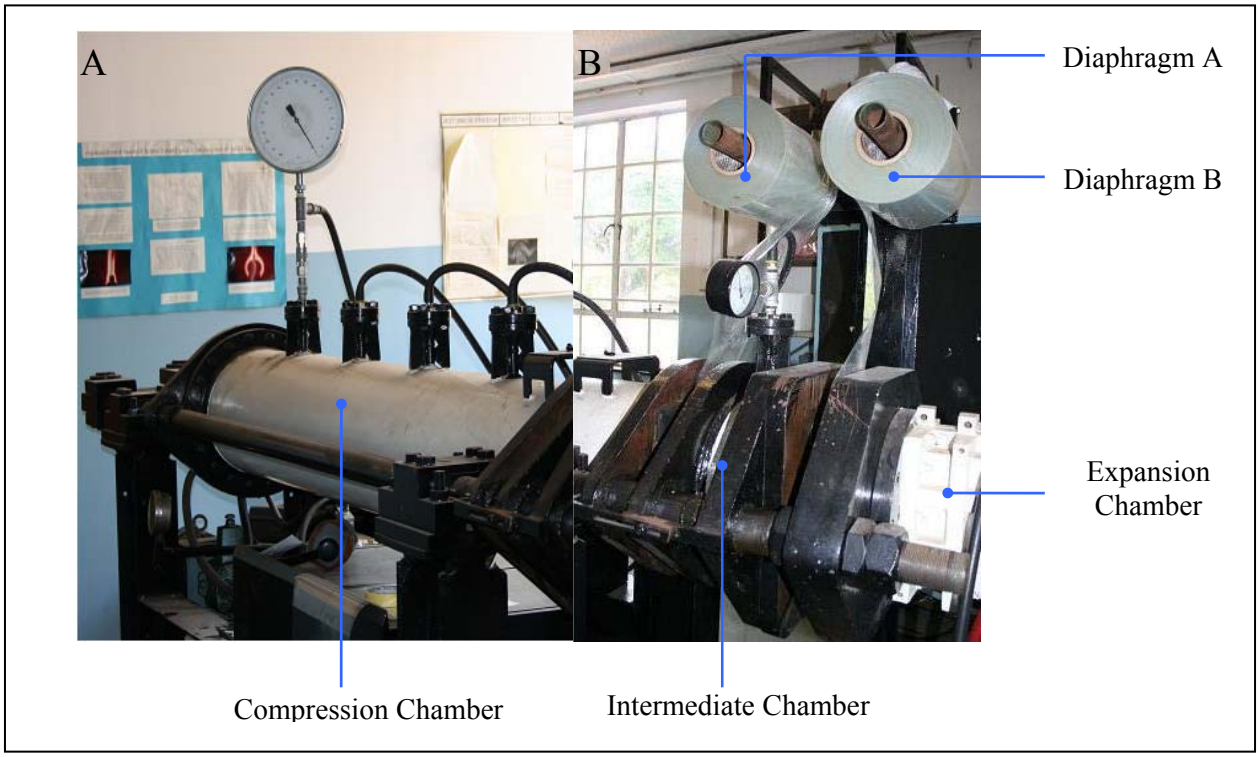


Figure 28: Photographs of the Driver Section of the Shock Tube

4.2.2.2 The Expansion Chamber

The expansion chamber has a length of 6 m and is constructed from cast-iron sections, as cast- iron has superior damping properties when compared to other metals. This damping property of cast-iron significantly reduces wall vibrations to the extent that the outputs from pressure transducers are not affected by wall resonance. The internal cross section of the expansion chamber is 180 mm x 76 mm with a wall thickness of 50 mm. Each section of the expansion chamber incorporates flanges and stiffening

webs as the chamber and test section are required to operate at vacuum pressures as low as 2 torr in order to produce Mach numbers greater than 1.55.

Pressure ports are situated at 450 mm intervals along the length of the expansion chamber. The two ports closest to the test section are fitted with pressure transducers, which are used to determine the Mach number obtained during testing and for initiating the recordings of the transducers in the test section. The expansion chamber is mounted on self aligning V-stands. The stands allow movement in the axial direction, which eliminates induced longitudinal stresses in the structure of chamber.

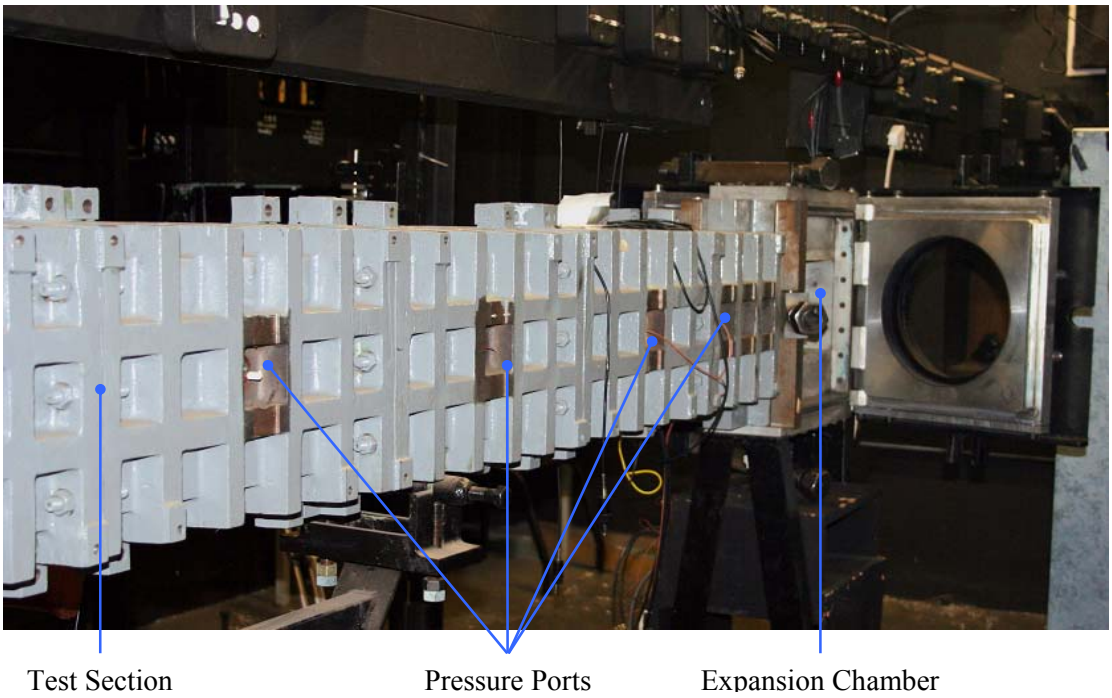


Figure 29: Photograph of the Expansion Chamber and the Test Section

4.2.2.3 The Test Section

The test section is a continuation of the expansion chamber and has an internal length of 350 mm. Two large doors (500 mm x 470 mm) enclose the test section and are secured by means of four large bolts. Two large 55 mm thick borosilicate crown optical quality circular glass windows are situated on either side of the section. The windows are placed in the doors of the test section and have a diameter of 260 mm, producing a minimum viewing area of 180 mm x180 mm. These doors are hinged to allow easy opening between tests to facilitate cleaning and changing of the test specimens.

A solid aluminium door also exists in which pressure transducers may be mounted. One of the optical doors may be removed and replaced with the aluminium door if pressure traces on the side wall of the test section are required.

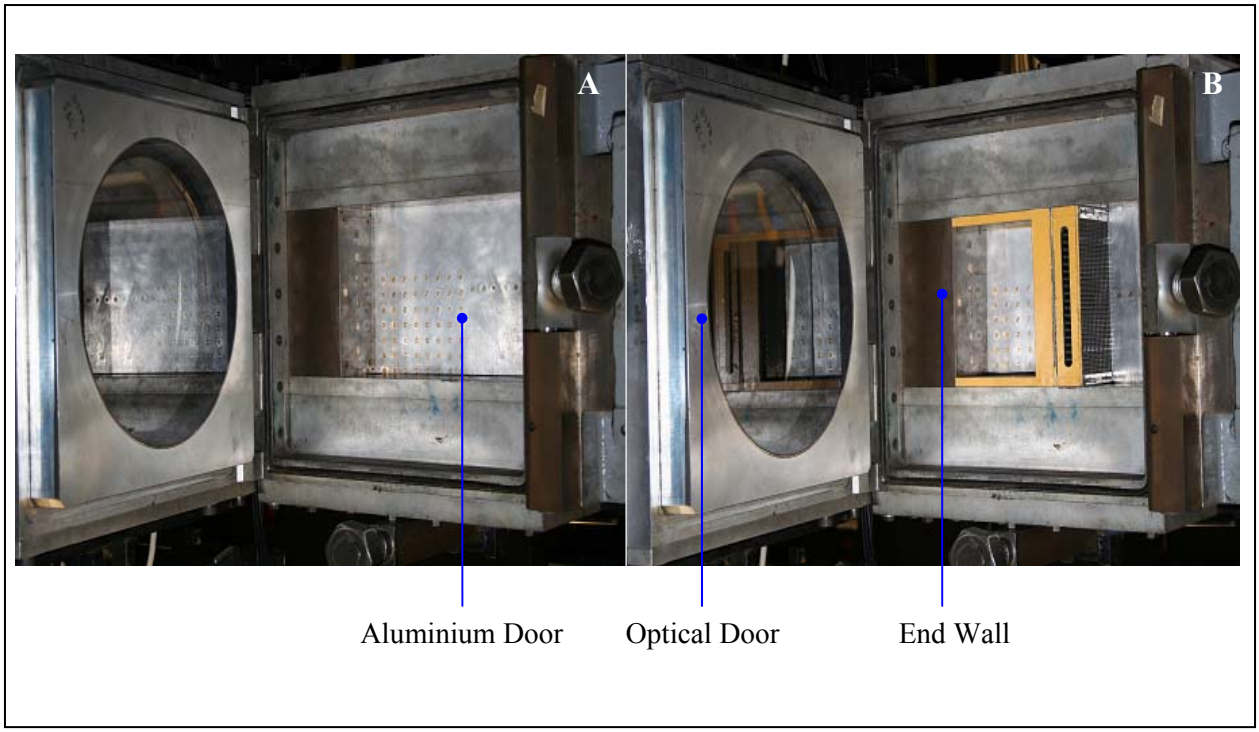


Figure 30: Photograph of the Test Section: A) With Test Specimens and B) Without Test Specimens

Transducer ports are also situated along the centre line of the floor and roof of the test section and are spaced 30 mm apart. Since the roof and floor transducer ports are offset, staggering of these ports occurs with a 15 mm distance between successive ports. In this study, the pressure transducers located in the roof and floor of the test section were removed and some of these ports were used to secure the mounting system of the test specimens. The remaining ports were replaced with blanks.

For experiments involving the capturing of photographic images of the test section, both optical doors were used. However, in order to obtain pressure readings along the length of the test section, the right (looking downstream) optical door was removed and replaced with the aluminium pressure transducer door. This was necessary, as the majority of transducer ports located in the roof and the floor of the test section were covered by the test specimen mounting system.

An 83 mm thick block forms the end wall of the test section in which eight transducer ports are present. Six of these transducer ports are situated along the vertical centre line with 25 mm spacings between adjacent ports. The remaining two transducer ports are situated along the horizontal centre line with a 50 mm distance between them, as shown in Figure 31.

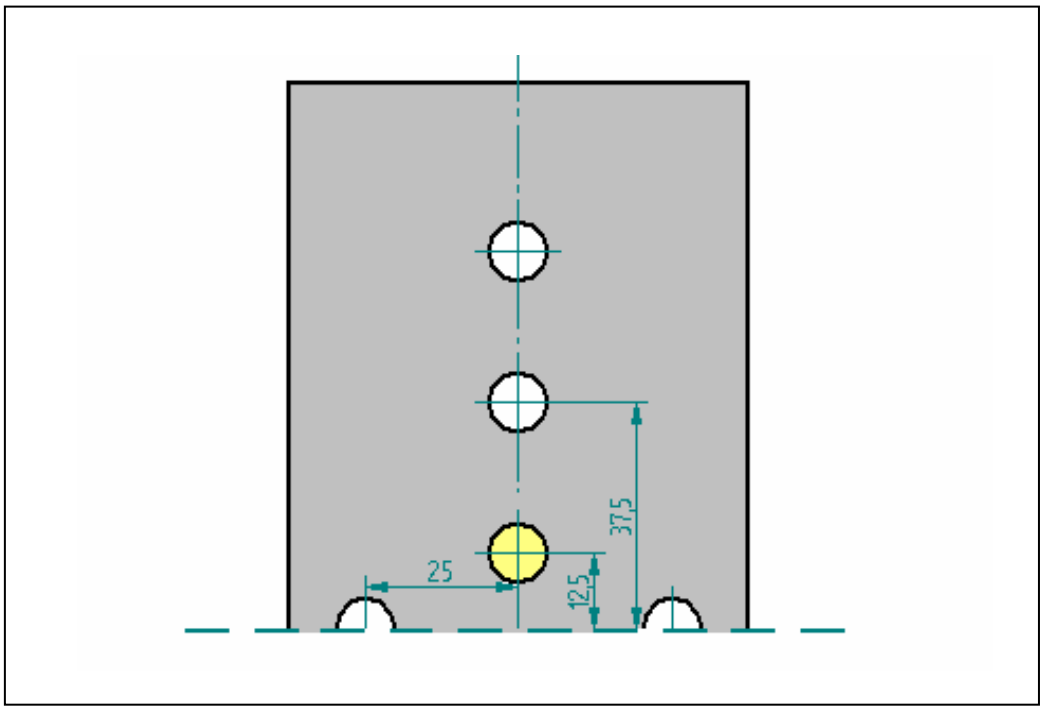


Figure 31: Location of Pressure Transducers on the End Wall of the Shock Tube

Only two of the eight pressure transducers ports in the end wall of the test section were used. This is in accordance with the findings of Hattingh (2000), whom upon calibration of the pressure transducers found that the two pressure transducer ports situated on either side of the horizontal axis of symmetry (as highlighted in the figure above) were most accurate since they were least affected by edge effects. The remaining six transducers were replaced with blanks.

4.3 The Data Acquisition System

The data acquisition system is situated in the Expansion Chamber room and comprises a Pentium IV, 3.2 GHz personal computer, three data acquisition cards, and TLC software which controls the capture of data and the operation of the shock tube. The PC has a 120 GB hard drive, 512MB RAM, CD - writer, 19 inch monitor and Windows XP Professional software installed on it.

The data acquisition cards are used to convert the analogue output signals from all measuring devices, to digitized signals for further processing by the TLC software. Two high speed data acquisition cards (NI 6110 cards) are used to give simultaneous sampling on a total of 8 channels at a maximum of 5 MHz per channel. These cards were used to capture the data recorded by the pressure transducers. The acquisition driver of these cards, use a small FIFO buffer of 8192 samples to transfer acquired data to the PC. The TLC software controls both the acquisition rate and the amount of points to acquire. The limit was set at 16 million points per card or 4 million points per cycle. A NI 6224 card was used to capture the data of the steady state variables such as the ambient pressure and temperature. This card was used to give precision output bit pattern (16 bit resolution) and to provide up to 32 channels of multiplexed data acquisition, sampling up to 250 kHz overall. The interface between the data acquisition cards, measuring devices and the PC is provided by means of connector blocks.

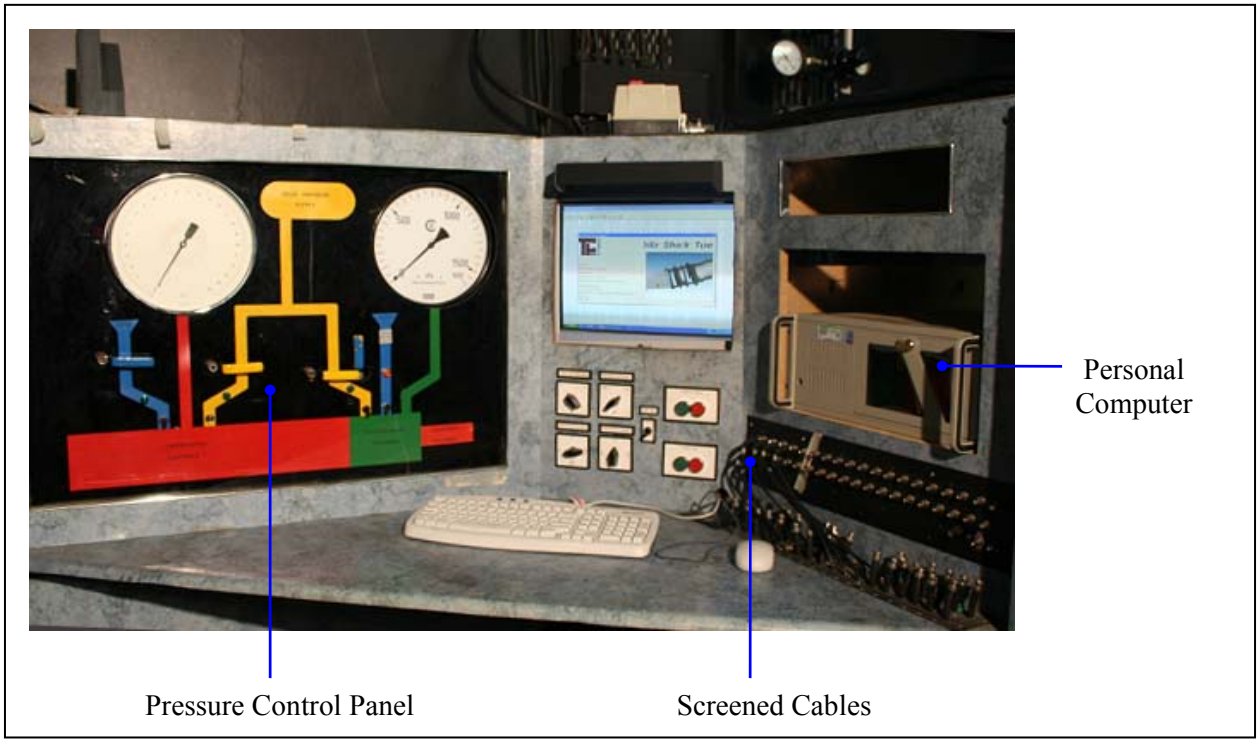


Figure 32: Photograph of the Control Console

4.4 Instrumentation and Calibration

4.4.1 Static Pressure and Temperature Measurement

Ambient temperature measurements were recorded using an LM35DZ integrated temperature sensor, which is mounted above the test section. The sensor has an accuracy of 0.25 ˚C within a normal room-temperature operating range.

The expansion chamber barometric pressure was measured using a Berotek B1000 pressure transducer which has an operating range of 800 - 1000 mbar (ambient pressure in the laboratory averages 830 mbar) and a resolution of 0.4 mbar. [Seitz (2001)]

4.4.2 Driver Section Pressure Measurement

A Schaevitz P1041 high-pressure transducer is used to measure the pressures in the compression and intermediate chambers. This transducer has a linear measuring range of 0 - 20 bar (gauge). The transducer is designed to withstand any rapid pressure changes, such as those caused by the rupturing of a diaphragm. [Bugarin (2003)]

4.4.3 High Speed Pressure Measurement

The accurate measurement of pressure fluctuations inside the shock tube, especially the test section, is accomplished using fast response PCB (Model 113A21 and A24) piezo-electric pressure transducers. This type of pressure transducer is specially designed for shock wave research and has a rise time of 1 μs. The output signals from these transducers are conditioned and amplified by externally powered PCB line power units, Model 482A. The output analogue signals are then captured by the NI 6110 data acquisition cards. [Seitz (2001)]

4.4.4 Calibration of the High Speed Pressure Transducers

In total, ten PCB transducers were used during experimentation. Preliminary test indicated that the transducer constants supplied with the transducers were no longer valid and that recalibration of the

transducers was required. In order to recalibrate the transducers, normal shock tests were run at three different Mach numbers for all transducers. The theoretical rise across the incident and reflected shock waves were then calculated using the equations listed in Section 1.5. For each pressure transducer six theoretical and six experimental pressure rises were obtained. The pressure traces were then scaled, by modifying the respective calibration constants, so that the pressures obtained experimentally correlated to those obtained theoretically. The results of the calibration procedure are listed in Appendix A.

4.4.5 Shock Tube Mach number Calibration

It must be noted that the properties and thicknesses of the diaphragms are manufacturer dependent. Since the diaphragms used in a test determine the Mach number that is achieved, a calibration routine was incorporated in the TLC Shock Tube Software in the event that new diaphragms are used. The routine was made user friendly and determines the range of Mach numbers achievable for the diaphragms available. The data obtained from the calibration tests are automatically saved and the plastics database is updated by the software. Therefore when the user inputs the Mach number for a test, the software is able to retrieve the diaphragm thicknesses required to attain the desired Mach number and prompts the user to load these diaphragms in the driver section of the shock tube.

Since new diaphragms were used in this study, the Mach Number Calibration routine had to be performed before testing could commence. The shock tube was calibrated using four diaphragms which allowed for a set Mach number in the range of M_{set} = 1.2 – 1.43. The diaphragm combinations and their corresponding Mach number ranges have been listed in Appendix B.

4.5 The Schlieren Optical System

The schlieren flow visualization method reveals density gradients across a flow field and is one of the most frequently used optical visualization system in aerodynamic laboratories, since it is a relatively simple optical arrangement with a high degree of resolution. The word schliere has been attributed to certain optical devices that allow one not only to qualitatively visualize flow inhomogeneities, but to also quantitatively measure the distribution of deflection angles or the variations in the index of refraction in the test field. This distribution is calculated directly from density variations present in the flow field which may be measured using a densitometer. The principle component of this system is a knife edge. Many modifications have been derived from the original Toepler system such as the one used in this study, which is referred to as the Z – configuration and is shown in Figure 33. The major differences

between these two configurations are that mirrors are used in the Z-configuration whereas lenses are used in the Toepler system. This allows for a large field of vision as spherical mirrors can be fabricated with a greater diameter than lenses. Furthermore, the mirrors in this configuration are tilted at an angle and the light source and the image are positioned off the axis of the mirrors which lead to optical aberrations of coma and astigmatism. These disturbances are acceptable if the angle in which the mirrors are tilted is small. [Merzkirch (1974)]

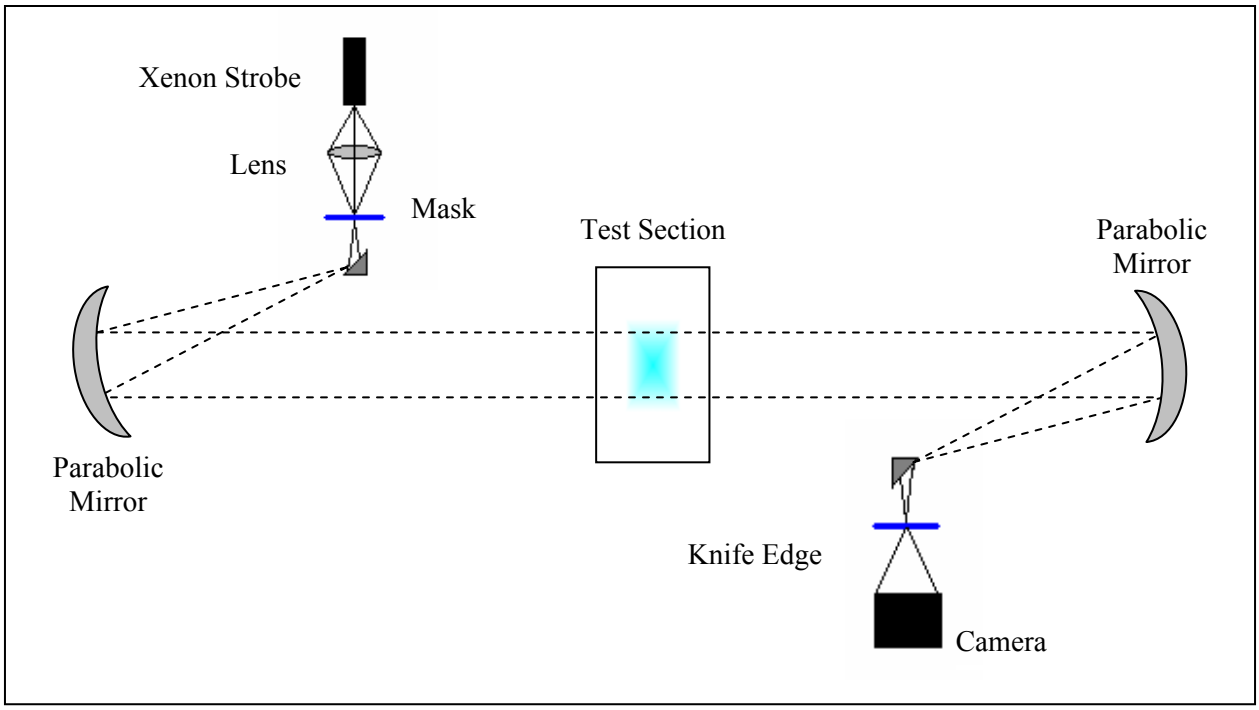


Figure 33: The Schlieren Optical System Used in the Study

The first optical component of the system used in the study is a light source, which was produced by using a Xenon strobe. The light produced by the strobe was passed through a converging lens and subsequently through a mask to improve the definition of the effective line light source. The diverging light from the line source is then reflected off a secondary 45˚ angled mirror onto a parabolic mirror (first schlieren head) which establishes a collimated (parallel) light beam passing through the test section. The light beam is then reflected off the second parabolic mirror (second schlieren head) which converges the light beam onto a secondary 45˚ angled mirror. The light beam is then directed and focused onto an adjustable knife edge which allows the variation of the sensitivity of the image captured by a digital camera.

The image captured by the camera will be uniformly bright if the flow is uniform. If there are density variations in the flow field there will be a change in the index of refraction of the fluid and some of the

light that would have passed by the knife edge in the uniform situation will instead be blocked by it and the image will have dark areas. Conversely, if some light rays were to pass the knife edge that would have been blocked in the uniform situation, the image will have light areas. Therefore by utilizing the knife edge the parallel light is cut off, with the diffracted light passing the knife edge and the photograph taken by the camera revealing the density gradients present in the flow field as either dark or light regions on a partially darkened background. Solid objects appear as silhouettes on schlieren photographs. [Seitz (2001)]

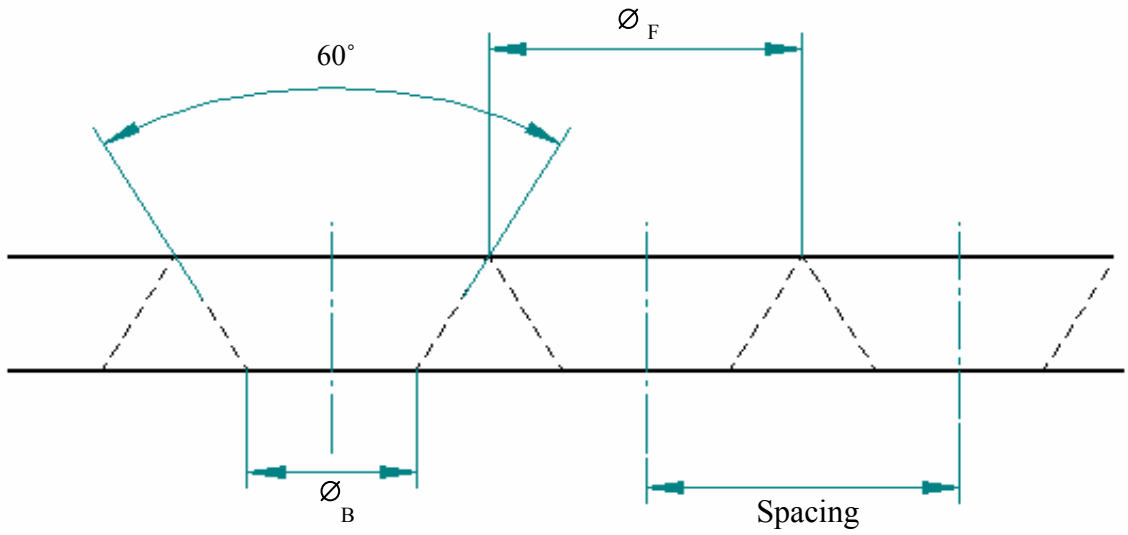
A digital camera was used during testing to determine the wave interactions that occurred in the test section. The camera used was a Fuji Finepix S3 Pro Body camera with a 23 x 15.5 mm sensor chip and 12.3 million effective pixels. The use of a digital camera greatly improved the testing procedure, as film did not have to be developed and images could be viewed and saved to hard disk immediately.

4.6 Test Specimens

4.6.1 Introduction

It was originally envisaged that the test specimens manufactured and used by Seeraj (2004, unpublished) would be used for testing purposes. However, initial tests revealed that the composite test specimens (see Section 3.2) were not suitable for testing purposes as they would have broken, or even shattered due to the large forces and bending moments acting on them when fixed in the test section.

Four steel specimens with tapered hole arrangements were used in testing. The tapered hole arrangement gives the specimens their directional properties and is similar in geometry to the wedge arrangement used in the trapping of shock waves by Skews and Broido (1992). Two hole diameters were chosen and three hole spacings were used. The front hole diameters used were 5 mm and 7.5 mm. These corresponded to back hole diameters of 1.54 mm and 4.04 mm respectively. The hole spacings used were 3 mm, 5 mm and 7.5 mm. These hole spacings were selected in order to obtain the overlapping of the tapered holes. This formed sharp edges over which it was hoped that the incident shock wave would reflect. Figure 34 that follows illustrates the typical cross section of the tapered hole used in the manufacture of the test specimens.



Where:

Ø B = Diameter of Back Hole

Ø F = Diameter of Front Hole

Figure 34: Cross Section of the Tapered Hole Geometry

Detailed engineering drawings of these specimens have been provided in the DVD accompanying this report. Figure 35 that follows is a photograph of test specimens. Please refer to Seeraj (2004, unpublished) for more information on the test specimens and its manufacturing processes.

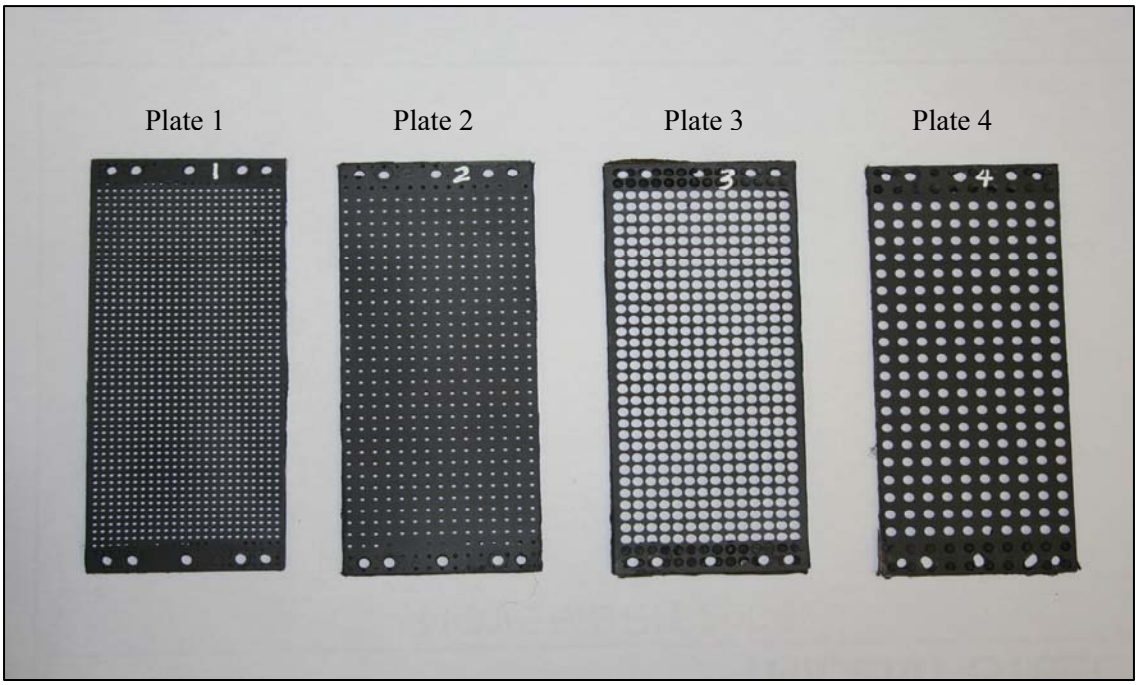


Figure 35: Photograph of the Metal Test Specimens

4.6.2 Test Specimen Properties

The following table summarizes the test specimen geometries and properties. The table lists the porosity of the plates which have been calculated after the placement of the metal plates necessary for mounting purposes. These metal plates do cover certain cut outs in the specimens, reducing their porosity. The porosity is quantified as the ratio of the area cut out of the specimen to its total area. The mass of the specimens have also been listed in the tables below.

Table 3: Summary of the Test Specimen Geometries and Properties

Plate	Front Hole Diameter [mm]	Back Hole Diameter [mm]	Plate Area [mm^2]	Mass [g]	Back Hole Area [mm^2]	Rows	Columns	No Of Holes	Cut Out Area [mm^2]	Porosity [%]
Plate 1	5	1.54	13500	137.4	1.86	52	24	1248	2325	17.2
Plate 2	5	1.54	13500	224.7	1.86	32	15	480	894	6.6
Plate 3	7.5	4.04	13500	120.2	12.79	31	14	434	5552	41.1
Plate 4	7.5	4.04	13500	208.1	12.79	20	10	200	2559	19.0

4.6.3 Mounting of the Test Specimens

During the initial tests, the metal test specimens were fixed in the test section using a simple four rod supporting structure and bolts. These specimens deformed along the longitudinal axis upon interaction with the incident shock wave as a result of the large bending moment experienced at the centre of the plate (when viewed side on). It was immediately decided that the composite test specimens could not be used for testing as they were not designed for such large bending moments and were less stiff along both axes than the metal plates. The mounting system shown below was therefore designed to provide both lateral as well as longitudinal support and stiffness to the test specimens in order to overcome the deformation of the metal test specimens. Detailed engineering drawings of the mounting system have been provided in the DVD accompanying this report.

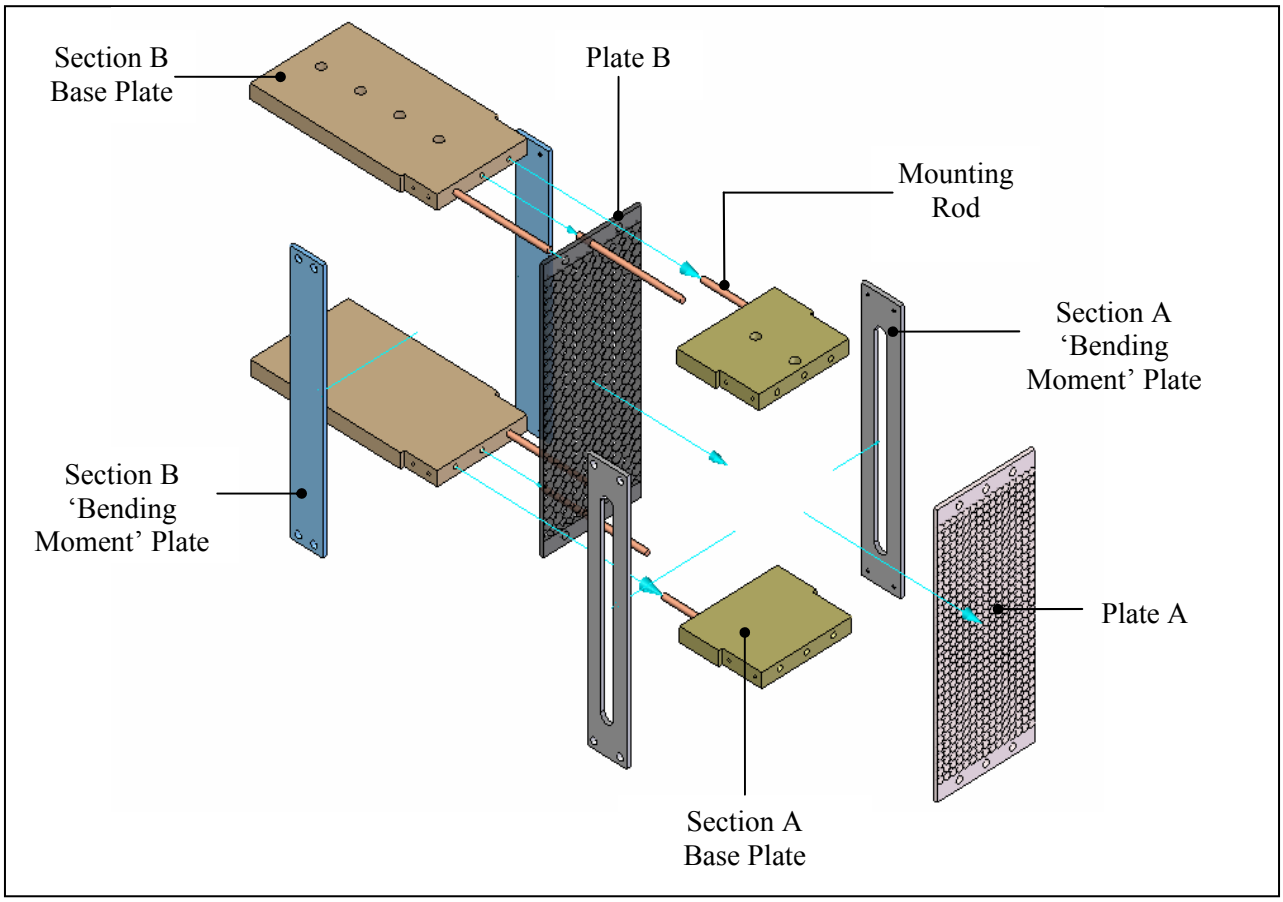


Figure 36: Exploded View of the Test Specimen Mounting System

The mounting system consists of two sections, as shown in the above figure. Section B creates a 140 mm long space between the downstream specimen (Plate B) and the end wall. Two 3mm thick 'bending moment' plates at the front of this section provide the longitudinal support and stiffness to prevent deformation of Plate B. Base plates provide this test specimen with lateral support and stiffness. They also allow for the fitting of mounting rods which hold Section A and the test specimens in place. The configuration of the Section B (excluding Plate B) remains the same for all tests.

Section A is similar to the Section B; however three configurations are possible as the distance between the test specimens may be varied using base plates with distances of 30 mm, 45mm or 60 mm. These base plates are also 10 mm thick and have holes drilled into them to allow for the mounting rods to pass through. Two 3 mm thick 'bending moment' plates, with sections cut out of them, provide the longitudinal stiffness to prevent deformation of the upstream test specimen (Plate A). The cut out regions in these support frames allow for the photographing of the wave system between the plates. The configuration for a 60 mm spacing between test specimens is shown in Figure 36. The first test specimen is held in place by means of six bolts which are tightened onto the mounting rods.

All base plates were manufactured from mild steel. As the 'bending moment' plates required being thin to reduce noise effects, they were manufactured from tool steel which has a higher yield stress than mild steel. The use of tool steel for these plates allowed for a 3mm thickness to provide sufficient longitudinal stiffness to the system for tests with an incident Mach number up to M = 1.6.

The mounting system is secured in the test section by means of bolts which pass through the transducer ports located on the floor and roof of the shock tube and fasten into the base plates of both sections.

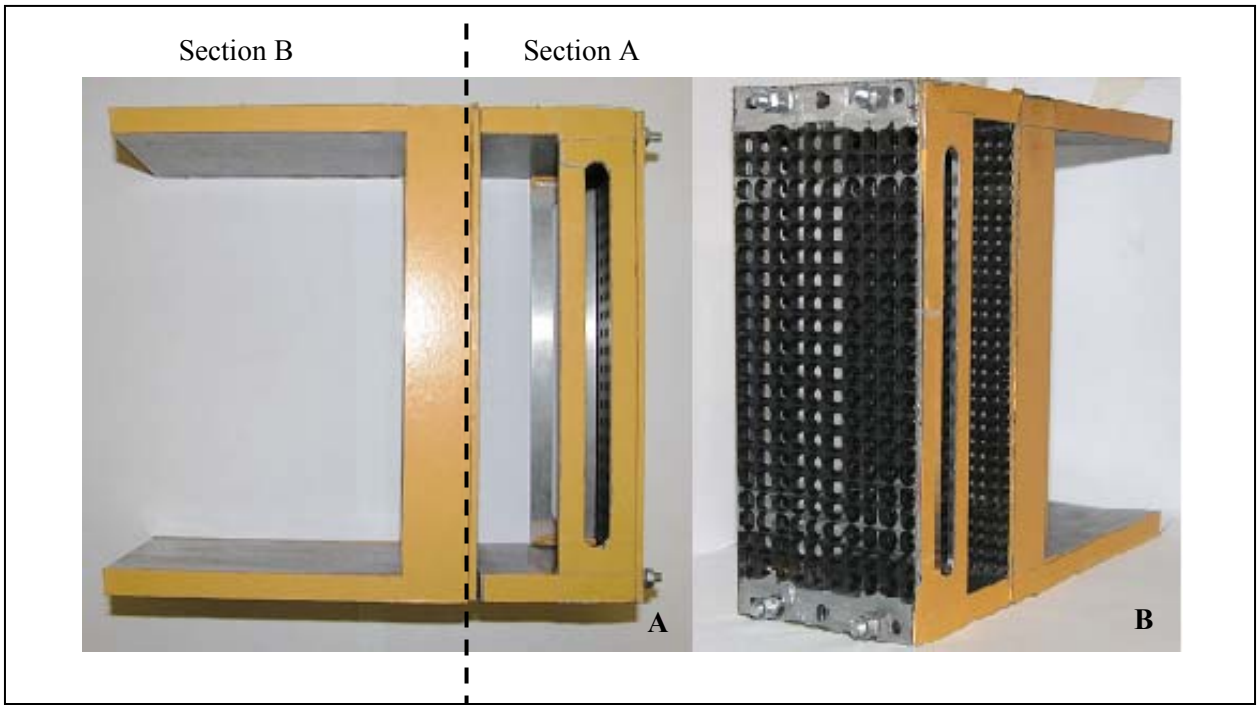


Figure 37: Photographs of the Assembled Test Specimen Mounting System

4.6.4 Plate Combinations and Their Representation

In each test two test specimens are mounted in the test section. Since four test specimens were used in this study, it is possible to arrange them in twelve combinations as each plate may be paired with one of the three remaining plates.

Furthermore, each plate may have either its front or back facing the incident shock wave. This results in a possibility of four arrangements for each combination of plates. The four arrangements possible for each plate combination are, Front & Front, Front & Back, Back & Front and Back & Back. In total forty-eight plate configurations are available, as each of the twelve plate combinations has four possible plate arrangements. Please refer to Table 4 that follows.

Table 4: Plate Combination and Arrangement Matrix

Downstream Plate	Plate Arrangement	Upstream Plate	Plate Arrangement
Plate 1	Front or Back	Plate 2	Front or Back
		Plate 3	Front or Back
		Plate 4	Front or Back
Plate 2	Front or Back	Plate 1	Front or Back
		Plate 3	Front or Back
		Plate 4	Front or Back
Plate 3	Front or Back	Plate 1	Front or Back
		Plate 2	Front or Back
		Plate 4	Front or Back
Plate 4	Front or Back	Plate 1	Front or Back
		Plate 2	Front or Back
		Plate 3	Front or Back

The naming of plate combinations for tests follows the format of the matrix above. The downstream plate number (closest to the end wall) and it's face is written first, which is then followed by the upstream plate number and it's face written second e.g. Pl1Fr&Pl2Bk means that Plate 1 is situated downstream with its front facing the incident shock and Plate 2 is situated upstream with is back facing the incident shock.

4.7 Modification of the Aluminium Test Section Door

As the test specimen mounting system covered the existing transducer ports located in the roof and floor of the test section, an existing aluminium test section door was modified to obtain pressure trace data along the length of the test section. The original door was designed to obtain pressure trace data near the end wall of the shock tube. Therefore transducer ports were located towards the back of the test section and not along its whole length. In order to obtain pressure traces across the entire mounting system for this study, six more transducer ports were machined into the door. The modified transducer door is shown in the figure that follows. Detailed engineering drawings of the modified test section door have been included in the DVD accompanying this report for further reference.

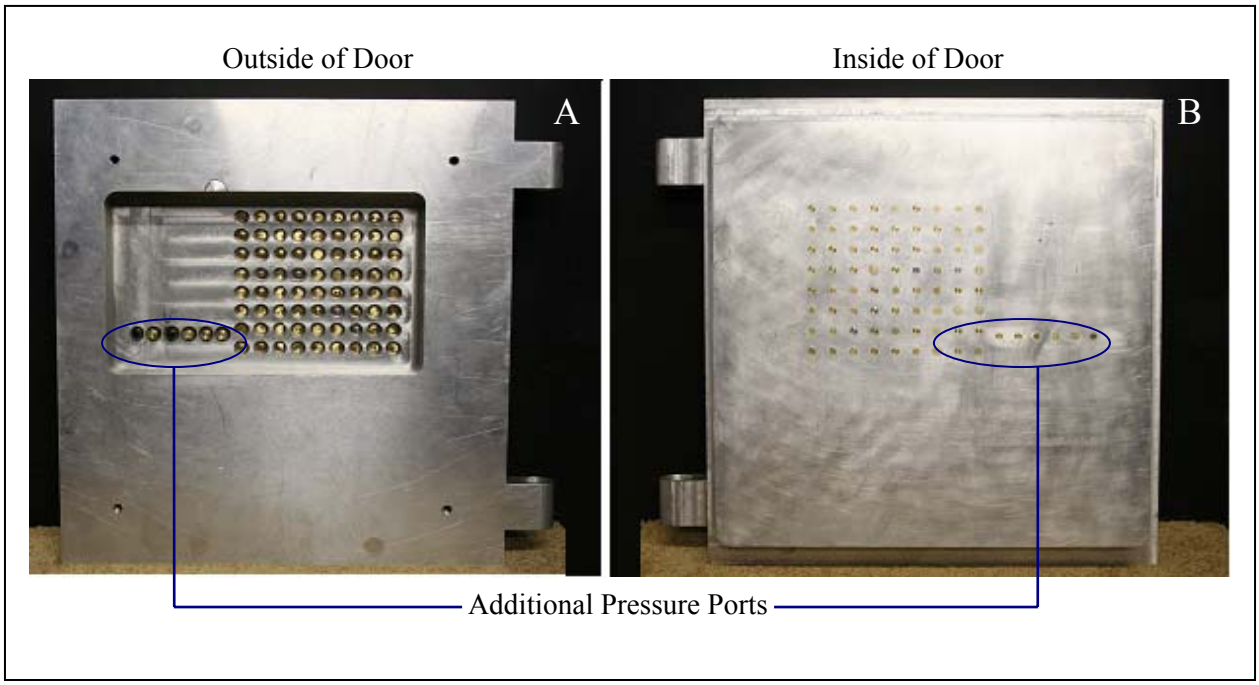


Figure 38: Photographs of the Modified Aluminium Test Section Door

The placement of these pressure ports allowed for the acquisition of pressure traces upstream of the mounting system, in between test specimens and in between the second specimen and the end wall of all configurations tested.

4.8 Location of Pressure Transducers

Eight pressure transducers were activated for all tests performed. Two transducers viz. Transducer 1 and 2 were situated upstream of the test section and were used to calculate the actual Mach number for tests. The remaining six transducers were positioned in the test section as follows:

- Transducer 3 - Upstream of the plate arrangement, recording the reflected pressure data.
- Transducer 4 - In between the two test specimens, recording the trapped pressure data.
- Transducer 5 & 6 - Located downstream of the second test specimen, but before the end wall of the shock tube, recording pressure data downstream of the plate arrangement.

- Transducer 7 & 8 - Located in the end wall of the shock tube from which the initial peak pressure and impulse amelioration values of the tests were calculated.

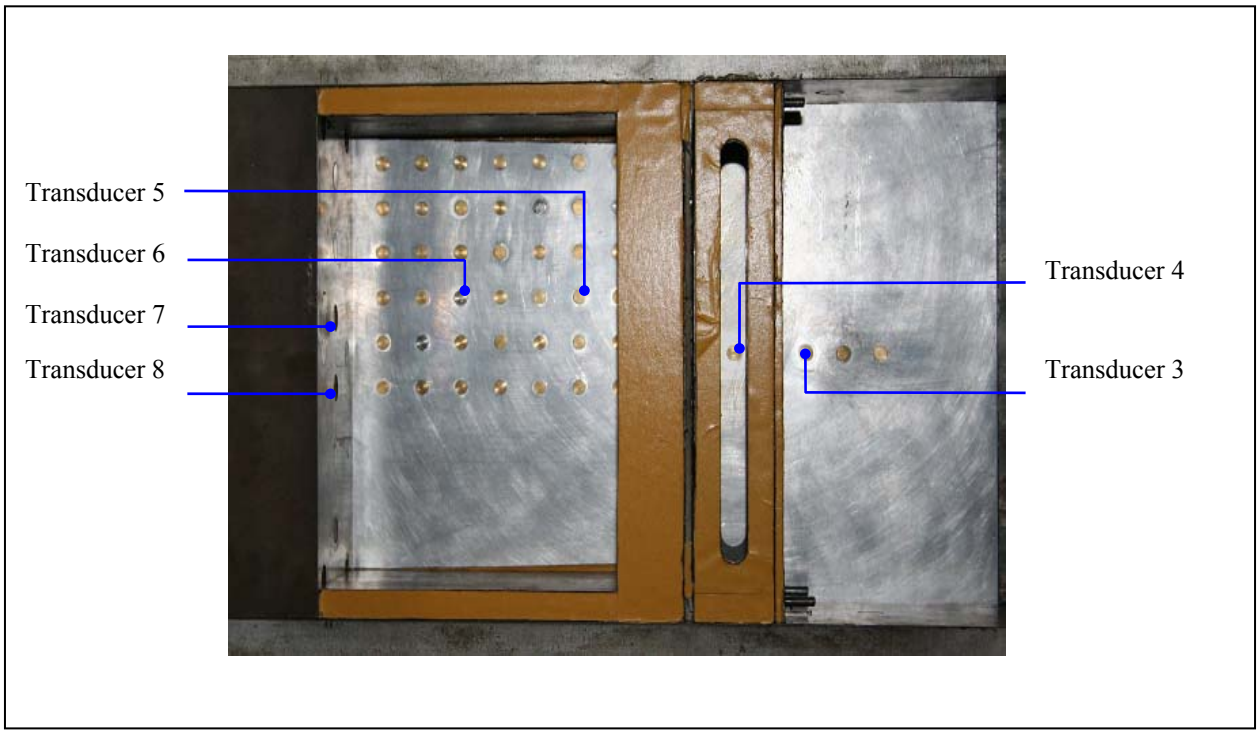


Figure 39: Location of the Test Section Pressure Transducers

5 Experimental Procedure and Precautions

5.1 Orifice Plate Calibration Procedure

A brass orifice plate was manufactured to determine the air flow rate passing through the Calibration Duct when determining the directional properties of the metal test specimens. This orifice plate had to be calibrated before the tests in the calibration duct could be performed. The calibration procedure followed is outlined below.

1. A suitable range of pressure differentials across the orifice plate was selected to be tested
2. The ambient air pressure was recorded.
3. A pressure differential value was chosen from the range initially selected (refer to 1 above).
4. The power of the duct's motor was increased until the pressure drop measure across the orifice plate equaled that selected in 3.
5. The flow in the duct was allowed to settle.
6. The temperature upstream of the orifice plate was recorded.
7. The exiting air speed at the end of the calibration duct was measured using the electronic vane anemometer.
8. The power setting on the ducts motor was decreased back to zero.
9. Steps 4 - 8 were repeated at least three times and the average value of the exiting air speed for the pressure differential selected was recorded.
10. Steps 3 - 9 were repeated until the range of selected pressure differentials were tested.

5.2 Orifice Plate Calibration Precautions

1. It must be ensured that the mounting flange around the orifice plate is sealed and that there are no leaks in the calibration duct during testing.

2. It must be ensured that the electronic vane anemometer is perpendicular to the airflow at the exit of the duct and that the distance from the exit is not varied throughout calibration of the orifice plate. The anemometer should be mounted directly in front of the duct exit.
3. It must be ensured that the pressure tapping tubes are not pinched when taking the pressure readings.
4. The electronic manometer must be zeroed after each reading.

5.3 Operation of the Calibration Duct

The procedure followed in order to determine the pressure drop across each of the test specimens for both the conditions of the front and the back of the specimen facing the oncoming airflow is outlined below.

1. The test specimen was mounted in the test section of the duct so that the front of the specimen faced the oncoming air flow.
2. The orifice plate was then secured in the duct.
3. The ambient air pressure was recorded.
4. A range of (at least three) orifice pressure differentials for each specimen was selected and their corresponding air speeds, obtained from the calibration of the orifice plate, were noted.
5. The power to the motor was increased until the predetermined pressure differential was achieved across the orifice plate.
6. The electronic manometer was connected to the pressure tappings across the test section.
7. The reading was allowed to settle before recording the data.
8. The temperature of the airflow upstream of the orifice plate was then recorded.
9. Steps 5 - 8 were then repeated for the remaining airflow rates selected for the test specimen.
10. Steps 1 - 9 above were then repeated with the test specimen turned around so that the back of the specimen faced the oncoming air flow.

5.4 Calibration Duct Operating Precautions

1. It must be ensured that the motor speed is increased and decreased gradually. Do not increase or decrease the speed abruptly as the motor might burn out.
2. It must be ensured that the direction of the specimen facing the oncoming flow is noted correctly for every test.
3. Protective ear muffs must be worn when operating the motor at high speeds.
4. It must be ensured that the pressure tapping tubes are not pinched when taking the pressure readings.
5. The electronic manometer must be zeroed after each reading.

5.5 Operation of the Shock Tube

Prior to each testing session, all the instrumentation was switched on and sufficient time was allowed to pass in order for the instrumentation to reach operating conditions (approximately 30 minutes). The procedure followed for each test undertaken in the 'Seitz' shock tube is outlined below.

1. The supply pressure from the supersonic wind tunnel receiver was checked to ensure that sufficient pressure was available for the required Mach number (above 500 kPa).
2. Both the doors of the test section were then opened.
3. The compression chamber and expansion chamber were blown clean using high pressure air in order to remove any diaphragm fragments from the previous test.
4. The desired test specimens were secured in the mounting system of test section and the distance between plates was adjusted depending on the test configuration that was being investigated.
5. Both doors of the test section were closed and secured.
6. The desired Mach number was entered into the Shock Tube software. The computer then displayed the diaphragm thicknesses required.

7. The correct thickness diaphragms were then placed between the compression and intermediate chambers and between the intermediate and expansion chambers.
8. The camera was focused on the test section and it was ensured that the shutter triggering device was connected.
9. The instruction prompts displayed by the computer program were then followed, during which the software prompts the user to perform safety checks on the valves of the shock tube and enter the relevant information about the test.
10. The ambient conditions are displayed by the software once the test is ready to be executed. This data was then recorded in the logbook.
11. The lights in the expansion chamber room were switched off and the shutter of the camera was opened.
12. The test was then executed.
13. Upon completion of the test, the shutter of the camera was closed and the lights in the room were switched on.
14. The actual Mach number achieved during the test as well as the date and time of the test were then recorded.
15. The test specimens and mounting system configuration tested were recorded in the logbook.
16. The doors to the test section were opened once the shock tube was vented completely.

Please note that when tests were performed to obtain pressure traces, photographs of the test section could not be taken. During such tests points 8, 11 and 13 listed above were ignored.

5.6 Shock Tube Operating Precautions

1. It must be ensured that there is sufficient pressure in the supply tank.
2. The power supply to the hydraulic ram must be switched on and the yellow pressure valve in the compression chamber room must be opened.

3. It must be ensured that the intermediate chamber valve is opened and that the compression chamber valve is closed on the control panel
4. All switches on the control panel must be switched to automatic and not manual.
5. It must be ensured that the test section doors are open prior to blowing down the tube.
6. Protective ear muffs must be worn while cleaning out the tube chambers and upon execution of a test.
7. When performing photographic tests, it must be ensured that the optical system is set up correctly and that the test section windows are dirt free. Furthermore, the shutter triggering device must be correctly connected.
8. It must be ensured that the test section doors are secured before running a test.
9. The operator must remember not to switch on the expansion chamber room light until the camera shutter is closed.
10. The compression chamber must not be opened unless it has been fully vented.

6 Observations

This section lists the observations recorded during the calibration of the orifice plate and the Calibration Duct tests performed in order to verify the directional properties of the metal test specimens. Furthermore, the data obtained during shock tube testing are also discussed.

6.1 Orifice Plate Calibration Observations

Two test sets of data have been listed in the tables that follow. Pressure differential values that occurred across the orifice plate ranged between 0-147 Pa for both test sets. For each of these values, three values of the exiting flow speed, V_{Exit}, were recorded and the average flow rate was then calculated.

Table 5: Orifice Plate Calibration Data Set 1

Test Set 1: 07/06/2007								
Temp = 18.00 C								
Po = 834.40 ѵlb								
Test #	**δ $P_{Orifice}$** [Pa]	**V_{Exit} Reading # 1** [m/s]	**V_{Exit} Reading # 2** [m/s]	**V_{Exit} Reading # 3** [m/s]	**Average V_{Exit}** [m/s]	**Average Flow Rate** [m^3/s]	**Theory Flow Rate** [m^3/s]	**Deviation** %
1	0	0.00	0.00	0.00	0.00	0.000	0.000	0
2	4	1.70	1.71	1.70	1.70	0.023	0.024	-2.6%
3	7	2.26	2.27	2.27	2.27	0.031	0.031	-2.0%
4	11	2.84	2.83	2.83	2.83	0.038	0.039	-2.3%
5	15	3.27	3.27	3.25	3.26	0.044	0.046	-3.6%
6	18	3.55	3.54	3.56	3.55	0.048	0.050	-4.3%
7	23	4.08	4.09	4.06	4.08	0.055	0.057	-2.8%
8	27	4.51	4.52	4.53	4.52	0.061	0.061	-0.5%
9	31	4.84	4.85	4.87	4.85	0.066	0.066	-0.3%
10	40	5.42	5.48	5.35	5.42	0.073	0.075	-2.1%
11	43	5.68	5.68	5.69	5.68	0.077	0.077	-0.9%
12	52	6.22	6.21	6.22	6.22	0.084	0.085	-1.4%
13	63	6.85	6.85	6.86	6.85	0.093	0.094	-1.3%
14	71	7.26	7.25	7.26	7.26	0.098	0.099	-1.5%
15	84	7.94	7.94	7.93	7.94	0.107	0.108	-1.0%

Table 5 continued.

Test #	$\delta P_{Orifice}$ [Pa]	V_{Exit} Reading # 1 [m/s]	V_{Exit} Reading # 2 [m/s]	V_{Exit} Reading # 3 [m/s]	Average V_{Exit} [m/s]	Average Flow Rate [m^3/s]	Theory Flow Rate [m^3/s]	Deviation %
16	97	8.54	8.52	8.51	8.52	0.115	0.116	-1.0%
17	107	8.93	8.93	8.96	8.94	0.121	0.122	-1.2%
18	128	9.79	9.78	9.80	9.79	0.132	0.134	-1.0%
19	147	10.52	10.52	10.52	10.52	0.142	0.143	-0.8%

Table 6: Orifice Plate Calibration Data Set 2

Test Set 2:	10/6/2006							
Temp =	18.00	˚C						
Po =	834.40	Mb						
Test #	**$\delta P_{Orifice}$** [Pa]	**V_{Exit} Reading # 1** [m/s]	**V_{Exit} Reading # 2** [m/s]	**V_{Exit} Reading # 3** [m/s]	**Average V_{Exit}** [m/s]	**Average Flow Rate** [m^3/s]	**Theory Flow Rate** [m^3/s]	**Deviation** %
1	0	0.00	0.00	0.00	0.00	0.000	0.000	0
2	4	1.70	1.71	1.73	1.71	0.023	0.024	-2.0%
3	7	2.21	2.20	2.20	2.20	0.030	0.031	-4.8%
4	10	2.69	2.68	2.69	2.69	0.036	0.037	-2.8%
5	13	3.05	3.02	3.01	3.03	0.041	0.043	-4.0%
6	16	3.39	3.40	3.37	3.39	0.046	0.047	-3.2%
7	20	3.76	3.77	3.78	3.77	0.051	0.053	-3.6%
8	25	4.25	4.25	4.24	4.25	0.057	0.059	-2.9%
9	35	5.03	5.06	5.05	5.05	0.068	0.070	-2.5%
10	40	5.30	5.47	5.35	5.37	0.073	0.075	-2.8%
11	44	5.65	5.61	5.65	5.64	0.076	0.078	-2.8%
12	52	6.18	6.17	6.16	6.17	0.083	0.085	-2.2%
13	62	6.79	6.79	6.78	6.79	0.092	0.093	-1.4%
14	71	7.24	7.27	7.26	7.26	0.098	0.099	-1.5%
15	84	7.89	7.87	7.89	7.88	0.106	0.108	-1.6%
16	92	8.30	8.29	8.28	8.29	0.112	0.113	-1.2%
17	98	8.57	8.53	8.54	8.55	0.115	0.117	-1.3%
18	114	9.23	9.25	9.24	9.24	0.125	0.126	-1.0%
19	141	10.34	10.34	10.31	10.33	0.139	0.140	-0.5%

6.2 Observations of Pressure Differentials that Occurred Across Test Specimens

The pressure drop that occurred across each specimen for the instances of the front and the back of the specimen facing the oncoming flow are listed in the tables that follow. Each specimen was tested at three orifice plate differential pressures ranging from 10 - 40 Pa, which corresponds to an air flow rate range of 0.036 – 0.073 m^3/s, as determined by the calibration of the orifice plate. The testing procedure was conducted twice in order to validate the data obtained and the average pressure drop value for each test is listed in the table that follows.

Table 7: Pressure Differentials That Occurred Across Metal Test Specimens for Selected Flow Rates

Plate	Face	$\delta P_{Orifice}$ [Pa]	V_{Exit} [m/s]	Flow Rate [m^3/s]	Ave. Δ P [Pa]	Face	$\delta P_{Orifice}$ [Pa]	V_{Exit} [m/s]	Flow Rate [m^3/s]	Ave. Δ P [Pa]
1	Front					Back				
		10	2.69	0.036	95		10	2.69	0.036	130
		20	3.77	0.051	192		20	3.77	0.051	259
		40	5.4	0.073	367		40	5.4	0.073	524
2	Front					Back				
		10	2.69	0.036	603		10	2.69	0.036	745
		15	3.26	0.044	929		15	3.26	0.044	1038
		20	3.77	0.051	1183		20	3.77	0.051	1378
3	Front					Back				
		10	2.69	0.036	15		10	2.69	0.036	20
		20	3.77	0.051	30		20	3.77	0.051	41
		40	5.4	0.073	59		40	5.4	0.073	83
4	Front					Back				
		10	2.69	0.036	91		10	2.69	0.036	137
		20	3.77	0.051	180		20	3.77	0.051	256
		40	5.4	0.073	351		40	5.4	0.073	524

6.3 Shock Tube Testing Observations

Upon completion of a successful test the TLC Software that controls the operation of the shock tube automatically saves the test data in *.TLCDAT file format. The file is named according to the date and time of the test and the user may specify the directory in which it is saved. This file format may only be read by TLC Software, which displays the pressure traces and does not allow for further data processing. However, the software does allows for the conversion of files to Matlab data file, *.mat, and Excel spreadsheet, *.xls, formats if further data processing is required. Conversion of the TLC data files to an Excel spreadsheet format was not viable due to the large number of data points saved during a test. Therefore each TLC data file was converted into a Matlab data file for further processing and analysis.

Upon completion of a test, the pressure traces were viewed on the TLC software to confirm the success of the test and the relevant test information entered into the logbook. Thereafter, the TLC data file was converted to Matlab format for processing in order to extract useful information from the test.

6.3.1 Description of Test Data Files

The TLC data file for each test contains general information about the test such as ambient temperature and pressure, the set Mach number and the actual Mach number. This data is then followed by the voltage readings recorded by each pressure transducer activated and the time at which the readings were taken. When this file is converted to a Matlab data file format, the general information of the test is lost. Therefore it was necessary to enter such details into the logbook upon the completion of each test.

The pressure trace data extracted is saved in matrix format within the Matlab data file. An extract of such a matrix, for a test which had eight transducers activated and a sampling frequency of 2.5 MHz, is shown in Table 8 that follows.

Table 8: Extract from a Matlab Data File (*.mat)

2.15956E-02	0.9155	0.6836	0.7471	0.5371	0.7471	0.835	0.7178	0.6177
2.15960E-02	0.9131	0.686	0.7471	0.5347	0.7495	0.8374	0.7178	0.6201
2.15964E-02	0.9131	0.6836	0.7471	0.5371	0.7471	0.835	0.7178	0.6177
2.15968E-02	0.9131	0.6836	0.7471	0.5371	0.7495	0.8374	0.7178	0.6201
2.15972E-02	0.9131	0.686	0.7471	0.5371	0.7495	0.835	0.7178	0.6201
2.15976E-02	0.9131	0.6836	0.7446	0.5347	0.7495	0.835	0.7178	0.6201
2.15980E-02	0.9131	0.6836	0.7471	0.5371	0.7471	0.835	0.7178	0.6177
2.15984E-02	0.9131	0.6836	0.7495	0.5371	0.7495	0.835	0.7202	0.6201
2.15988E-02	0.9131	0.6812	0.7495	0.5371	0.752	0.8374	0.7178	0.6201
2.15992E-02	0.9131	0.6836	0.7471	0.5371	0.7495	0.835	0.7178	0.6177
2.15996E-02	0.9131	0.6812	0.7471	0.5371	0.7495	0.835	0.7178	0.6177

The first column of the matrix contains the time data of the test. The values in this column begin at zero and increase in increments of the sampling frequency. Each column that follows contains the voltage values recorded by an activated pressure transducer. Values along the row are taken at the time listed at the beginning of the row. The sequence of the transducers follow the sequence entered in the TLC software settings e.g. the transducer labeled as 1 in the TLC software settings will correspond to column 2 of the matrix and that labeled as 2 will correspond to column 3 of the matrix.

7 Shock Tube Data Processing Description

A Matlab M- File was written to convert the voltage values stored in the *.mat files to pressure readings and made the processing of test data less tedious (refer to Section 6.3). The M-File written also incorporates a data filtering procedure and a numerical integration procedure that calculates the impulse per unit area experienced by specified pressure transducers. Upon running the M-file, filtered pressure traces are plotted in a Matlab Figure window and the values of impulse per unit area of the selected traces are displayed in the command window. These values of impulse per unit area for selected transducers were then entered into an Excel spreadsheet in order to calculate the impulse amelioration experienced for each test. Values of initial and the final pressures experienced by the end wall of the shock tube were then read of the pressure traces and entered into this spreadsheet. The M-file used in the processing of test data has been included in the DVD accompanying this report for further reference and examples of filtered pressure traces of tests have been listed in Appendix C.

Filtering of the original pressure traces was required as they were noisy and made the reading of pressure values difficult. The filtering procedure averaged every ‘filtervalue’ number of data points to clarify the pressure traces. The value selected for the variable ‘filtervalue’ depended on the sampling frequency of the test being analyzed. Values of this variable used during this study ranged between 5 - 50 data points. The following figures illustrate the difference between an unfiltered and a filtered trace. The pressure traces shown are for a test with a sampling frequency 2.5 MHz and a ‘filtervalue’ of 25. Notice that the filtered pressure trace allows for pressure values to be read off more accurately as the noise in the trace is reduced.

In total 97 tests were performed during which pressure trace data was recorded, 63 photographic tests and 26 transducer calibration tests were performed over the duration of this study, excluding preliminary tests. The data files of all tests performed over the duration of this study, together with their processed pressure traces and photographs have been included in the DVD accompanying this report.

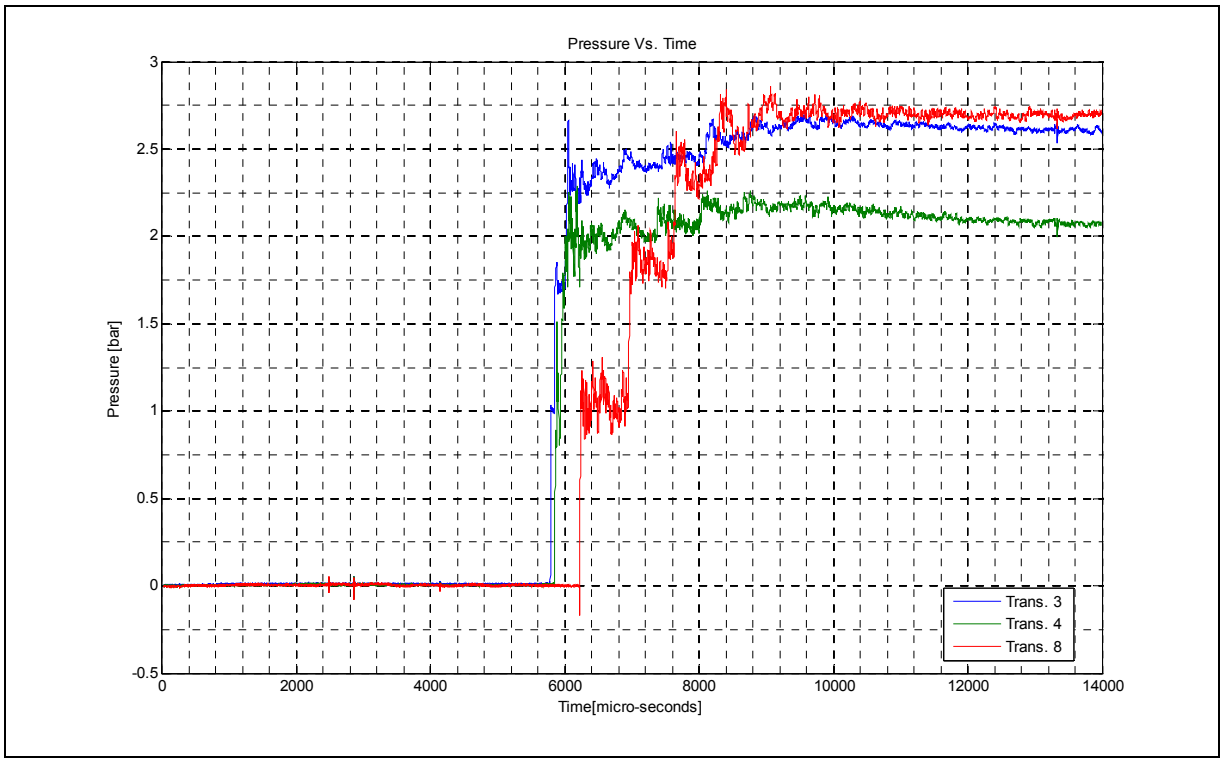


Figure 40: Unfiltered Pressure Traces for Pl1Fr&Pl3Fr - M_{set} = 1.42, P_o = 0.83 bar



Figure 41: Filtered Pressure Traces for Pl1Fr&Pl3Fr - M_{set} = 1.42, P_o = 0.83 bar

8 Processed Shock Tube Data

The tables listed in the subsections that follow summarize the processed data obtained from the 97 pressure trace tests performed. For all these tests, eight transducers were activated. Two transducers were situated upstream of the test section and were used to calculate the actual Mach number for the tests and the remaining six transducers were positioned in the test section. Please refer to Section 4.8, where the locations of the transducers situated in the test section are described.

Note that the 'final' pressure, P_F, listed in the tables that follow is equivalent to the pressure experienced when an incident normal shock wave reflects of the end wall of the tube.

Furthermore, as noted by Britan (2006), the analysis of the impulse results is noted to be the more suitable amelioration measure, as it focuses on the rate of pressure increase dp/dt, acting on the end-wall of the shock tube since most structures are able to withstand a gradual pressure rise better than an instantaneous rise in pressure.

For all tests performed:

- Gauge pressure values are listed i.e. referenced from P_o.
- The atmospheric pressure measured, P_o, was measured to be 0.83 bar
- The time period used for the integration of the end wall pressure traces was 9 250 μs as measured from the first rising edge of the pressure traces.

8.1 Normal Test Data

Normal shock tube tests were performed to obtain the values of initial peak pressure and impulse experienced by the end wall of the shock tube with no test specimens present in the test section. These values were necessary to calculate the initial peak pressure and impulse amelioration percentages of the tests that followed. Section B of the mounting system was present during these tests, as it does affect the normal wave system in the test section; however minimally.

Table 9: Processed Normal Test Data

		Impulse			Pressure	
M_{set}	M_{actual}	End Wall 1 [Pa.s]	End Wall 2 [Pa.s]	Ave. End Wall [Pa.s]	Init. Peak Press. [Bar]	Final Pressure [Bar]
1.42	1.431	2527	2550	2538	3.4	2.75
1.42	1.429	2527	2546	2537	3.4	2.75
1.42	1.417	2563	2571	2567	3.25	2.75
1.42	1.429	2525	2536	2531	3.3	2.75
1.42	1.430	2547	2559	2553	3.5	2.75
1.35	1.355	1752	1761	1756	2.5	2.00
1.23	1.242	1158	1163	1160	1.45	1.25

From the data obtained in the table above, it was decided that the following normal wave initial peak pressure and impulse values would be used in the calculation of the amelioration values for tests that followed.

Table 10: Normal Wave End Wall Initial Peak Pressure and Impulse Values

M_{set}	Initial Peak Pressure [bar]	Impulse [Pa.s]
1.23	1.5	1160
1.35	2.5	1756
1.42	3.4	2544

8.2 Plate Configuration Test Data

This set of tests was performed in order to determine the effect that the plate arrangements and plate combinations had on the end wall initial peak pressure and impulse ameliorations. All tests were performed for a 30 mm distance between plates and for a set Mach number of 1.42. In total 48 tests were performed as each plate combination (12 in total) has four different plate arrangements viz. Front & Front, Front & Back, Back & Front and Back & Back. The processed data for this set of tests are listed in the table that follows.

Table 11: Processed Plate Configuration Test Data

			Impulse						Pressure		
Plate Combo	**Plate Arrangement**	**M_{actual}**	**Ref. Wave** [Pa.s]	**Trapped Wave Data** [Pa.s]	**End Wall 1** [Pa.s]	**End Wall 2** [Pa.s]	**Ave. End Wall** [Pa.s]	**Amelio-ration** [%]	**Init. Peak** [bar]	**Final Press.** [bar]	**Amelio-ration** [%]
Pl1 &Pl2	Fr & Fr	1.422	2545	1180	1736	1747	1742	31.5%	0.43	2.75	87.4%
	Fr & Bk	1.430	2561	877	1715	1725	1720	32.4%	0.45	2.75	86.6%
	Bk & Fr	1.426	2509	811	1716	1727	1722	32.3%	0.45	2.75	86.6%
	Bk & Bk	1.427	2565	1356	1679	1687	1683	33.8%	0.35	2.75	89.6%
Pl1 &Pl3	Fr & Fr	1.423	2473	2043	2289	2292	2291	9.9%	1.15	2.75	65.9%
	Fr & Bk	1.428	2501	2040	2291	2279	2285	10.2%	1.05	2.75	68.8%
	Bk & Fr	1.422	2507	2087	2293	2305	2299	9.6%	1.05	2.75	68.8%
	Bk & Bk	1.426	2553	2080	2323	2337	2330	8.4%	1.05	2.75	68.8%
Pl1 &Pl4	Fr & Fr	1.424	2490	1799	2220	2232	2226	12.5%	0.80	2.75	76.3%
	Fr & Bk	1.428	2539	1917	2225	2238	2232	12.3%	0.75	2.75	77.7%
	Bk & Fr	1.428	2556	1863	2251	2268	2260	11.2%	0.75	2.75	77.7%
	Bk & Bk	1.429	2533	1947	2195	2215	2205	13.3%	0.70	2.75	79.2%
Pl2 &Pl1	Fr & Fr	1.423	2528	2101	1843	1834	1839	27.7%	0.35	2.75	89.6%
	Fr & Bk	1.425	2536	2165	1828	1819	1824	28.3%	0.33	2.75	90.4%
	Bk & Fr	1.427	2557	2087	1824	1837	1830	28.0%	0.30	2.75	91.1%
	Bk & Bk	1.423	2541	2104	1791	1802	1796	29.4%	0.30	2.75	91.1%
Pl2 &Pl3	Fr & Fr	1.427	2526	2125	1893	1884	1889	25.8%	0.60	2.75	82.2%
	Fr & Bk	1.426	2535	2132	1895	1883	1889	25.7%	0.58	2.75	82.9%
	Bk & Fr	1.431	2552	2119	1874	1882	1878	26.2%	0.55	2.75	83.7%
	Bk & Bk	1.428	2547	2207	1865	1881	1873	26.4%	0.50	2.75	85.2%
Pl2 &Pl4	Fr & Fr	1.424	2526	1960	1842	1836	1839	27.7%	0.40	2.70	88.1%
	Fr & Bk	1.429	2564	1925	1854	1839	1846	27.4%	0.40	2.75	88.1%
	Bk & Fr	1.428	2539	1933	1817	1830	1824	28.3%	0.35	2.75	89.6%
	Bk & Bk	1.427	2555	2077	1809	1819	1814	28.7%	0.33	2.75	90.2%
Pl3 & Pl1	Fr & Fr	1.425	2530	1941	2301	2321	2311	9.2%	1.30	2.75	61.4%
	Fr & Bk	1.431	2567	1982	2294	2315	2304	9.4%	1.25	2.75	62.9%

Table 11 continued

Plate Combo	Plate Arrangement	M_{actual}	Ref. Wave [Pa.s]	Trapped Wave Data [Pa.s]	End Wall 1 [Pa.s]	End Wall 2 [Pa.s]	Ave. End Wall [Pa.s]	Amelio-ration [%]	Init. Peak [bar]	Final Press. [bar]	Amelio-ration [%]
Pl3 & Pl1	Bk & Fr	1.425	2553	1968	2323	2345	2334	8.3%	1.28	2.75	62.2%
	Bk & Bk	1.423	2538	1976	2273	2293	2283	10.2%	1.15	2.75	65.9%
Pl3 & Pl2	Fr & Fr	1.425	2537	1225	1744	1756	1750	31.2%	0.55	2.75	83.7%
	Fr & Bk	1.432	2595	844	1763	1776	1770	30.4%	0.58	2.75	82.9%
	Bk & Fr	1.422	2528	1134	1734	1746	1740	31.6%	0.55	2.75	83.7%
	Bk & Bk	1.429	2551	770	1688	1699	1694	33.4%	0.53	2.75	84.4%
Pl3 & Pl4	Fr & Fr	1.407	2542	1769	2325	2346	2336	8.2%	1.35	2.75	59.9%
	Fr & Bk	1.423	2513	1851	2266	2285	2275	10.6%	1.25	2.75	62.9%
	Bk & Fr	1.424	2521	1804	2281	2312	2297	9.7%	1.30	2.75	61.4%
	Bk & Bk	1.431	2583	1758	2331	2353	2342	7.9%	1.25	2.75	62.9%
Pl4 & Pl1	Fr & Fr	1.422	2558	2060	2272	2283	2277	10.5%	0.80	2.75	76.3%
	Fr & Bk	1.430	2567	2065	2240	2260	2250	11.5%	0.80	2.75	76.3%
	Bk & Fr	1.429	2569	1931	2258	2271	2264	11.0%	0.78	2.75	77.0%
	Bk & Bk	1.427	2529	1947	2191	2187	2189	14.0%	0.75	2.75	77.7%
Pl4 & Pl2	Fr & Fr	1.431	2562	1293	1779	1787	1783	29.9%	0.45	2.75	86.6%
	Fr & Bk	1.428	2563	1168	1725	1734	1730	32.0%	0.40	2.75	88.1%
	Bk & Fr	1.428	2560	1255	1738	1748	1743	31.5%	0.38	2.75	88.9%
	Bk & Bk	1.433	2586	854	1725	1737	1731	32.0%	0.38	2.75	88.9%
Pl4 & Pl3	Fr & Fr	1.430	2528	2111	2343	2365	2354	7.5%	1.35	2.75	59.9%
	Fr & Bk	1.420	2502	2051	2305	2298	2302	9.5%	1.30	2.75	61.4%
	Bk & Fr	1.427	2521	2136	2305	2329	2317	8.9%	1.25	2.75	62.9%
	Bk & Bk	1.428	2569	2124	2342	2343	2343	7.9%	1.20	2.75	64.4%

8.3 Plate Separation Distance Test Data

This set of tests was performed in order to determine the effect that the separation distance between test specimens had on the end wall initial peak pressure and impulse ameliorations. Each plate combination was tested at three separation distances viz. d = 30 mm, d = 45 mm and d = 60 mm. It was originally planned to use larger separation distances between plates viz. a maximum of 90 mm. However due to the limiting length of the test section, a maximum separation distance of 60 mm was possible. All tests were performed for a Back & Back plate arrangement and a set Mach number of 1.42.

Table 12: Processed Plate Separation Distance Test Data

			Impulse				Pressure		
Plate Combo.	**Distance** [mm]	**M_{actual}**	**End Wall 1** [Pa.s]	**End Wall 2** [Pa.s]	**Ave. End Wall** [Pa.s]	**Amelioration** [%]	**Init. Peak Press.** [bar]	**Final Press.** [bar]	**Amelioration** [%]
Pl1 & Pl2	30	1.433	1698	1706	1702	33.1%	0.38	2.75	88.9%
	45	1.428	1622	1631	1627	36.1%	0.35	2.75	89.6%
	60	1.431	1583	1592	1587	37.6%	0.35	2.75	89.6%
Pl1 & Pl3	30	1.428	2279	2297	2288	10.0%	1.05	2.75	68.8%
	45	1.427	2294	2310	2302	9.5%	1.05	2.75	68.8%
	60	1.433	2336	2352	2344	7.9%	1.05	2.75	68.8%
Pl1 & Pl4	30	1.426	2179	2203	2191	13.9%	0.68	2.75	80.0%
	45	1.429	2165	2180	2172	14.6%	0.65	2.75	80.7%
	60	1.428	2160	2174	2167	14.8%	0.63	2.75	81.5%
Pl2 & Pl1	30	1.429	1805	1800	1802	29.1%	0.30	2.75	91.1%
	45	1.432	1784	1777	1780	30.0%	0.30	2.75	91.1%
	60	1.424	1751	1760	1756	31.0%	0.30	2.75	91.1%
Pl2 & Pl3	30	1.43	1880	1887	1884	26.0%	0.50	2.75	85.2%
	45	1.43	1858	1851	1854	27.1%	0.48	2.75	85.9%
	60	1.431	1874	1887	1881	26.1%	0.48	2.75	85.9%
Pl2 & Pl4	30	1.423	1793	1801	1797	29.4%	0.33	2.75	90.4%
	45	1.432	1802	1808	1805	29.0%	0.32	2.75	90.5%
	60	1.425	1754	1759	1756	31.0%	0.32	2.75	90.5%
Pl3 & Pl1	30	1.427	2269	2286	2278	10.5%	1.05	2.75	68.8%
	45	1.429	2271	2286	2279	10.4%	1.05	2.75	68.8%
	60	1.424	2211	2227	2219	12.8%	1.05	2.75	68.8%
Pl3 & Pl2	30	1.428	1726	1735	1730	32.0%	0.53	2.75	84.4%
	45	1.429	1663	1672	1668	34.4%	0.53	2.75	84.4%
	60	1.429	1601	1609	1605	36.9%	0.53	2.75	84.4%
Pl3 & Pl4	30	1.429	2289	2303	2296	9.7%	1.15	2.75	65.9%
	45	1.427	2255	2274	2264	11.0%	1.15	2.75	65.9%
	60	1.425	2237	2254	2246	11.7%	1.10	2.75	67.4%

Table 12 continued

Plate Combo.	Distance	M_{actual}	End Wall 1	End Wall 2	Ave End Wall	Amelioration	Init. Peak Press.	Final Press.	Amelioration
	[mm]		[Pa.s]	[Pa.s]	[Pa.s]	[%]	[bar]	[bar]	[%]
Pl4 & Pl1	30	1.428	2176	2199	2188	14.0%	0.68	2.75	80.0%
	45	1.429	2176	2190	2183	14.2%	0.70	2.75	79.2%
	60	1.427	2156	2172	2164	14.9%	0.65	2.75	80.7%
Pl4 & Pl2	30	1.431	1715	1725	1720	32.4%	0.38	2.75	88.9%
	45	1.428	1634	1643	1638	35.6%	0.36	2.75	89.3%
	60	1.429	1571	1581	1576	38.1%	0.35	2.75	89.6%
Pl4 & Pl3	30	1.429	2298	2304	2301	9.5%	1.15	2.75	65.9%
	45	1.431	2348	2363	2355	7.4%	1.15	2.75	65.9%
	60	1.427	2308	2325	2316	8.9%	1.10	2.75	67.4%

8.4 Mach number Test Data

The table that follows lists the processed data for the three plate combinations analyzed in order to determine the effect that incident Mach number had on end wall initial peak pressure and impulse ameliorations. The plate combinations were chosen randomly and each was tested for set Mach numbers of 1.23 and 1.35. The data obtained for M_{set} = 1.45 were taken from the Plate Configuration Test Data (Please refer to Table 11) listed previously. All tests were performed for a 30 mm separation distance between plates and a Back & Back plate arrangement.

Table 13: Processed Mach number Test Data

			Impulse				Pressure		
Plate Combo	M_{set}	M_{actual}	End Wall 1 [Pa.s]	End Wall 2 [Pa.s]	Ave. End Wall [Pa.s]	Amelioration [%]	Init. Peak [Bar]	Final Press. [Bar]	Amelioration [%]
Pl4 & Pl3	1.23	1.244	1061	1067	1064	8.3%	0.65	1.25	55.2%
	1.35	1.346	1603	1613	1608	8.4%	0.94	1.95	62.4%
	1.42	1.427	2309	2326	2318	8.9%	1.15	2.75	65.9%
Pl3 & Pl2	1.23	1.244	775	778	777	33.1%	0.28	1.22	81.0%
	1.35	1.343	1174	1180	1177	33.0%	0.45	1.88	82.0%
	1.42	1.429	1602	1610	1606	36.9%	0.55	2.68	83.7%
Pl3 & Pl4	1.23	1.245	1032	1037	1034	10.9%	0.63	1.26	56.6%
	1.35	1.331	1558	1569	1563	11.0%	0.90	1.90	64.0%
	1.42	1.425	2240	2257	2248	11.6%	1.20	2.75	64.4%

9 Results and Discussion

9.1 Orifice Plate Calibration

A brass orifice plate was manufactured and calibrated in order to determine the air flow rate passing through the Calibration Duct when determining the directional properties of the metal test specimens. Table 5 and Table 6 list the data obtained during the calibration of the orifice plate. For each pressure differential value that occurred across the orifice plate, three values of flow rate were recorded during testing in order to verify the data and to ensure that the exiting air flow was steady. For both test data sets, the average of these flow rate values were then calculated and are plotted against the corresponding pressure differential values that occurred across the orifice plate in the figure below. Using the equations and the iterative procedure set out by the British Standards Institution (BS EN ISO 5167-1: 1997 with Amendments until Feb 1999), values of the theoretical flow rates were calculated and are also illustrated on the plot.

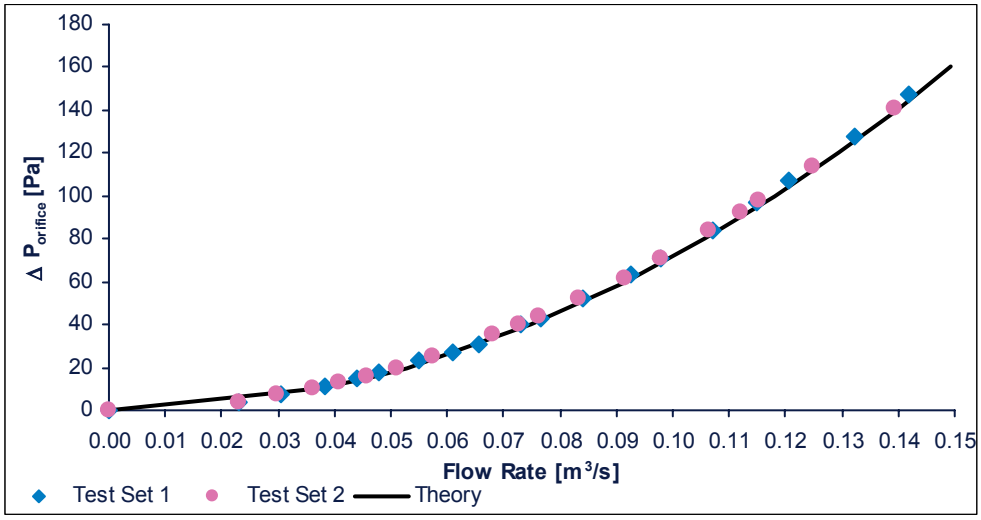


Figure 42: Orifice Plate Calibration Curve

The figure above indicates that the data obtained during the calibration process was highly accurate as it does not deviate greatly from the theoretical line. For all data points collected, the maximum deviation from the theoretical flow rate was calculated to be within 5 % as noted in Table 5 and Table 6.

9.2 Directionality of Test Specimens

Tests measuring the pressure differentials that occurred across each specimen for both instances of the front and the back of the specimen facing the oncoming flow were conducted in order to determine the directional properties of the test specimens and to obtain an indication of their resistance to flow. Table 7 lists the data obtained for these pressure differential tests. Each specimen was tested at three different air flow rates for both the instances of its front and back facing the oncoming flow. The air flow rates chosen for testing fell in the range between 0.036 m^3/s to 0.073 m^3/s. This range was selected as it provided the most steady air flow through the duct and allowed for accurate pressure measurements to be taken. Due to the high resistance of Plate 2 (with its back facing the oncoming flow), the maximum flow rate achievable through the duct was approximately 0.051 m^3/s. Therefore the flow rates at which tests were performed on this specimen had to be lower in value and differ from the flow rates selected for the other test specimens, as seen in Table 7.

The pressure differential results that occurred across Plate 1 for both instances of the front and the back of the specimen facing the oncoming flow are illustrated in the figure below.

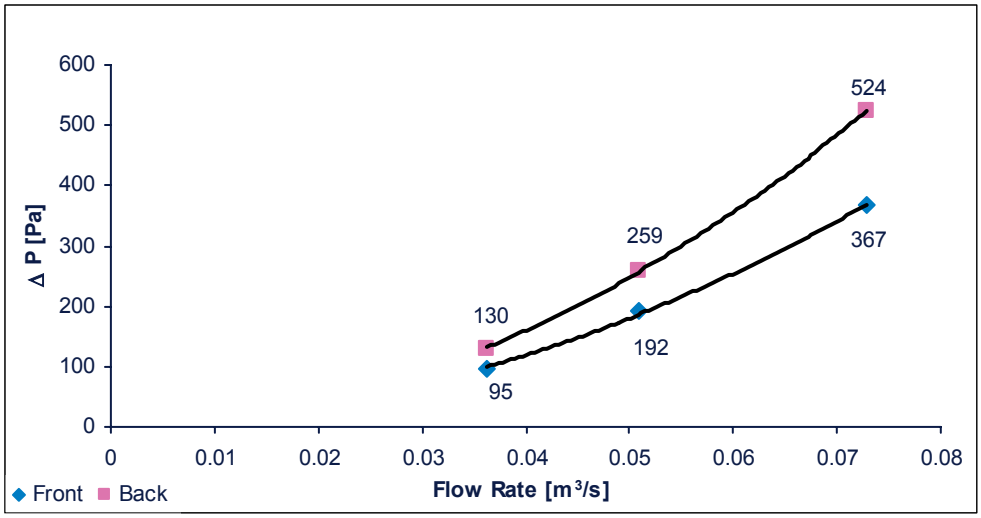


Figure 43: Pressure Differential Results for Plate 1

The figure clearly indicates the directional properties of the test specimen, as lower pressure differential values were recorded with the front of the plate facing the oncoming flow. This result was expected, for the holes with the larger diameter were facing the flow in this testing condition offering a lower resistance to the air flow and thus producing lower drag coefficient for the plate. Furthermore, a quadratic curve fit

best describes the trend of data for both the front and the back of the plate facing the oncoming flow, which is characteristic of drag coefficient, C_d, versus dynamic pressure, q, plot.

The pressure differential results that occurred across plate 2 are shown in the figure below.

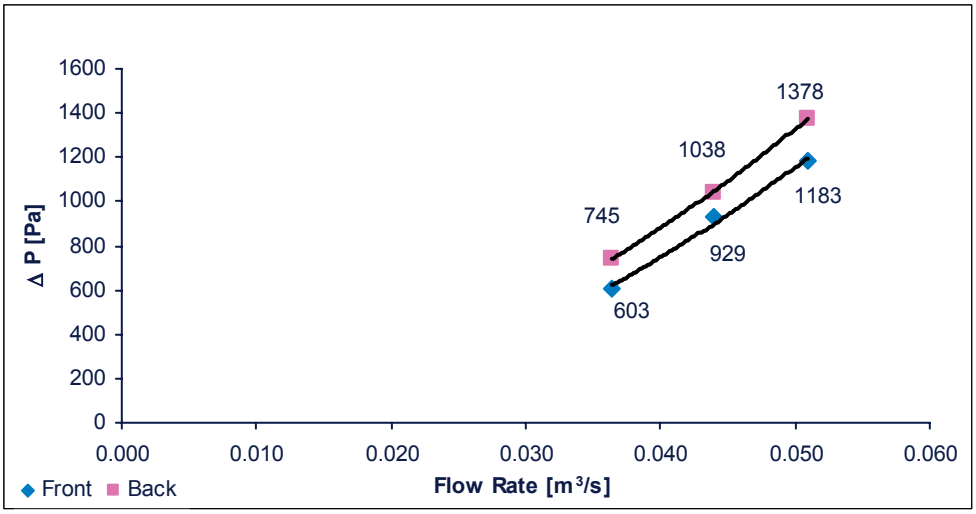


Figure 44: Pressure Differential Results for Plate 2

As noticed the results reveal the same data trends noted for Plate 1. It is noticed that lower pressure differential values are obtained with the front of the plate facing the oncoming flow indicating the directionality of the specimen and that a quadratic curve fits best describe the trend of data for both the front and the back of the plate facing the oncoming flow.

Since the results of the remaining specimens also exhibit the same data trends, their figures have been omitted; however these figures have been included in the DVD accompanying this report for further reference.

Table 14, that follows, summarizes the pressure differential results, extracted from Table 7 that occurred across each specimen for an air flow of 0.036 m^3/s, which corresponds to a 10 Pa pressure differential across the orifice plate i.e. $\delta P_{Orifice} = 10$ Pa.

Table 14: Summarized Pressure Differential Results for Test Specimens - Air Flow Rate = 0.036 m^3/s

Plate	Porosity	$\delta P_{Orifice}$	V_{Exit}	Flow Rate	Front ΔP	Back ΔP	Difference
	[%]	[Pa]	[m/s]	[m^3/s]	[Pa]	[Pa]	[%]
Plate 1	17.2	10	2.69	0.036	94.5	130	37.6%
Plate 2	6.6	10	2.69	0.036	603	745	23.5%
Plate 3	41.1	10	2.69	0.036	14.5	20	37.9%
Plate 4	19	10	2.69	0.036	91	136.5	50.0%

These results have been plotted in the figure that follows according to the plate number. The figure clearly indicates that the back of the plate offers greater resistance to the oncoming air flow and therefore a greater pressure differential occurs across all the plates.

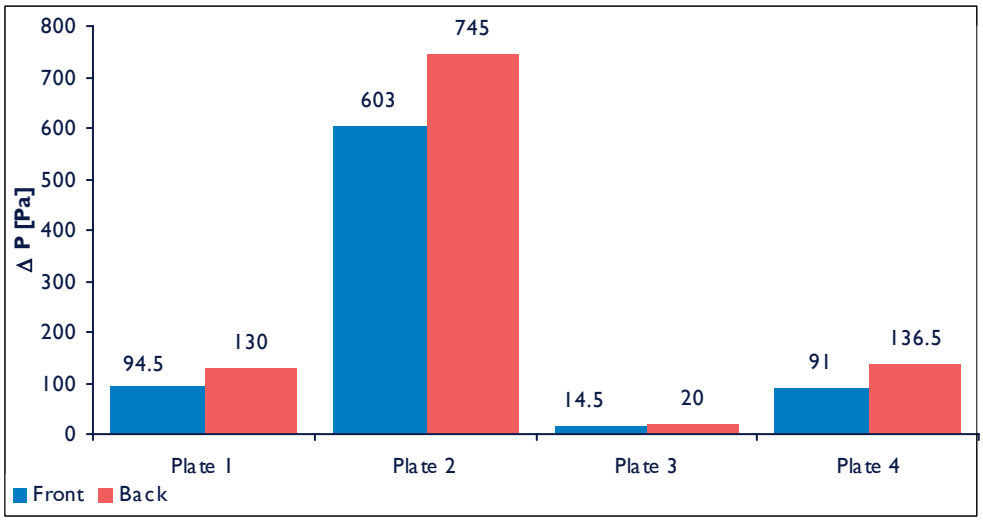


Figure 45: Pressure Differential Results for Test Specimens - Air Flow Rate = 0.036 m^3/s

In Figure 46, that follows, the data listed in Table 14 has been plotted according to increasing plate porosity. The percentage difference, by which the pressure differential for the back of the plate facing the oncoming flow is greater than when the front of the plate faces the oncoming flow, is also illustrated in the figure in order to illustrate the directionality of each plate.

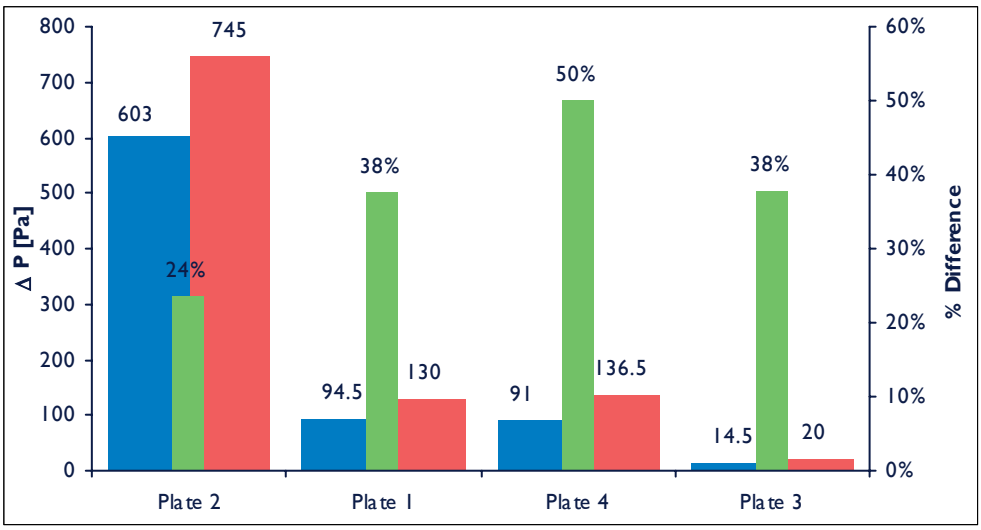


Figure 46: Pressure Differential Results for Test Specimens Arranged According to Increasing Plate Porosity - Air Flow Rate = 0.036 m^3/s

As expected, the pressure differential that occurs across each plate reduces in value as the porosity of the plate increases and offers less resistance to the oncoming flow. Plate 2 has the greatest resistance to flow and this result corresponds to it having the lowest porosity (6.6 %). Similarly, Plate 3 has the least resistance to flow as it has the highest porosity (41.1 %). Since the porosities of Plate 1 and Plate 4 are similar, so are the pressure differentials that occur across them.

The directionality of the plates is also noted to increase as the porosity increases until a maximum value of 50 % is reached. Thereafter the further increase in porosity reduces the directionality of the plate. Plate 3 is noted to have a large porosity (41.1 % as compared to 19 %, 17.2 % and 6.6 %) which corresponds to an open structure. Therefore the resulting reduction in directionality may be attributed to the fact that as the porosity of the plate increases, the plate becomes largely open in structure which reduces its directional properties.

9.3 Normal Shock Tube Tests

The values of the initial peak pressure and impulse experienced by the end wall of the shock tube with no test specimens present in the test section, i.e. P_{Bare} and I^*_{Bare}, had to be determined first in order to calculate the initial peak pressure amelioration and impulse amelioration that occurred for each test. These values were obtained by conducting normal shock tests with Section B of the Mounting System present in the test section, since this mounting section is present in the test section for all tests and does affect the pressure readings captured by the test section transducers. The presence of Section B of the mounting system reduces the effective area exposed to the incident shock wave and reflects part of the incident wave before it impacts off the end wall. Therefore, in order to eliminate the pressure effects caused by Section B, it is taken as the base case to which the results obtained for tests conducted in this study were compared.

Since the majority of tests in this study were performed for a set incident Mach number of 1.42, five normal shock tests were performed for this Mach number and the average values of initial peak pressure and impulse experienced by the end wall of the shock tube were then used in calculations. The results of these tests are listed in Table 9. It was found that the values obtained for these tests varied within 2 % of each other and repetition of tests was not required as the values recorded were sufficiently accurate. Therefore only one test was performed for each of the remaining set incident Mach numbers viz. M_{set} = 1.23 and M_{set} = 1.35. The results of these tests are listed in Table 9.

The following figure displays the pressure experienced by the end wall of the shock tube upon impact with a normal shock wave set at M = 1.42, for the instances when Section B is absent (blue trace) and present (red trace) in the test section.

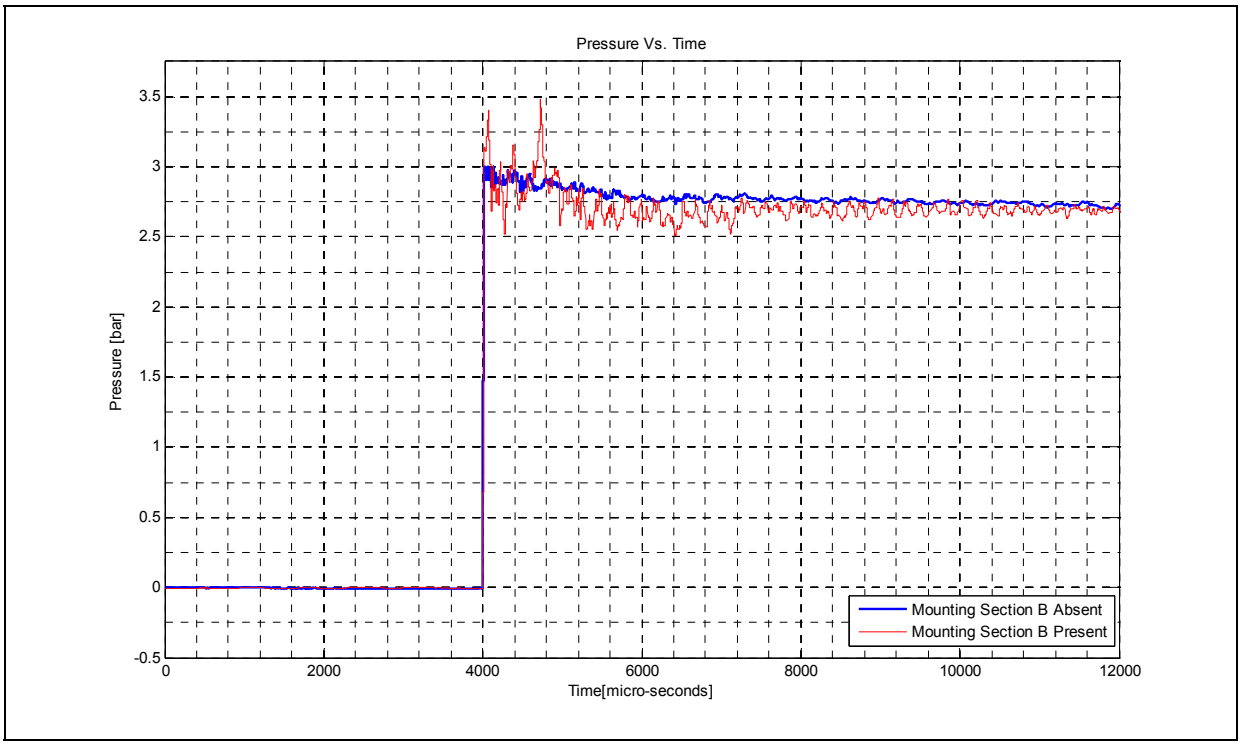


Figure 47: Overlay of Normal Pressure Traces with Section B of Mounting System Present and Absent In Test Section

The pressure trace with Section B present in the test section is nosier than that obtained with it absent due to the wave reflections caused by the edges of the base and 'bending moment' plates. Comparison of the pressure traces also reveal that the impulse experienced is lower and that the initial peak pressure experienced is higher in the case with Section B present. The majority of the pressure trace obtained when Section B is present, is seen to be below the trace obtained for when the section was absent and therefore the impulse value recorded was found to be lower for this case. Reduced impulse values, although little (ranging between 2 % to 4 %), were obtained for all tests performed when Section B was present in the test section. As mentioned earlier this reduction in impulse is due to the presence of the mounting system which reflects part of the incident wave before it impacts of the end wall. Furthermore, a portion of the incident wave's energy and impulse is also dissipated through turbulence created upon interacting with the mounting section. It must be noted that the difference in impulse amelioration values calculated using the values of impulse obtained either with or without Section B present in the test section, are small and may be neglected.

The initial increase in peak pressure was calculated to be approximately 10 % greater than the absent case. This increase could be attributed to the process of the incident shock moving into a reduced test section area, 'converging duct', as well as the reinforcement of the reflected waves created off the edges

of the base plates as shown in the schlieren photograph that follows. It must be noted that the use of the higher initial peak pressure value obtained with Section B present in the test section leads to a conservative approach being adopted in the calculation of the initial peak pressure amelioration values.

The turbulent flow created by the presence of the 'bending moment' plates is clearly shown in the schlieren photograph below. This turbulent flow contributes to the pressure fluctuations that occur in the end wall pressure traces. The reflected waves of the base plates are also clearly visible in the photograph and are noted to be out of plane as they travel upstream.

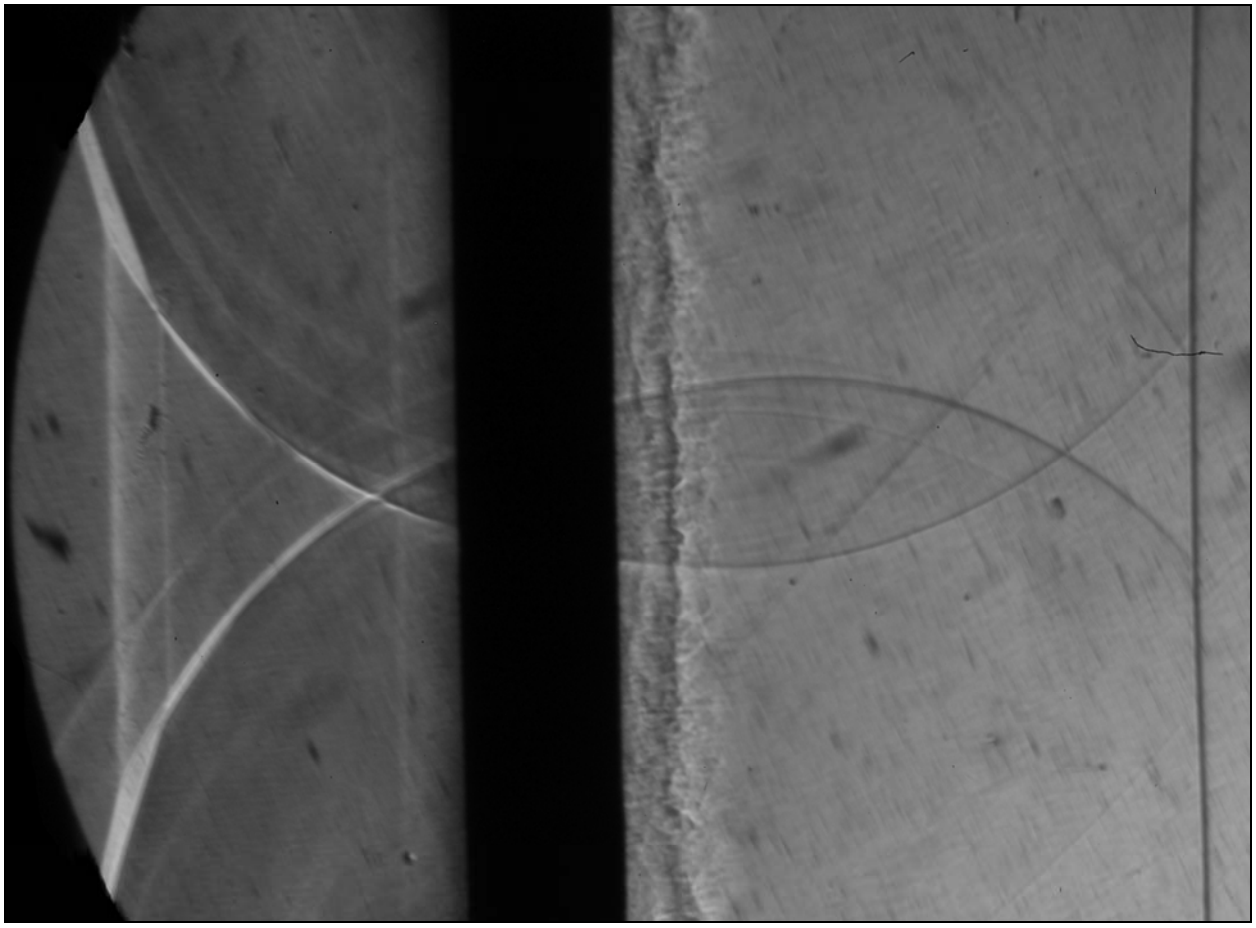


Figure 48: Photograph of a Normal Shock Wave Passing Through the Test Section with Mounting Section B Present

The end wall of the shock tube is situated to the right of the picture shown above. It is noticed that slight distortion of the incident shock wave occurs at either end. However the shock wave remains plane and normal in the center of the test section, where all pressure readings were taken during testing.

9.4 Analysis of the Effects of Plate Arrangement

As two plates are mounted in the test section for each test, and since four test specimens were used in this study, twelve plate combinations are possible. Furthermore, since each plate may have either its front or back facing the incident shock wave, four arrangements for each plate combination is achievable. Therefore, in order to determine the effects that the plate properties and their placement have on the end wall impulse, all forty-eight different plate configurations were tested. Please refer to Section 4.6.4 for a detailed explanation of the calculation of the plate configurations possible.

The initial peak pressure and impulse amelioration results obtained for the forty eight tests are listed in Table 11. It is important to note that all tests were performed with a 30 mm separation distance between plates and for a set Mach number of 1.42 i.e. M_{set} =1.42. The ambient atmospheric pressure, P_o, was measured to be 0.83 bar and the time period used for the integration of the end wall pressure traces was 9 250 μs as measured from the first rising edge of the of these pressure traces. Please refer to Table 11.

In order to determine the effects of plate arrangement on the end wall initial pressure and impulse amelioration, each plate combinations was tested for the four plate arrangements. The four pressure trace results obtained for each plate combination were then over-laid for comparison. The figure that follows displays the results obtained for plate combination Pl1&Pl2. The pressure trace of a normal shock wave, M_{set} =1.42, is also overlaid in the figure to illustrate the significant initial peak pressure amelioration achieved.

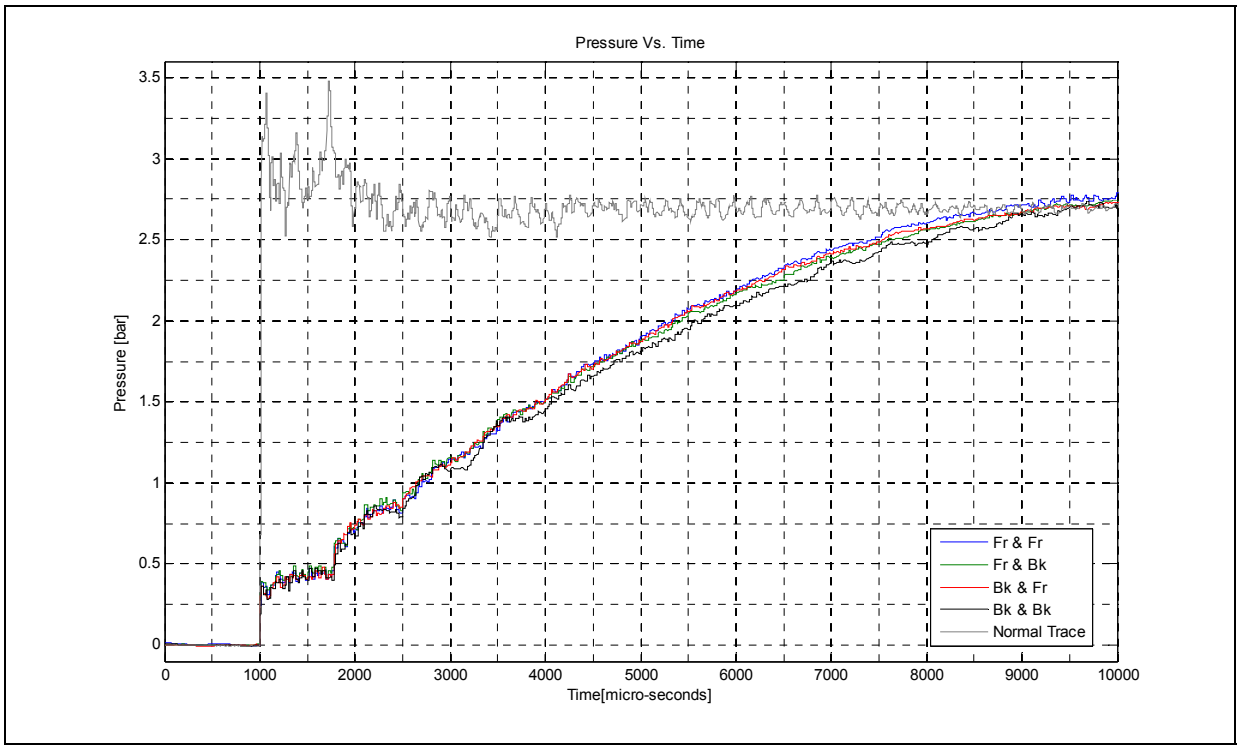


Figure 49: Overlay of End Wall Plate Arrangement Pressure Traces for Pl1&Pl2 - M_{set} =1.42

For all twelve plate combinations, it was found that the pressure trace plots obtained for each plate arrangement varied slightly from each other as seen in the figure above. However, for all twelve plate combinations the pressure trace for Back & Back arrangement deviates from the traces of the other arrangements some time (approximately 4000 μs in the above diagram) after incidence with the end wall, displaying lower pressure readings and taking longer to reach P_F, 'final' pressure.

9.4.1 The Effects of Plate Arrangement on the Initial Peak Pressure Amelioration Experienced by the End Wall

Figure 50 illustrates the values of initial peak pressure amelioration obtained for each of the forty eight plate configurations possible. By grouping the data according to plate arrangement, the general data trend is illustrated. The figure indicates that for each plate combination, the initial peak pressure amelioration values are similar for the four plate arrangements. However, upon closer inspection it is noticed that the general trend of data indicates that the Back & Back plate arrangement produces the greatest initial peak pressure amelioration for each plate combination, while the Front & Front arrangement produces the lowest.

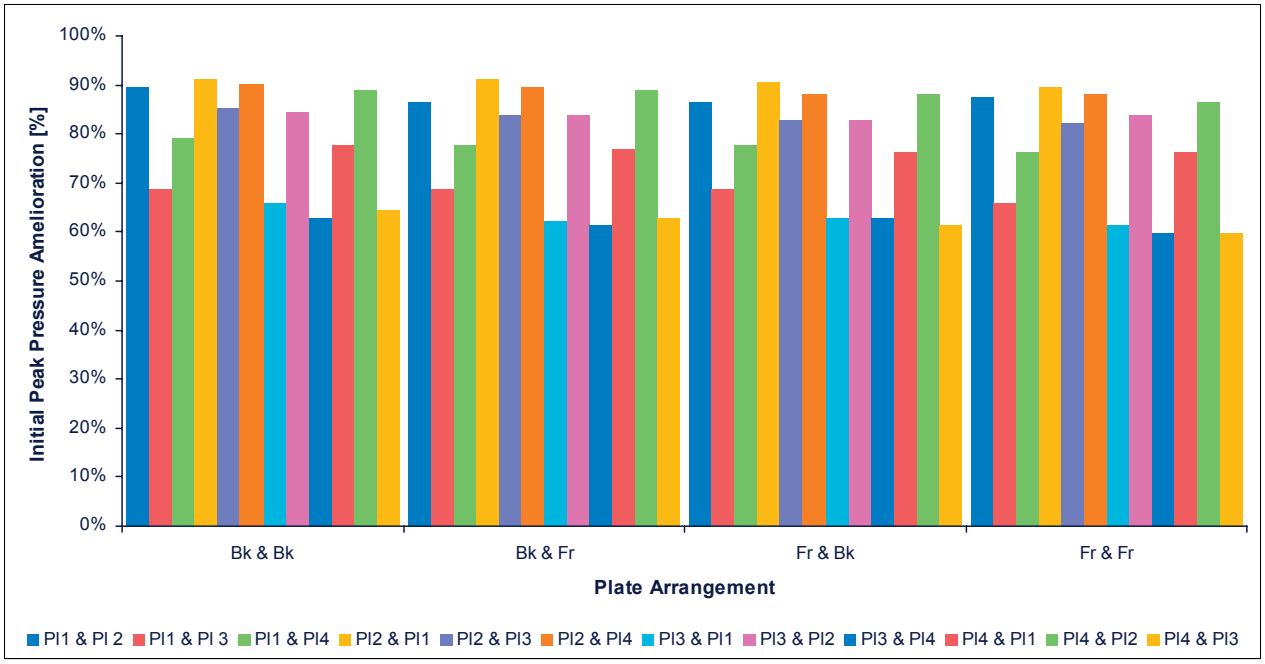


Figure 50: Initial Peak Pressure Amelioration Values Obtained for the Various Plate Arrangements

Figure 51 that follows illustrates the initial peak pressure amelioration experienced by the end wall of the shock tube, with the results rearranged and grouped according to plate combination. By regrouping the results according to plate combination, the plate combinations that produce the largest initial peak pressure amelioration are easier to distinguish. Furthermore, it is also easier to distinguish the general trend that the Back & Back plate arrangement produces the greatest initial peak pressure amelioration and that the Front & Front arrangements produce the lowest initial peak pressure amelioration for each plate combination.

It is noted that combinations Pl1&Pl2, Pl2&Pl1, Pl2&Pl4, Pl3&Pl2 and Pl4&Pl2 produce the greatest initial peak pressure amelioration, with amelioration values greater than 80 %. The remaining plate combinations produced end wall pressure amelioration values less than 80 %, but greater than 50 %.

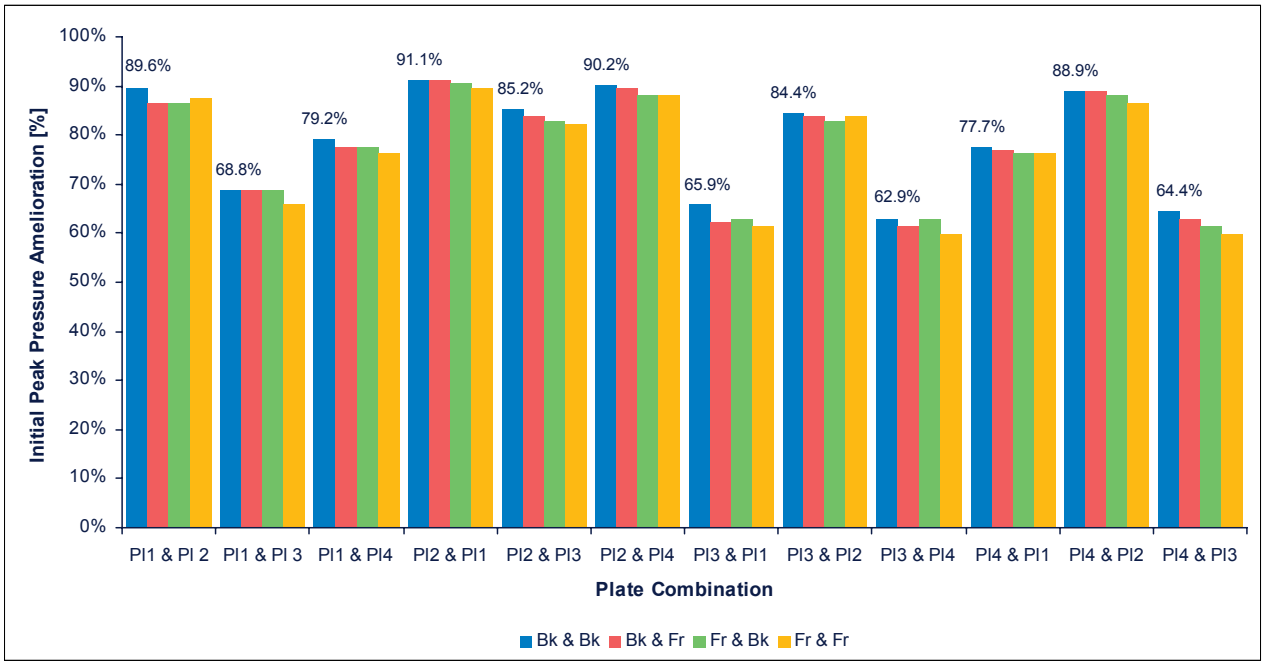


Figure 51: Initial Peak Pressure Amelioration Values Obtained for the Various Plate Combinations

In order to verify that the Back & Back arrangement produces the greatest initial peak pressure amelioration and that the Front & Front arrangements produce the lowest pressure amelioration for each plate combination, the average pressure amelioration value was calculated for each plate arrangement and the results are illustrated in the figure below.

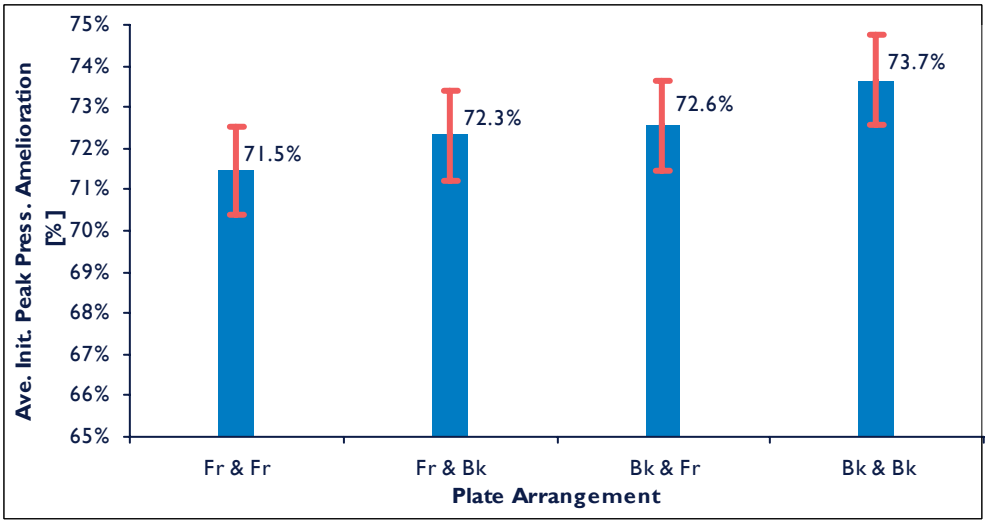


Figure 52: Average Initial Peak Pressure Amelioration Values Obtained For Each Plate Arrangement

Using a conservative approach, it was estimated that the initial peak pressure amelioration values had an uncertainty of approximately 1.5 % and these error bounds have been included in the previous figure. Taking these error bounds into consideration, it is clearly noticeable that the Front & Front arrangements produced the lowest initial peak pressure amelioration with an average value of 71.5 %, while the Back & Back arrangement produced the greatest pressure amelioration with an average value of 73.7 %. However one cannot differentiate which of the Front & Back and Back & Front arrangements produce greater amelioration when one takes the uncertainty of their values into account. These arrangements produce similar average initial peak pressure amelioration values with negligible difference, which fall in between the lowest and highest amelioration values i.e. 71.5 % and 73.7 % respectively.

These results are attributed to the fact that the Back & Back plate arrangement poses the greatest resistance to the incident shock wave and produces the greatest average initial peak pressure amelioration. However; the Front & Front arrangement poses the least resistance and therefore produces the lowest average initial peak pressure amelioration. Since the Front & Back and Back and Front arrangements have the similar resistance, they produce average pressure amelioration values that deviate little from each other.

9.4.2 The Effects of Plate Arrangement on the Impulse Amelioration Experienced by the End Wall

The results of the end wall impulse amelioration analysis reveal similar results obtained from the analysis of the initial peak pressure amelioration values. This was expected as both quantities illustrate the extent of damage that an incident shock wave is capable of inflicting. As noted previously, the impulse amelioration analysis is a more suitable measure of the destructive capability of an incident shock or blast wave, as it also incorporates the effect of the rate of pressure increase acting on the end-wall of the shock tube. Furthermore, it was found that the results obtained from the impulse amelioration analysis reveal more distinct/clear data trends.

Figure 53 that follows, illustrates the values of impulse amelioration obtained for each of the forty eight plate configurations. By grouping the data according to plate arrangement, it is noticed that for each plate combination, the amelioration values are similar. Upon further inspection, it is seen that the general trend of data indicates that the Back & Back plate arrangement produces the greatest impulse amelioration for each plate combination, while the Front & Front arrangement produces the lowest.

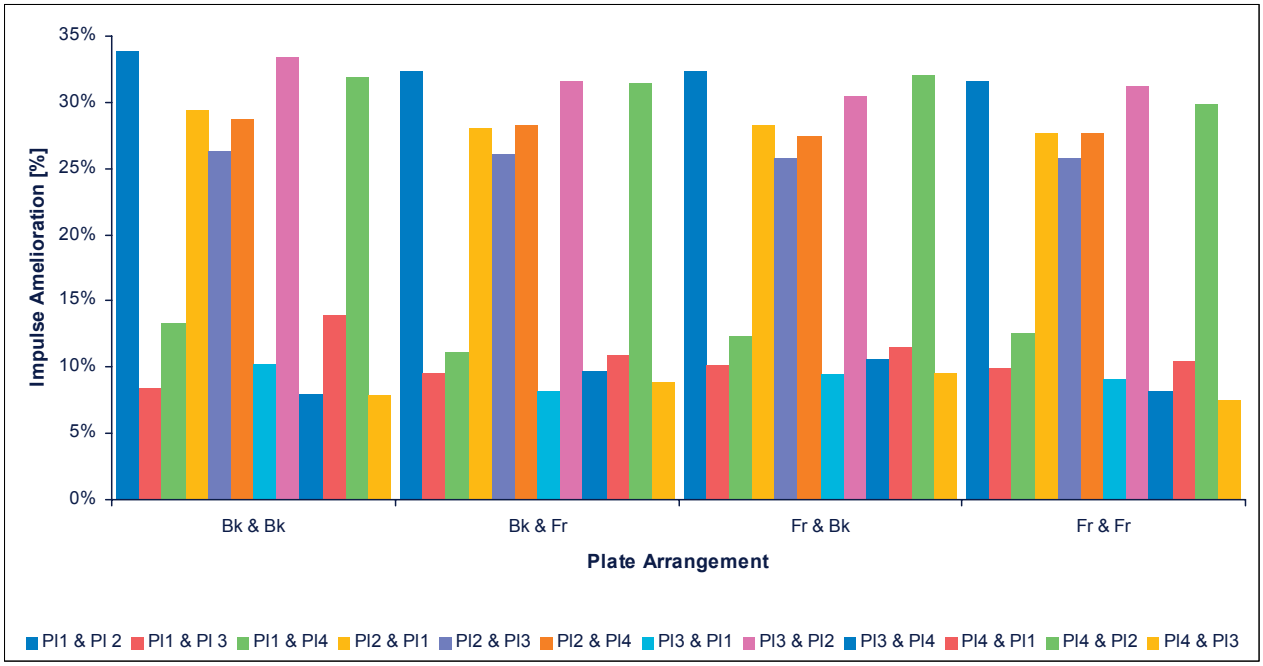


Figure 53: Impulse Amelioration Values Obtained for the Various Plate Arrangements

Figure 54 that follows, illustrates the impulse amelioration experienced by the end wall of the shock tube, with the results rearranged and grouped according to plate combination. By regrouping the results according to plate combination, the plate combinations that produce the largest impulse amelioration are easier to distinguish. It is also easier to distinguish the general trend that the Back & Back plate arrangement produces the greatest impulse amelioration and that the Front & Front arrangements produce the lowest impulse amelioration for each plate combination.

It is noted that combinations Pl1&Pl2, Pl3&Pl2 and Pl4&Pl2 produce the greatest end wall impulse amelioration for each arrangement, with impulse amelioration values greater than 30 %. Furthermore, the amelioration values obtained for combinations Pl2&Pl1, Pl2&Pl3 and Pl2&Pl4 are also large, with values greater than 25 %. The remaining plate combinations produced end wall pressure amelioration values less than 15 %.

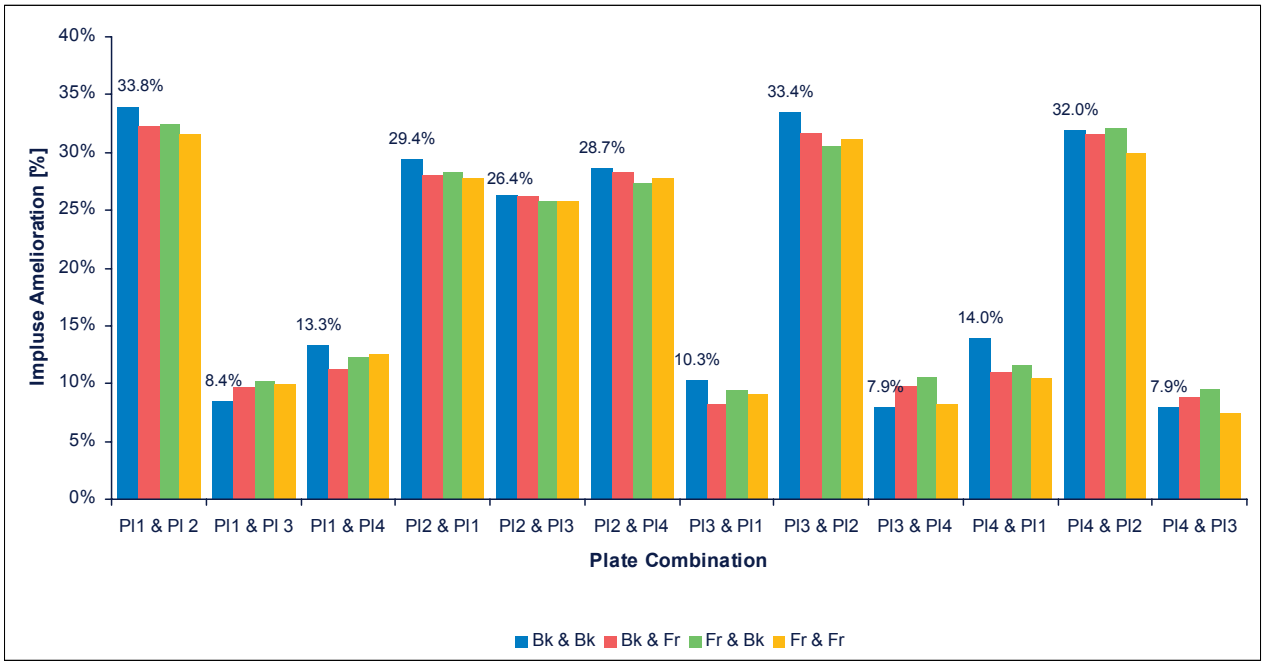


Figure 54: Impulse Amelioration Values Obtained for the Various Plate Combinations

As previously performed in the initial peak pressure amelioration analysis, the average impulse amelioration value was calculated for each plate arrangement and the results are illustrated in the figure below.

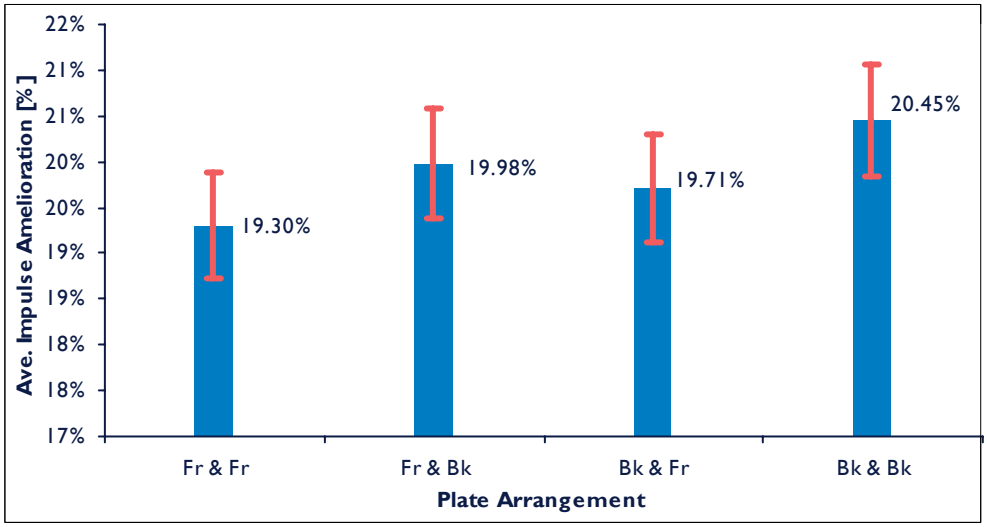


Figure 55: Average Impulse Amelioration Obtained For Each Plate Arrangement

An error analysis of the impulse readings was performed since the average impulse values obtained for each of the plate arrangements were so similar. Using a conservative approach, it was estimated that the

impulse amelioration values had a 3 % uncertainty and these error bounds have been included in the previous figure. Taking these error bounds into consideration it is clearly noticeable that the figure illustrates the same data trend noticed in the average initial peak pressure results (please refer to Figure 52). The Front & Front arrangements produced the lowest impulse amelioration with an average value of 19.3 %, while the Back & Back arrangement produced the greatest impulse amelioration with an average value of 20.45 %. Once again, one cannot differentiate which of the Front & Back and Back & Front arrangements produce greater amelioration when one takes the uncertainty of their values into account. These arrangements produce average amelioration values with negligible difference, which fall in between the lowest and highest amelioration values viz. 19.3 % and 20.45 % respectively.

As explained previously, these results are attributed to the fact that the Back & Back plate arrangement pose the greatest resistance to the incident shock wave and produces the greatest average impulse amelioration. However; the Front & Front arrangement poses the least resistance and therefore produces the least average impulse amelioration. Since the Front & Back and Back & Front arrangements have the same resistance, they produce similar average impulse amelioration values. These results indicate that the resistance to the oncoming flow is the more dominant feature than the process of shock wave trapping, as the Back & Back plate combinations produce higher amelioration values than the Back & Front plate arrangement. Furthermore, since the calculation of the impulse amelioration values incorporate the effect of the rate of pressure increase acting on the end-wall of the shock tube, larger differences between impulse amelioration values for plate combinations are noticed when compared to the results obtained for the initial peak pressure amelioration analysis. For example, consider the Back & Back plate arrangement for plate combinations Pl1&Pl2 and Pl1&Pl3. The initial peak pressure ameliorations are 89.6 % and 68.8 % respectively; whereas the impulse amelioration values for these combinations are 38.8 % and 8.4 % respectively.

Therefore, from the analysis of results for the plate arrangement tests it is concluded that the Back & Back plate arrangement produces the greatest initial peak pressure and impulse amelioration values in general. Therefore, in order to reduce the number of tests to be performed it was decided that the Back & Back arrangement would be used for the remaining tests of the study.

9.5 Analysis of the Effects of Plate Combination

In this section, the initial peak pressure amelioration and the impulse amelioration results obtained for the Back & Back plate arrangement are analyzed in order to determine the effects that the plate combinations have on the end wall amelioration values. As noted previously, the results of the Back & Back plate arrangements are only analyzed as it was determined that in general this plate arrangement produces the greatest initial peak pressure and impulse amelioration values.

The data used in this section was extracted from Table 11 and is therefore the same data used in the Plate Arrangement analysis. The figures that follow illustrate the initial peak pressure amelioration and the impulse amelioration achieved on the end wall of the shock tube for the twelve plate combinations used in this study.

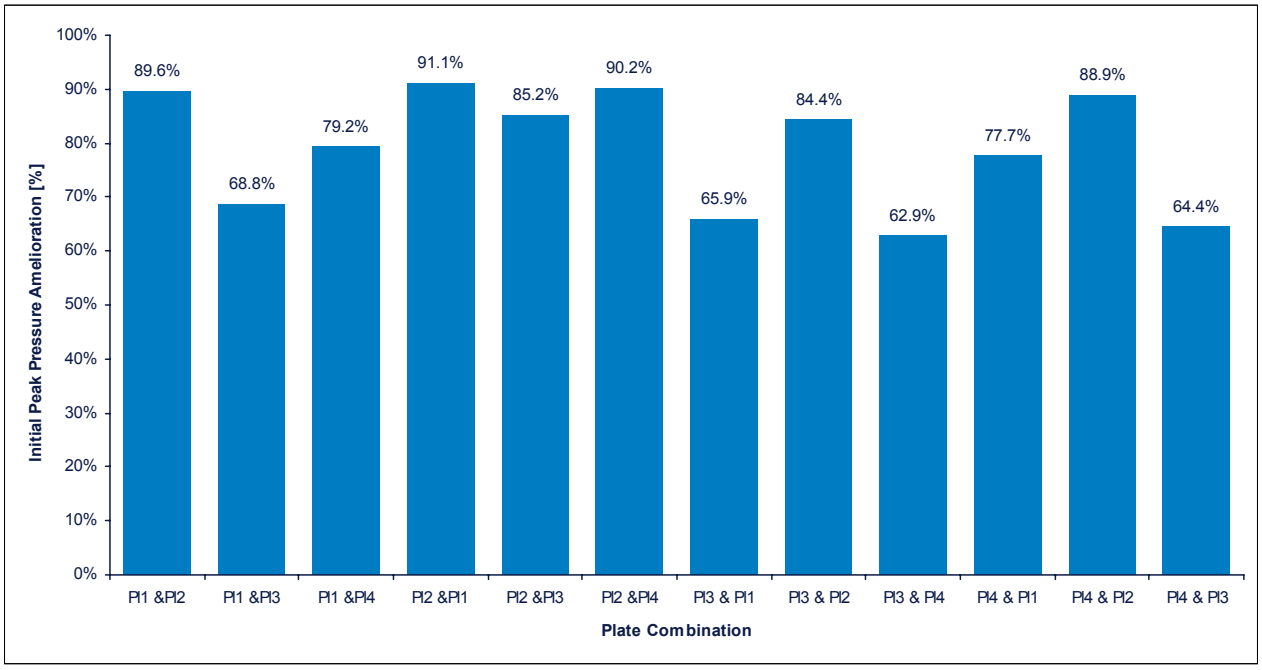


Figure 56: Initial Peak Pressure Amelioration Values Obtained for the Various Plate Combinations - Back & Back Plate Arrangement

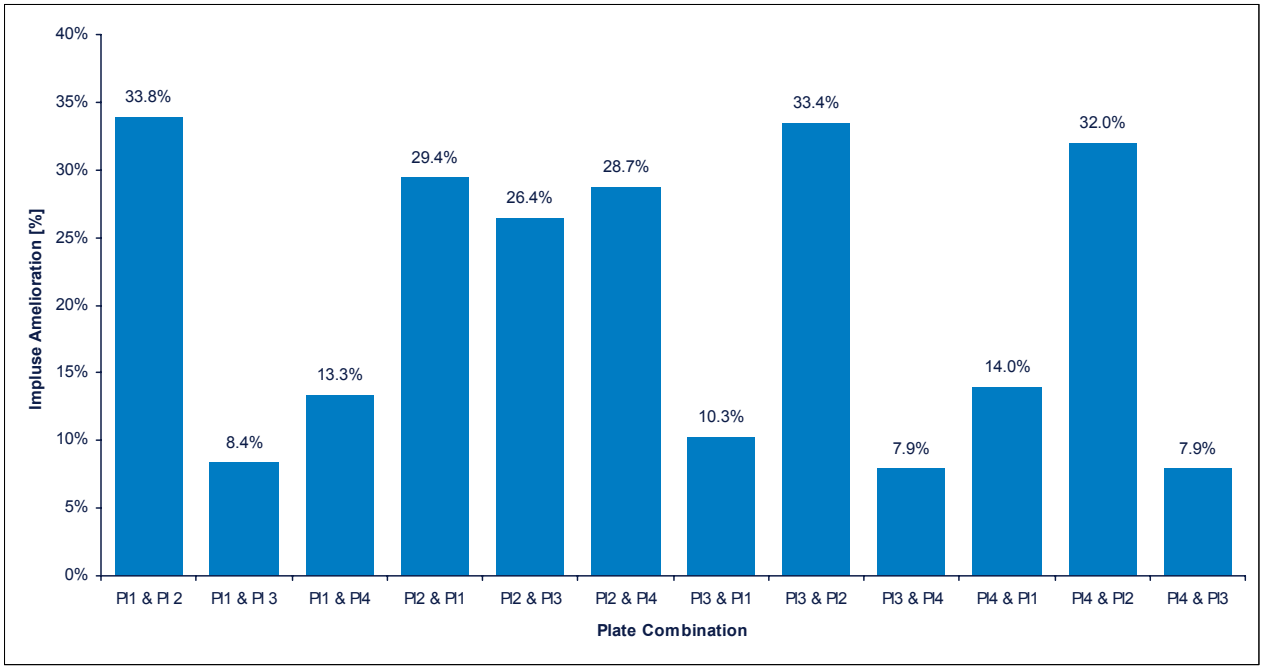


Figure 57: Impulse Amelioration Values Obtained for the Various Plate Combinations - Back & Back Plate Arrangement

In the previous figures, it is noticed that combinations in which Plate 2, which has the lowest porosity, is present produce the highest initial peak pressure and impulse ameliorations. The remaining plate combinations, in which Plate 2 is absent, produce significantly lower initial peak pressure and impulse amelioration values. It is also noticed that complementary plate combinations e.g. Pl1&Pl2 and Pl2&Pl1, produce differing initial peak pressure and impulse amelioration results. This result was expected as different wave interactions occur when plate positions, either upstream or downstream, are interchanged.

The initial peak pressure amelioration results indicate that for all complementary plate combinations, the combinations which have the lower porosity plates, with higher resistances to the oncoming flow, situated downstream produce larger amelioration values. The difference in initial peak pressure amelioration values for all complementary plate combinations is small (< 3 %) though. These results indicate that maximum initial pressure amelioration is achieved by placing the less porous of any two plates under consideration downstream, just before the end wall of the shock tube.

The impulse amelioration results indicate that for all sets of complementary plate combinations, the combinations in which the lower porosity plates are situated upstream produce greater impulse amelioration values. This is clearly visible for plate combinations in which Plate 2 is present, due to the large difference in impulse ameliorations achieved for complementary combinations. This trend is also noted for the complementary plate combinations which have small differences (< 3 %) in impulse

amelioration values. Complementary plate combinations Pl3&Pl1 and Pl1&Pl3 have the largest difference in impulse amelioration values. This is due to the large difference in porosities of the plates. Plate 1 has the lowest porosity, excluding Plate 2, of 17 % and Plate 3 has the highest porosity of 41 %. Furthermore, since Plate 1 and Plate 4 have similar porosity value, the difference of the impulse amelioration value for their complementary combinations is negligible (0.7 %). Plate combinations Pl3&Pl4 and Pl4&Pl3 are the only combinations that produce the same impulse amelioration values. This is attributed to the fact that these plates have the highest porosity values and the order in which they are placed has negligible effect on the end wall impulse amelioration.

The initial peak pressure amelioration results indicate that for a complementary plate combination set, the combination which has the lower porosity plate situated downstream produce larger initial peak amelioration values. On the other hand the impulse amelioration results indicate when the lower porosity plate is situated upstream, greater impulse amelioration is achieved. This apparent contradiction is attributed to the fact that the impulse amelioration results are time dependant and take the effect of the rate of pressure increase acting on the end-wall of the shock tube, dp/dt, into account. Even though larger initial peak pressure ameliorations are recorded when a less porous plate is situated downstream of the testing configuration, the rate of pressure increase is greater and more ‘wave energy’ is trapped between the end wall and the downstream plate (which has a lower porosity) which decreases the impulse amelioration experienced by the end wall. Similarly when a more porous plate is situated downstream of the testing configuration, less ‘wave energy’ is trapped between the end wall and the downstream plate (which has a higher porosity) which increases the impulse amelioration experienced by the end wall.

For all tests performed in this study, the time period used for the integration of the end wall pressure traces was 9 250 μs as measured from the first rising edge of these pressure traces. As Britan (2006) states that an acceptable closing time for a blast valve in a shelter’s ventilation system is approximately 4 000 μs, the impulse amelioration values for plate combinations Pl1&Pl2 and Pl3&Pl4 were recalculated for comparative purposes. These plate combinations were selected, as Pl1&Pl2 produced the greatest impulse amelioration whereas Pl3&Pl4 produce the least.

Table 15: Comparison of Impulse Amelioration Values Obtained for Different Time Periods of Integration viz. 9 250 μs and 4 000μs.

Plate Combo.	Plate Arrangement	Integration Time [μs]	Impulse Amelioration [%]
Pl1&Pl2	Back & Back	4000	60.8%
	Back & Back	9250	33.8%
Pl3&Pl4	Back & Back	4000	20.3%
	Back & Back	9250	7.9%

It is noticed, that using the 4 000 μs time period for integration produces greater impulse amelioration values. This result occurs as the rate of pressure rise, dp/dt, is initially lower at the beginning of the end wall pressure trace and therefore produces a larger impulse amelioration value. From these results, it is concluded that plate combination Pl3&Pl4, with the lowest impulse amelioration value (7.9 %) in this study, will produce quite significant impulse amelioration (20.3%) if it were to be used in a shelter's ventilation system.

9.5.1 The Effects of Combined Plate Porosity on the Initial Peak Pressure and Impulse Ameliorations Experienced by the End Wall

A more detailed analysis of the effects that plate combination porosity had on the end wall amelioration values was conducted, as the analysis of the initial peak pressure and impulse amelioration results revealed that maximum amelioration is achieved for combinations in which the least porous plate specimen with the greatest resistance to flow is present i.e. Plate 2.

The porosity of an individual plate specimen is easy to quantify and is defined as the ratio of area open to air flow (cut-out area) to the area of the entire plate. In order to determine the porosity of a combination of plates, the product of porosities were calculated as the plates are placed in series. For example, consider plate combination Pl1&Pl2, the combined plate porosity is equivalent to 17 % x 7 % = 1.14 %. The results of initial peak pressure and impulse ameliorations for the plate combinations were then arranged according to the increasing plate combination porosities and are displayed in the figures that follow.

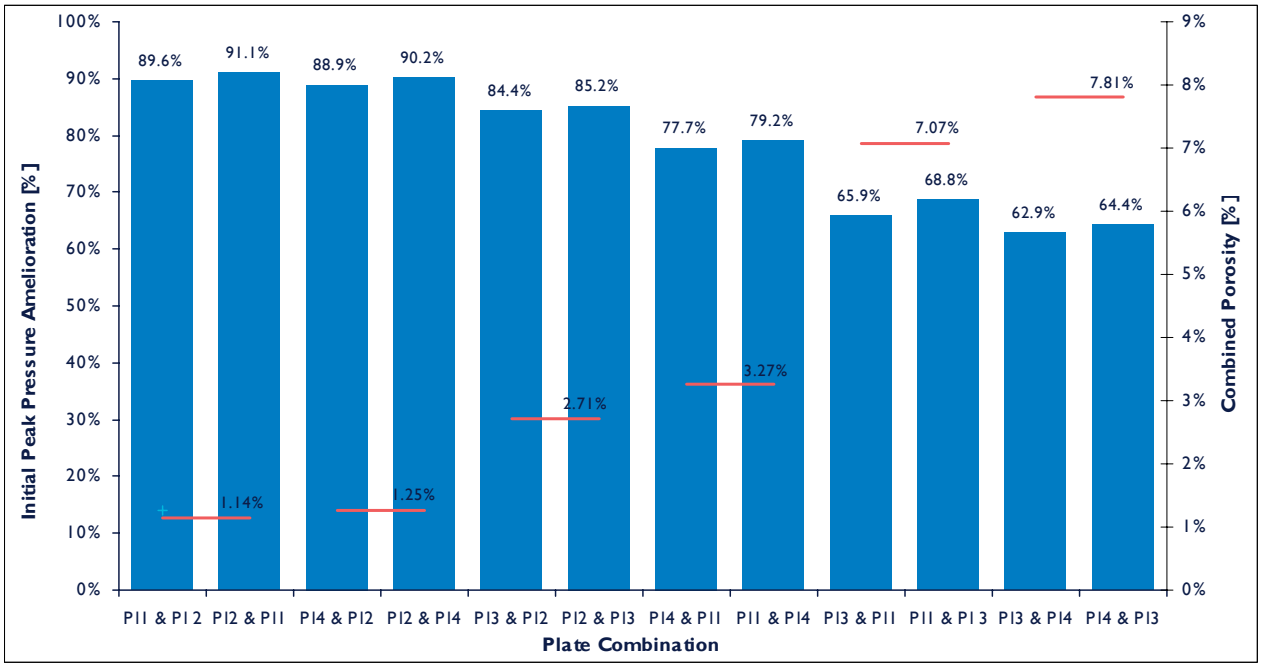


Figure 58: The Relationship between Initial Peak Pressure Amelioration and Increasing Plate Combination Porosity

The figure above clearly indicates that the initial peak pressure amelioration is clearly dependant on the combined porosities of the plates in a plate combination i.e. plate combination porosity. As the porosity of the combination increases the initial peak pressure amelioration experienced by the end wall of the shock tube decreases. This corresponds to a higher initial peak pressure experienced by the end wall as the resistance of the combination of plates decreases. Furthermore, note that the figure clearly illustrates that for all complementary plate combinations, the combinations which have the lower porosity plates, providing a higher resistance to the oncoming flow, situated downstream produces larger initial peak amelioration values. This indicates that maximum initial pressure amelioration is achieved by placing the less porous of any two plates under consideration downstream, just before the end wall of the shock tube.

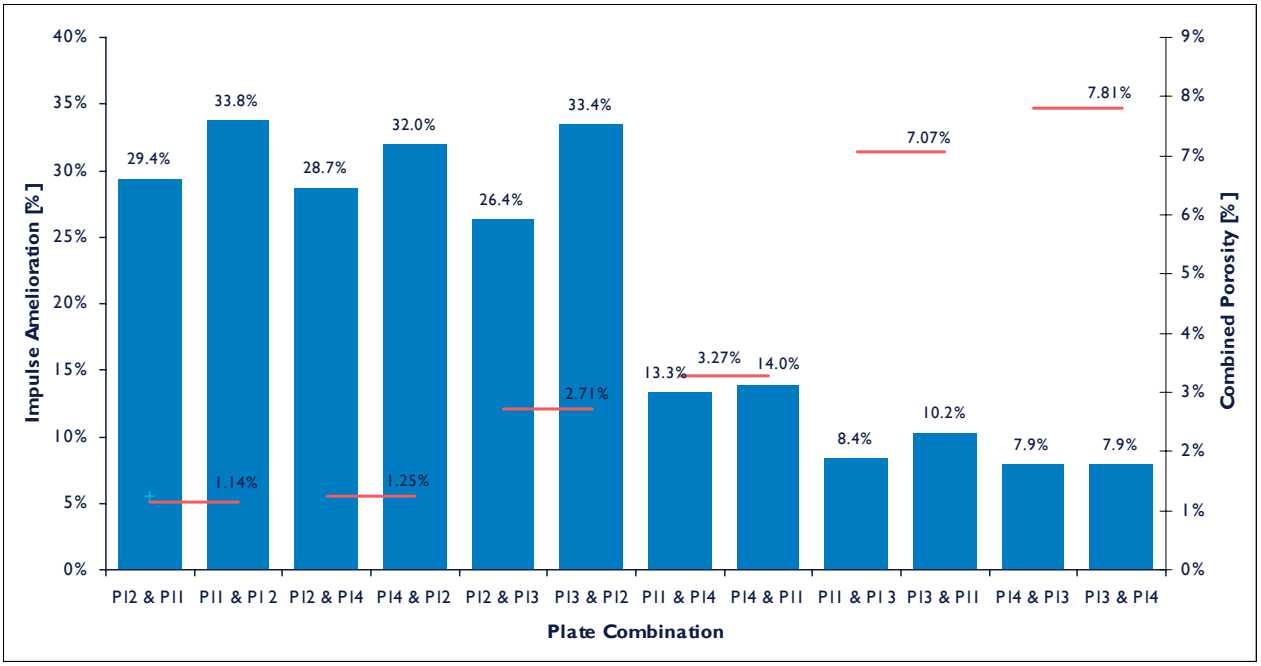


Figure 59: The Relationship between End Wall Impulse Amelioration and Increasing Plate Combination Porosity

Figure 59 above, also illustrates that the end wall impulse amelioration is dependant on the plate combination porosity. It is clearly noticed that as the porosity of the plate combination increases, the values of impulse amelioration experienced by the end wall of the shock tube decreases. Therefore as the combined resistance of the plate specimens increases, the impulse experienced by the end wall of the shock tube increases, lowering the achieved amelioration value. Furthermore, the graph clearly illustrates that for all sets of complementary plate combinations, the combinations in which the lower porosity plates are situated upstream, produce greater impulse amelioration values i.e. consider plate combinations Pl1&Pl2, Pl4&Pl2, Pl3&Pl2, Pl4&Pl1, Pl3&Pl1 and Pl3&Pl4. These plate combinations have the lower porosity plates situated upstream and produce greater impulse amelioration values when compared to their respective complementary combinations.

It must be noted that the porosity of the combined plates have an overriding influence on the end wall initial peak pressure and impulse amelioration values when compared to the effect that plate arrangement (i.e. geometrical influences) has. Similarly, it was found by Britan et al (2006) that the amplitude of the initial first pressure jump experienced by the end wall increases as the porosity of the barrier increases. Furthermore, the attenuation of the transmitted shock wave did not show any dependence on the specific geometry of the barriers tested, but rather on their porosities. Please refer to Section 3.2.

9.5.2 Analysis of the Trapped Wave Data

In this section, the impulse values obtained by the transducer located in the airspace between the plate specimens are analyzed in order to determine the effects the plate combinations have on 'shock wave trapping' as well as the effects on the impulse amelioration experienced by the end wall of the shock tube.

The Trapped Wave Impulse data was calculated from the pressure traces recorded by Transducer 4, which was located in the air space between the two plate specimens. These impulse values are calculated from the first rising edge of the pressure traces until the time period of 9 250 μs for the end wall pressure traces had been completed. As the method and time period that were used in the calculation of these values were kept constant for the various tests, one may use these impulse values for comparative purposes.

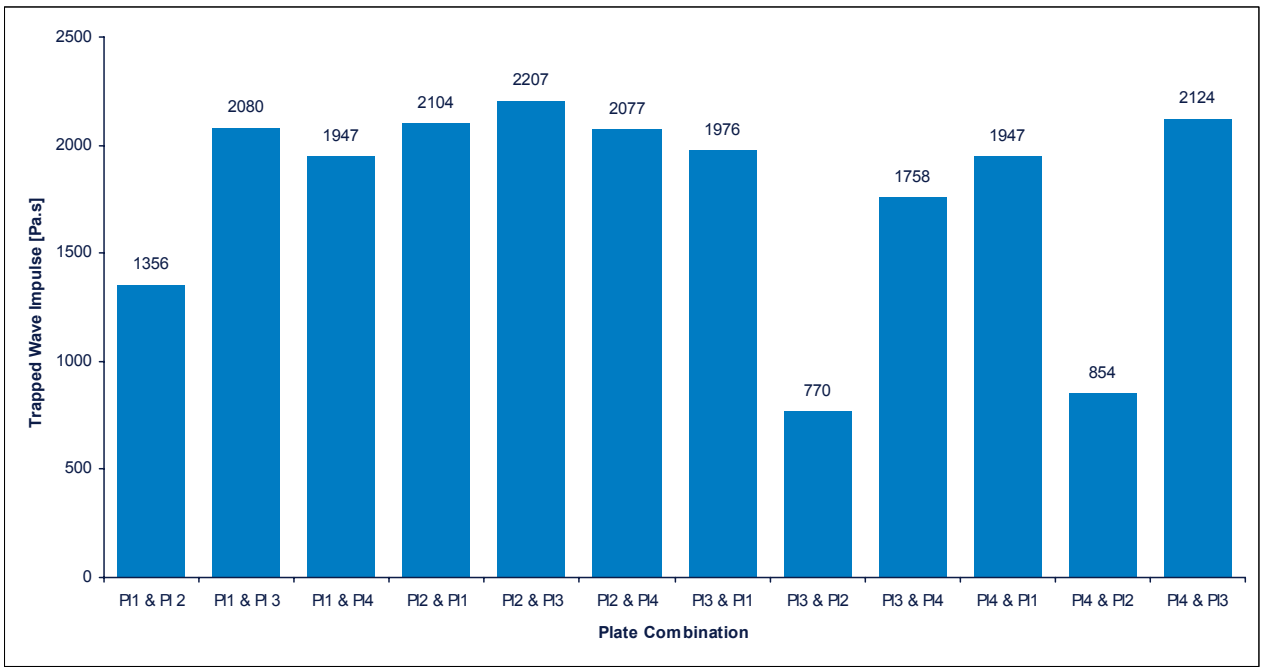


Figure 60: Trapped Wave Impulse Values Obtained for the Various Plate Combinations - Back & Back Plate Arrangement

From the figure above, it is noticed that plate combinations Pl1&Pl2, Pl3&Pl2 and Pl4&Pl2 produce the minimum Trapped Wave Impulse (< 1400 Pa.s), which corresponds to the highest values of end wall impulse amelioration (> 30 %). These results indicate that the presence of the lowest porosity plate, Plate 2 (6.6 %) which is situated upstream in the test section, produces weak transmitted shock waves into the airspace between the plate specimens and the air space between the downstream plate and the end wall in which complex wave interactions occur. The pressure traces obtained for these plate combinations indicate that destructive wave interactions probably occur as compression waves are formed and the rate

of pressure rise experienced by both the end wall and Transducer 4 are low. Therefore the impulse experienced by the end wall of the shock tube and Transducer 4 are low in magnitude for these plate combinations.

Plate combinations Pl2&Pl1, Pl2&Pl3 and Pl2&Pl4, which produce high end wall impulse ameliorations values (> 25 %), do not produce low Trapped Wave Impulse values even though they are complementary to the ones listed above. This is attributed to the fact that in these combinations the lower porosity plate, Plate 2 (6.6 %) is situated downstream and effectively traps more 'wave energy' between the two plate specimens as well as the airspace between the end wall and the downstream plate. Therefore larger Transducer 4 impulse values and lower end wall impulse amelioration values are recorded for these combinations when compared to their respective complementary combinations. Furthermore, analysis of the pressure traces for these combinations indicate that destructive wave interference probably occurs to a lesser extent, as the pressure traces recorded on the end wall and by Transducer 4 have a higher rate pressure rise when compared to their respective complementary combinations.

The effect of the lower porosity plate which is situated downstream resulting in greater Trapped Wave Impulse is also noted for the remaining complementary plate combinations which exclude Plate 2. In all cases, greater Trapped Wave Impulse values are attained when the lower porosity plate is situated downstream. Only plate combinations Pl1&Pl4 and Pl4&Pl1 produce exactly the same value of Trapped Wave Impulse, as their porosities are similar.

For all the pressure traces obtained in this study, it was noticed that unlike the other pressure traces, the trace recorded by Transducer 4 never reached P_F. This result may be attributed to the fact that destructive inference occurs in the airspace between the plate specimens as well as the possibility that the pressure trace recorded by the transducer is affected by wave interactions with the edges of the cut-out region of the 'bending moment' plate of Section A of the mounting system. Furthermore a boundary layer may exist which may also affect the pressure reading of this transducer as it is fitted flush with the Aluminium door and the 'bending moment' plate which is 3 mm thick. Consider the pressure traces obtained for plate combinations Pl2&Pl1, Pl3&Pl1 and Pl4 &Pl1, which are listed in Appendix C.

Analysis of the pressure traces recorded by Transducer 4 indicate that the 'settled' pressure in the airspace between the plate specimens is approximately 10 % lower than P_F and is the lowest deviation obtained for all plate combinations. Therefore, this result may be largely attributed to the wave interactions and boundary layer created by the presence of the cut-out in the 'bending moment' plate. The pressure traces for the remaining plate combinations have much greater deviations and therefore for these cases the

results may be attributed largely to the destructive wave interactions that occur. It is suggested that a numerical analysis be performed in future in order to further investigate the cause of the discrepancies and possibly verify the suggested explanations.

9.5.3 Analysis of the Reflected Wave Data

The Reflected Wave Impulse data was calculated from the pressure traces recorded by Transducer 3, which was located 12 mm in front of the upstream plate specimen. These impulse values are calculated from the first rising edge of the pressure traces until the time period of for the end wall pressure traces had been completed. Figure 61 illustrates the Reflected Wave Impulse values for the Back & Back plate arrangements listed in Table 11.

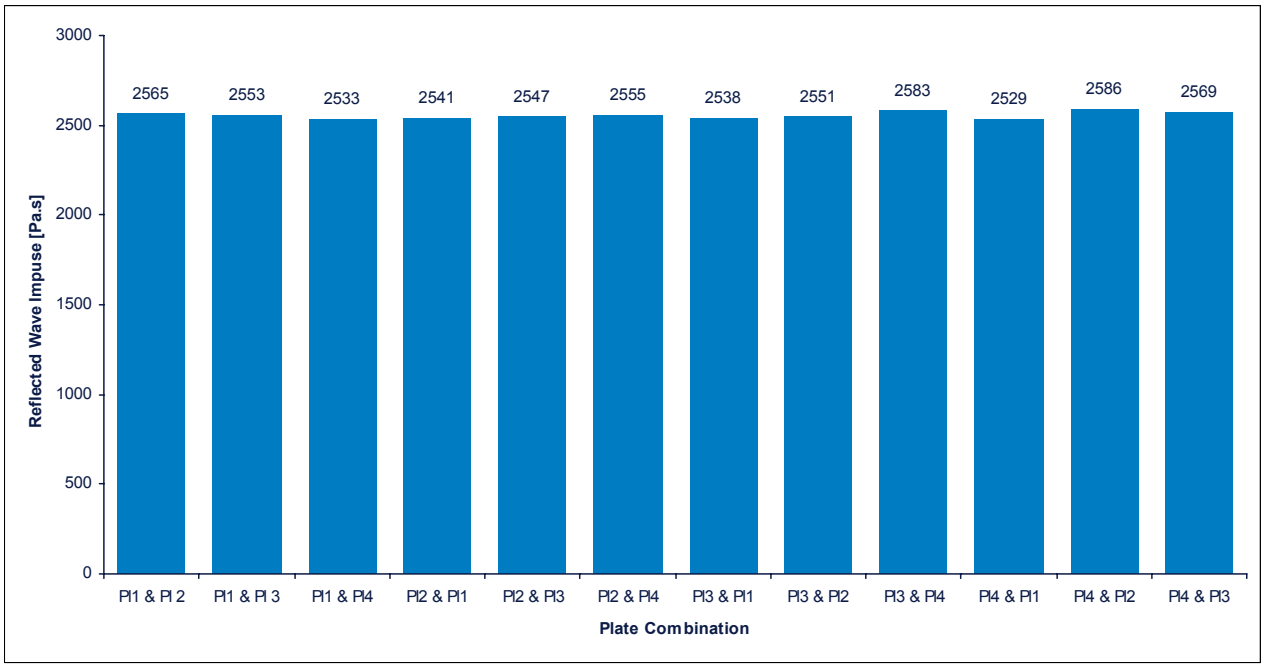


Figure 61: Reflected Wave Impulse Values Obtained for the Various Plate Combinations - Back & Back Plate Arrangement

From the figure above, it is noticed that data obtained for all the plate combinations is similar (within 2 % variation from the average). Therefore little information can be extracted from these results. Analysis of the pressure traces reveals that the wave forms recorded for plate combination in which Pl2 is situated upstream are most similar to the form of a plane wave reflection. When the remaining plates, with lower porosities than Plate 2, are situated upstream they produced a more distinct stepped form as waves are reflected from the air space between the two plate specimens. However, not much can be said, as these pressure traces are extremely noisy and within a short time period (approximately 500 μs) reach P_F. In

hindsight, the Transducer 3 should have been situated further upstream of Plate A. This probably would have allowed for the collection of more useful data.

9.6 Analysis of Pressure Traces

The pressure profiles of the end wall pressure transducers for the twelve combinations were analyzed. It was found that in general, three end wall pressure profiles exist for all twelve plate combinations. Furthermore, it was found that the initial peak pressure and impulse amelioration results are similar for plate combinations in each group due to the group's characteristic pressure profile. Please refer to Appendix C, in which the pressure trace data from transducers 3, 4 and 8 are listed for each of the plate combinations. Note that these pressure plots correspond to the 30 mm plate separation distance tests listed in Table 12.

9.8.2 End Wall Pressure Trace Analysis of Pl1&Pl2, Pl3&Pl2 and Pl4&Pl2

Plate combinations Pl1&Pl2, Pl3&Pl2 and Pl4&Pl2 were found to produce end wall pressure traces that are similar in profile. Figure 62 illustrates the end wall pressure trace data obtained for Pl1&Pl2. A normal pressure trace, $M_{set} = 1.42$, for the end wall when no tests specimens are present in the shock tube is also illustrated in the figure for comparative purposes.

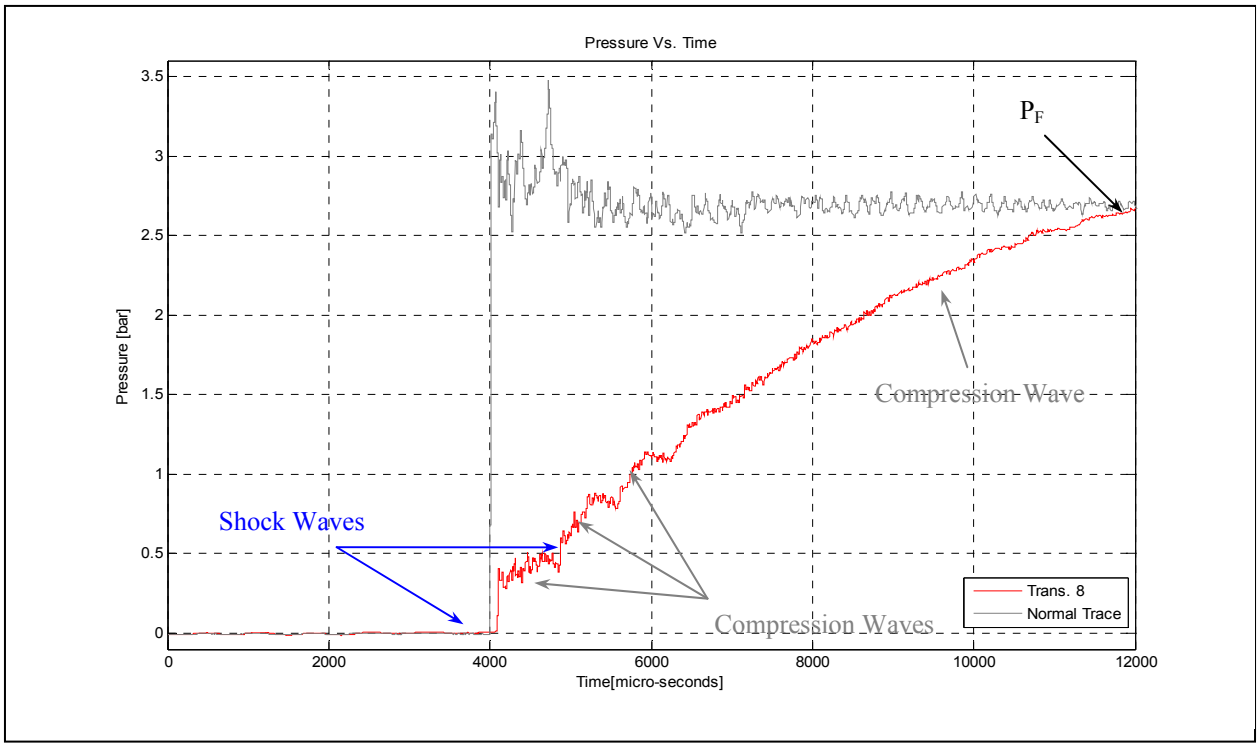


Figure 62: End Wall Pressure Trace for Pl1&Pl2 - M_{set} = 1.42, Po = 0.83 and d = 30 mm

It is noticed that these plate combinations all have Plate 2, the least porous plate specimen, situated upstream in the test section. The presence of Plate 2 in this position produces the characteristic end wall pressure profiles for these combinations. Upon collision of the incident shock wave with Plate 2, a weak shock wave is transmitted into the air space between the two plate specimens. This transmitted shock wave then interacts with the downstream plate and is further weakened in strength before colliding with the end wall of the shock tube producing a low initial peak pressure. The weak shock wave is quickly dissipated through a system of complex wave interactions which causes the end wall to experience a compression wave. These complex interactions occur in the airspace between the plate specimens and the airspace between the end wall and the downstream plate specimen.

Since Plate 1 and Plate 4 are of similar porosities, plate combinations Pl1&Pl2 and Pl4&Pl2 produce similar end wall pressure traces. For both plate combinations, the end wall pressure profile is initially seen to be step like in form with a low initial peak pressure. After approximately 6200 μs, the profile becomes a compression wave. Due to the few weak shock waves colliding with the end wall and the rapid transformation of the pressure profile into to compression wave, the impulse experienced by the end wall is greatly reduced. This is clearly visible, as the area under the end wall pressure trace is slightly greater than half the area under the normal shock pressure trace.

Plate combination Pl3&Pl2 exhibits a similar end wall pressure profile as plate combinations P1&Pl2 and Pl2&Pl4, with a low initial peak pressure. However its pressure profile has a more distinct step like form than the other plate combinations. Furthermore, the time taken for the end wall pressure trace to become a compression wave is greater. This is attributed to the fact that Plate 3 is much more porous than either Plate 1 or Plate 4. Therefore stronger and distinct reflections occur in the air spaces between Plate 2 and the end wall due to the high resistance of Plate 2 to the flow.

This group of plate combinations produce the greatest initial peak pressure and impulse amelioration values.

9.8.2 End Wall Pressure Trace Analysis of Pl2&Pl1, Pl2&Pl3 and Pl2&Pl4

Plate combinations Pl2&Pl1, Pl2&Pl3 and Pl2&Pl4 were found to produce the second set of end wall pressure traces similar in profile. Figure 63 illustrates the end wall pressure trace data obtained for Pl2&Pl3. A normal pressure trace, M_{set} = 1.42, for the end wall when no tests specimens are present in the shock tube has also been illustrated in the figure for comparative purposes.

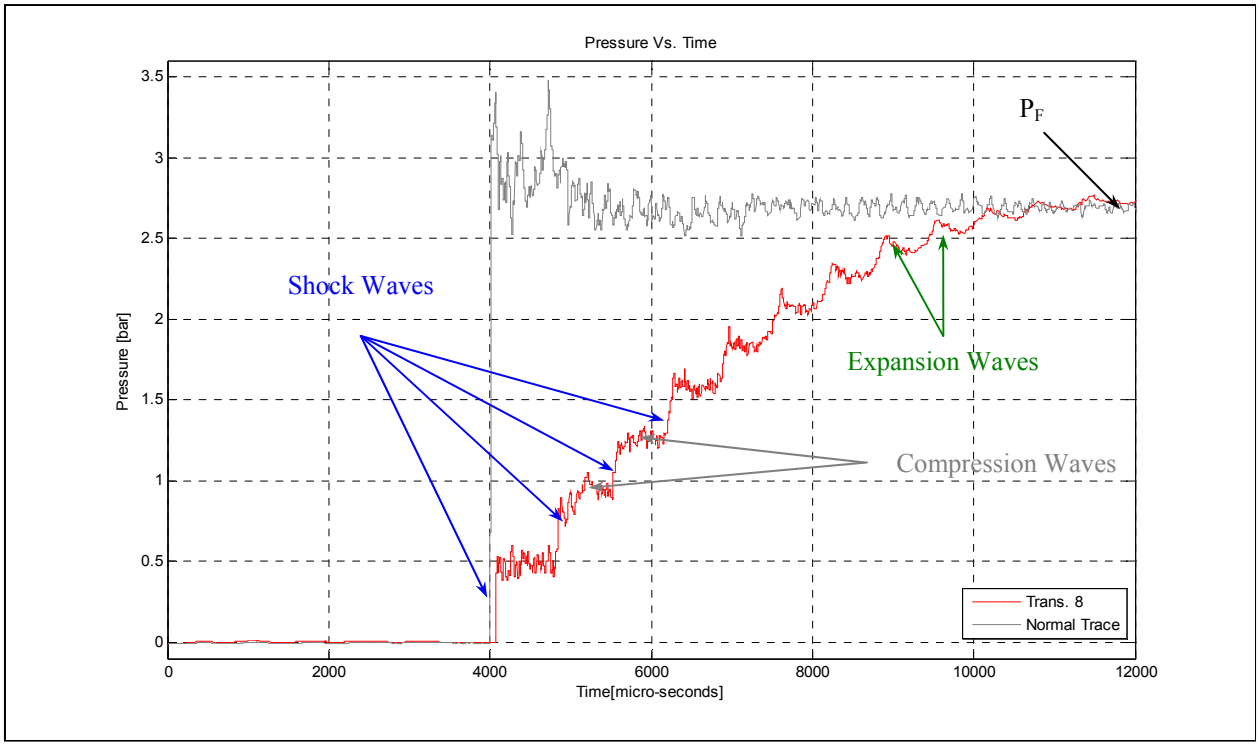


Figure 63: End Wall Pressure Trace for Pl2&Pl3 - M_{set} = 1.42, Po = 0.83 and d = 30 mm

These three plate combinations have Plate 2 situated downstream in the test section and therefore their pressure traces are similar in form. In this set of plate combinations, it was noticed that plate combinations Pl2&Pl1 and Pl2&Pl4 produce similar end wall pressure traces as the porosities of Plate 1 and Plate 4 are similar. These pressure traces have a low initial peak pressure and are step like in form until the 'final' pressure, P_F, is reached. It is noticed that these plate combinations have the highest frequency of 'steps' from all the end wall pressure traces. This is due to the position of Plate 2. It is noticed that that more shock reflections occur in the air space between the downstream plate and the end wall as Plate 2 is the least porous plate specimen and therefore offers the greatest resistance to flow. This effectively traps more of the incident wave's energy in this airspace which results in successive wave reflections and produces a more step like form for the end wall pressure trace than when compare to the plate combinations in which Plate 2 is positioned upstream in the test section.

Due to the presence of Plate 3 in plate combination Pl2&Pl3, the initial peak pressure experienced by the end wall is slightly greater and the stepped profile is more pronounced as shown in the figure above. These results are attributed to the fact that Plate 3 is much more porous than either Plate 1 or Plate 4. Therefore much stronger and more distinct shock wave reflections occur in the air space between Plate 2 and the end wall as compared to when Plate 1 and Plate 4 are present.

The figure above also illustrates that significant end wall impulse amelioration is achieved by these plate combinations as the area under the end wall pressure is much less than that under the normal shock pressure trace. However, since these plate combinations have a greater rate of pressure rise, dp/dt, than plate combinations their complementary plate combinations the impulse experienced by the end wall for these combinations is greater.

9.8.2 End Wall Pressure Trace Analysis of the Remaining Plate Combinations

Finally, plate combinations Pl1&Pl3, Pl1&Pl4, Pl3&Pl1, Pl3&Pl4, Pl4&Pl1 and Pl4&Pl3 were found to produce the third set of end wall pressure traces that are similar in profile. It is noted that for this group, the initial peak pressure and impulse amelioration values produced are lower than the previous two groups. The 'stepped' like end wall pressure profiles obtained for these plate combinations are most similar in profile to those obtained by Britan et al (2006). Please refer to Figure 16. This result is attributed to the fact that these plate combinations have large combined porosities as Plate 2 is absent. Figure 64 that follows, illustrates the end wall pressure trace data obtained for Pl1&Pl3 as well a normal pressure trace obtained for the end wall.

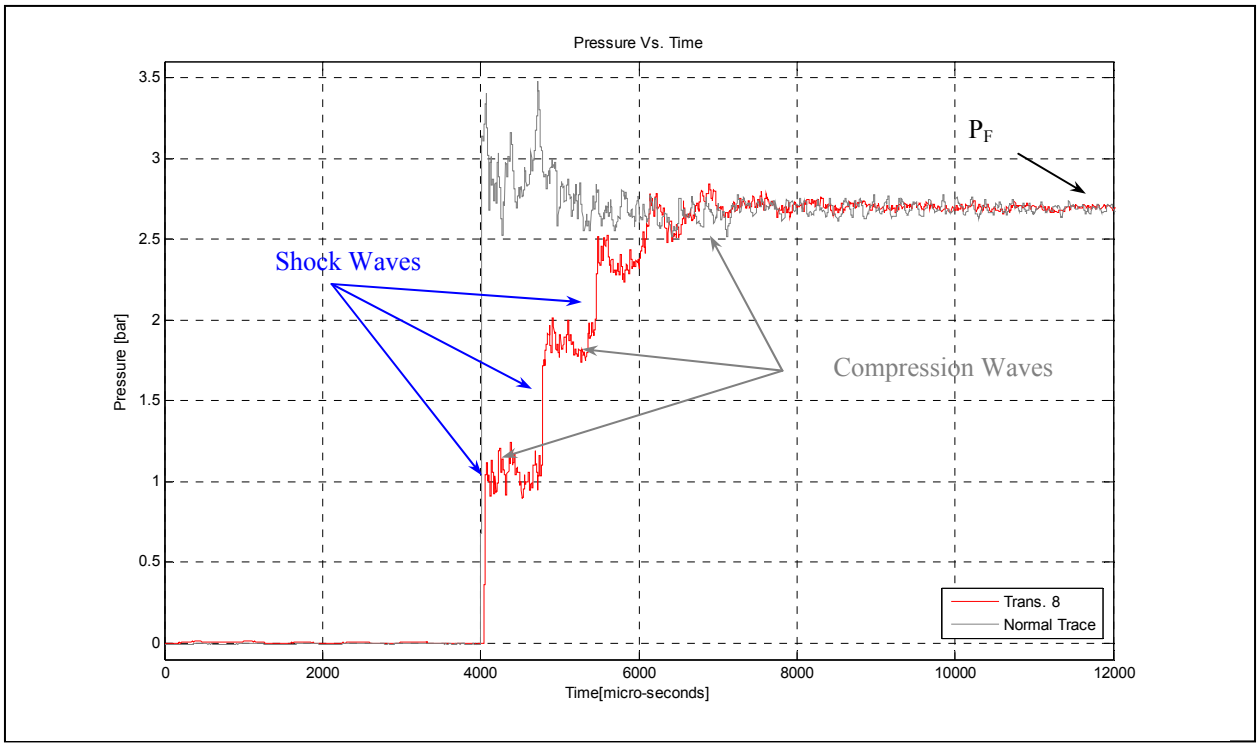


Figure 64: End Wall Pressure Trace for Pl1&Pl3 - M_{set} = 1.42, Po = 0.83 and d = 30 mm

The profile of the end wall pressure traces for these six plate combinations produce large initial peak pressures when compare to those combinations in which Plate 2 is present. Furthermore, these pressure traces have a distinct 'stepped' profile which indicates that a relatively strong shock wave (when compared to combinations in which Plate 2 is present) undergoes successive reflections in the airspace between the downstream plate and the end wall until the 'final' pressure, P_F, in the shock tube is reached. This is attributed to the fact that the combined plate combination porosities are much higher than those plate combinations in which Plate 2 is present, thereby offering a lower resistance to flow. Therefore, the initial peak pressure experienced by the end wall of the shock tube and the rate of pressure rise, dp/dt, is greater for these plate combinations. Furthermore, notice that the frequency of 'steps' in the pressure profile is reduced when compared to combinations in which Plate 2 is situated downstream. This reduction of frequency occurs due to the higher porosities of the downstream plates which do not trap as much of the reflected wave energy (off the end wall).

9.7 Analysis of Pressure Plots

Upon further analysis of all three transducer traces (i.e. traces from transducers 3,4 and 8), it was found that the pressure trace plots obtained for the majority of plate combinations were not exclusive i.e. certain plate combinations had similar pressure profiles for all three transducers. For example, consider the pressure plots of Pl1&Pl2 and Pl4&Pl2 that are illustrated below. Notice that the pressure profiles obtained for each transducer in both plots are similar i.e. the pressure traces for all transducers in Figure 65 are similar in profile to the pressure traces for corresponding transducers in Figure 66.

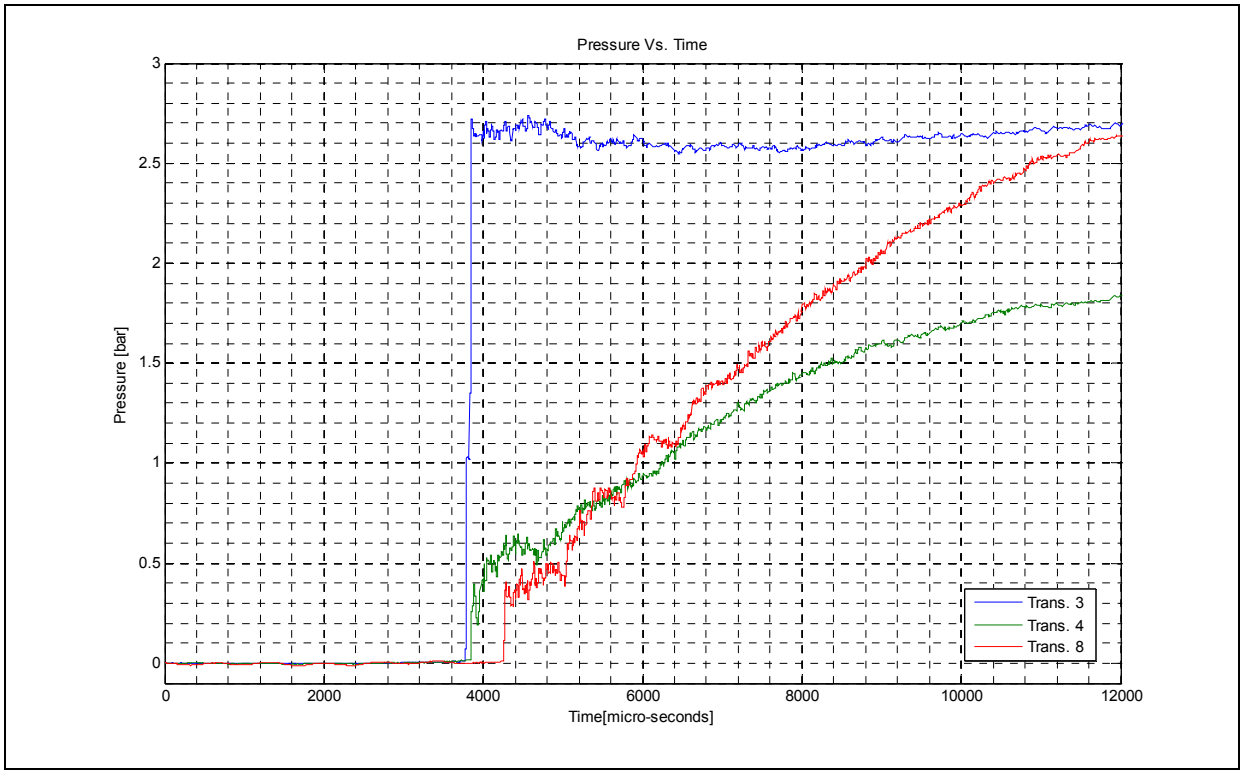


Figure 65: Pressure Plot for Pl1&Pl2 - M_{set} = 1.42, Po = 0.83 and d = 30 mm

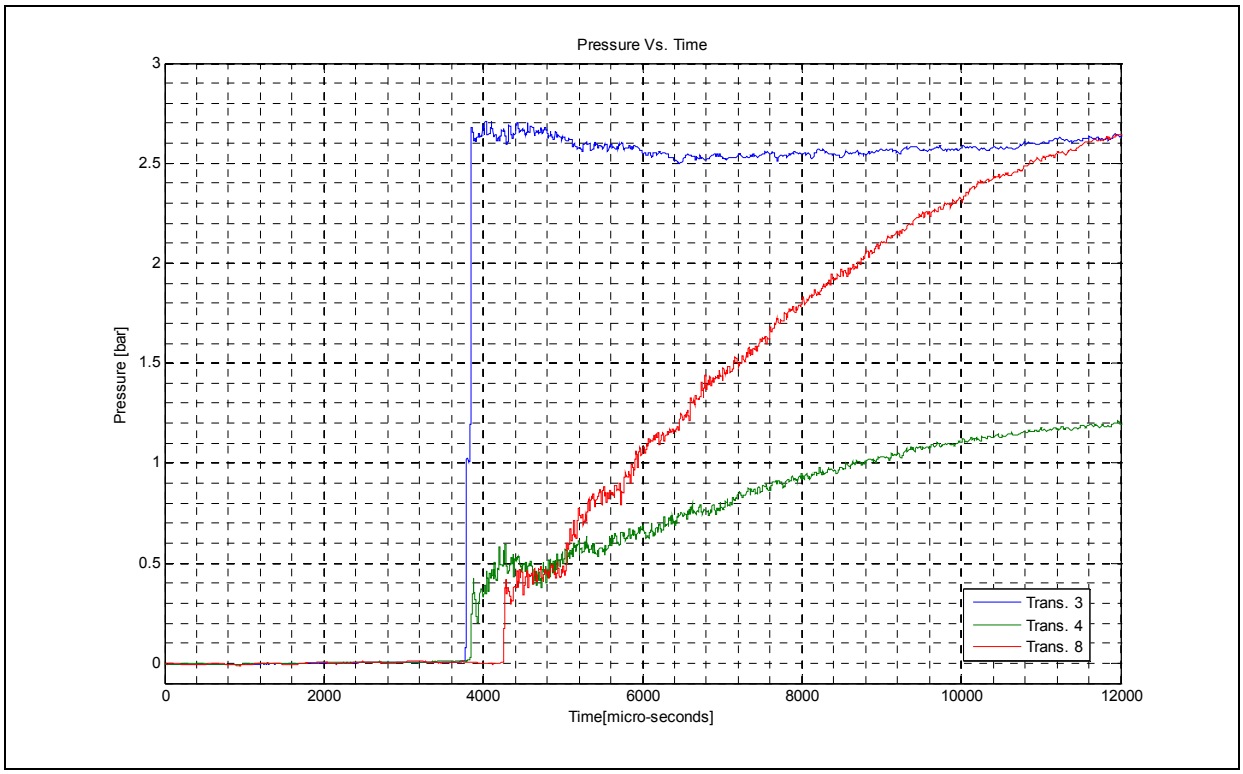


Figure 66: Pressure Plot for Pl4&Pl2 - M_{set} = 1.42, Po = 0.83 and d = 30 mm

It was found that only plate combinations Pl2&Pl3 and Pl3&Pl2 had distinct pressure plots. All other plate combinations had a corresponding plate combination, for which their pressure profiles were similar. These pairs of plate combinations with similar pressure plots have been listed in the table below.

Table 16: Mapping of Plate Combinations with Similar Pressure Plots

Plate Combination	Corresponds To	Plate Combination
Pl1&Pl2	↔	Pl4&Pl2
Pl2&Pl1	↔	Pl2&Pl4
Pl1&Pl3	↔	Pl4&Pl3
Pl1&Pl4	↔	Pl4&Pl1
Pl3&Pl1	↔	Pl3&Pl4

The table illustrates that these relationships are attributed to the fact that Plate 1 and Plate 4 have similar porosity values corresponding to 17 % and 19 % respectively. Therefore, replacing one plate by the other has little effect on the pressure profiles recorded.

Plate combinations Pl2&Pl3 and Pl3&P2 produce end wall pressure traces that are similar in profile. However the profiles obtained for the pressure traces from Transducer 3 and Transducer 4 vary greatly. This is due to the positioning of Plate 3, the highest porosity plate, relative to Plate 2, the lowest porosity plate. When Plate 3 is place downstream stream of Plate 2 i.e. Pl3&Pl2, it is noted that the rate of pressure rise, dp/dt, is lower in the airspace between the two plates and therefore a lower impulse is recorded. The opposite occurs when Plate 3 is situated upstream of Plate 2 i.e. Pl2&Pl3, as more wave energy is let into the airspace between the two plates due to the high porosity of Plate 3. Furthermore, from the pressure trace obtained from Transducer 4, it is also noticed that a series of strong reflections occur for plate combination Pl3&Pl2 as Plate 2, the lower porosity plate is placed upstream of Plate 3. This 'stepped' profile is not noticed for plate combination Pl2&Pl3.

It was previously mentioned that plate combinations Pl1&Pl3, Pl1&Pl4, Pl3&Pl1, Pl3&Pl4, Pl4&Pl1 and Pl4&Pl3 were found to produce end wall pressure traces similar in profile. From Table 16, it is noticed that these six plate combinations can be further grouped into pairs as shown in the last three rows of the table. Each pair of plate combinations have almost exact pressure plots, further distinguishing the profiles of end wall pressure traces of this large group of plate combinations.

9.8 Analysis of the Effects of Plate Separation Distance

This set of tests was performed in order to determine the effects that the separation distance between plate specimens had on the end wall initial peak pressure and impulse amelioration results. The twelve plate combinations were tested using three different separation distances viz. 30 mm, 45 mm and 60 mm. All tests were performed for a Back & Back plate arrangement and a set Mach number of 1.42. The ambient atmospheric pressure, P_o, was measured to be 0.83 bar and the time period used for the integration of the end wall pressure traces was 9 250 ms as measured from the first rising edge of these pressure traces. The results of these tests are listed in Table 12. Furthermore, it must be noted that the pressure trace data obtained during this set of tests correspond extremely well to the pressure trace data obtained during previous tests, listed in Table 11, thus verifying the repeatability of tests**.**

The pressure trace results obtained for each plate combination were over-laid for comparison. The figure that follows displays the results obtained for plate combination Pl4&Pl2 and serves as an example of such

a figure produced for each plate combination. The pressure trace of a normal shock wave, M_{set}=1.42, is also plotted in the figure to illustrate the significant initial peak pressure amelioration achieved.

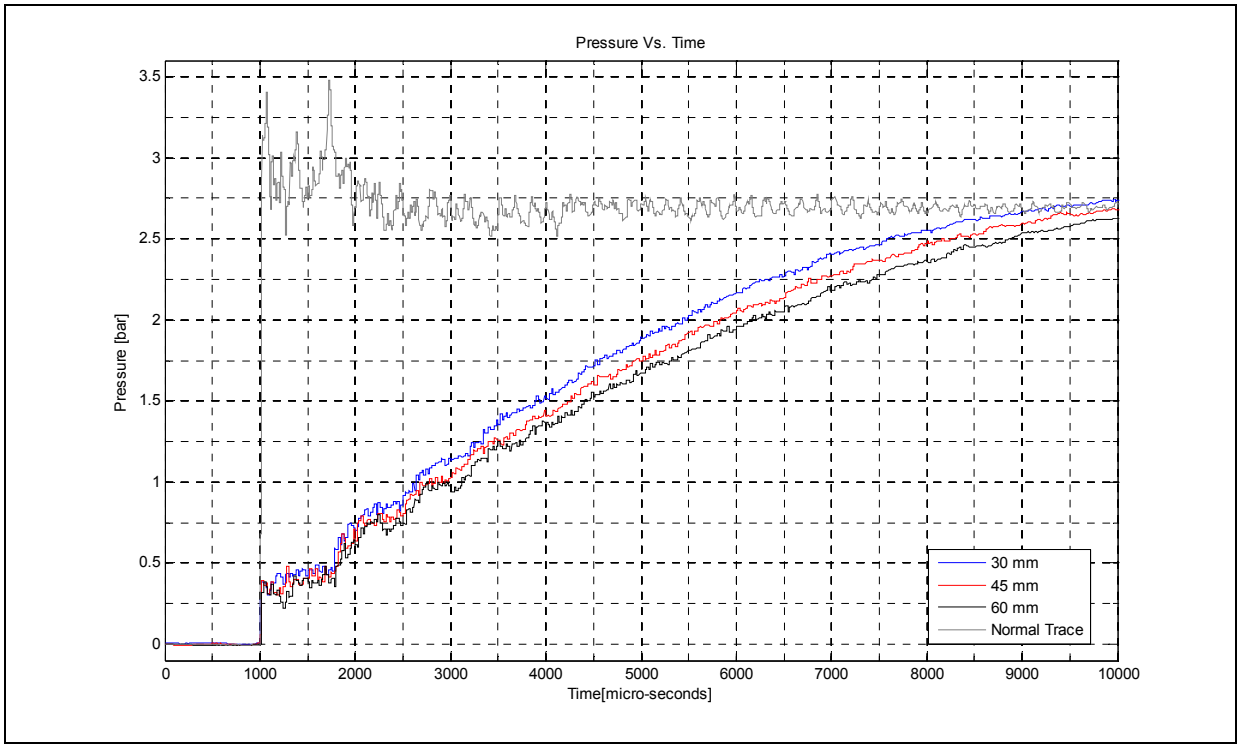


Figure 67: Overlay of End Wall Plate Separation Distance Pressure Traces for Pl4&Pl2 - M_{set} =1.42, Back & Back Plate Arrangement

The pressure trace results obtained for all plate combinations revealed that initial peak pressure experienced by the end wall were similar (within 5 % of the average initial peak pressure obtained for the three distances) irrespective of the separation distance. However, deviations of the pressure traces were noted to occur at some time (1750 μs in the above diagram) after incidence with the end wall. For all the plate combinations tested lower pressure readings were obtained and the pressure trace took longer to reach P_F i.e. the gradient of the pressure trace decreased as the separation distance between the plates was increased. This characteristic of the pressure traces is clearly shown in the figure, as the staggering of the overlaid pressure traces is clearly noticeable.

The general form of the pressure traces obtained for each plate combination was relatively unaltered as the separation distances were varied. The wave forms were noted to be more distinct as the separation distance was increased. This is attributed to the fact that fewer wave reflections occurred between the two

plates, due to the larger distance between them, which resulted in fewer transmitted waves travelling towards the end wall of the shock tube producing a 'cleaner' end wall pressure trace.

The results listed in Table 12 have been plotted in the figures that follow, in order to determine the effect that the plate separation distance have on the end wall initial peak pressure amelioration and impulse amelioration.

9.8.2 The Effects of Plate Separation Distance on the Initial Peak Pressure Amelioration Experienced by the End Wall

Figure 68 that follows, illustrates the results obtained for the initial peak pressure amelioration for each of the plate separation distances. The figure indicates that the results obtained for the three separation distances are similar. Plate combinations Pl1&Pl2, Pl3&Pl2, Pl4&Pl2, Pl2&Pl1, Pl2&Pl3 and Pl2&Pl4 produce the greatest initial peak pressure amelioration with values greater than 70 %. The remaining plate combinations in which Plate 2, the least porous plate, is absent produce initial peak pressure values below 70 %.

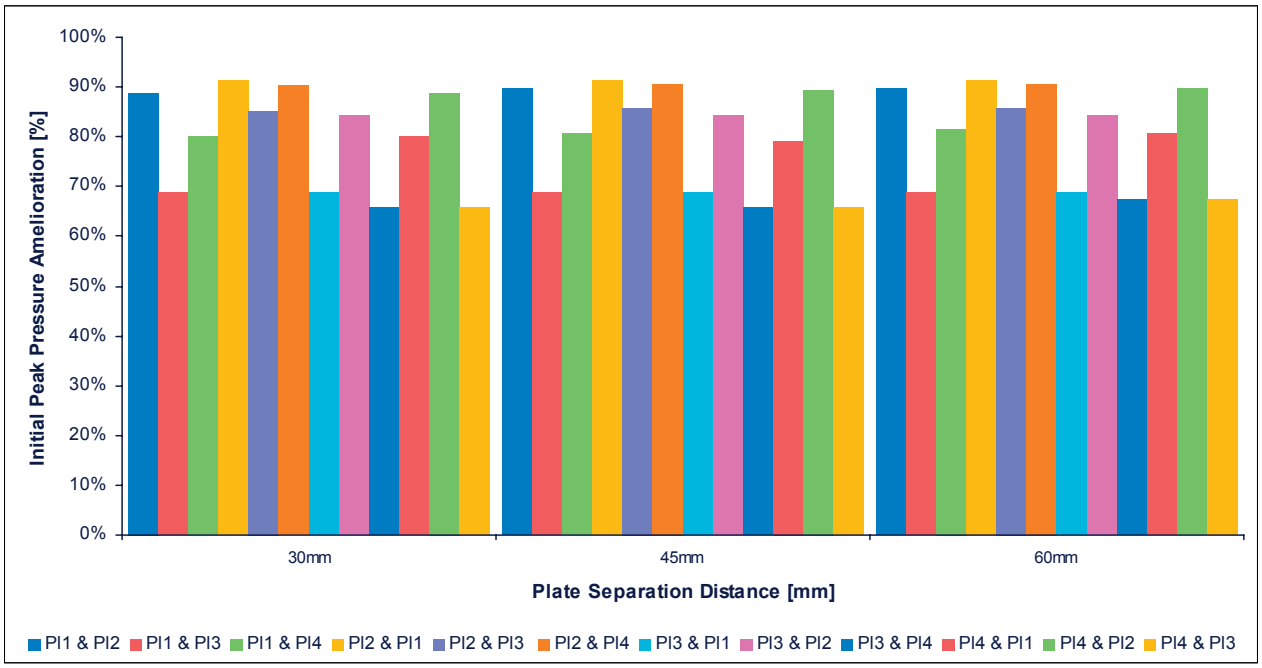


Figure 68: Initial Peak Pressure Amelioration Results Obtained for the Various Plate Separation Distances

In Figure 69, that follows, the initial peak pressure amelioration experienced by the end wall of the shock tube is rearranged and grouped according to plate combination. By regrouping the results according to

plate combination, the plate combinations that produce the largest initial peak pressure amelioration are easier to distinguish. Furthermore, it is easier to distinguish the similarity of the initial peak pressure amelioration values obtained for each plate combination even though plate separation distances differ. For each plate combination, the initial peak pressure values were found to be within 5 % of the average initial peak pressure obtained for the three distances. Therefore, for each plate combination the amelioration percentages for the three separation distances differed by no more than approximately 1.5 % from each other.

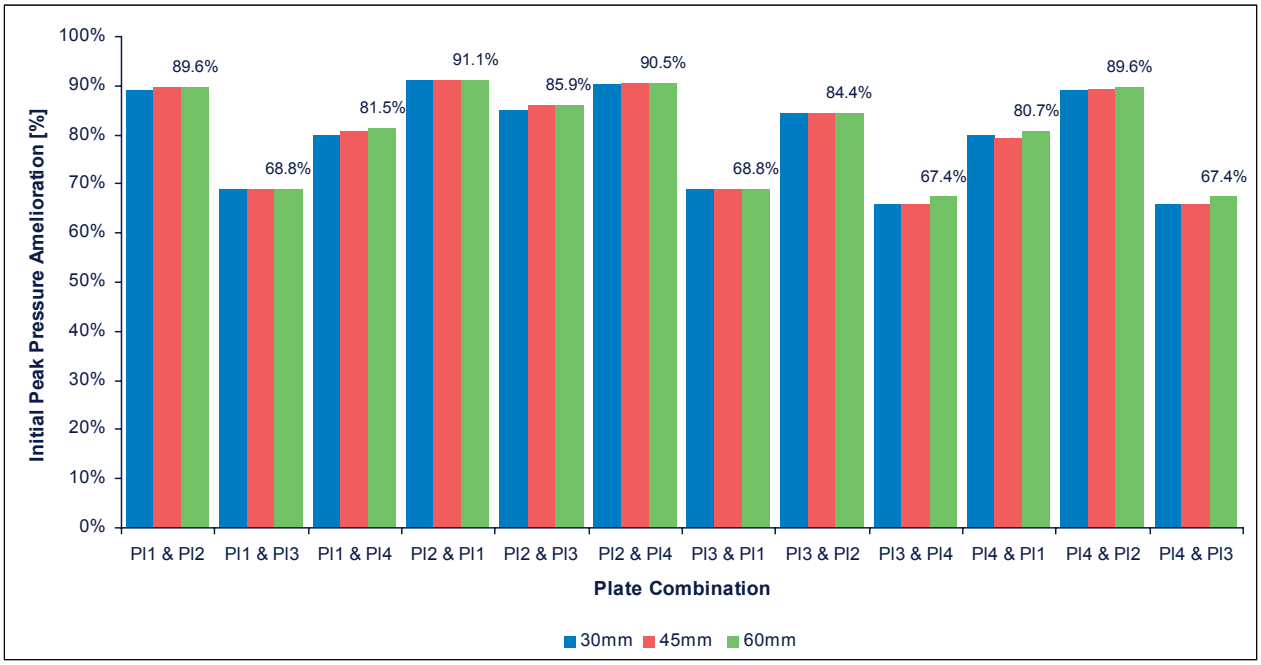


Figure 69: Initial Peak Pressure Amelioration Results Obtained for the Various Plate Combinations

An average initial peak pressure amelioration value for the twelve plate combinations was calculated for each plate separation distance and the results are listed in the figure that follows.

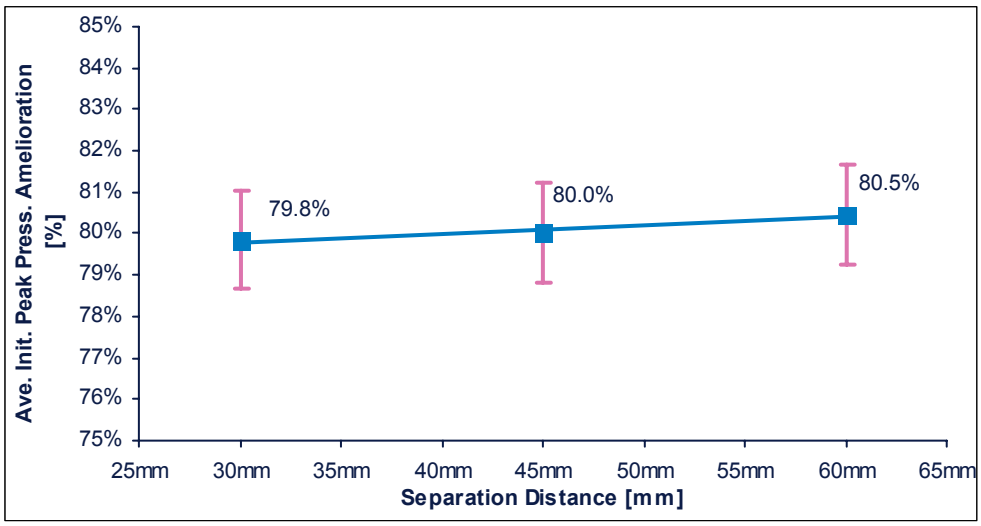


Figure 70: Average Initial Peak Pressure Amelioration Vs Plate Separation Distance

It is noticed that the average initial peak pressure increases marginally as the plate separation increases. However, as this increase is negligible, it is concluded that plate separation distance does not have a significant effect on the end wall initial peak pressure amelioration.

9.8.2 The Effects of Plate Separation Distance on the Impulse Amelioration Experienced by the End Wall

Figure 71 that follows, displays the end wall impulse amelioration values obtained for each plate combination which have been grouped according to plate separation distance. The general trend of data indicates that the impulse amelioration values increase as the plate separation distance increases. It is noted that combinations Pl1&Pl2, Pl3&Pl2, Pl4&Pl2, Pl2&Pl1, Pl2&Pl3 and Pl2&Pl4 produce the greatest end wall impulse amelioration for each separation distance, with amelioration values greater than 25 %. The remaining plate combinations produced end wall pressure amelioration values less than 15 %. These results obtained correlates well with those obtained for the plate arrangement analysis (see Figure 53) and reinforce the findings of the analysis.

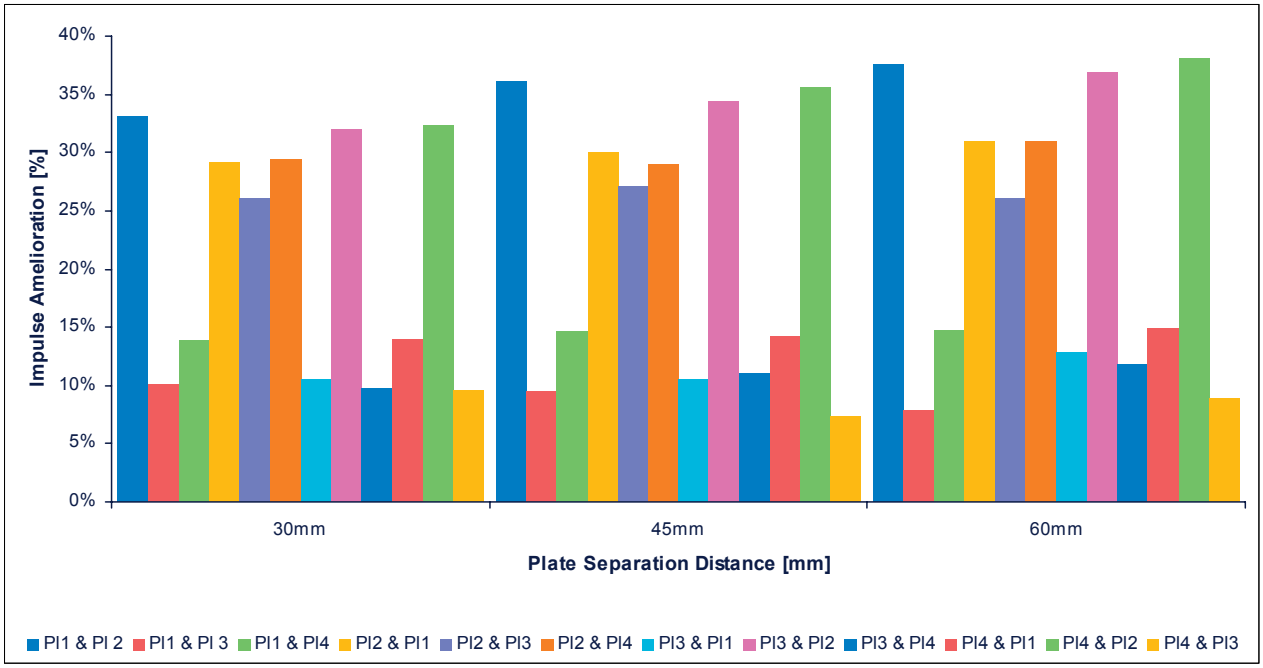


Figure 71: Initial Peak Pressure Amelioration Results Obtained for the Various Plate Separation Distances

In Figure 72 that follows, the impulse amelioration results have been rearranged and grouped according to plate combination. By regrouping the results according to plate combination, the plate combinations that produce the largest initial peak pressure amelioration are easier to distinguish. Furthermore, it is also easier to distinguish the general trend of data which indicates that for each plate combination, the impulse amelioration values increase as the plate separation distance increases. Furthermore, it is important to note that for each plate combination, the impulse amelioration values for the various plate separation distances differ more greatly from each other than when compared to the initial peak pressure results.

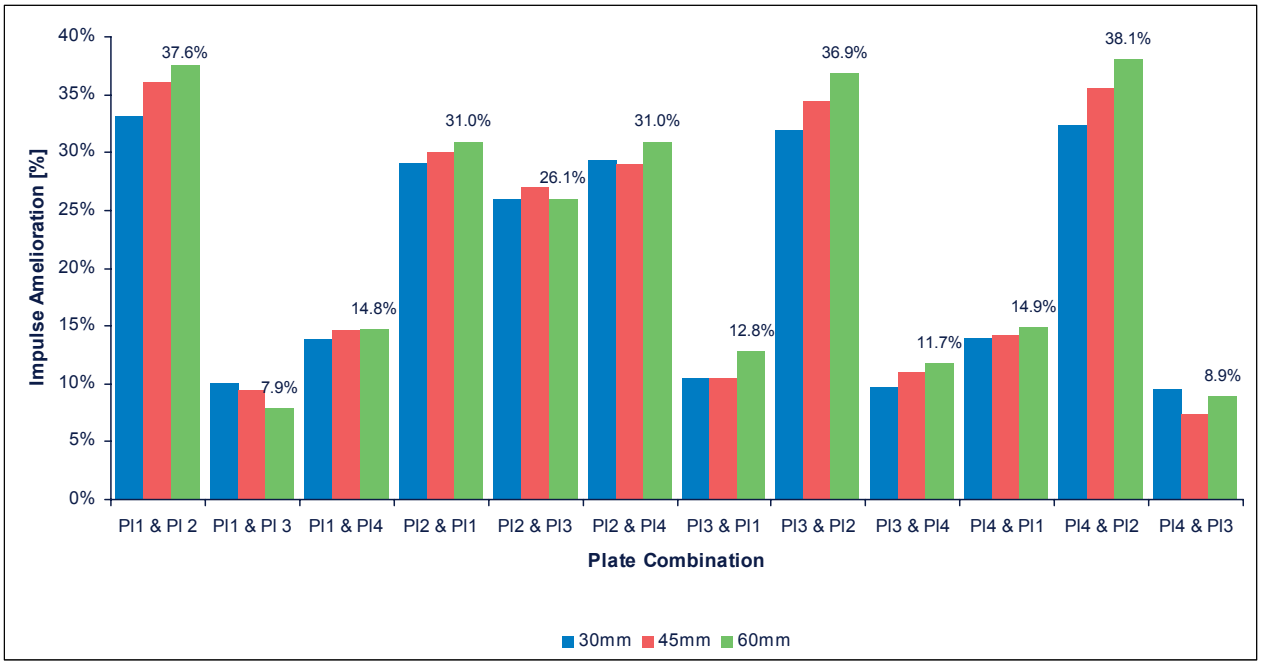


Figure 72: Impulse Amelioration Results Obtained for the Various Plate Combinations

An average initial peak pressure amelioration value for the twelve plate combinations was calculated for each plate separation distance in order to verify the general data trend that the impulse amelioration values increase as the plate separation distance increases. The results are shown in the figure that follows.

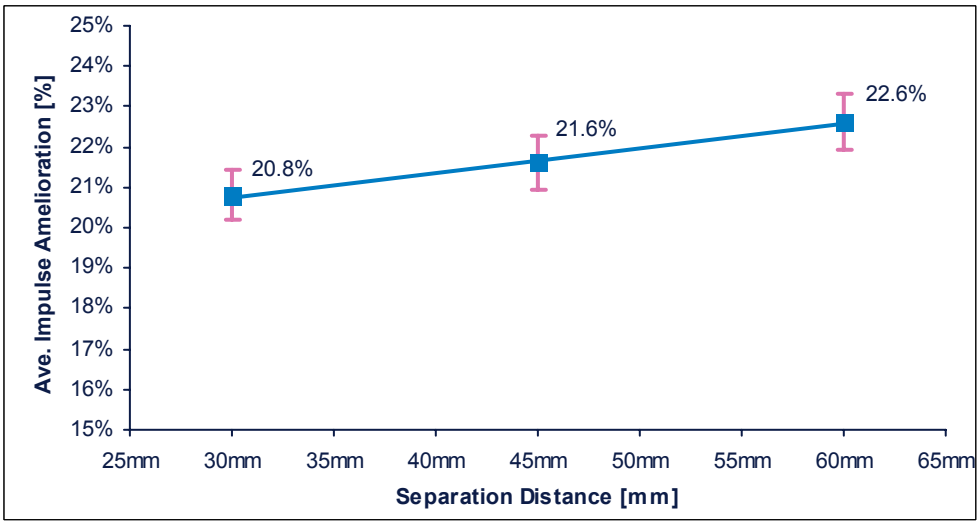


Figure 73: Average Impulse Amelioration Vs Plate Separation Distance

The graph displays a linear relationship between the average impulse amelioration experienced by the end wall and the range of plate separation distances tested. The 30mm separation distance between plates corresponds to an average amelioration value of 20.8 % and that for the 60mm separation distance

corresponds to a value of 22.6 %. Therefore, if the separation distance is increased by 15mm the average impulse amelioration increases approximately 1 %.

It must be noted that the range of separation distances used during testing is relatively small when compared to distances that are possible to attain in real situations such as in ventilation ducts and channels. This range, with a maximum separation distance of 60mm, was selected due to the limiting length of the test section. One may argue that the results listed above is insignificant depending on the application, as the average impulse amelioration increases merely 1 % for every 15 mm increase in separation distance. In particular, this result would not be beneficial in instances where duct length is limited. Nonetheless, the results of the analysis (although small) indicate that impulse amelioration increases as the separation distance between the plates is increased.

9.9 Analysis of the Effects of Incident Mach number

Three plate combinations were randomly selected and tested at varying Mach numbers in order to determine the effect that the incident shock wave Mach number had on the initial peak pressure and impulse ameliorations experienced by the end wall of the shock tube. Tests were performed at set Mach numbers of M_{set} = 1.23 and M_{set} = 1.35. Data obtained for M_{set} = 1.42 were taken from tests previously performed (refer to Table 11), for the third Mach number. All tests were performed for a 30 mm separation distance between plates and a Back & Back plate arrangement. It is also important to note that for all tests, the time period used for the integration of the end wall pressure traces was 9 250 μs and the ambient atmospheric pressure, P_o, was measured to be 0.83 bar.

The pressure trace results obtained for each plate combination were then over-laid for comparison. The figure that follows, displaying the results obtained for plate combination Pl4&Pl3, serves as an example of such a figure produced for each plate combination.

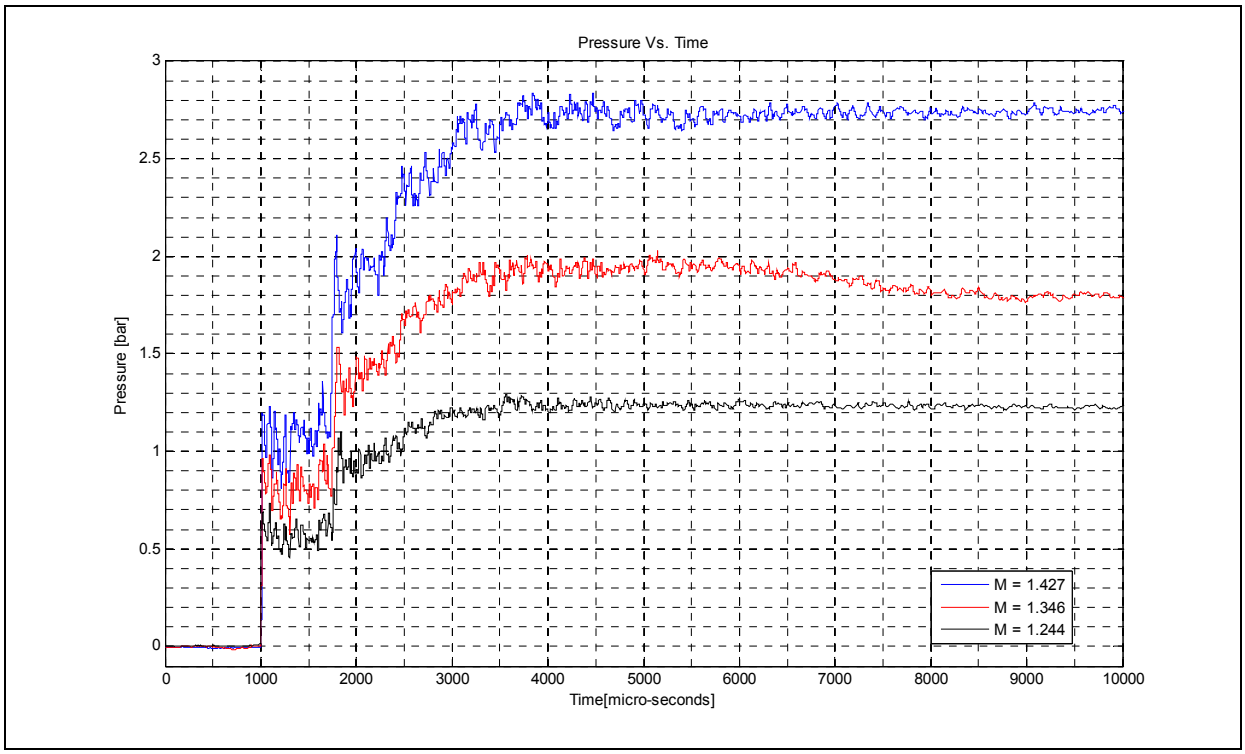


Figure 74: Overlay of End Wall Pressure Traces for Pl4&Pl3 Obtained for Three Different Incident Mach numbers

The pressure trace results obtained for all three plate combinations reveal that as the incident Mach number was increased, the amplitude of the entire pressure trace was increased which resulted in a greater initial peak pressure and impulse experienced by the end wall of the shock tube. The wave form remains similar for all cases and as expected is only dependant on the plate combination used. The figures that follow illustrate the relationship of the initial peak pressure and the impulse experienced by the end wall of the shock tube and the incident Mach number. This data has been extracted from Table 13.

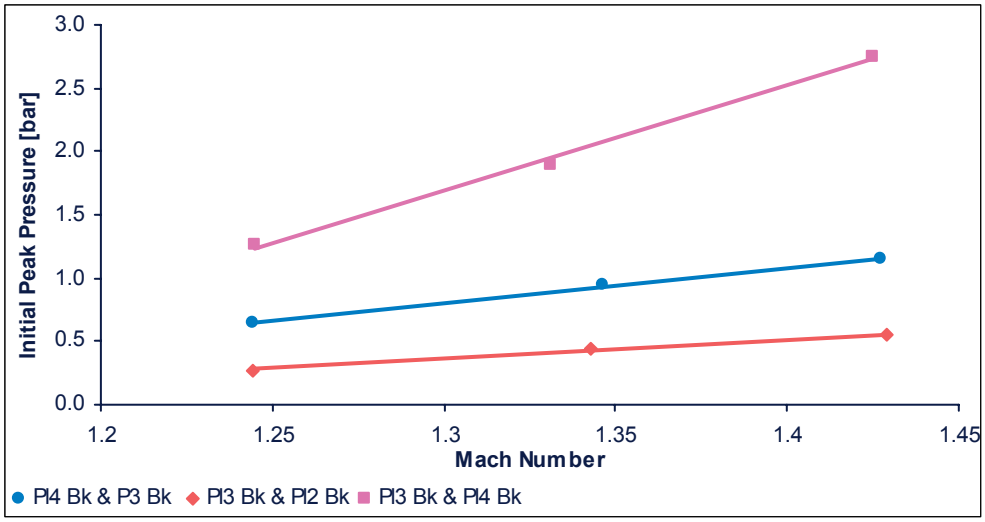


Figure 75: End Wall Initial Peak Pressure Vs Incident Mach number

Figure 75, indicates that the initial peak pressure experienced by the end wall increases as the incident Mack number is increased. It was found that this data was best described by a linear cure fit (minimal error). Therefore, for each plate combination the initial peak pressure experienced by the end wall is directly proportional to the incident Mack number. These results correlate well with the findings of Britan et al (2006), which states that the amplitude of the initial pressure jump experienced by the end wall decreased as the incident Mach number decreased and that this pressure amplitude reduces linearly with increasing distance between the end-wall and the barrier. Please refer to Section 3.2.

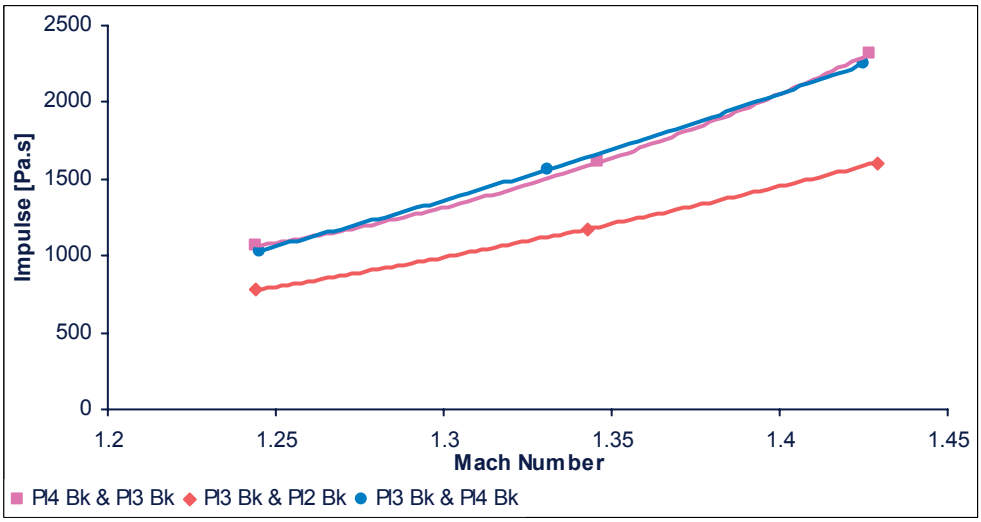


Figure 76: End Wall Impulse Vs Incident Mach number

Figure 76, clearly shows that the impulse experienced by the end wall increases as the incident shock wave Mach number was increased and it was found that a quadratic curve fit best describes (minimal error) the trend of data obtained for each combination tested.

These results were expected since the pressure ratio across the incident shock wave increases as the Mach number is increased and causes the increase in both the initial peak pressure and impulse experienced by the end wall. Once again, it is noted that the plate combination in which Plate 2 is present produces the lowest initial peak pressure and impulse values.

The values of impulse amelioration obtained for each plate combination are plotted in the figure that follows.

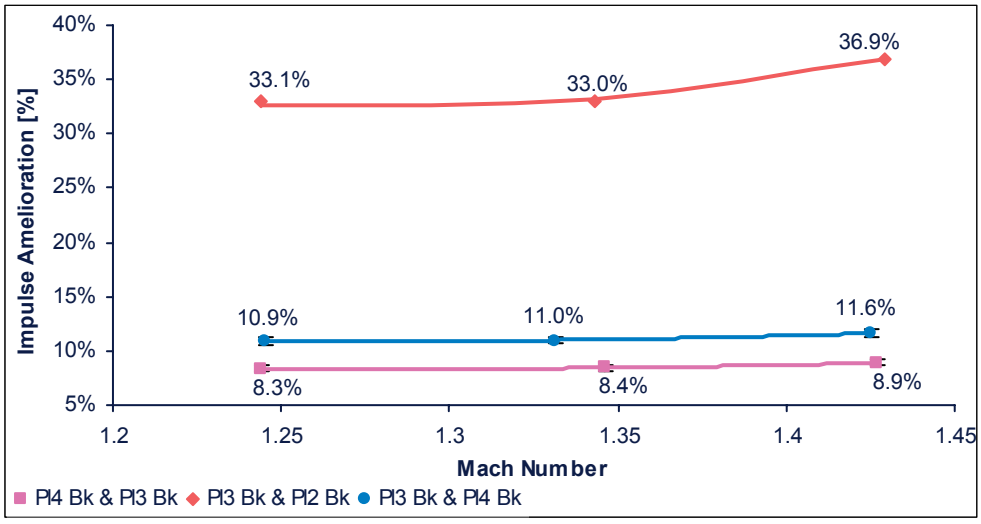


Figure 77: End Wall Impulse Amelioration Vs Incident Mach number

Since the integration time period is constant for all tests performed, the figure indicates the measure of the amelioration efficiency as a function of the Mach number. The general data trend indicates that small increases in the impulse amelioration values occur as the Mach number increases. These results may be attributed to the larger entropy changes that occur for higher Mach numbers, in which system losses increase causing impulse amelioration to increase.

9.10 Wave Diagrams

The wave process that occurs when the incident shock wave interacts with the test specimens is highly complex. Figure 78 below, illustrates a simplified approximate wave diagram of the wave processes that occur when the incident shock wave interacts with the plate specimens and the end wall of the shock tube.

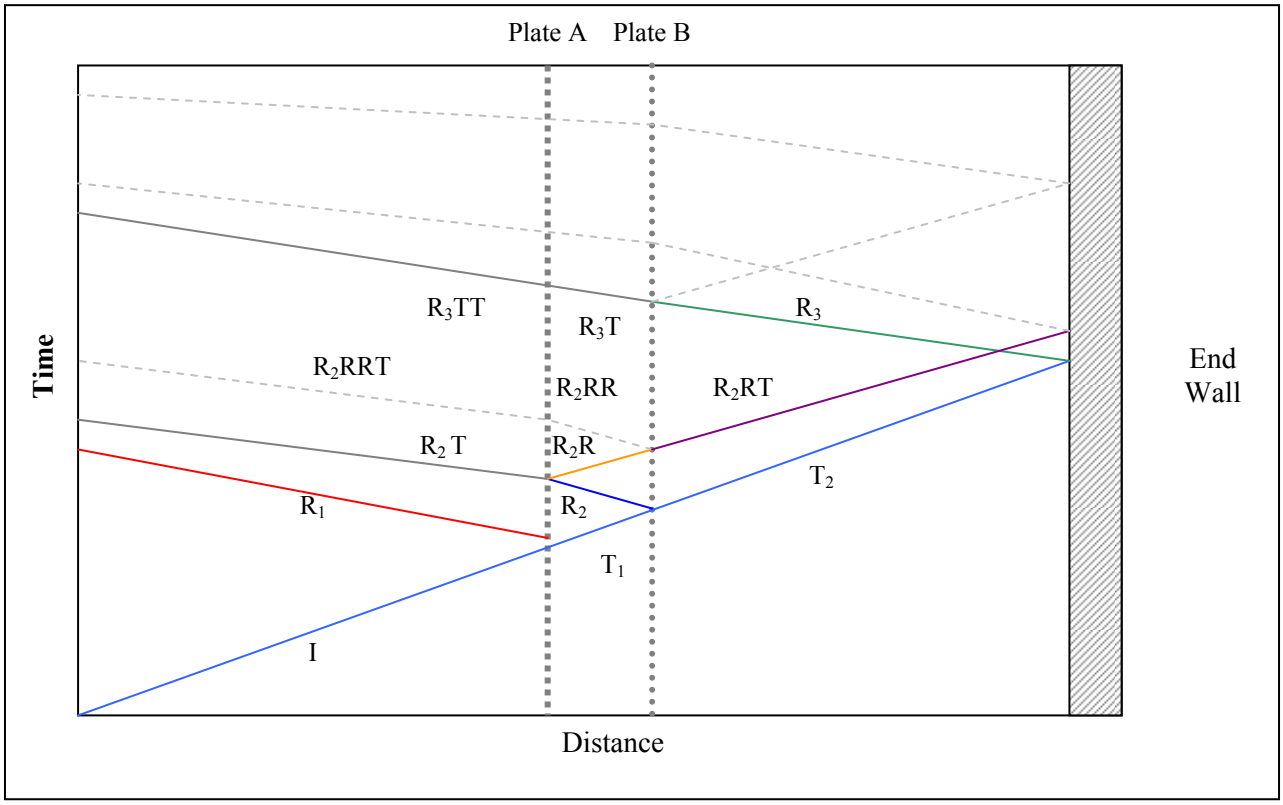


Figure 78: Wave Diagram Illustrating the Wave Processes that Occur

Upon a head on collision between the incident shock wave (I) and the upstream plate specimen (Plate A), a reflected shock (R_1) propagates from the barrier and a transmitted shock (T_1) propagates towards the downstream plate. Once the transmitted shock collides head on with the downstream barrier, a reflected shock (R_2) is propagated towards the upstream plate and a transmitted shock (T_2) propagates toward the end wall of the shock tube. This is the beginning of multiple reflections that occur in the airspace between the two plate specimens. When the transmitted shock (T_2) reaches the end wall of the shock tube, it is reflected (R_3) back towards the downstream barrier and this is the beginning of multiple reflections in the airspace between the end wall and the downstream plate specimen. It must be noted that for every reflection that occurs off the downstream plate in the airspace between the plate specimens, a transmitted shock is propagated (e.g. R_2RT) and this shock further interacts with the wave system that exists in the

airspace between the end wall and the downstream plate specimens. Similarly, for every reflection that occurs off the downstream plate in the airspace between the end wall and the downstream plate, a transmitted shock is propagated (e.g. R_3T) and this shock further interacts with the wave system that exists in the airspace between the plate specimens.

It is know that when an incident shock wave interacts with a porous barrier, the flow immediately behind the barrier is highly unsteady and non-uniform (inhomogeneous and non-isotropic) with viscous and heat transfer processes contributing to the significant energy dissipation of the flow in this region. Greatest attenuation of the transmitted wave occurred in this zone just downstream of the barrier where the flow is highly turbulent due to interactions of the jets and wakes produced by the barrier. Please refer to Britan et al (2004) and Dosanjh (1956). Therefore, in this study, the significant attenuation of the incident shock wave is attributed to the system of multiple reflected and transmitted waves that are produced by the presence of the plate specimens in series. This increases the frequency of shock and barrier interactions, when compared to just using a single barrier, creating regions of highly unsteady flow, especially in the air space between the plate specimens. Furthermore, the presence of the series of plates also allows for wave resonance to occur which may further attenuate the strength of the incident shock wave. It has been noted previously that destructive wave interference mostly likely occurs in which some of the incident wave's energy is dissipated.

The pressure trace data for plate combinations Pl1&PL2, Pl3&Pl2 and Pl3&Pl4 with Back & Back plate arrangements and a plate separation distance of 30 mm, were used to construct approximate wave diagrams. These plate combinations were selected as they produce distinct 'step like' pressure traces, making the identification of shock waves from the pressure trace data easier. Due to the complex nature of the wave interactions that occur in the test section and the fact that transverse waves caused by the shape of the holes effect the pressures traces, making the flow become 3-dimensional, these diagrams could not be completed. Therefore, as a dispersion of waves occurs which does not allow one to monitor distinct waves, these wave diagrams reveal little information.

As an example of the data acquired, the pressure plot and the incomplete wave diagram for plate combination Pl3&Pl2 have been listed.

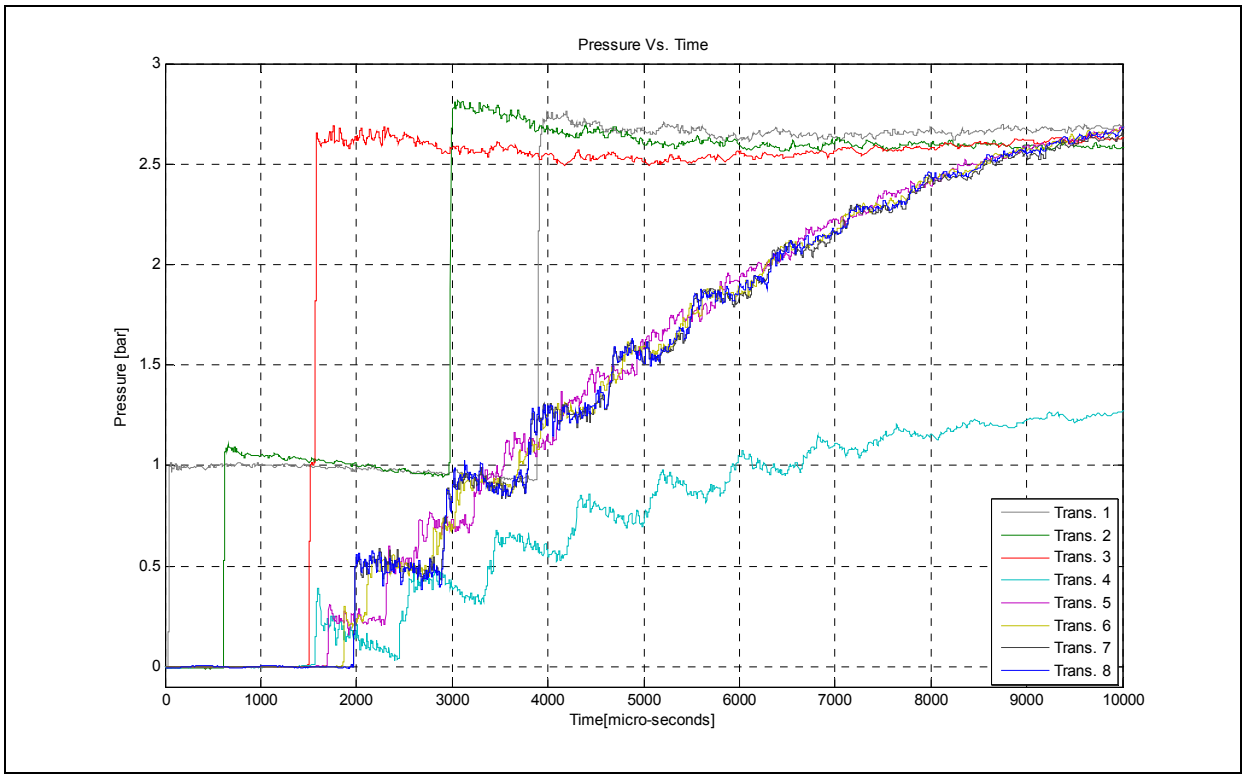


Figure 79: Pressure Plot for Pl3&Pl2 - M_{set} = 1.42, d=30mm, Back & Back Plate Arrangement

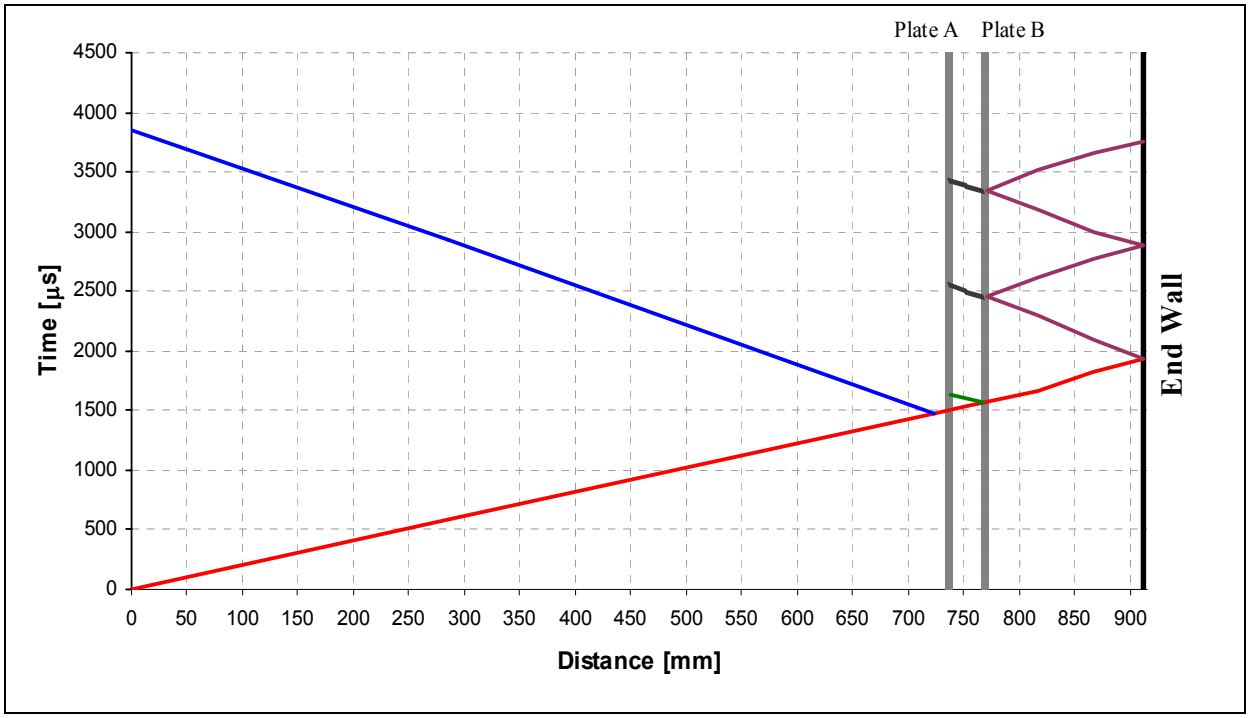


Figure 80: Approximate Incomplete Wave Diagram for Pl3&Pl2 - M_{set} = 1.42, d=30mm, Back & Back Plate Arrangement

From the approximate wave diagram it is noticed that after t > 1600 μs the diagram is incomplete for the region downstream of Plate A. This is attributed to the fact that the complex wave interactions which are on longer 1 - dimensional occur in the airspace between the two plates, making the distinctive shock waves difficult to distinguish in this region. It must be noted that wave reflections occur in this airspace, which produces transmitted waves both upstream of Plate A and downstream of plate B. These transmitted waves affect the pressure readings of the transducers situated in these regions, but these waves could not be indicated in the above diagram due to 3-dimensional effects.

The wave that is reflected in the air space between the end wall and Plate B remains strong and 1 - dimensional for a longer time though. Its multiple reflections are clearly noticed in the diagram above. This is attributed to the fact that Plate 2 has the lowest porosity of all the plates used in this study. It therefore, effectively traps the transmitted wave, T_2. The dashed black lines in the wave diagram indicated the transmitted shock waves due to the shock reflections which occur in the airspace. These waves correspond to the stepped increase in pressure for Transducer 4, as seen in the pressure plot figure. It must be noted that the transmitted waves due to the multiple reflections that occur in the air space between the plates also affects the wave system between the end wall and the downstream plate; however these effects have been neglected in the approximate wave diagram.

It is suggested that future studies regarding this topic include numerical techniques i.e. the use of computational fluid dynamic software, in order to further investigate the complex wave processes that occur upon interaction with the plate specimens. The use of such techniques would confirm the major loss mechanisms of the system and possibly allow for construction of more accurate wave diagrams.

9.11 Schlieren Photographs

Schlieren photograph tests were performed to track the motion of the incident wave shock wave and to visualize the process of wave interactions that occurred in the test section. Six plate combinations, viz. Pl4&Pl2, Pl4&Pl1, Pl1&Pl3, Pl2&Pl4, Pl3&Pl2 and Pl3&Pl4, with Back & Back plate arrangements were randomly selected for the photographic tests. In total, approximately 63 photographic tests were performed. All tests were performed using a set Mach number of M_{set} =1.42 and a separation distance of 30 mm between plate specimens. Ten photographs were taken over a 325 μs interval using a time delay of 1425 μs for each plate combination. During this time interval the incident shock wave interacts with both plate specimens.

As the photographs for the six combinations are similar in nature, the summarized results of plate combination Pl2&Pl4 are only discussed in this section. The photographic results for all six plate combinations may be referred to in the DVD accompanying this report. Furthermore, the complete set of photographic results for plate combinations Pl2&Pl4 and Pl3&Pl4 have been listed in Appendix D. The summarized results obtained for plate combination Pl2&Pl4 are illustrated in the Figure 81 that follows.

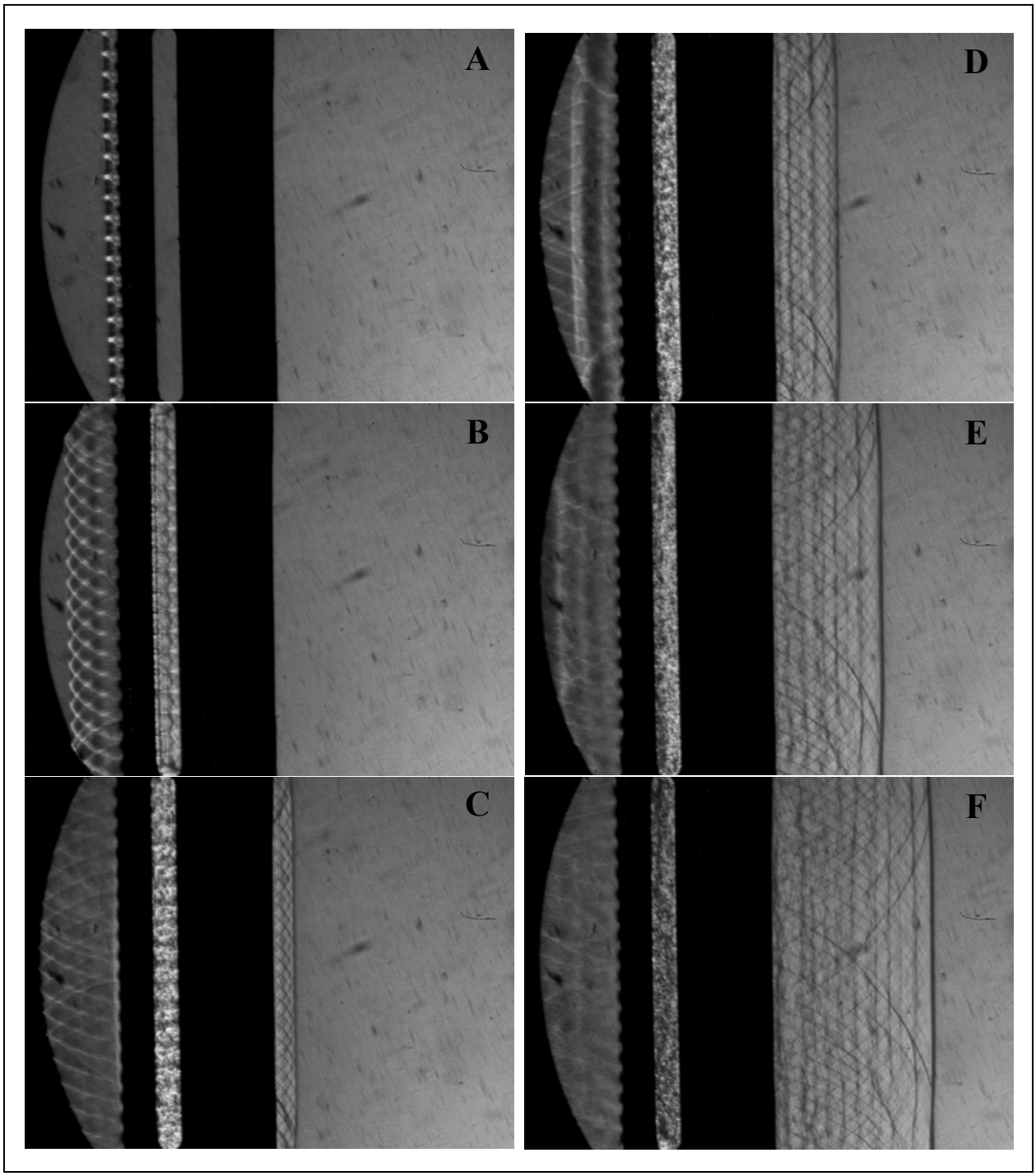


Figure 81: Schlieren Photographs of Pl2&Pl4 at Time Delays of A) t = 1500 μs, B) t = 1550 μs, C) t = 1650 μs, D) t = 1700 μs, E) t = 1750 μs and F) t = 1800 μs

In Picture A, that follows, the incident shock wave is seen to interact with the upstream plate specimen, producing both a reflected wave and a transmitted wave. The reflected wave is seen in the figure; however the transmitted wave is not visible as yet.

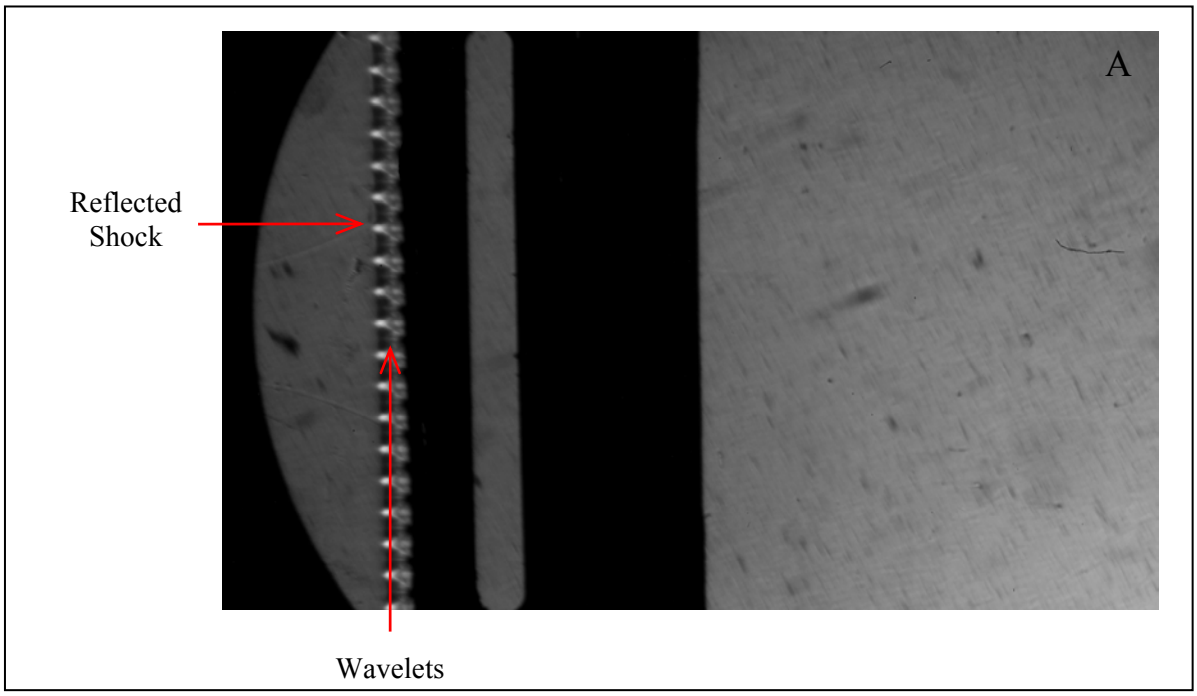


Figure 82: Schlieren Photograph of Pl2&Pl4 at a Time Delay of t = 1500 μs

In Picture B, that follows, the transmitted wave is seen in the air space between the two plate specimens and the reflected shock wave is seen to travel further upstream of Plate A. The flow in this air space is noted to exhibit structure as this transmitted wave has not interacted with the downstream plate, Plate B, as yet. Note that when this transmitted wave collides with the downstream plate, part of it will be transmitted towards the end wall of the shock tube and part of it will be reflected upstream towards Plate A.

As noted previously, it is in this region between the plate specimens that the significant attenuation of the incident shock wave occurs due to the multiple reflections that occur increasing the frequency of shock and barrier interactions, when compared to just using a single barrier, thus creating highly unsteady flow. Furthermore, destructive wave interference mostly likely occurs in this region causing a portion of the incident wave's energy to be dissipated.

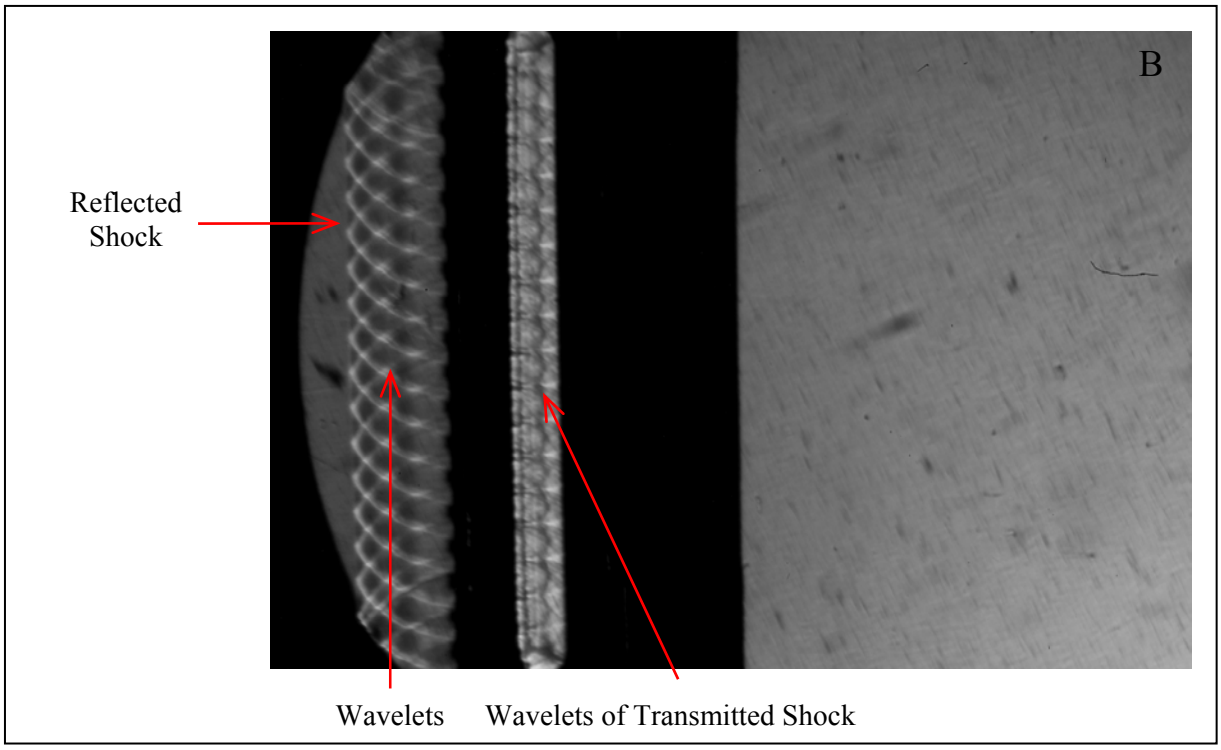


Figure 83: Schlieren Photograph of Pl2&Pl4 at a Time Delay of t = 1550 μs

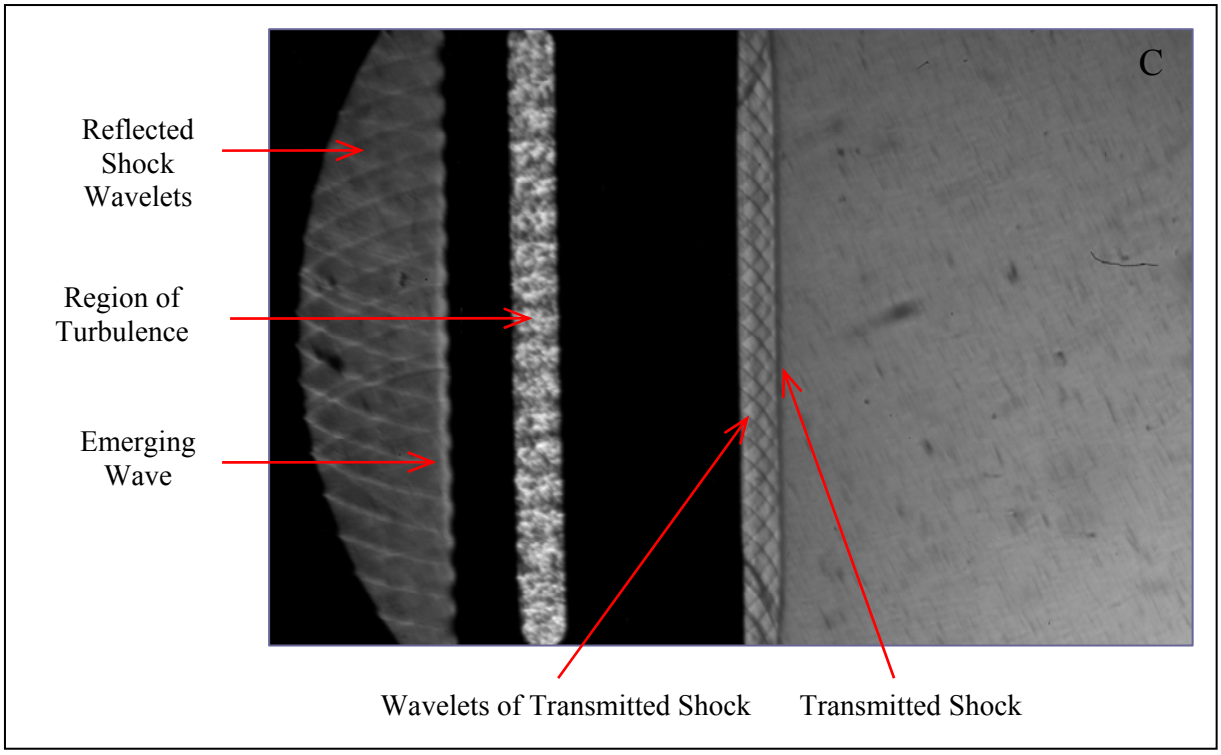


Figure 84: Schlieren Photograph of Pl2&Pl4 at a Time Delay of t = 1650 μs

In Picture C, the second transmitted wave (T_2) is seen to emerge after passing through the downstream plate, Plate B, and travels towards the end wall of the shock tube. It is also noticed that the flow in the airspace between the two plate specimens has become highly turbulent due to the passing of the reflected wave (R_2) originating from the transmitted wave interacting with Plate B. This reflected wave which is traveling upstream collides with Plate A and the processes of transmission and reflection again occur. The transmitted part of this wave is noticed to emerge just in front of Plate A in this picture as well.

In Picture D, it is noticed that a transmitted wave has emerged after interacting with Plate B i.e. R_2RT. This is indicated by a region of strong turbulence just after the 'Bending Moment' Plate B of the mounting system. This result is supported by the pressure trace data.

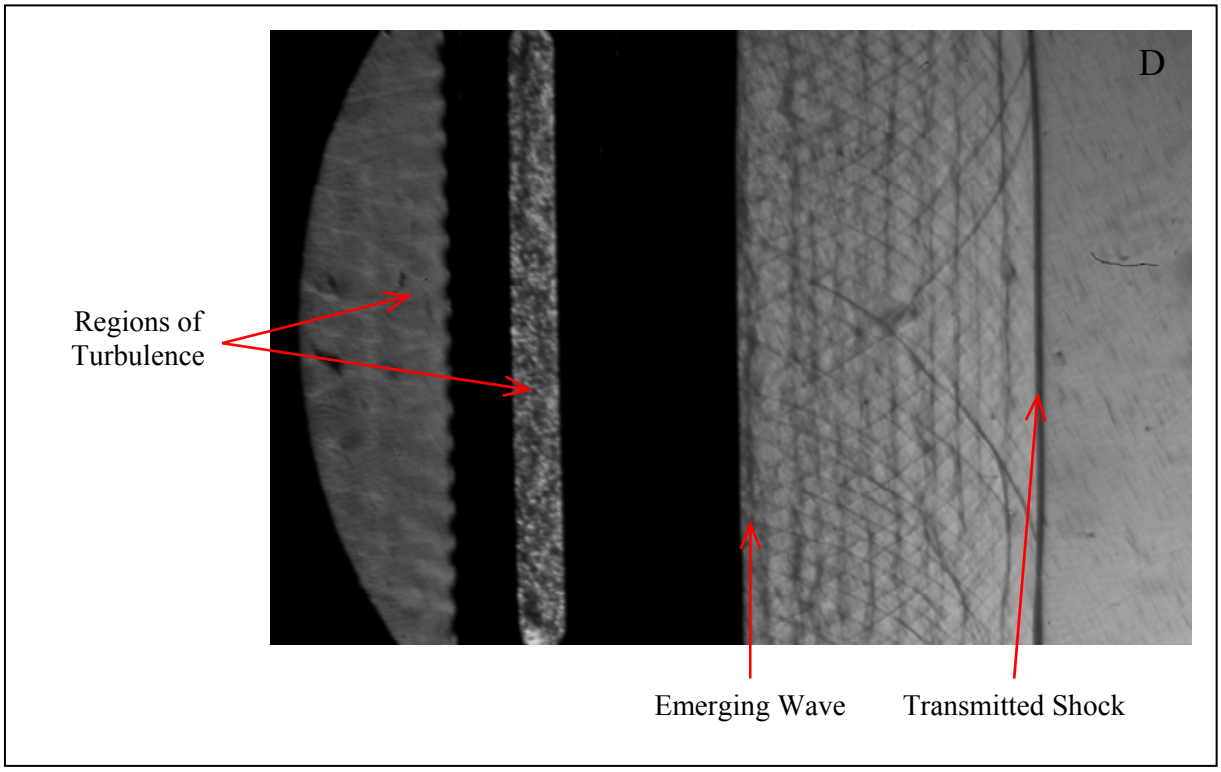


Figure 85: Schlieren Photograph of Pl2&Pl4 at a Time Delay of t = 1700 μs

Pictures E and F illustrates the strengthening (darkening of the line) of the total transmitted wave front (which includes T_2, R_2RT etc.) as it travels towards the end wall of the shock tube. The flow in the airspace is seen to remain turbulent as successive reflections occur between the two plate specimens. The flow upstream of Plate A is also noted to become more turbulent due to transmission of waves from the air space between the plate specimens.

10 Conclusion

The metal test specimens were found to have directional properties as lower pressure differential values were recorded across each test specimen with their fronts facing the oncoming flow when compared to the backs of the specimens facing the oncoming flow. This result was expected; for the holes with the larger diameter were facing the flow in this testing condition (i.e. front facing) offering a lower resistance to the air flow and thus producing lower drag coefficients for the plates. Plate 2 was found to have the greatest resistance to flow and this result corresponds to it having the lowest porosity (6.6 %). Plate 3 was found to have the least resistance to flow as it has the highest porosity (41 %). Since the porosities of Plate 1 (17 %) and Plate 4 (19 %) are similar, so were their resistances to the oncoming flow.

From the analysis of results for the plate arrangement tests it was found that the Front & Front plate arrangement produced both the lowest initial peak pressure and impulse amelioration values with average values of 71.5 % and 19.3 % respectively. The Back & Back plate arrangement produced the greatest initial peak pressure and impulse amelioration with an averages values of 73.7 % and 20.45 % respectively. One cannot differentiate which of the Front & Back and Back & Front plate arrangements produce greater amelioration values when one takes the uncertainty of these values into account. Therefore it was concluded that the Back & Back plate arrangement produced the greatest initial peak pressure and impulse amelioration values in general and in order to reduce the number of tests to be performed it was decided that the Back & Back arrangement would be used for the remaining tests of the study. It was found that plate combinations Pl1&Pl2, Pl2&Pl1, Pl2&Pl4, Pl3&Pl2 and Pl4&Pl2 produce the greatest initial peak pressure amelioration, with amelioration values greater than 80 %. The remaining plate combinations produced end wall pressure amelioration values less than 80 %, but greater than 50 %. Plate combinations Pl1&Pl2, Pl3&Pl2 and Pl4&Pl2 produce the greatest end wall impulse amelioration, with impulse amelioration values greater than 30 %. Furthermore, the impulse amelioration values obtained for combinations Pl2&Pl1, Pl2&Pl3 and Pl2&Pl4 were also large, with values greater than 25 %. The remaining plate combinations produced end wall impulse amelioration values less than 15 %.

The analysis of the plate combination tests revealed that combinations in which Plate 2 (which had the lowest porosity) was present, produced the highest initial peak pressure and impulse amelioration values. The remaining plate combinations, in which Plate 2 was absent, produce significantly lower initial peak pressure and impulse amelioration values. It was also noticed that complementary plate combinations e.g. Pl1&Pl2 and Pl2&Pl1, produce differing initial peak pressure and impulse amelioration results. This result was expected as different wave interactions occur when plate positions, either upstream or downstream, are interchanged. The initial peak pressure amelioration results indicated that for all

complementary plate combinations, the combinations which had the lower porosity plates, with higher resistances to the oncoming flow, situated downstream produce larger amelioration values. The difference in amelioration values were found to be small (< 3 %) though. The impulse amelioration results indicated that for all sets of complementary plate combinations, the combinations in which the lower porosity plates that were situated upstream produced greater impulse amelioration values. These results indicate that maximum impulse amelioration was achieved by placing the less porous of any two plates under consideration upstream in the test section.Upon further analysis of the plate combination tests data, it was found that the initial peak pressure and impulse amelioration values were clearly dependant on the combined porosities of the plates in a plate combination i.e. plate combination porosity. As the porosity of the combination increased the initial peak pressure amelioration experienced by the end wall of the shock tube decreased. This corresponded to a higher initial peak pressure being experienced by the end wall as the resistance of the combination of plates decreased. The end wall impulse amelioration was also found to decrease as the porosity of the plate combination increased. Therefore as the combined resistance of the plate specimens increased, the impulse experienced by the end wall of the shock tube increased, lowering the amelioration value achieved. It was concluded that the porosity of the combined plates have an overriding influence on the end wall initial peak pressure and impulse amelioration values when compared to the effect that plate arrangement (i.e. geometrical influences) has.

For all tests performed in this study, the time period used for the integration of the end wall pressure traces was 9 250 μs as measured from the first rising edge of the of these pressure traces. As Britan (2006) states that an acceptable closing time for a blast valve in a shelter's ventilation system is approximately 4 000 μs, the impulse amelioration values for plate combinations Pl1&Pl2 and Pl3&Pl4 were recalculated, using this shorter time period, for comparative purposes. These plate combinations were selected, as Pl1&Pl2 produce the greatest impulse amelioration whereas Pl3&Pl4 produce the least. It was found that using the 4 000 μs time period for integration produced greater impulse amelioration values as the rate of pressure rise, dp/dt, was initially lower at the beginning of the end wall pressure trace and therefore produced a larger impulse amelioration value. It was concluded that plate combination Pl3&Pl4, which produced the lowest impulse amelioration value (7.9 %) in this study, would produce significant impulse amelioration (20.3 %) if it were to be used in a shelter's ventilation system.

The results obtained during this study are promising as significant initial peak pressure and impulse amelioration values were obtained. The significant attenuation of the incident shock wave obtained during this study is attributed to the system of multiple reflected and transmitted waves that are produced by the presence of the plate specimens in series. This increases the frequency of shock wave and barrier interactions, when compared to just using a single barrier, creating regions of highly unsteady flow,

especially in the air space between the plate specimens. Please refer to Section 3.2. Furthermore, the presence of the series of plates also allows for wave resonance to occur which may further attenuate the strength of the incident shock wave. It has been noted previously that destructive wave interference mostly likely occurs in which some of the incident wave's energy is dissipated. The construction of wave diagrams was attempted in order to shed further light upon the wave interactions that occurred. However; it was found that the wave interactions were complex and rapidly became three dimensional, making the distinctive shock waves difficult to identify and therefore the wave diagrams could not be completed. It is suggested that future studies regarding this topic include numerical techniques in order to further investigate the complex wave processes that occur upon interaction with the plate specimens. The use of such techniques would confirm the major loss mechanisms of the system and possibly allow for construction of more accurate wave diagrams.

Changes in the separation distance between plates were found to have insignificant effects on the end wall initial peak pressure amelioration values achieved. However; a linear relationship was found to exist between the average impulse amelioration experienced and the plate separation distances tested. The average impulse amelioration value was found to increase approximately 1 % for a 15mm increase in the distance between plates. It must be noted that the range of separation distances used during testing were relatively small when compared to distances that are possible to attain in real situations such as in ventilation ducts and channels. In such situations significant impulse amelioration benefits may be possible by distancing the plates as far apart from each other as possible.

Finally, the analysis of the incident Mach number tests reveal that the amplitude of the entire end wall pressure trace is increased as the Mach number is increased. This results in a greater initial peak pressure and impulse experienced by the end wall. The wave form produced was found to remain similar for all cases and was only dependant on the plate combination used. These results were expected since the pressure ratio across the incident shock wave increases as the Mach number is increased and causes the increase in both the initial peak pressure and impulse experienced by the end wall.

11 Recommendations for Future Studies

Further experimental testing should be performed:

- In order to determine the effects that plate separation distances larger than 60 mm have on the end wall impulse and initial peak pressure amelioration values. Due to the limiting length of the test section, a maximum separation distance of 60mm was selected in this study. Future studies should use separation distances much larger than this in order to fully analyze the effects of plate separation distance on the end wall amelioration values.

- In order to determine the effect that the distance between the end wall and the downstream plate specimen has on both the end wall impulse and initial peak pressure amelioration values. In this study a fixed distance of 140 mm was used.

- In which Transducer 3 is situated further upstream of Plate A in the test section so that more useful results may be obtained on the Reflected Wave Impulse.

- In which Transducer 4 is relocated such that wave interference from the 'bending moment' plate of the mounting system is reduced or possibly eliminated.

Intersecting wedge geometries, that are sufficiently strong to withstand a collision with an incident shock wave of at least M=1.6, should be designed and tested. It was originally envisaged that the test specimens manufactured and used by Seeraj (2004, unpublished) would be used for testing purposes. However, initial tests revealed that these composite test specimens were not suitable for testing purposes as they would have broken, or even shattered due to the large forces and bending moments acting on them when fixed in the test section. This, intersecting wedge geometry is most similar to that investigated by Skews and Broido (1992) and might produce more promising results than that obtained using the tapered hole arrangement.

12 References

Baker W.E. (1973), Explosions In Air, Southwest Research Institute, University of Texas Press, Austin and London

Bird G.A. (1958), The Effect of Wall Shape On the Reinforcement of A Shock Wave Moving Into A Converging Channel, Journal of Fluid Mechanics, pp 60 - 66

Britan A., Karpov A.V., Vasilev E.I., Igra O., Ben-Dor G., Shapiro E. (2004), Experimental and Numerical Study of Shock Wave Interaction With Perforated Plates, Journal of Fluid Mechanics, May 2004, Vol. 126, pp 399 - 409

Britan A., Igra O., Ben-Dor G., Shapiro H. (2006), Shock Wave Attenuation by Grids and Orifice Plates, Shock Waves, Vol. 16, pp 1 - 15

British Standards Institution (BS EN ISO 5167-1: 1997 with Amendments until Feb 1999), Measurement of Fluid Flow by Means of Pressure Differential Devices – Part 1. Orifice Plates, Nozzles and Venturi Tubes Inserted in Circular Cross Section Conduits Running Full, The British Standards Institution, 389 Chiswick High Road, London W4 4AL

Bugarin S. (2003), The Interaction of Shock Waves with Textiles, Masters of Science Dissertation, The University of the Witwatersrand, Johannesburg, South Africa

Clemedson C.J. and Jonsson A. (1976), Effects of the Frequency Content in Complex Air Shock Waves on Lung Injuries in Rabbits, Journal of Aviation, Space and Environmental Medicine, Vol. 47, pp 1143 - 1152

Colovos N. (2001), Blast Injuries, FACEP Article, www.mediccom.org, last updated 30 June 2001, last accessed: 21 January 2007

Cooper G.J. (1996), Protection of the Lung from Blast Overpressure by Thoracic Stress Wave Decouplers, Journal of Defence Science, Vol. 1, No.1, pp 85 - 93

Dosanjh D.S. (1956), Interaction of Grids with Traveling Shock Waves, National Advisory Committee for Aeronautics Technical Note 3680, John Hopkins University

Glass I.I. (1974), Shock Waves and Man, The University of Toronto Press, Institute for Aerospace Studies, University of Toronto, Canada

Hattingh T.S. (2000), The Interaction of Shock Waves with Porous Textiles, Masters of Science Dissertation, University of the Witwatersrand, Johannesburg, South Africa

Hirsch M. and Bazini J. (1969), Blast Injury of the Chest, Journal of Clinical Radiology, Vol. 20, pp 362 - 370

Huller T. and Bazini Y. (1970), Blast Injuries of the Chest and Abdomen, Archives of Surgery, Vol. 100, pp 24 - 30

John J.E.A. (1969), Gas Dynamics, Allan Bacon Inc., 470 Atlantic Avenue, Boston

Kinney G.F. (1962), Explosive shocks in Air, The MacMillan Company, New York, The United States of America

Lavonas E. (2003), Blast Injuries, eMedicine Article, www.eMedicine.com, last updated 30 December 2003, last accessed: 21 January 2007

Lavonas E. (2006), Blast Injuries, eMedicine Article, www.eMedicine.com, last updated 17 January 2006, last accessed: 21 January 2007

Leibovici D., Gofrit O.N., Stein M., Shapira S.C., Noga Y., Heruiti R.J. and Shemer J. (1996), Blast Injuries: Bus Versus Open Air Bombings, Comparative Study of Injuries In Survivors of Open-Air Versus Confined Space Explosions, Journal of Trauma: Injury Infection and Critical Care, Vol. 41, No. 6, pp 1030 - 1035

Mayo A. & Kluger Y. (2006), Blast Induced Injury of Air Containing Organs, ADF Health, Vol. 7, April 2006, http://www.defence.gov.au- last accessed: 21 January 2007

Merzkirch W. (1974), Flow Visualization, Academic Press Inc, 111 Fifth Avenue, New York, 10003, pp 86 - 100

Seeraj S. (2004, unpublished), Shock Wave Interaction with Porous Barriers, Fourth Year Research Project, The University of the Witwatersrand, Johannesburg, South Africa

Seitz M.W. (2001), Shock Wave Interaction with Porous, Compressible Foams, Doctor of Philosophy Thesis, University of the Witwatersrand, Johannesburg, South Africa

Skews B.W. & Broido P.E. (1992), Shock Attenuation Through A Grid of Obstacles, 4th International Symposium on Explosions Technology and Ballistics, Pretoria, South Africa

Skews B.W., Draxl M.A. Felthun L. & Seitz M.W. (1998) Shock Wave Trapping, Shock Waves Vol. 8, pp 23-28

Whitehouse J.L. (2003), The Pressure Distribution in the Wake of a Supersonic Aircraft Entering a Valley, Research Project, The University of the Witwatersrand, Johannesburg, South Africa

Wright J.K. (1961), Shock Tubes, John Wiley and Sons Inc., London, Meuthen & Co Ltd

Zuckerman S. (1940), Experimental Study of Blast Injuries to the Lungs, The Lancet, Vol. 239, pp 219 – 223

Appendices

Appendix A Transducer Calibration Constants

The results of the calibration procedure performed on the high speed PCB pressure transducers are listed in the table that follows. Please refer to Section 4.4.4 for a detailed description of the calibration procedure.

Table: Transducer Calibration Constants Used in the Study

Transducer Serial Number	**Calibration Constant**	
	[V/bar]	[mV/psi]
A21-SN 5924	2.687	25.66
A21-SN 4817	3.314	20.80
A21-SN 7938	2.831	24.35
A21-SN 10624	3.293	20.93
A24-SN 6709	13.747	5.02
A21-SN 7342	2.570	26.83
A21-SN 8287	2.763	24.95
A21-SN 8288	2.839	24.28
A21-SN 5477	3.097	22.26

Appendix B: Shock Tube Mach number and Diaphragm Calibration

The shock tube was recalibrated using four diaphragms which allowed for a set Mach number in the range of M_{set} = 1.2 – 1.43. The diaphragm combinations and their corresponding Mach number ranges have been listed in the table below. The compression and intermediate chamber pressures have also been included in the table.

Table: Shock Tube Mach number and Diaphragm Calibration

Upstream	**Downstream**				
Plastic A [μm]	**Plastic B** [μm]	**Mach Number** [bar]	**P_{comp}** [bar]	**P_{exp}** [bar]	**P_o** [bar]
23	3	1.20	1.61	1.07	0.83
		1.21	1.66	1.12	0.83
		1.22	1.7	1.16	0.83
		1.23	1.74	1.2	0.83
23	23	1.235	1.76	1.23	0.83
		1.24	1.9	1.36	0.83
		1.25	1.93	1.4	0.83
		1.26	1.96	1.42	0.83
46	23	1.3	2.28	1.28	0.83
		1.31	2.35	1.35	0.83
		1.32	2.43	1.43	0.83
		1.325	2.46	1.46	0.83
50	23	1.34	2.54	1.09	0.83
		1.35	2.63	1.17	0.83
		1.36	2.71	1.26	0.83
		1.37	2.8	1.34	0.83
		1.38	2.88	1.43	0.83
		1.39	2.96	1.51	0.83
50	46	1.415	3.27	1.81	0.83
		1.42	3.32	1.87	0.83
		1.43	3.44	1.99	0.83

Appendix C: Examples of Pressure Plots for all Plate Combinations Tested

The pressure plots listed in this Appendix correspond to the Plate Separation Distance Tests listed in Table 12 of this report. All tests were performed for a set Mach number of 1.42, a 30 mm separation distance and the Back & Back plate arrangement. The data sampling frequency was set at 2.5 MHz and a 'Filtervalue' of 25 was used to filter the pressure traces.

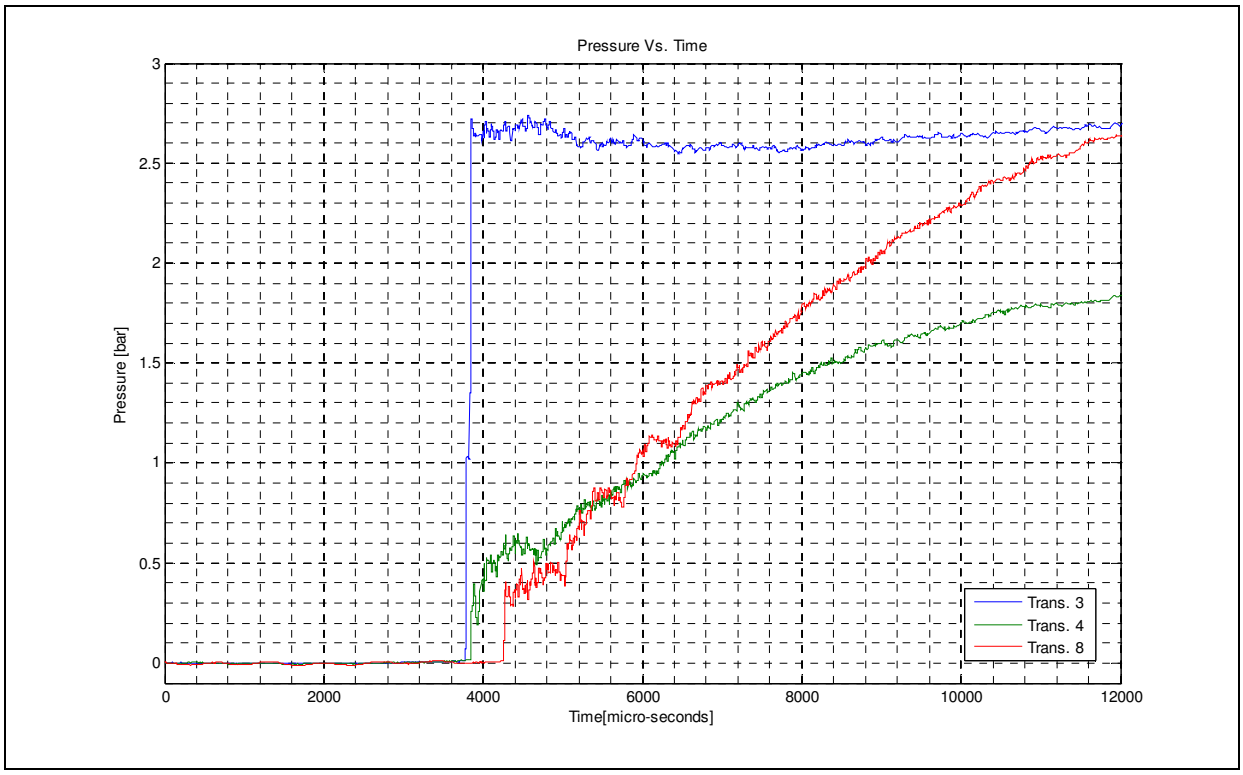


Figure: Pressure Plot for Pl1&Pl2

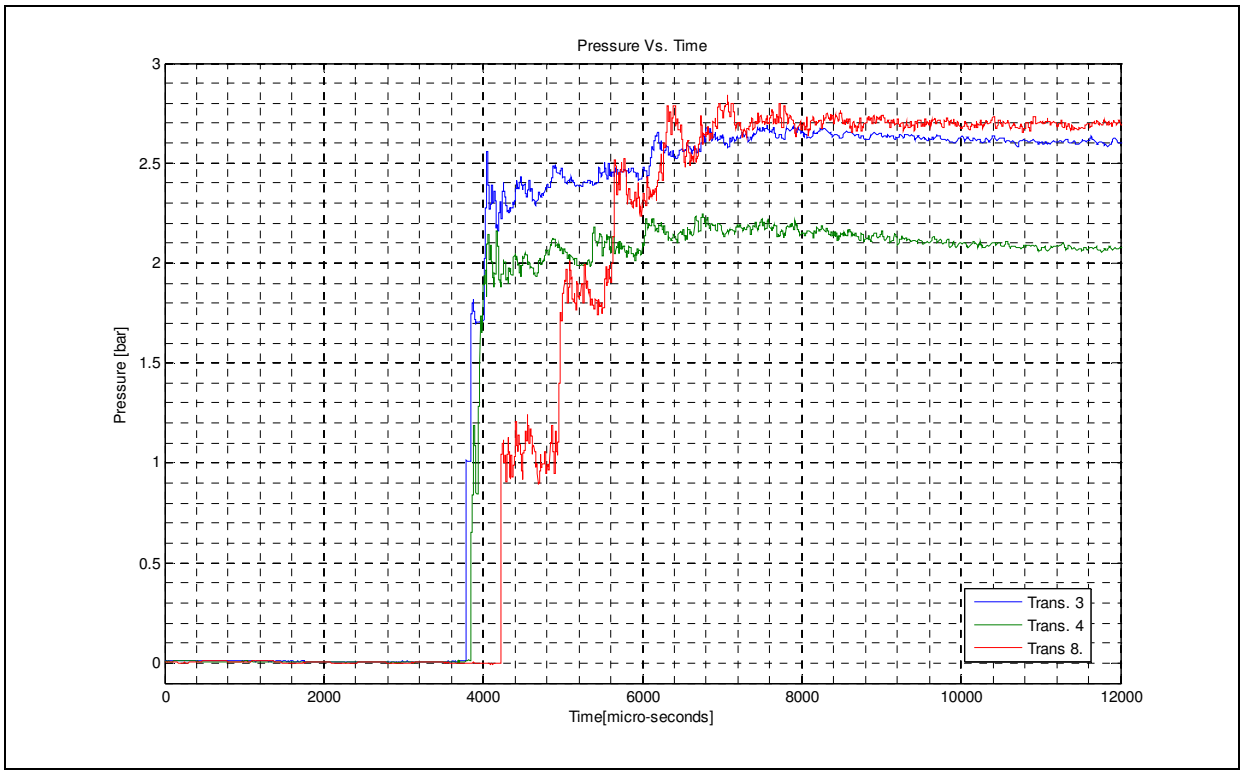


Figure: Pressure Plot for Pl1&Pl3

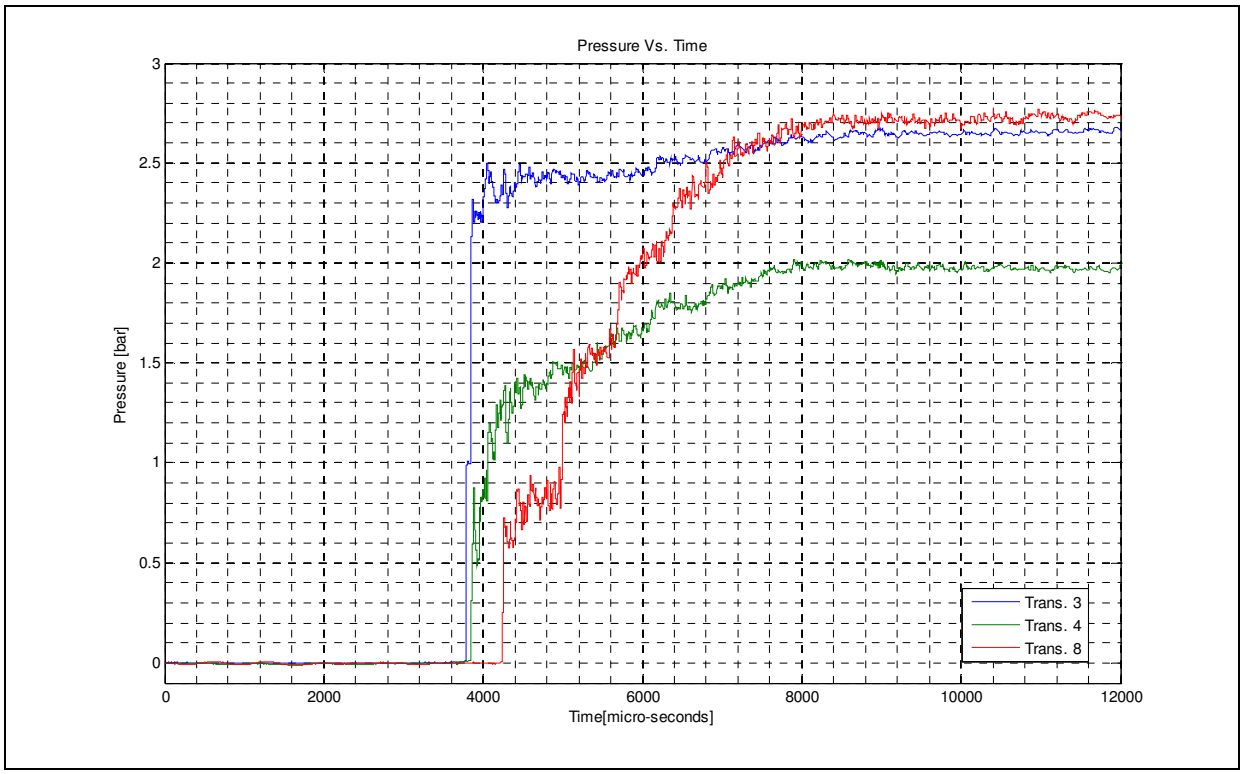


Figure: Pressure Plot for Pl1&Pl4

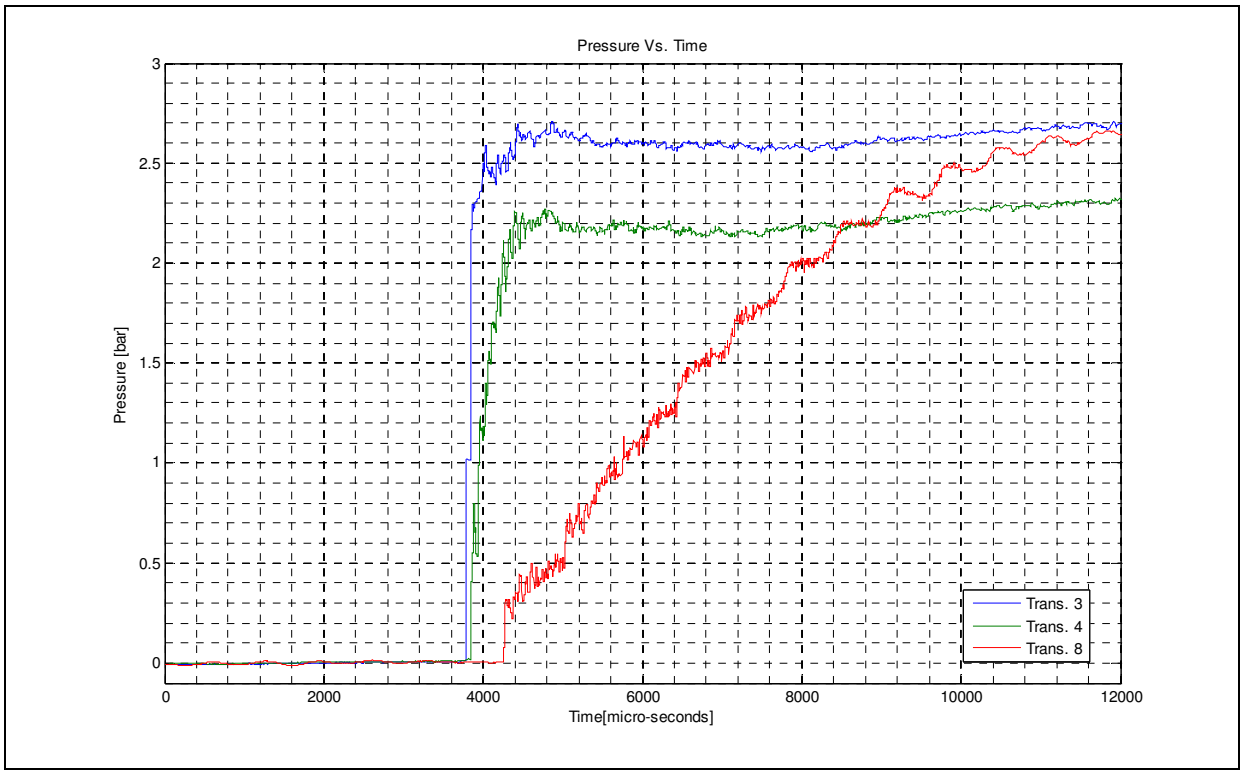


Figure: Pressure Plot for Pl2&Pl1

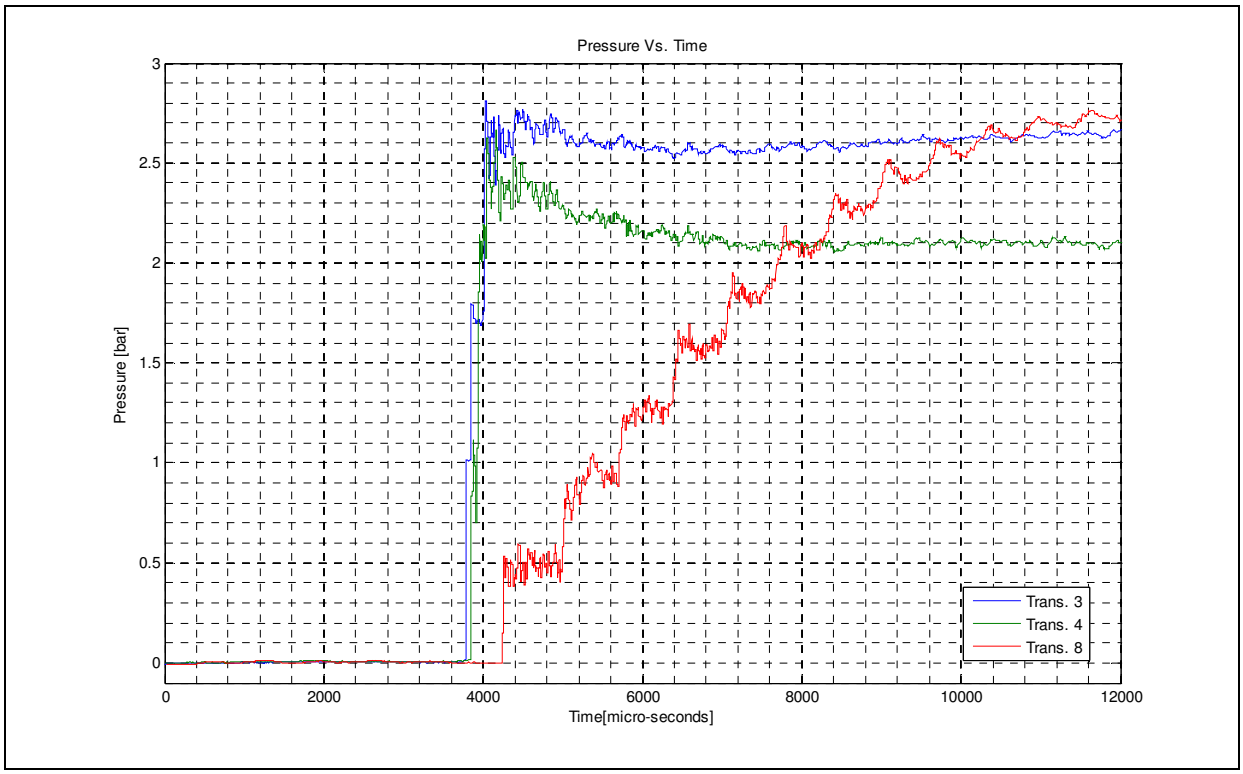


Figure: Pressure Plot for Pl2&Pl3

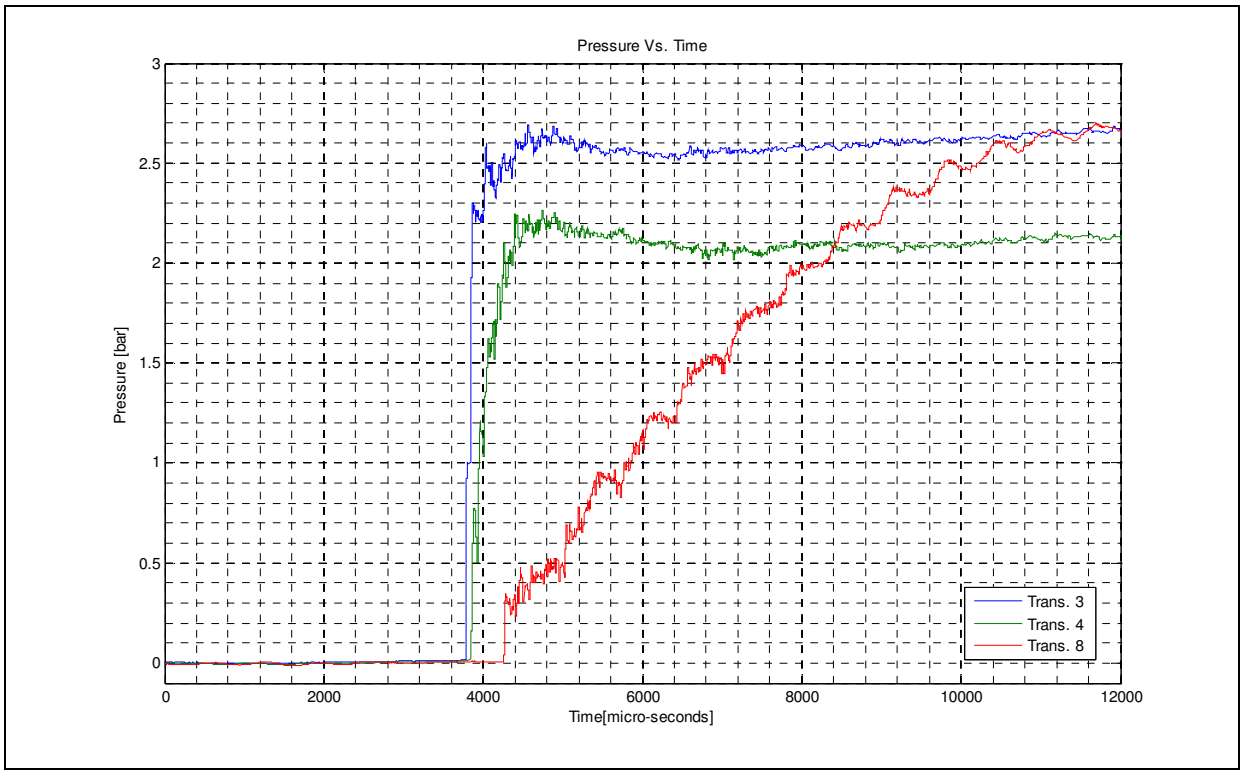


Figure: Pressure Plot for Pl2&Pl4

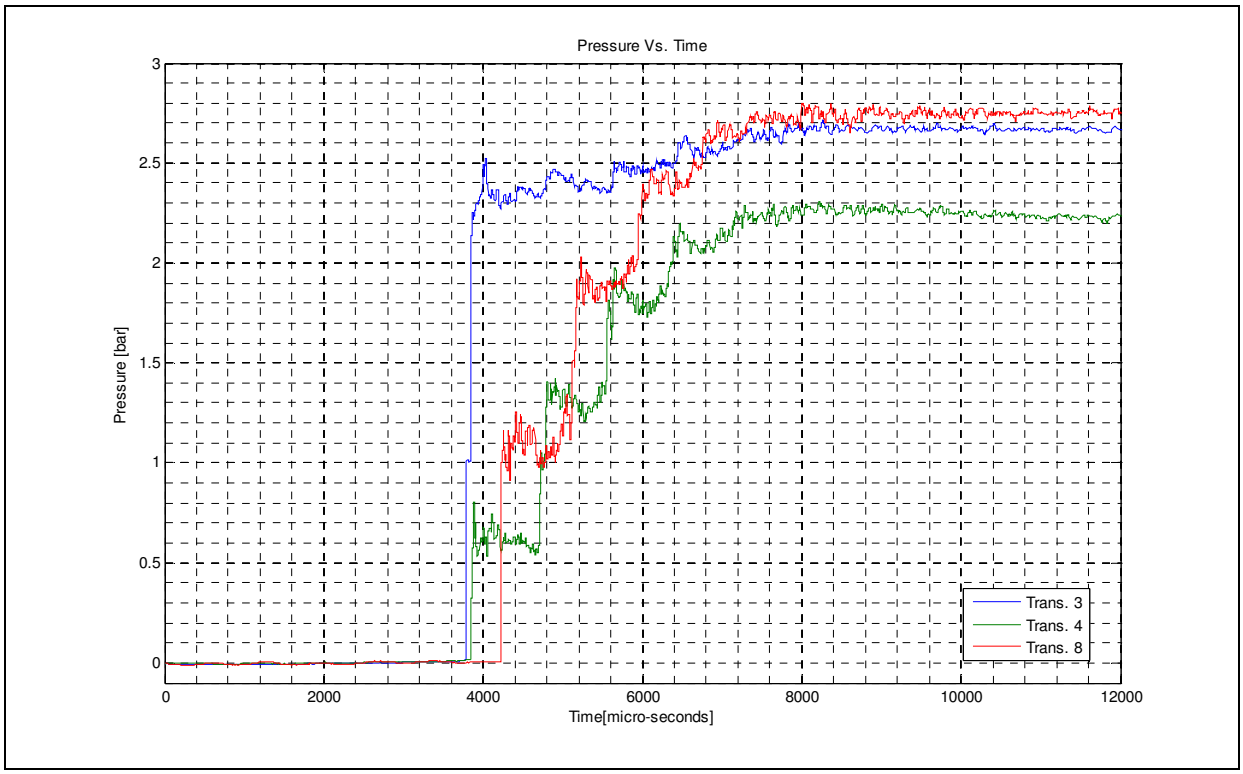


Figure: Pressure Plot for Pl3&Pl1

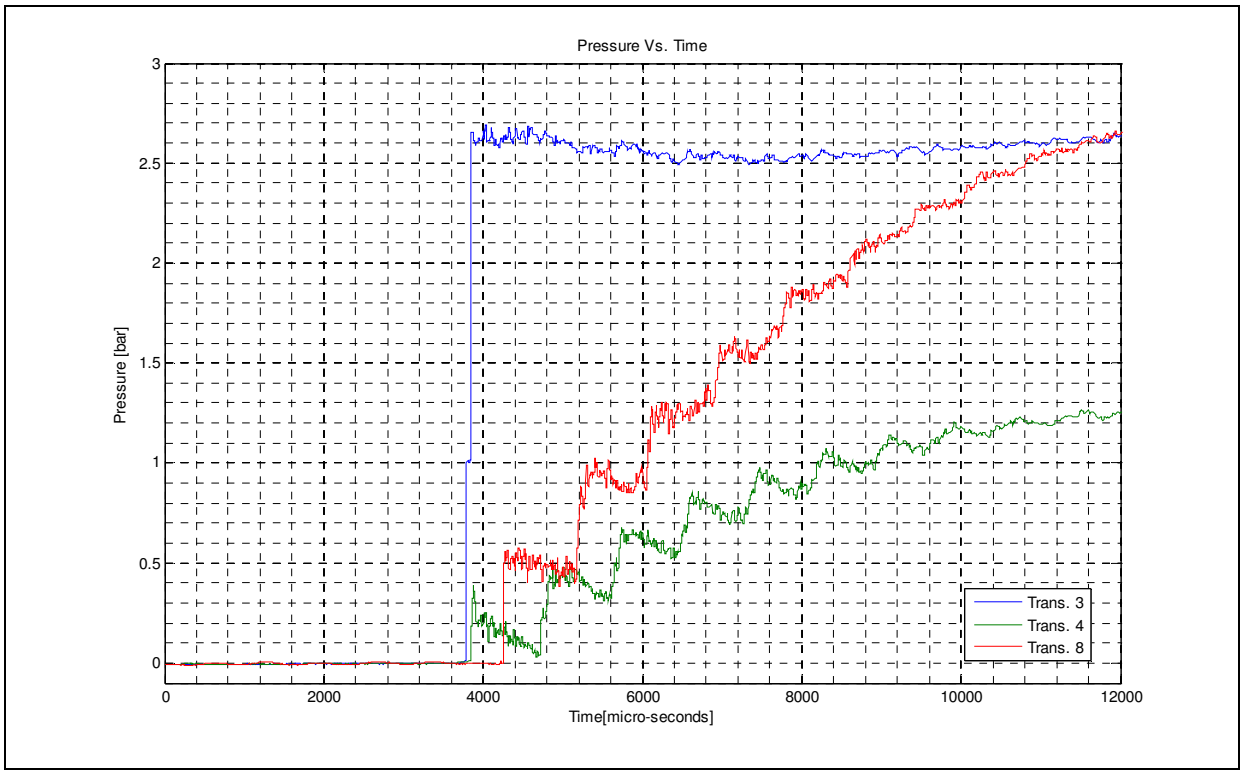


Figure: Pressure Plot for Pl3&Pl2

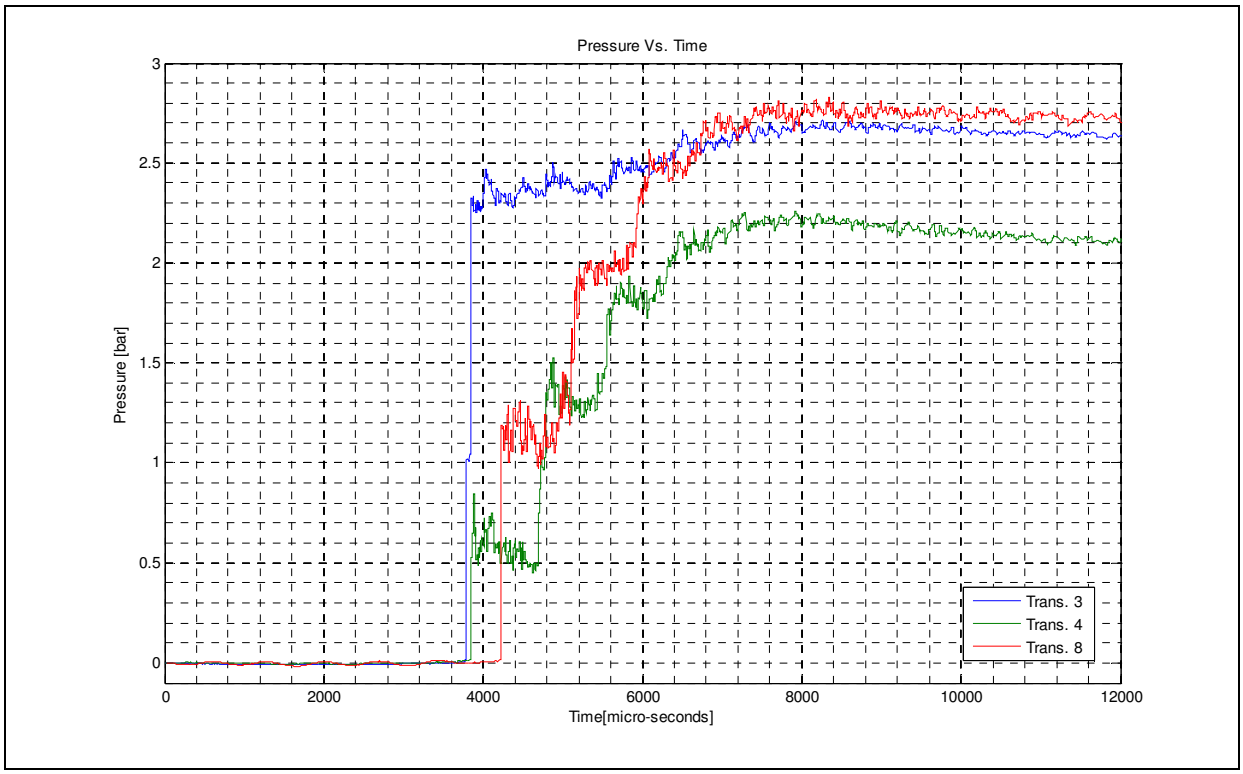


Figure: Pressure Plot for Pl3&Pl4

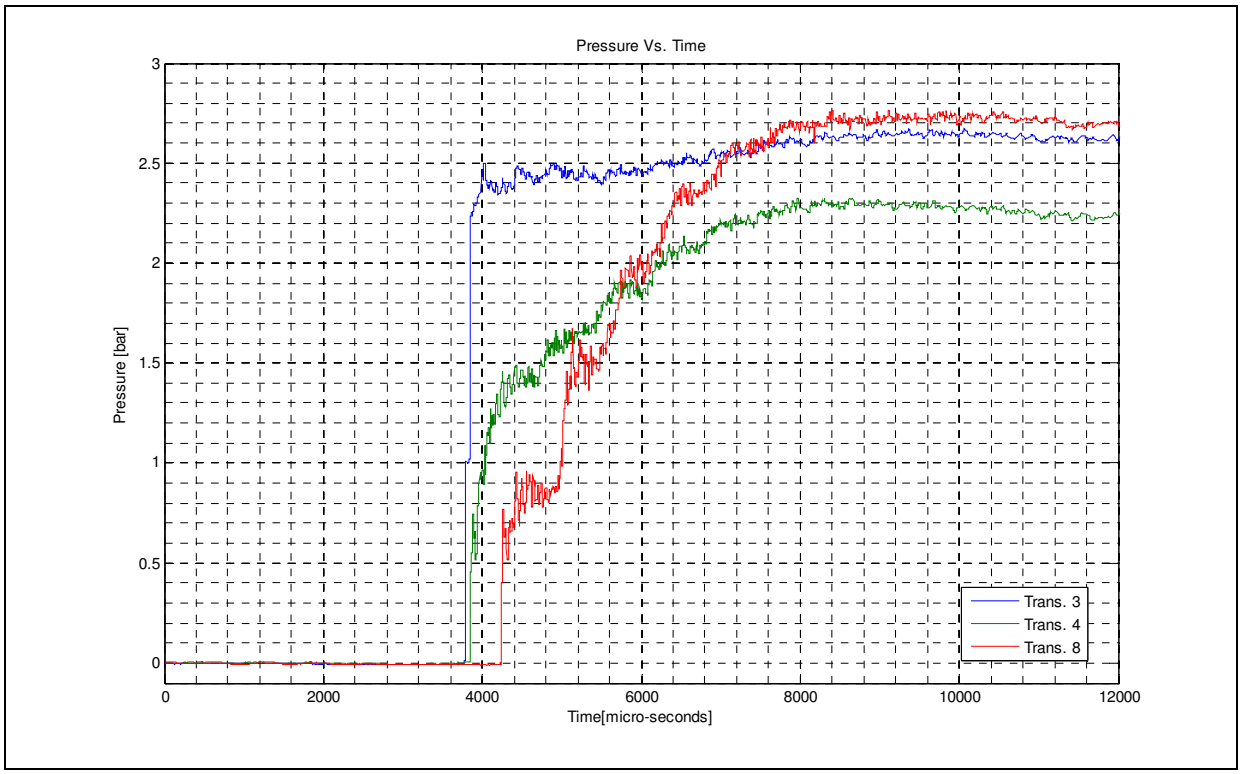


Figure: Pressure Plot for Pl4&Pl1

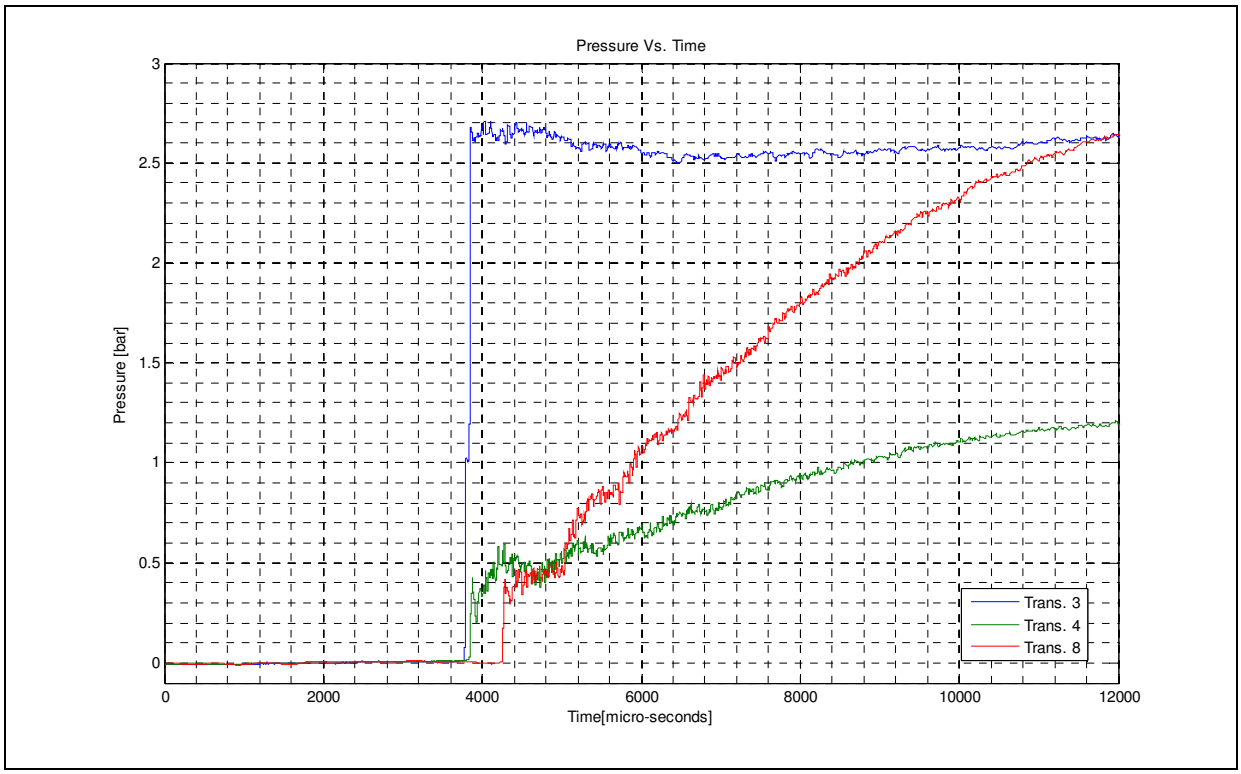


Figure: Pressure Plot for Pl4&Pl2

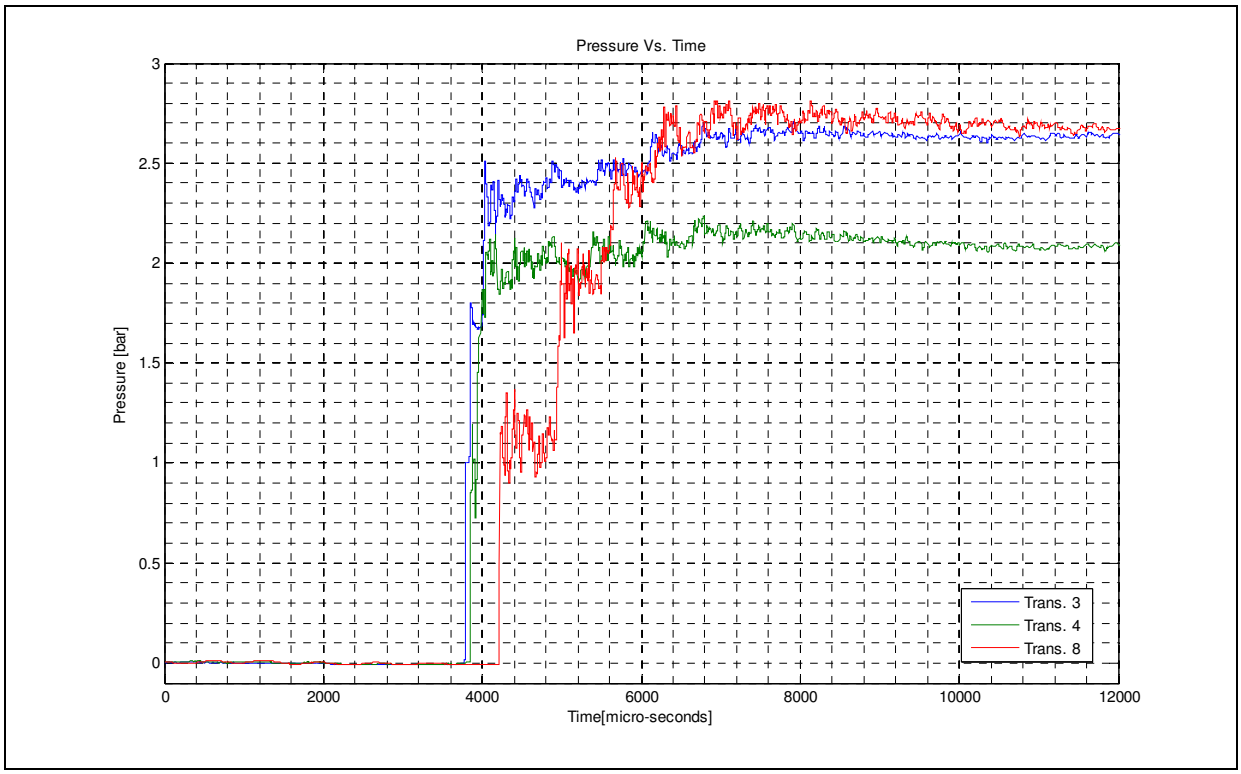


Figure: Pressure Plot for Pl4&Pl3

Appendix D: Schlieren Photographs

The complete set of photographic results for plate combinations Pl2&Pl4 and Pl3&Pl4 have been listed in this Appendix. The photographic results for all six plate combinations viz. Pl4&Pl2, Pl4&Pl1, Pl1&Pl3, Pl2&Pl4, Pl3&Pl2 and Pl3&Pl4 may be referred to in the DVD accompanying this report. All tests were performed using a set Mach number of M_{set} =1.42 and a separation distance of 30 mm between plate specimens. Ten photographs were taken over a 325 μs interval using a time delay of 1425 μs for each plate combination.

Photographs for Pl2&Pl4

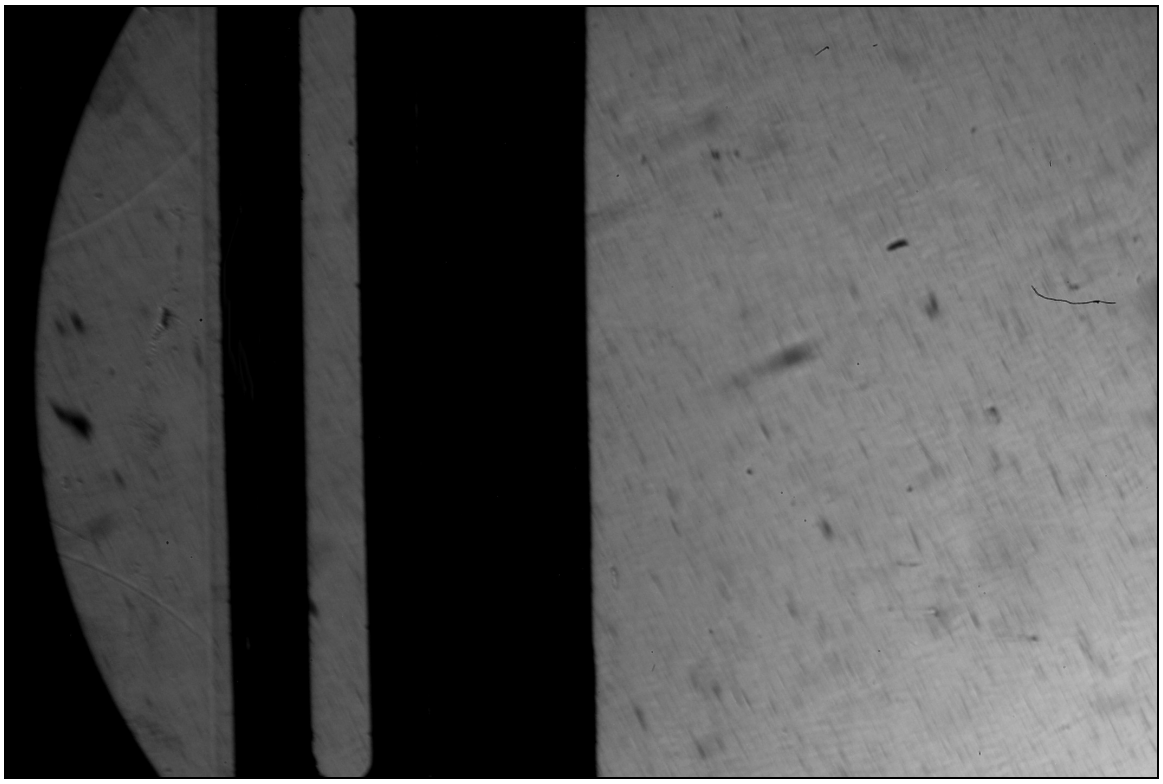


Figure: Schlieren Photograph of Pl2&Pl4, t = 1475 μs

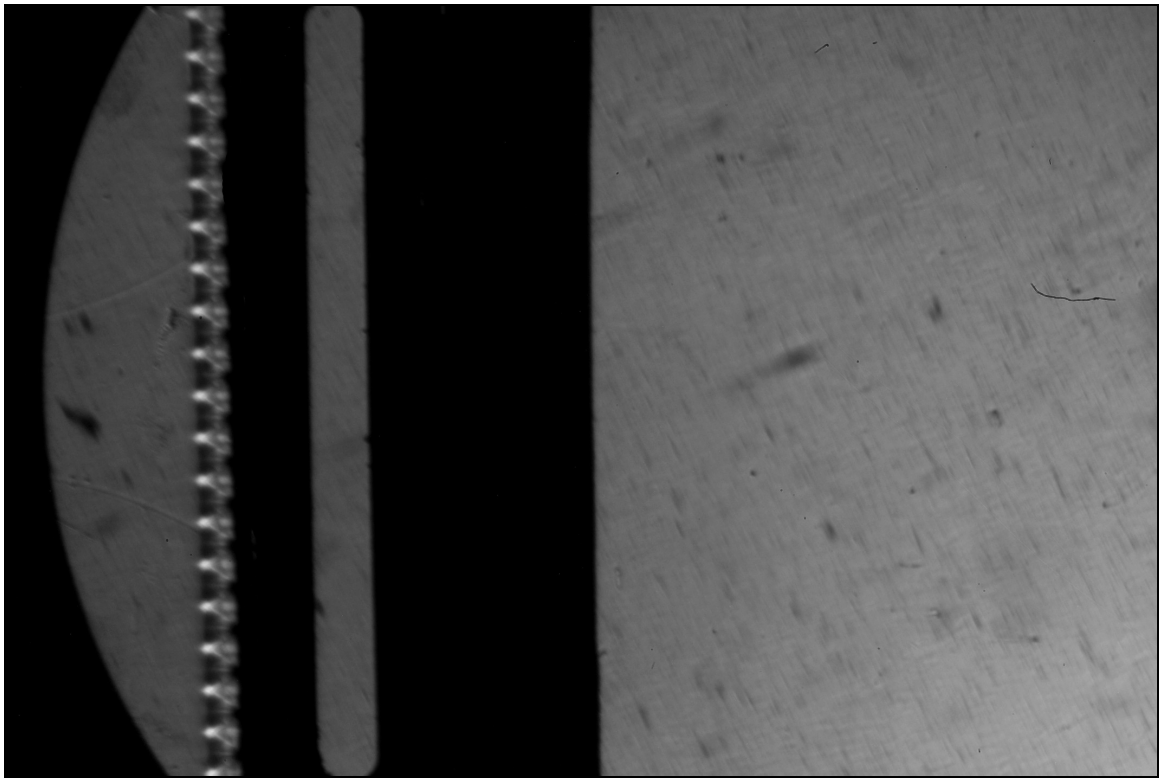


Figure: Schlieren Photograph of Pl2&Pl4, t = 1500 μs

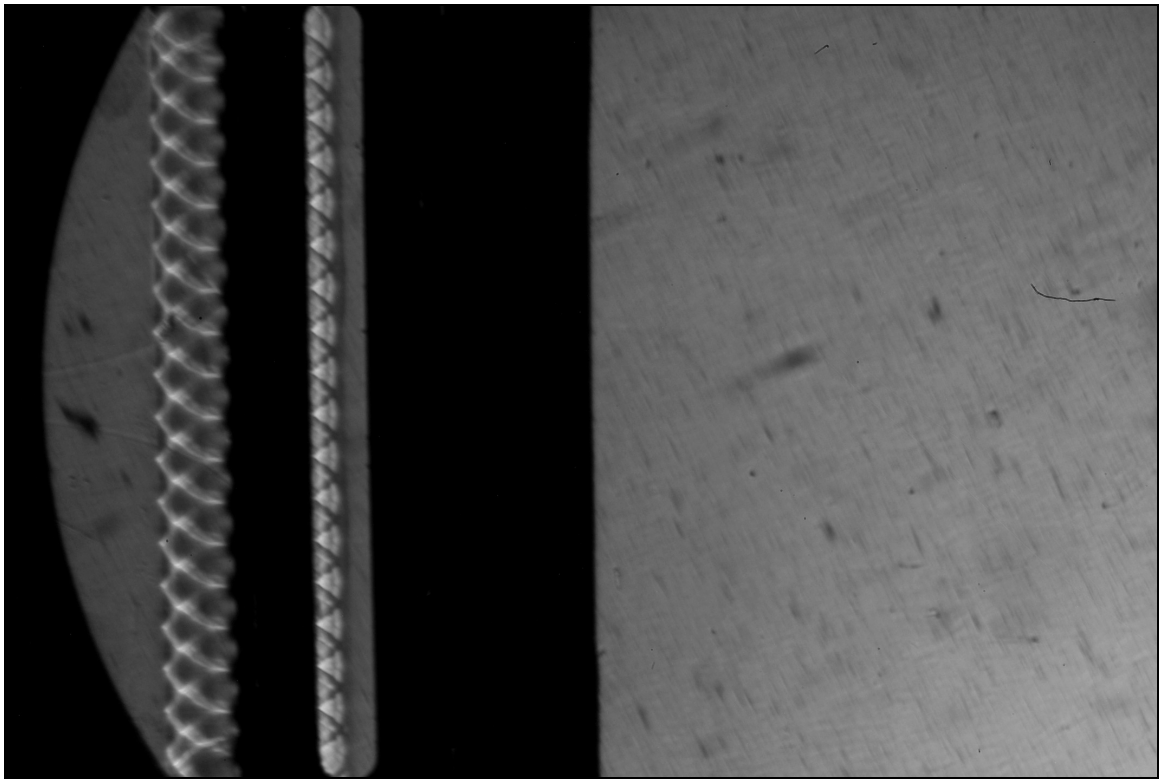


Figure: Schlieren Photograph of Pl2&Pl4, t = 1525 μs

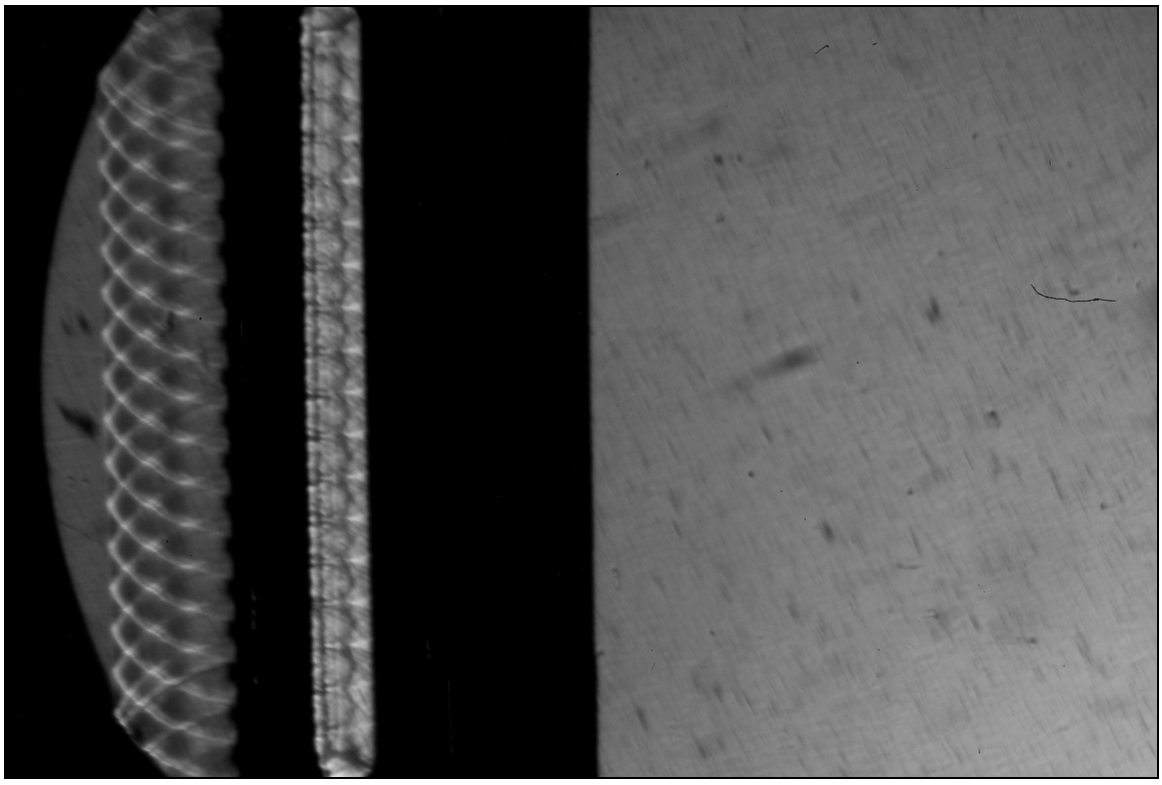


Figure: Schlieren Photograph of Pl2&Pl4, t = 1550 μs

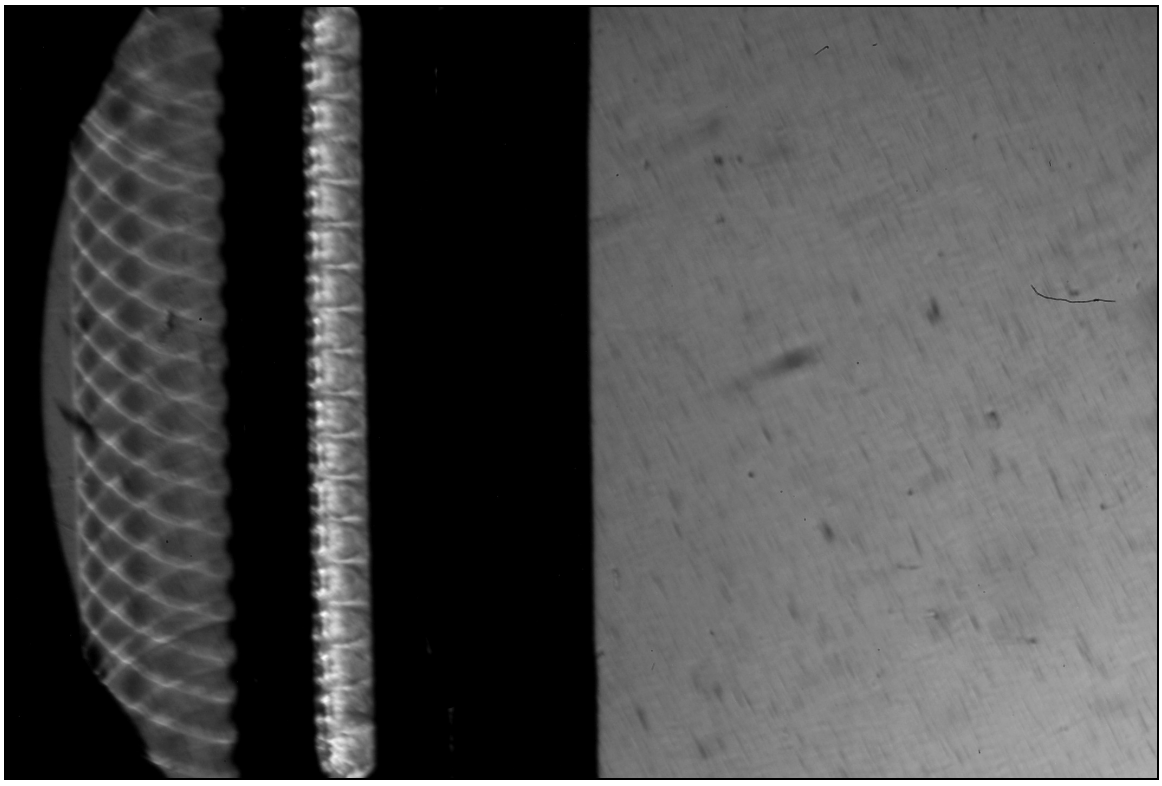


Figure: Schlieren Photograph of Pl2&Pl4, t = 1575 μs

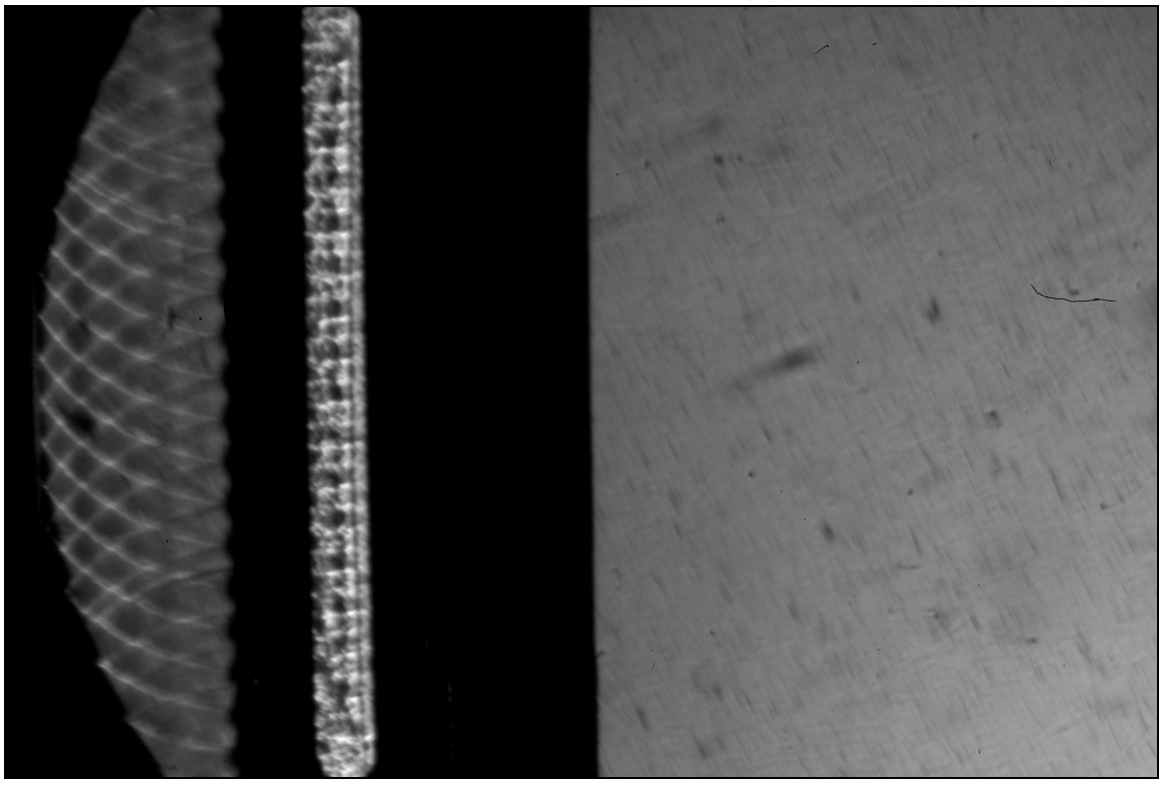


Figure: Schlieren Photograph of Pl2&Pl4, t = 1600 μs

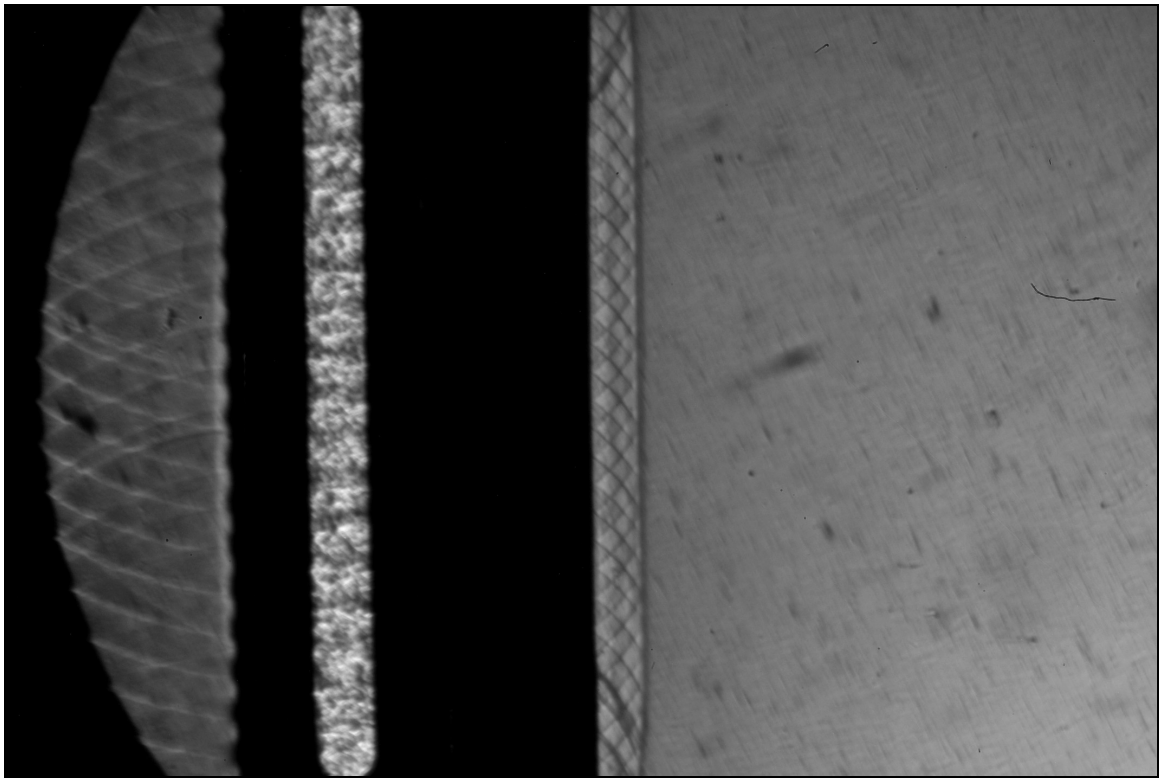


Figure: Schlieren Photograph of Pl2&Pl4, t = 1650 μs

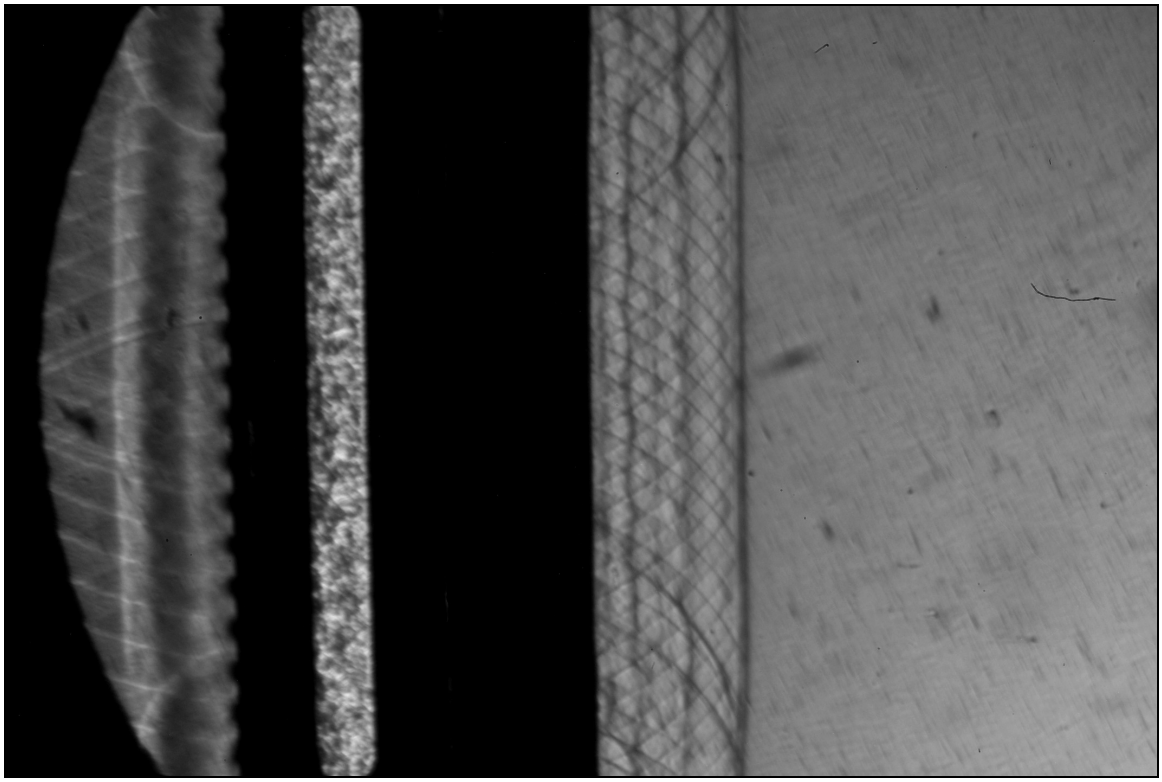


Figure: Schlieren Photograph of Pl2&Pl4, t = 1700 μs

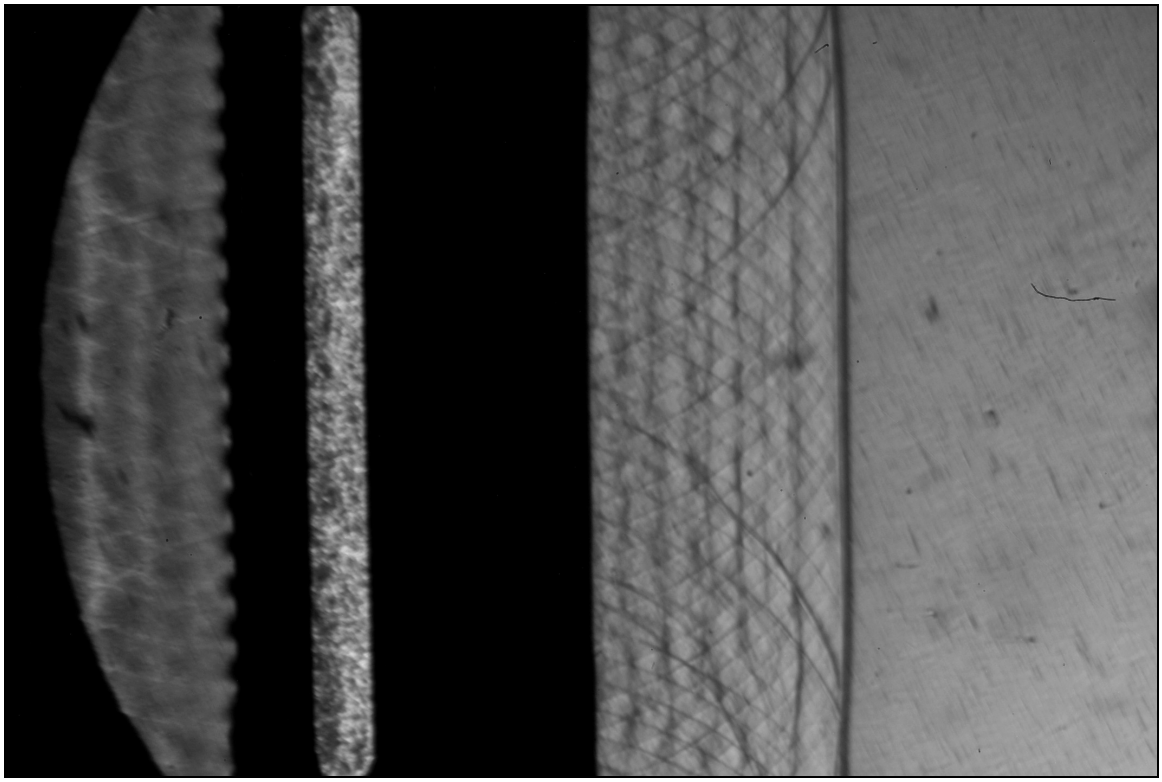


Figure: Schlieren Photograph of Pl2&Pl4, t = 1750 μs

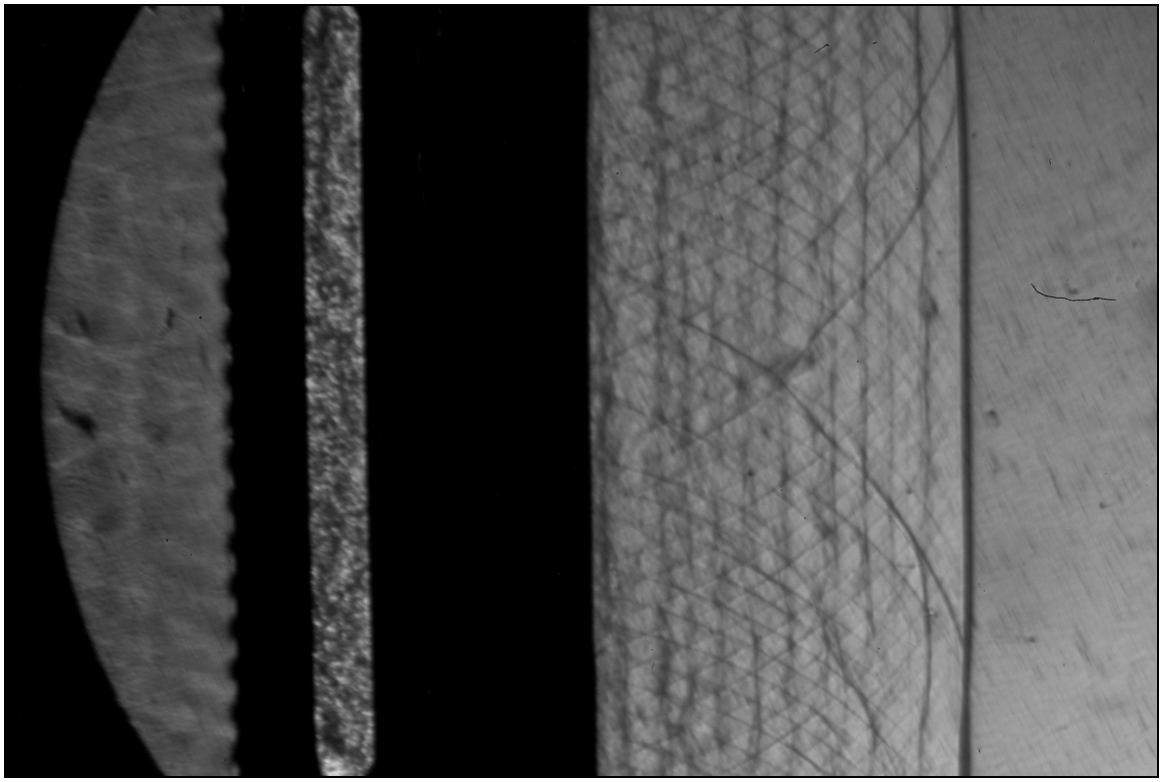


Figure: Schlieren Photograph of Pl2&Pl4, t = 1800 μs

Photographs for Pl3&Pl4

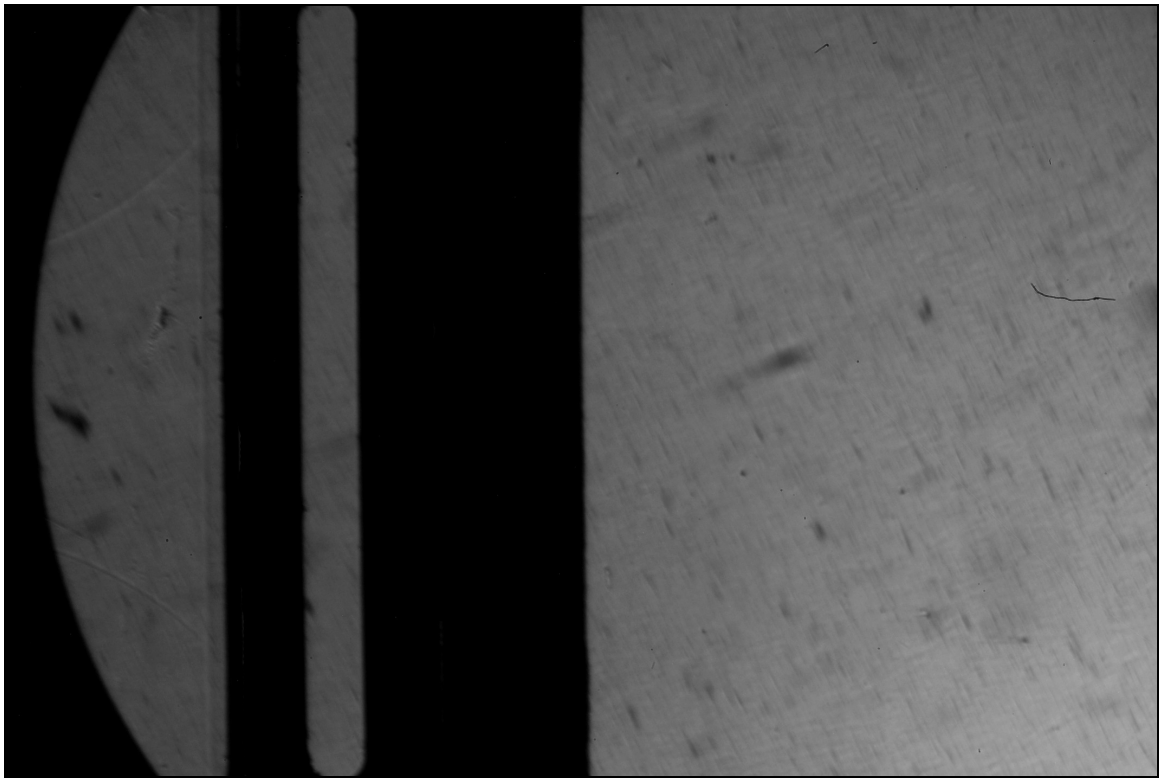


Figure: Schlieren Photograph of Pl3&Pl4, t = 1475 μs

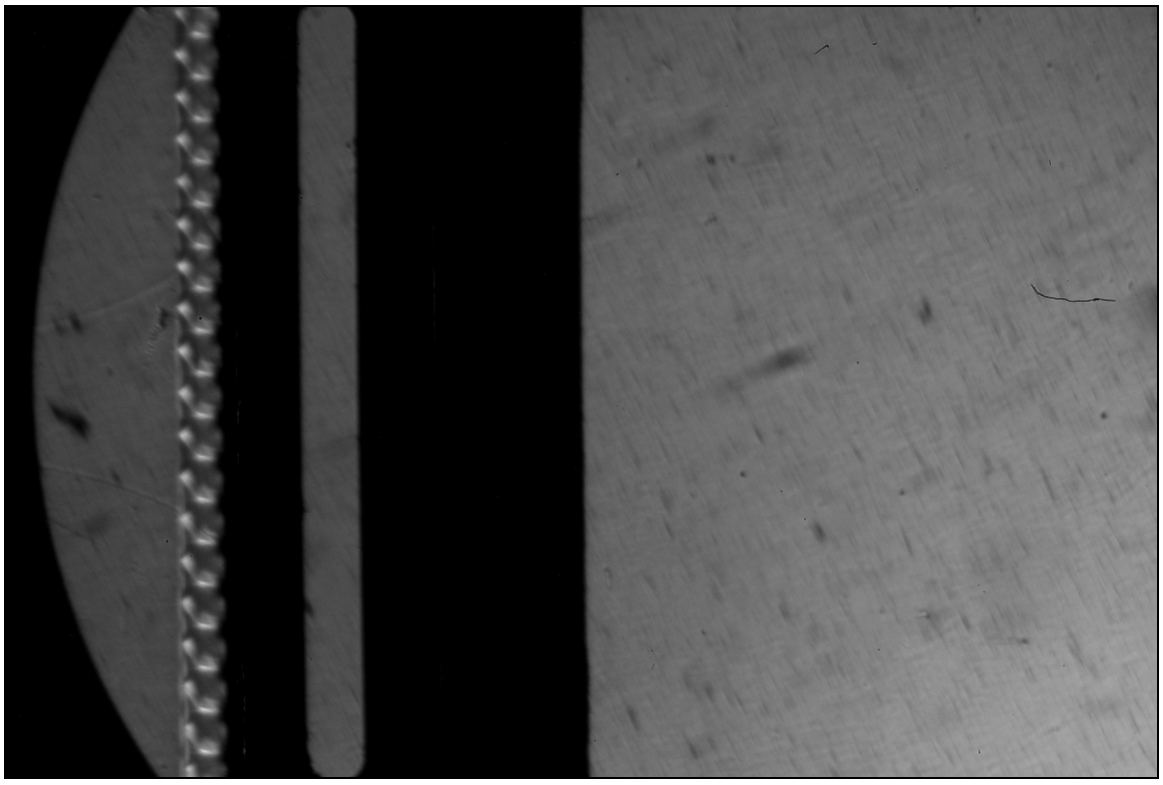


Figure: Schlieren Photograph of Pl3&Pl4, t = 1500 μs

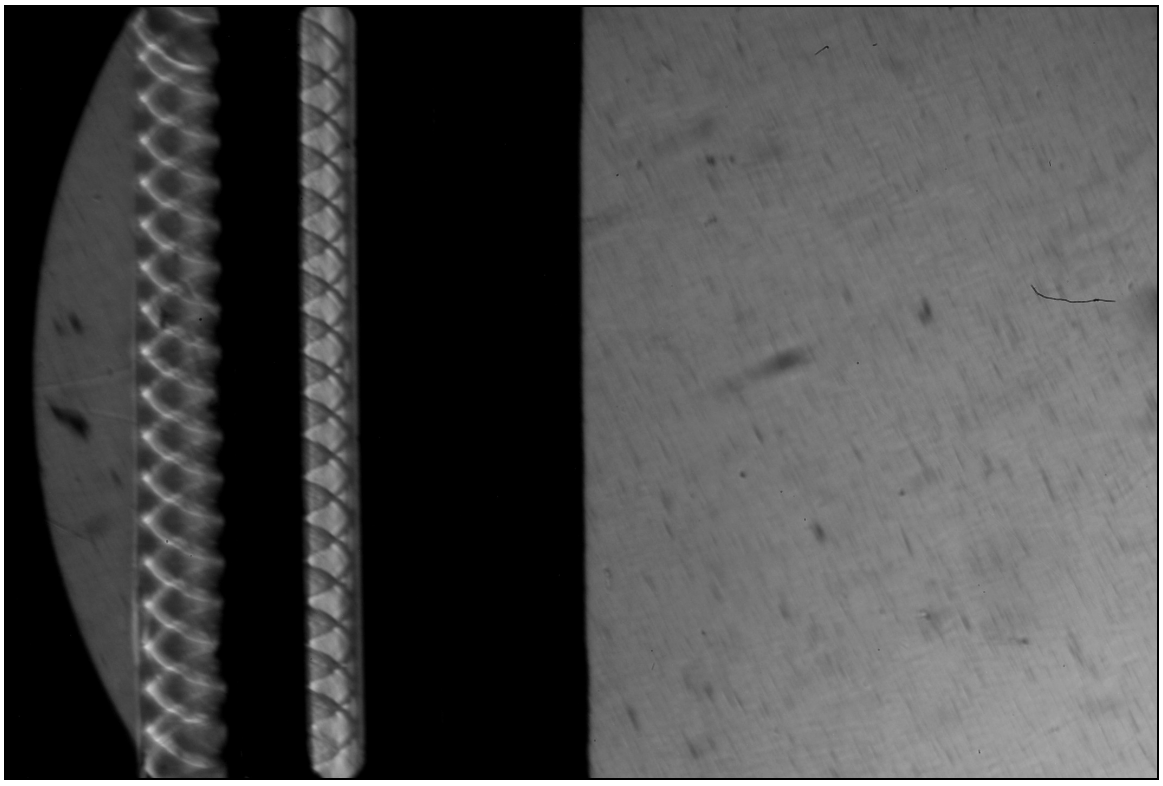


Figure: Schlieren Photograph of Pl3&Pl4, t = 1525 μs

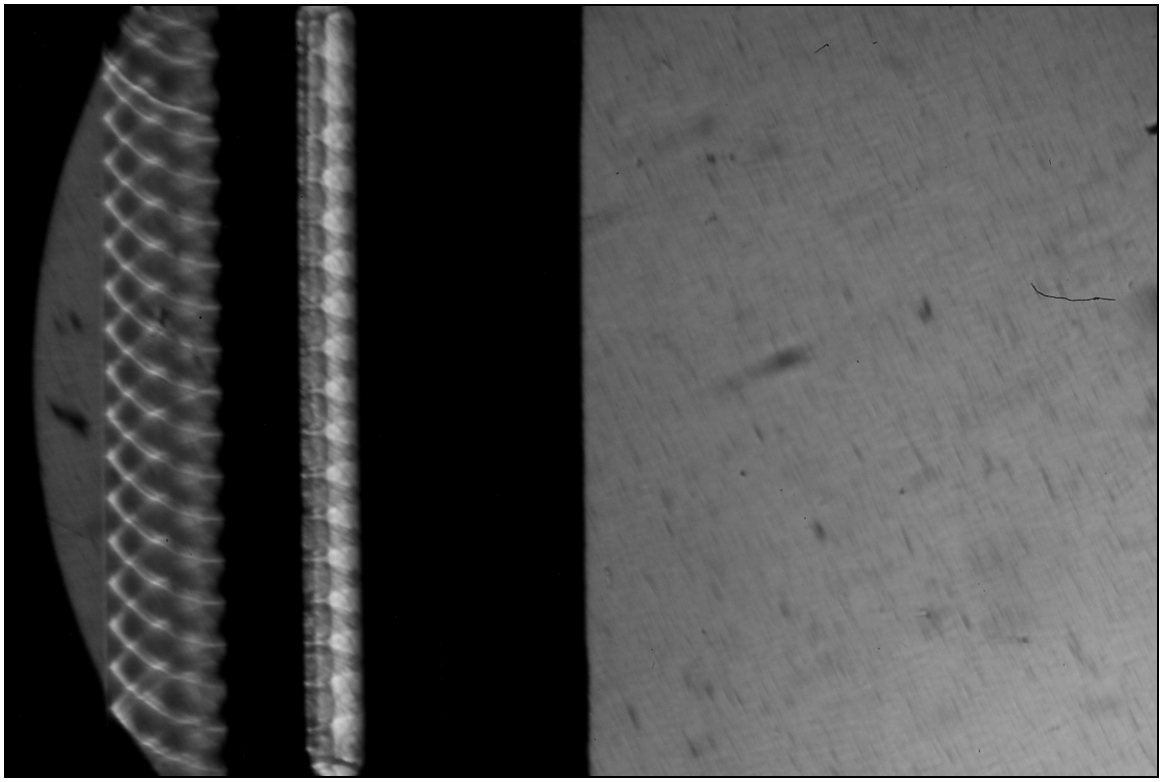


Figure: Schlieren Photograph of Pl3&Pl4, t = 1550 μs

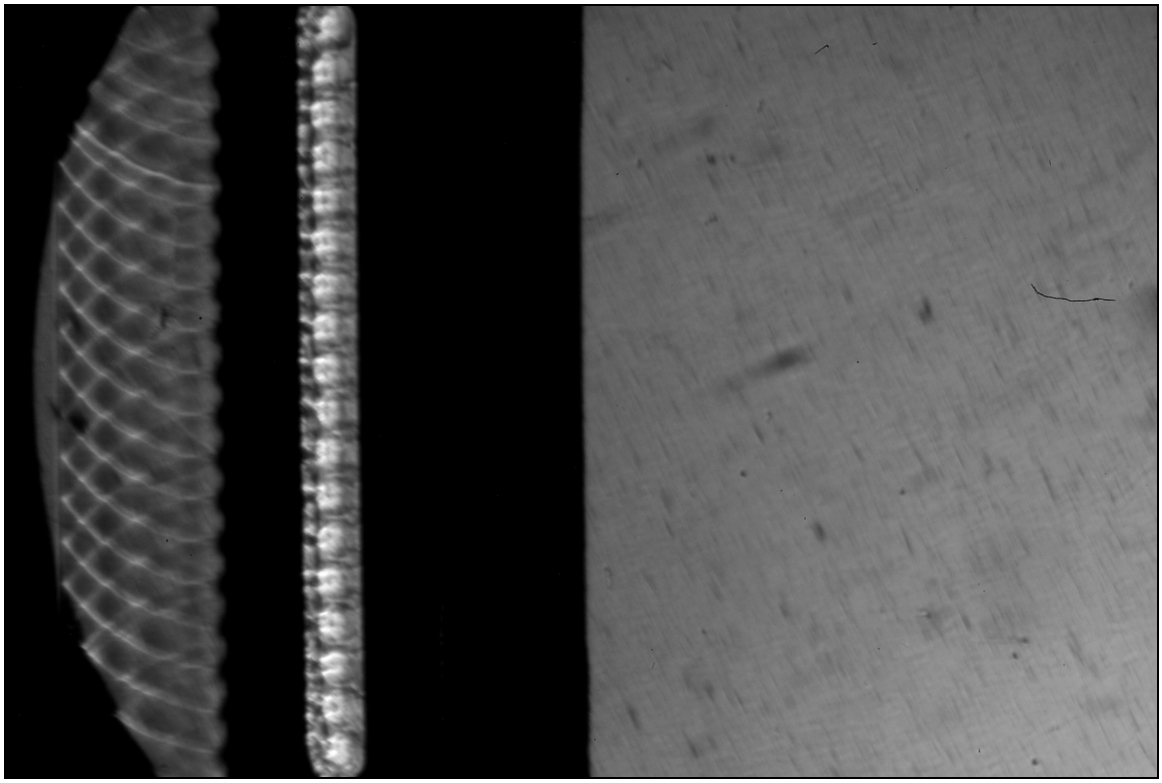


Figure: Schlieren Photograph of Pl3&Pl4, t = 1575 μs

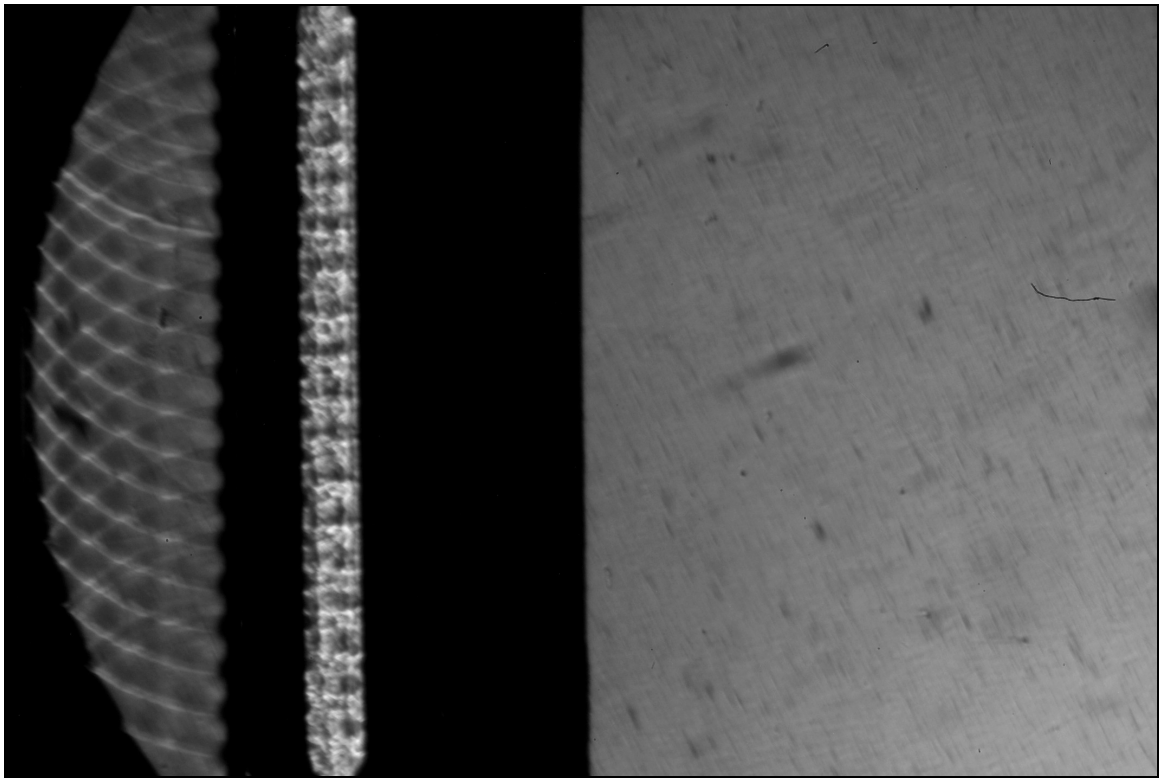


Figure: Schlieren Photograph of Pl3&Pl4, t = 1600 μs

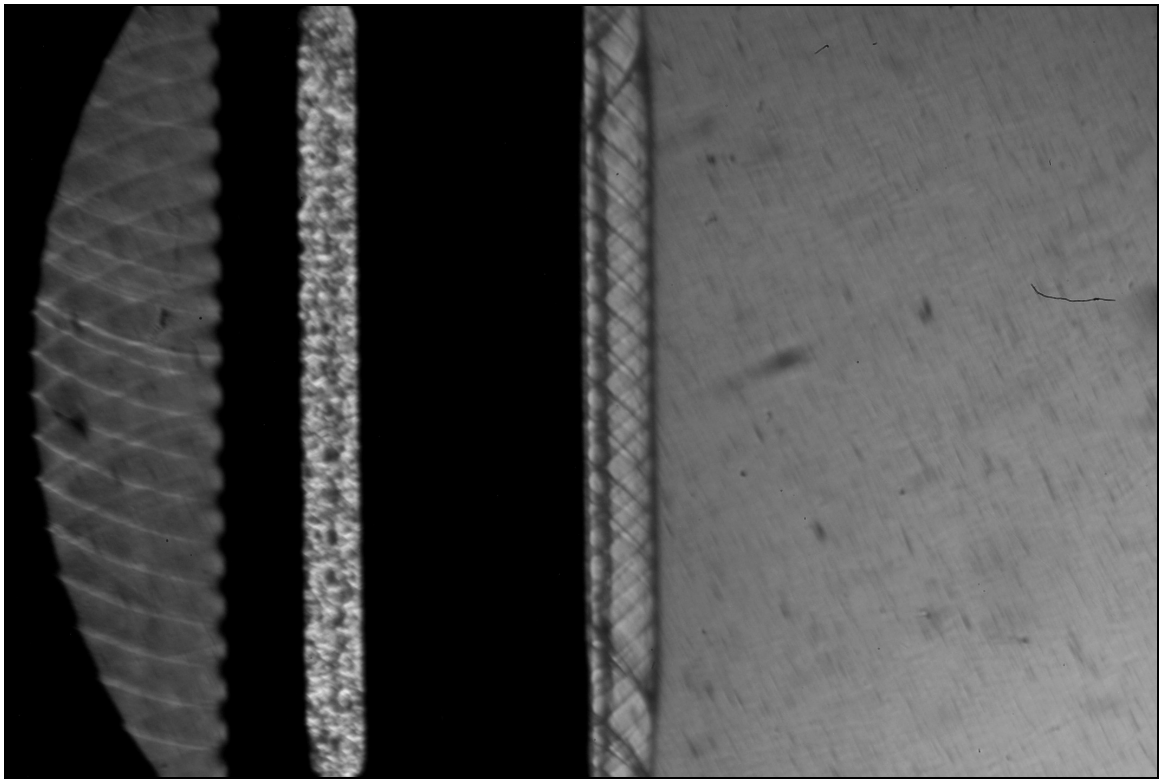


Figure: Schlieren Photograph of Pl3&Pl4, t = 1650 μs

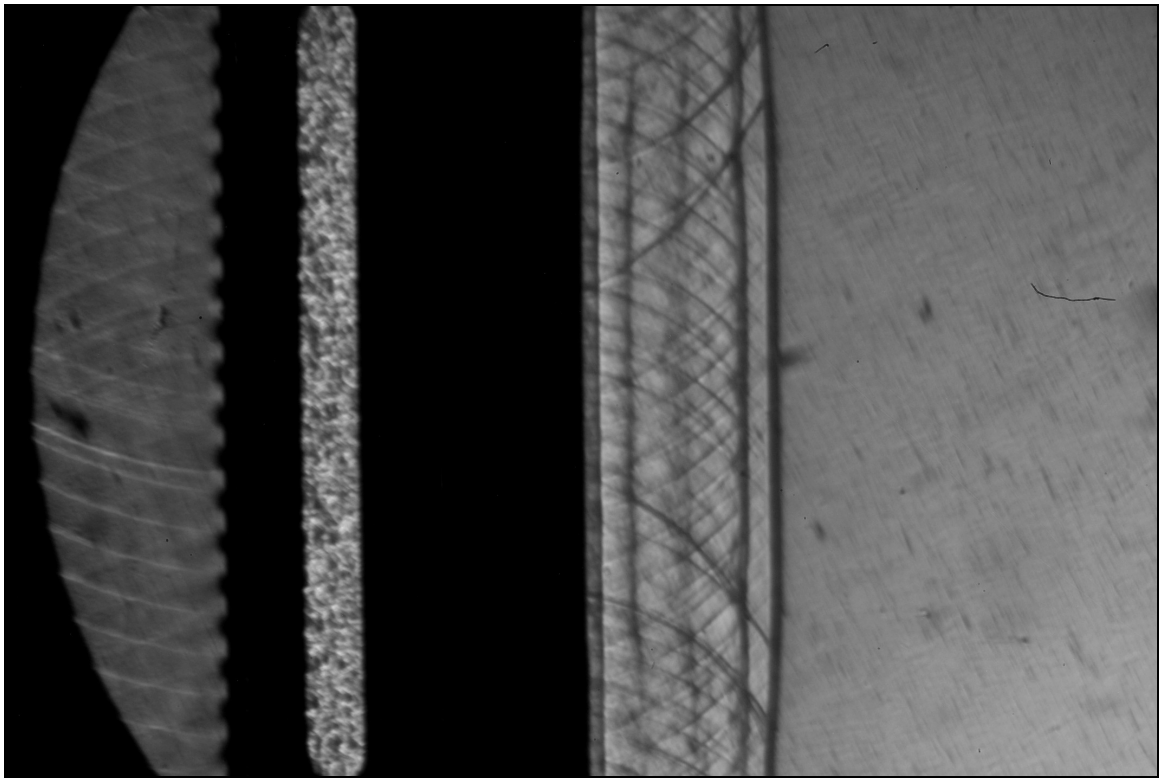


Figure: Schlieren Photograph of Pl3&Pl4, t = 1700 μs

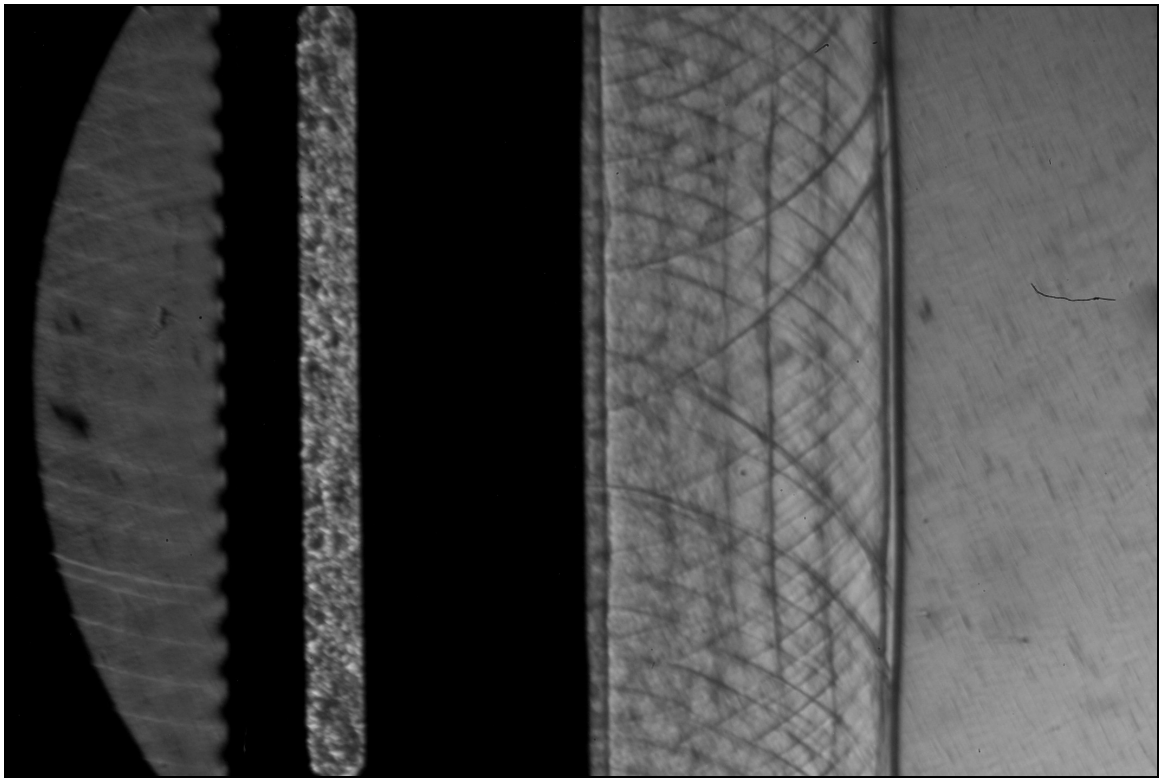


Figure: Schlieren Photograph of Pl3&Pl4, t = 1750 μs

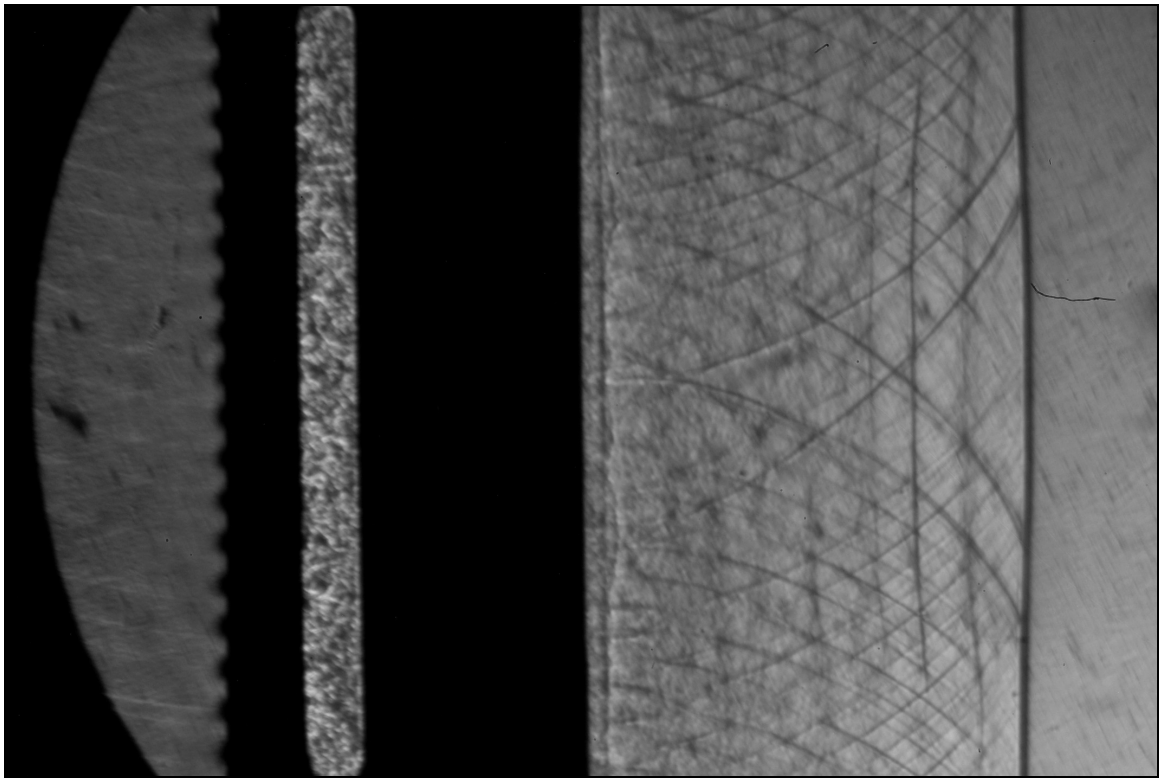


Figure: Schlieren Photograph of Pl3&Pl4, t = 1800 μs